UNIVERSITY OF CALIFORNIA, SAN DIEGO

An Investigation in the Hygrothermal Degradation of an E-glass/vinyl-ester Composite in Humid and Immersion Environments

A Dissertation submitted in partial satisfaction of the
Requirements for the degree of Doctor of Philosophy

in

Structural Engineering

by

Stephanie Laura Svetlik

Committee in charge:

Professor Vistasp M. Karbhari, Chair
Professor Francesco Lanza di Scalea
Professor Yu Qiao
Professor Lea Rudee
Professor Jan Talbot

2008

The Dissertation of Stephanie Laura Svetlik is approved, and it is acceptable in quality and form for publication on microfilm:

_____

_____

_____

_____

_____
Chair

University of California, San Diego

2008

DEDICATION

In loving memory of Dr. Francis Byron Nickerson.

To my parents, Frank and Barbara Svetlik, without whom I could not have completed this degree.

To my companion in life, David Haley, whose words of encouragement were instrumental in my success.

TABLE OF CONTENTS

LIST OF FIGURES

LIST OF TABLES

ACKNOWLEDGEMENTS

First and foremost, I would like to acknowledge Professor Vistasp Karbhari for his support and guidance through the completion of my studies. His patience, knowledge, and experience were absolutely instrumental in my success.

I must also acknowledge the support of the California Department of Transportation whose generous support enabled the completion of these studies.

I would like to acknowledge the deep support staff who serviced the numerous pieces of equipment without which this research could not have been conducted, including Ken Hughson as well as Bob Parks and Charlie Stearns of the Powell Structures Laboratory.

I would also like to acknowledge Evelyn York at the Scripps Institute of Oceanography for her indispensable assistance in performing scanning electron microscopy.

I would like to acknowledge the fellow inhabitants, current and former, of University Center 409 in the Department of Structural Engineering. Be they fellow graduate students, staff members, or rambunctious critters, their interactions helped to preserve my sanity outside of the laboratory.

I would also like to acknowledge the support of the Southern California women's lacrosse community who helped me to see the big picture both on and off the field.

Finally, I would like to acknowledge the faculty of the Pomona College Department of Physics and the Harvey Mudd College Department of Engineering who

provided invaluable guidance as I entered my graduate studies. Their instruction provided me with the solid foundation upon which I began to construct a strong, flexible continuing education.

VITA

2004	Bachelor of Arts, Pomona College
2005	Master of Science, University of California, San Diego
2005 – 2008	Research Assistant, Department of Structural Engineering University of California, San Diego
2007 – 2008	Teaching Assistant, Department of Structural Engineering University of California, San Diego
2008	Doctor of Philosophy, University of California, San Diego

ABSTRACT OF THE DISSERTATION

An Investigation in the Hygrothermal Degradation of an E-glass/vinyl-ester Composite in Humid and Immersion Environments

by

Stephanie Laura Svetlik

Doctor of Philosophy in Structural Engineering

University of California, San Diego, 2008

Professor Vistasp M. Karbhari, Chair

The main goal of this research is to gain a fundamental understanding of the synergistic mechanisms of degradation for a model E-glass/vinyl-ester composite exposed to humid environments and to compare them to the mechanisms of degradation resulting from water immersion. Moisture sorption kinetics are assessed in terms of structural modification diffusion in order to understand how water sorption phenomena and leaching of low molecular weight species may be responsible for changes in material properties.

Plasticization is identified using dynamic mechanical thermal analysis (DMTA) and is correlated to reversible degradation of the longitudinal tensile strength and short beam shear (SBS) strength. Tensile strength is also seen to decrease as a

result of minimally reversible interfacial degradation, also identified through DMTA and SBS testing. Exposure to 18%RH and 50%RH results in material properties which remain within initial scatter except where increases in the glass transition temperature and SBS strength indicate matrix dominated strengthening also identified in material exposed to 99%RH and immersion at elevated temperatures. Tensile, SBS, and DMTA results all reveal degradation of the fiber resulting from exposure to high humidity and immersion environments at elevated temperatures. Scanning electron microscopy confirms the occurrence of interfacial debonding and fiber pitting. In material exposed to 80°C immersion, pitting of the fiber surface was identified at sites adjacent to kaolin clay, a hydrophilic particulate filler commonly used as a lubricant in pultrusion.

Predictive degradation models are applied to tensile strength, SBS strength, and tensile failure strain results for 99%RH and immersion exposures, where irreversible degradation occurred at elevated temperatures. Degradation resulting from exposure to 99%RH and immersion is found to be equivalent. Predictive models show significant scatter based on the inability to isolate specific mechanisms. Further work is indicated in this area to ensure that safety factors are appropriately selected.

1. Introduction

1.1 Motivation

Glass fiber composites are commonly selected for civil applications due to their low cost, despite their known susceptibility to stress corrosion cracking [1-4]. As glass fiber composites are implemented more frequently in structural applications, it is important to understand the behavior of these materials over long periods of time. While composites have been in service for several years, the technology continues to progress. Thus, the performance of composites put in-service thirty years ago may not accurately reflect the performance of a composite designed today.

Because moisture, alkalinity, and temperature are the main factors affecting the durability of composite materials [5], the durability of composites is assessed through investigations of the effects of water on a particular system [6,7,8]. Immersion in liquid water addresses the worst case scenario where a composite is in continuous contact with liquid water in service. Accelerated testing is also conducted by immersing composite material in liquid water at elevated temperatures to accelerate the diffusion of water and mechanisms of degradation. Similarly, the effects of alklanity are addressed through exposure to alkaline solutions at elevated temperatures [5].

Photo-degradation of polymeric materials is well known to result form exposure to ultraviolet (UV) radiation [9,10,11], and temperature and moisture are known to produce a synergy leading to accelerated degradation [12]. Exposure to the

UV spectrum has been observed to result in degradation of the first 10 μm of the polymer resin in composite material [9]. While the loss of material properties will occur within this surface layer and the tensile strain has been shown to decrease with increased UV exposure [13], the degradation of material properties should not significantly affect the material properties of the bulk material [9,14]. Furthermore, composites in structural applications are generally utilized on surfaces which are not exposed to direct sunlight.

The main goal of this research is to establish a fundamental understanding of the mechanisms of degradation in humid environments as compared to those which result from exposure to water immersion at similar temperatures. Because hot water immersion is a standard test methodology for accelerated testing of composite durability, it is important to understand the mechanisms of degradation in these standard test environments and how they relate to degradation experienced in in-service humid environments in the absence of UV radiation.

Hygrothermal degradation of glass fiber composites primarily results from the degradation of the glass reinforcement, polymer resin matrix, and fiber/matrix interface, which is often characterized by an interphase characterized by the interdiffusion of the polymer resin and coupling agent [7]. Hydrolytic attack on the glass fiber surface results in pitting which leads to decreases in mechanical strengths and strains. The resin matrix serves in part to slow the progression of water to the glass surface, thereby protecting the glass reinforcement from hydrolytic attack [15]. Interfacial degradation may result from hydrolytic attack of the fiber/matrix interphase

and may also be aggravated by hygrothermal swelling stresses [15]. Increased interfacial bonding generally leads to increased durability of the interphase, as long as the interphase is not hydrophilic [7,15]. Reversible degradation of the polymer resin is attributed to the physical effects of water including plasticization and swelling [7,16], while irreversible degradation of the polymer resin is attributed to hydrolysis, microcracking, polymer relaxation resulting from physical aging, and the formation of microvoids resulting from water clustering [7,16].

Despite the available knowledge regarding the mechanisms of degradation of the glass fiber and polymer matrix in moist environments, it is difficult to isolate the specific modes of degradation of a polymer matrix composite which has been exposed to moisture. The longitudinal tensile strength of a composite depends upon the strength and strain of the constituent materials but is also strongly dependent upon the interphasial bond. The gradual sorption of moisture into the bulk composite further complicates degradation mechanisms as the diffusion profile changes. For instance, degradation of the interphase at higher temperatures may lead to pitting of the fiber reinforcement which is not so predominant at lower temperatures of exposure. Because it is so difficult to isolate the mechanisms of degradation and because there is interaction between the participating modes of degradation, it is desirable to implement a test program which allows for monitoring of specific modes of degradation.

The hygrothermal degradation of reinforced epoxy composites has been studied at length [8,15,16,17-32]. However, studies indicate that vinyl-ester

reinforced composites demonstrate increased durability over epoxy based composites [33]. Therefore, vinyl-ester epoxy based resins are often selected as the matrix for their low cost, high durability, and resistance to chemical attacks [33-35].

Because of their predominance in civil infrastructure applications, it is imperative to understand the mechanisms of degradation in E-glass/vinyl-ester composites. Accelerated durability studies have been performed previously on glass/vinyl-ester composites [36-41]; however, there is still a lack of understanding of how these materials actually perform in the long term. With a thorough understanding of the mechanisms of degradation, the structure may be optimally designed for resistance to degradation.

1.2 Service Life Prediction of Composite Materials

With the long term application of polymeric materials, durability testing is a major concern in the broad field of polymer science and can vary depending upon the specific application of the material. Composites in civil infrastructure are expected to perform at or above the design level for decades. The implementation of composites in civil infrastructure design for structures such as bridges is currently hindered by a lack of comfort with composites in the design and construction industry which also slows progress in the development of a sophisticated design code for composite materials in civil applications. Once composite has been used in civil applications, it is difficult to perform an inspection which may provide information on the material performance beyond a qualitative analysis of the adhesion of the composite to the substrate.

The coatings industry may have similar in-service exposure conditions, but the service life, end goal for accelerated testing, and metrics for success and failure [42] are different from those sought in the structural composites field, where knowledge of a design parameter over time is desirable. Specifically, coatings service life prediction (SLP) predicts time to failure of a critical mass of a larger population exposed to accelerated conditions [42], where these times to failure are years rather than decades long. While the mechanisms of degradation in coatings represent those experienced by the composite matrix, failure is detected by the progression of parameters such as glossiness, color index, and blistering beyond a critical level.

The composites industry implements a failure detection approach where designers require a certain design parameter, such as modulus or strength, to hold above a critical level for a specified service life. The design process includes a scaled factor allowing for durability considerations [43].

Well known degradation models exist to predict the change in material properties over time [44-46]. While predictive degradation models exist to account for humid environments [47,48], there are apparently no studies implementing the degradation model to composite materials exposed to humid environments. Durability models must be conservative in order to ensure that a material property is above the critical value for the service life; however, they should not be overly conservative so that the cost and weight of the structure may be minimized.

1.3. Goals and Objectives

While hot water immersion accelerated testing is standard for durability testing of composite materials, exposure to liquid water at elevated temperatures is not likely for composites used in civil applications. Composites used in civil infrastructure, rather, will be exposed to humid environments, and these environments will be transient in nature. Before time-variant hot and humid environmental conditions may be considered, it is imperative to gain a thorough understanding of the mechanisms of degradation of glass composites in static, humid environments since it is difficult to isolate the various mechanisms of degradation in the fiber, matrix, and interphase.

The main goal of this research is to gain a fundamental understanding of the synergistic mechanisms of degradation for a model E-glass/vinyl-ester composite exposed to humid environments and to compare them to the mechanisms of degradation resulting from immersion in deionized water. Gravimetric studies are conducted to gain an understanding of the modes of moisture sorption in this glass composite system in humid and immersion environments. Mechanical and physical testing of the composite is conducted in order to monitor the mechanisms of degradation which lead to decreases in longitudinal tensile properties. A comparison of reversible and irreversible degradation trends is made in order to shed light on possible mechanisms of degradation. Where environmental exposure results in degradation of material properties, predictive degradation models are implemented and compared. Degradation trends resulting from immersion in liquid water are compared to those resulting from exposure to humid environments.

1.4 References

1. Liao, K. and E.Y.M. Tan. "In situ tensile strength degradation of glass fiber in polymer composite." *Scripta mater.* 44 (2001) 785-789.

2. Kawada H. and A. Kobiki. "A study on stress-corrosion cracking using single fiber model specimen: Degradation properties of GFRP caused by water absorption." *JSME International Journal A.* 46 **3** (2003) 303-307.

3. Akdemir, A., N. Tarakcioglu, and A. Avci. "Stress corrosion crack growth in glass/polyester composites with surface crack." *Composites: Part B.* 32 (2001) 123-129.

4. Bunker, B.C. "Molecular mechanisms for corrosion of silica and silicate glasses." *Journal of Non-Crystalline Solids* Vol. 179 (1994), pp300-308.

5. Nkurunziza, G., A. Debaiky, P. Cousin, and B. Benmokrane. "Durability of GFRP bars: A critical review of the literature." *Progress in Structural Engineering and Materials*. Vol. 7 (2005) 194-209.

6. Liao, K., C.R. Schultheisz, D.L. Hunston, and L.C. Brinson. "Long-term Durability of Fiber-Reinforced Polymer-Matrix Composite Materials for Infrastructure Applications: A Reivew." *Journal of Advanced Materials*. Vol. 30, No. 4 (1998) 3-40.

7. Schutte, C.L. "Environmental durability of glass-fiber composites." *Materials Science and Engineering*. Vol. R13 (1994) 265-324.

8. Lee, M.C. and N.A. Peppas. "Water transport in epoxy resins." *Progress in Polymer Science*. Vol. 18, No. 5 (1993) 947-961.

9. Bank, L.C., T.R. Gentry, and A. Barkatt. "Accelerated Test Methods to Determine the Long-Term Behavior of FRP Composite Structures: Environmental Effects." *Journal of Reinforced Plastics and Composites.* Vol. 14 (1995) 559-587.

10. Fedor, G.R. and P.J. Brennan. "Comparison between natural weathering and fluorescent UV exposures: UVA-340 Lamp Test Results." *Durability Testing of Nonmetallic Materials, ASTM STP 1294*. R.J. Herling, Ed., American Society for Testing and Materials, 1996.

11. Verdu, J., X. Colin, B. Fayolle, and L. Audouin, "Methodology of Lifetime Prediction in Polymer Aging," *Journal of Testing and Evaluation*. Vol. 35, No. 3 (2007) 289-296.

12. Nguyen, T., J. Martin, E. Byrd, and N. Embree. "Relating Laboratory and Outdoor Exposure of Coatings: II. Effects of Relative Humidity on

Photodegradation and the Apparent Quantum Yield of Acrylic-Melamine Coatings." *Journal of Coatings Technology*. Vol. 74, No. 932 (2002) 65-80.

13. Larena, A., S. Jimenez de Ochoa, and F. Dominguez. "Dynamic-mechanical analysis of the photo-degradation of long glass fibre reinforced polypropylene: Mechanical properties' changes." *Polymer Degradation and Stability*. Vol. 91 (2006) 940-946.

14. Correia, J.R., S. Cabral-Fonseca, F.A. Branco, J.G. Ferreira, M.I. Eusebio, and M.P. Rodrigues. "Durability of pultruded glass-fiber-reinforced polyester profiles for structural applications." *Mechanics of Composite Materials.*. Vol. 42, No. 4 (2006) 325-338.

15. Koenig, J.L. and H. Emadipour. "Mechanical Characterization of the Interfacial Strength of Glass-Reinforced Composites." *Polymer Composites*. Vol. 6, No. 3 (1985) 142-150.

16. Antoon, M.K. and J.L. Koenig. "The Structure and Moisture Stability of the Matrix Phase in Glass-Reinforced Epoxy Composites." *Journal of Macromolecular Science – Reviews in Macromolecular Chemistry*. Vol. C19, No. 1 (1980) 135-173.

17. Romans, J.B., A.G. Sands, and J.E. Cowling. "Fatigue Behavior of Glass Filament-Wound Epoxy Composites in Water." *Industrial & Engineering Chemistry Product Research and Development.* Vol. 11, No. 3 (1972) 261-268.

18. Ishai, O. "Environmental Effects on Deformation, Strength, and Degradation of Unidirectional Glass-Fiber Reinforced Plastics. II. Experimental Study." *Polymer Engineering and Science*. Vol. 15, No. 7 (1975) 491-499.

19. Shen, C.-H. and G.S. Springer. "Effects of Moisture and Temperature on the Tensile Strength of Composite Materials." *Journal of Composite Materials*. Vol. 11 (1977) 2-16.

20. Shen, C.-H. and G.S. Springer. "Environmental Effects on the Elastic Moduli of Composite Materials." *Journal of Composite Materials.* Vol. 11 (1977) 250-264.

21. Adamson, M.J. "Thermal expansion and swelling of cured epoxy resin used in graphite/epoxy composite materials." *Journal of Materials Science*. Vol. 15 (1980) 1736-1745.

22. Dewimille, B. and A.R. Bunsell. "The modeling of hydrothermal aging in glass fibre reinforced epoxy composites." *Journal of Physics D: Applied Physics*. Vol. 15 (1982) 2079-2091.

23. Aronhime, M.T., S. Neumann, and G. Marom. "The anisotropic diffusion of water in Kevlar-epoxy composites." *Journal of Materials Science*. Vol. 22 (1987) 2435-2446.

24. Hahn, H.T. "Hygrothermal Damage in Graphite/Epoxy Laminates." *Journal of Engineering Materials and Technology*. Vol. 109 (1987) 3-11.

25. Zheng, Q. and R.J. Morgan. "Synergistic Thermal-Moisture Damage Mechanisms and Their Carbon Fiber Composites." *Journal of Composite Materials*. Vol. 27, No. 15 (1993) 1465-1478.

26. Dufresne, A. and C. Lacabanne. "Thermo-stimulated creep analysis on the effect of water in glass bead-reinforced composites." *Polymer*. Vol. 36, No. 23 (1995) 4417-4424.

27. Lekatou, A. Faidi, S.E., D. Ghidaoui, S.B. Lyon, and R.C. Newman. "Effect of water and its activity on transport properties of glass/epoxy particulate composites." *Composites Part A*. Vol. 28A (1997) 223-236.

28. Jensen, R.E., C.E. Johnson, and T.C. Ward. "Investigation of a Waterborne Epoxy for E-glass Composites." *Journal of Polymer Science*. Vol. 38 (2000) 2351-2365.

29. Choi, H.S., K.J. Ahn, J.-D. Nam, and H.J. Chun. "Hygroscopic aspects of epoxy-carbon fiber composite laminates in aircraft environments." *Composites: Part A*. Vol. 32 (2001) 709-720.

30. Zhang, S., V.M. Karbhari, and D. Reynaud. "NOL-ring based evaluation of freeze and freeze-thaw exposure effects on FRP composite column wrap systems." *Composites: Part B*. Vol. 32 (2001) 589-598.

31. Patel, S.R. and S.W. Case. "Durability of hygrothermally aged graphite/epoxy woven composite under combined hygrothermal conditions." *International Journal of Fatigue*. Vol. 24 (2002) 1295-1301.

32. Mijovic, J. and H. Zhang. "Molecular Dynamics Simulation Study of Motions and Interactions of Water in a Polymer Network." *Journal of Physical Chemistry B*. Vol. 180, No. 8 (2004) 2557-2563.

33. Megel, M., L. Kumosa, T. Ely, D. Armentrout, and M. Kumosa. "Initiation of stress-corrosion cracking in unidirectional glass/polymer composite materials." *Composite Sceince and Technology*. Vol. 61 (2001) 231-246.

34. Auad, M.L., M. Aranguren, and J. Borrajo. "Epoxy-Based Divynyl Ester Resin/Styrene Copolymers: Composition Dependence of the Mechanical and Thermal Properties." *J. of Applied Polymer Science.* Vol. 66 (1997) 1059-1066.

35. Apicella, A., C. Migliaresi, L. Nicolais, L. Iaccarino, and S. Roccotelli. "The water aging of unsaturated polyester-based composites: influence of resin chemical structure." *Composites*. Vol. 14, No. 4 (1983) 387-392.

36. Ghorbel, I. and D. Valentin. "Hydrothermal Effects on the Physico-Chemical Properties of Pure and Glass Fiber Reinforced Polyester and Vinylester Resins." *Polymer Composites*. Vol. 14, No. 4 (1993) 324-334.

37. Liao, K., C.R. Schultheisz, and D.L. Hunston. "Effects of environmental aging on the properties of pultruded GFRP." *Composites: Part B*. Vol. 30 (1999) 485-493.

38. Chin, J.W., K. Aouadi, M.R. Haight, W.L. Hughes, and T. Nguyen. "Effects of Water, Salt Solution and Simulated Concrete Pre Solution on the Properties of Composite Matrix Resins Used in Civil Engineering Applications." *Polymer Composites*. Vol. 22, No. 2 (2001) 282-297.

39. Fraga, A.N., V.A. Alvarez, A. Vazquez, and O. de la Osa. "Relationship Between Dynamic Mechanical Properties and Water Absorption of Unsaturated Polyester and Vinyl Ester Glass Fiber Composites." *J. of Composite Materials.* Vol. 37, No. 17 (2003) 1553-1573.

40. Miyano, Y., M. Nakada, and N. Sekine. "Accelerated testing for long-term durability of GFRP laminates for marine use." *Composites: Part B*. vol. 35 (2004) 497-502.

41. Chu, W. and W. M. Karbhari. "Effect of Water Sorption on Performance of Pultruded E-Glass/Vinylester Composites." *Journal of Materials in Civil Engineering*. Vol. 17, No. 1 (2005) 63-71.

42. *Service Life Prediction of Organic Coatings: A Systems Approach*. D.R. Bauer and J.W. Martin, eds. American Chemical Society: Washington, DC, 1999.

43. ACI-440.2R-02. *Guide to the Design and Construction of Externally Bonded FRP Systems for Strengthening Concrete Structures*. American Concrete Institute: Farmington Hills, MI, 2002.

44. Litherland, K.L., D.R. Oakley, and B.A. Proctor. "The use of accelerated ageing procedures to predict the long term strength of GRC composites." *Cement and Concrete Research*. Vol. 11 (1981) 455-466.

45. Phani, K.K., and N.R. Bose. "Temperature Dependence of Hydrothermal Ageing of CSM-Laminate During Water Immersion." *Composites Science and Technology*. Vol. 29 (1987) 79-87.

46. Purnell, P. "Interpretation of climatic temperature variations for accelerated ageing models." *Journal of Materials Science*. Vol. 39 (2004) 113-118.

47. Jorgensen, G.J. "A Phenomenological Approach to Obtaining Correlations between Accelerated and Outdoor Exposure Test Results for Organic Materials." *Journal of Testing and Evaluation*. Vol. 32, No. 6 (2000) 494-499.

48. White, J.R. and A. Turnbull. "Weathering of polymers: mechanisms of degradation and stabilization, testing strategies and modeling." *Journal of Materials Science*. Vol. 29 (1994) 584-613.

2. Literature Review

2.1 Moisture Sorption in Composites

2.1.1 Effect of Moisture Sorption on Composites

The effect of moisture sorption on the degradation of polymer composite materials can be best understood by considering the effect of water on the constituent elements of the system. The degradation of polymers due to moisture can be broken up into chemical and physical degradation, where chemical changes include hydrolysis of the polymer matrix chain and interfacial bond, and physical degradation includes swelling, plasticization, and relaxation of the polymer [1,2]. Physio-mechanical degradation may also occur as swelling promotes microcracking in the hydrolyzed weakened resin and interfacial debonding at the hydrolyzed interface [1,3]. Table 1 summarizes the chemical, physical, and physio-mechanical degradation mechanisms and classifies them as reversible or irreversible. It should be noted that reversible processes will never be fully reversible since the rearrangement of molecules will always lead to increased entropy of the system. While hydrolysis is generally considered to be an irreversible degradation mechanism [1], there is evidence that hydrolyzed bonds can experience a condensation or hydration reaction which can partially reverse the effects of hydrolysis [4,5]. The following discussion addresses these degradation mechanisms in detail.

Table 1. Overview of moisture induced composite degradation mechanisms. F = Fiber, M = Matrix, I = Interphase. * Addresses processes which have been claimed as both reversible and irreversible.

Classification of Mechanism	Degradation Mechanism	Location			Reversible?
		F	M	I	Y/N
Chemical	Hydrolysis				
	Pitting	×			N*
	Chain Scission		×		N*
	Debonding			×	N*
Physical	Plasticization		×	×	Y*
	Swelling		×		Y*
	Leaching	×	×	×	N
	Relaxation (Physical Aging)		×		N
Physio-mechanical	Microcracking		×	×	N
	Microvoids		×	×	N

2.1.1.1 Polymer Matrix

It is well known that the ingress of water results in changes of bulk polymeric properties [6-10], as the water molecules interact with the polymer chains. The polymer matrix under consideration here, an epoxy based bisphenol-A vinyl-ester, may have a chemical structure similar to that provided in Figure 1. This chemical structure provides the mechanical properties of epoxy with the processability of polyesters while bisphenol-A reduces the number of ester bonds present in polyester and eliminates carboxyl and hydroxyl end groups, reducing the polymer's susceptibility to moisture degradation [11,12,13]. Furthermore, the presence of styrene in vinyl-ester reduces the viscosity, allowing for greater processability in the manufacturing of composites, but also increases shrinkage.

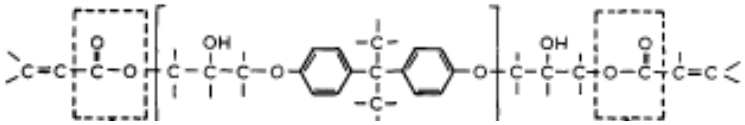

Figure 1. Possible structure of epoxy based bisphenol-A vinyl ester resin [12].

The polar nature of the water molecule enables it to establish hydrogen bonds with hydroxyl groups common on polymer chains, interrupting preexisting inter-chain hydrogen bonds [14-16]. Such modifications in hydrogen bonding between the polymer and water molecule result in plasticization as segmental mobility increases [15,17] and swelling as the inter-chain bond length increases [18,19].

Research indicates that hydrolysis of the ester group is a primary reason for chemical degradation of the polymer structure [8,12]. In the presence of alkaline solutions, the hydrolysis reaction where the ester reacts with hydroxide ions is known as saponification. Hydrolysis of the ester results in the formation of an additional polar hydroxyl group, increasing the number of site available for hydrogen bonding. Ether groups are also susceptible to hydrolysis, whereupon chain scission may occur and additional hydroxyl groups form.

Changes in the chemical structure of polymers with environmental exposure can be detected via spectroscopy, where the relative intensity of characteristic peaks attributed to chemical structures may be monitored as a function of exposure conditions [20-23]. In the case of vinyl-ester resin, the ether C-O band at 1182 cm^{-1} decreases with moisture sorption [20,21], indicating hydrolysis of ether bonds. Similarly, the ester band 1450 cm^{-1}, indicative of C-O stretch and O-H bend, in a vinyl-ester resin decreases with increasing exposure to immersion environments [21,22]. An increase in the O-H stretching band at 3473 cm^{-1} band was observed after exposure to water as hydrolysis increased the population of hydroxyl and carboxylic acid groups [20].

While it is expected that the C=O band at 1740 cm^{-1} would decrease as water hydrolyzes the ester, as is the case for an epoxy system [24], results for vinyl-esters are mixed. Studies on neat vinyl-ester resin exposed to moist environments show no significant difference in C=O and intensity at 1750 cm^{-1} [20,22,23], though one study does demonstrate an initial decrease in C=O band intensity at 1728 cm^{-1}. This band intensity subsequently increases with increasing exposure time, though it does not reach pre-exposure levels after 12,000 hours of exposure to immersion in water at 60°C [22]. It has been suggested that a shift in the C=O 1743 cm^{-1} peak of an epoxy to a lower frequency in the presence of water indicates the formation of hydrogen bonds between the ester and water [25].

Changes in the molecular weight of the polymer matrix may be detected through changes in the rubbery modulus, as detected in dynamic mechanical thermal analysis (DMTA) [27]. Classical rubber elasticity states that the average molecular weight between crosslinks, M_c, can be described via

$$M_c = \frac{3RT\rho}{E'_{rp}}. \tag{1}$$

where E'_{rp} is the rubbery modulus of the pure polymer, R is the gas constant, T is the temperature in Kelvin, and ρ is the density of the pure polymer. Equation 1 has been adapted for composites [24]

$$M_c = \frac{3RT\rho}{E'_{rp}\left(1 - V_f^{1/3}\right)}. \tag{2}$$

The average crosslink density, ρ_c, is calculated as the reciprocal of M_c. The molecular weight calculations should not be taken as an absolute value, despite the acceptable

order of magnitude [24]. Rather, the molecular weights should be taken as a qualitative representation of the changes in chemical structure of the composite matrix due to moisture sorption.

Previous studies on fiber reinforced epoxies reveal that hygrothermal degradation causes in a decrease in rubbery modulus [28], resulting in an increase of molecular weight between crosslinks and a decrease in crosslink density. This decrease in crosslink density indicates that chain scission occurs in the presence of water at elevated temperatures. Increasing styrene content is known to decrease the crosslink density of neat vinyl-ester resins [11,29,30]. Where styrene may leach out into a surrounding environment, the length of crosslinks is not reduced; rather, residual unreacted styrene and homopolymerized styrene are removed. Therefore, it may be expected that leaching of styrene also contributes to decreases in the average crosslink density of vinyl-ester composites.

Polymers typically exhibit a moisture uptake coefficient, β, relating the weight change of the polymer resulting from sorption of a solvent such as water to volumetric changes. The change is volume is used to determine the moisture induced strain, ε, using the moisture uptake, M_t, and a reference moisture uptake, M_o, below which no swelling occurs [8].

$$\varepsilon = \beta(M_t - M_o). \tag{3}$$

As water molecules interrupt inter-chain bonding by establishing water-polymer hydrogen bonds and water clusters, the inter-chain bond distance increases, resulting in dimensional changes of the bulk material [19,31]. In the case of composites, the

moisture uptake coefficient of glass and carbon fibers is much lower than those of typical polymer composite matrices [32]. Thus, the fiber dominated longitudinal direction of unidirectional composites will not experience noticeable swelling, whereas the transverse and through-thickness directions will experience clear dimensional changes with increased moisture uptake.

With these chemical and physical changes, LMWS may be formed due to chain scission of the polymer. When exposed to liquid water, low molecular weight degradation products may have the ability to diffuse out of the polymer matrix, especially at elevated temperatures. Similarly, LMWS residual from the initial polymerization reaction and cure may be driven out at elevated temperatures, resulting in an apparent weight loss of the polymer [33]. In the case of styrene, elevated temperatures may initiate further polymerization. Once all the reaction sites for styrene have been occupied, the residual styrene may then diffuse out of the polymer [33]. Evidence of this phenomenon may be identified through a residual post-cure followed by weight loss and further rise in glass transition temperature. Increases in the glass transition temperature resulting from exposure to hot water immersion have been attributed to leaching of LMWS [34]. Other LMWS diluents and additives which may desorb out are plasticizers, mold release agents, and other crosslinking agents [33,35]. Degradation of the interface, interphase, or glass reinforcement in GFRP can be observed through permanent weight loss not observed in neat resin [36,37], attributed to degradation of the silane coupling agent by some researchers [23].

Increased moisture content results in a plasticizing effect thereby decreasing the glass transition temperature, T_g. Plasticization is largely reversible in that the removal of water will result in a subsequent increase in T_g between the "wet" state and "dry" state [38]. The reversible nature of this process indicates that the presence of water increases the mobility of the polymer resin through a weak interaction [39-41]. An increase in T_g after exposure to water immersion at elevated temperatures has also been attributed to restrictions imposed on the polymer network due to tightly bound water molecules [38,41]. Increasing temperature of exposure is proposed to increase the amount of bound water [38], leading to higher T_g with increasing temperatures of immersion.

This change in polymer structure can sometimes be irreversible when the polymer has undergone chemical or physical aging. Chemical aging occurs as the polymer structure chemically reacts to form an aged polymer species [42,43]. In the case of physical aging, the morphology of the polymer chains adjusts so that the structure approaches thermodynamic equilibrium [42,44]. Residual stresses formed within the polymer network during curing and subsequent cooling may be relaxed toward an equilibrium state during the process of physical aging in an effort to balance a disparate stress state between lower and higher density cross-linked areas [42]. While thermoplastics may exhibit physical aging via crystallization, thermosets primarily exhibit relaxation phenomena due to physical aging. As the polymer ages, the highly cross-linked regions relax toward a nodular center due to contractive forces which develop as a result of cross-linking [42]. In a study of neat epoxy resin,

physical aging resulted in a higher equilibrium moisture content and lower diffusion coefficient [44], as expected when lower density regions physically age to become more dense and, therefore, result in a more tortuous path for penetrating water molecules. While some researchers argue that both aging processes can be observed via an increase in T_g [42], others have observed two regions of aging described as consolidation, where the T_g increases to a maximum with aging time, followed by degradation, where the polymer experiences a subsequent decrease in T_g [43].

Relaxation of the stressed state of the polymer network may occur with moisture ingress, as water molecules interact with polar sites on the polymer network. Water molecules are more likely to form hydrogen bonds with themselves rather than dissimilar polar sites on a polymer, so accumulation of several water molecules at a single polar site may occur with progressive hydrogen bonding, resulting in the formation of water clusters [45-50].

The ingress of moisture will lead to a differential stress state prior to saturation, where the stress distribution depends upon the moisture concentration. Equation 3, describing moisture induced swelling strain, states that there is some threshold moisture content which allows for a transition from compression to tension. With increasing moisture content, the swelling strain becomes more and more compressive. In the case of unidirectional composites, the largest stresses will develop transverse to the reinforcing fiber, where the development of the differential stress state through thickness is of particular interest since the highest stress gradients will develop in the smallest dimension. As moisture ingress occurs, the sum of forces

through the thickness must equal zero, so it is clear that the center of a sorbing species will experience tensile loading, leading to microcracking since polymers tend to be weak in tension [51].

2.1.1.2 Glass Fiber Reinforcement Degradation

Stress corrosion cracking of glass fibers and glass fiber composites is a well known phenomenon. After an induction period required for water to establish a high enough mobility on the glass surface [52], water molecules react with the silicon-oxide bonds near the surface of the glass structure, leading to a weakening of the fiber concurrent with pitting and cracking [52]. It is theorized that the hydrolysis reaction

$$H_2O + \text{Si-O-Si} \rightarrow \text{Si-OH} + \text{HO-Si} \quad (4)$$

occurs during the three step process of adsorption, reaction, and separation [53,54]. Here, adsorption is defined as the weak interaction of the water molecule with the Si-O bond. Definitions of adsorption will be discussed in detail in Section 2.1.2.

The hydrolysis reaction is thought to be partly reversible, where condensation reaction, or hydration, of the metal hydroxyls may reestablish a metal oxide [4,5].

$$\text{Si-OH} + \text{HO-Si} \rightarrow H_2O + \text{Si-O-Si} \quad (5)$$

Hydration of metal oxides concentrated at glass surfaces is thought to be characteristic of water adsorption on glass [52], so it would seem appropriate that heterogeneous non-silica metal-oxygen bonds would have a higher reactivity than the homogeneous silica bulk. Ion exchange reactions may occur when selective leaching of modifier cations are replaced by protons [4,55], resulting in the formation of silanol (-Si-OH) at heterogeneities.

The reaction described in Equation 4 may also occur where the silicon atoms are replaced with alternative metal ions commonly found in multicomponent glasses. These metal oxides make glass fiber intrinsically alkaline, where acidic and neutral water environments have less of an effect than alkaline ones [56]. In a study where the cladding of optical glass fiber was enhanced with metal ions, the rate of degradation varies with metal content as Mg > Al > Al + Zn > Mg + Al + Zn [57], indicating that the addition of metal oxides to glass fiber cladding increases their durability despite their reported ability to participate in ion exchange reactions [4,55]. Another study of zero stress aging of glass fibers revealed that the addition of B_2O_3 or Al_2O_3 reduced the fiber degradation in water environments [58]. The authors also noted that high amounts of modifiers in E-glass fibers are responsible for the higher rate of degradation [58].

The aggravating effect of stress in moist environments on the rate and degree of degradation, or corrosion, of glass fibers, can be observed on the macroscopic scale [59,60], microscopic scale [57], and nanoscale [4,61,62]. There is evidence that chemisorption of water to glass transitions from a thermodynamically unfavorable process to a thermodynamically favorable process with increasing stress [61], whereupon the hydrolytic attack on glass becomes more likely. Furthermore, applied stress increases the reactivity of the silica bonds [54,61]. As the number of bonds within a ring of silica decreases, the bonds become more stressed, and their reactivity increases correspondingly [4].

While liquid water proves to be the most aggressive environment for stress corrosion of silica, water vapor also proves detrimental, where an increased concentration at the surface of the crack results in increased reactivity [59,64]. As degradation progresses, nanoscale voids form within the glass, leading to accelerated transport of water and other species [4]. Surface pitting will occur at high energy sites on the glass surface where silica will preferentially desorb into the surrounding medium [55].

Because of this known susceptibility to hydrolytic attack, it is important to have a protective coating on the fiber reinforcement to minimize exposure to water adsorption. In general, a sizing which enhances interfacial adhesion will lead to decreased glass fiber degradation in moist environment [56].

2.1.1.3 Composite System Degradation

As water diffuses into the composites, stress gradients form at the macroscopic level and at the interfacial level. While the surface layers with higher water concentration develop compressive moisture stresses, the inner layers consequently develop tensile stresses in order to balance the stress state in the bulk material to zero [65]. These tensile stresses can lead to microcracking of the polymer composite and have been observed to be localized around voids in resin rich areas [3]. These microcracks consequently traverse through the resin to interfaces, where interfacial debonding may initiate. It has been argued that moisture induced compressive stresses may actually lead to relaxation of residual tensile stresses from the thermal gradient

established during high temperature curing, leading to an increase in strength [3] prior to moisture induced resin and interfacial degradation.

The disparate stress state developed with the local fiber-interphase-matrix region will nonetheless impose tensile forces on the fiber and compressive stresses on the matrix [66,67]. Depending on the loading conditions and material parameters, the interphase could develop a tensile or compressive stress [67], resulting in a high internal stress gradient. The combined effects of microcracking, high interfacial stress state, and hydrolytic attack on the silane coupling bonds reveal the serious susceptibility of the interphasial region and severe need for coatings which can withstand hygrothermal exposure.

It is often observed that the diffusion coefficient along the length of the fibers is higher than in the transverse direction [68,69]. A higher longitudinal diffusion coefficient is expected when interfacial debonding occurs since uptake of water through capillary action is effectively instantaneous [51]. Others assume that this elevated diffusion coefficient is a consequence of an elevated rate of sorption along the interphase [5], where polymer characteristics tend to vary from the bulk resin due to the resin's interaction with the fiber and sizing [5,70]. It has been observed that the presence of a glass filler in a polymer matrix results in an increased equilibrium moisture content in the resin matrix as compared to the neat resin [71-73], possibly due to preferential moisture sorption in the interphasial region [74]. Increasing glass filler content has also been observed to decrease the equilibrium moisture content [75], even when adjusted for fiber volume content. Glass filler is generally considered to

have low a low diffusion coefficient and maximum moisture content and, consequently, acts as a diffusion barrier. Therefore, the presence of glass filler will result in lower composite diffusion coefficients and maximum moisture contents. The effects of fiber reinforcement on the composite diffusion coefficient are addressed in detail in Section 2.4.1.1.

When interfacial debonding occurs, the fiber reinforcement becomes susceptible to hydrolytic attack. In the case of carbon fiber reinforced polymers, this debonding leads to a loss in strength directly related to the loss of interfacial adhesion. However, the presence of water along a glass fiber interface will inevitably lead to fiber degradation. Irreversible degradation can be observed through gravimetric measurements of GFRP which has been exposed to hydrolytic attack and subsequently redried, removing water and any degraded species [36,37,72].

The combination of physical and chemical degradation may weaken the polymer at the surface of the composite, leading to surface erosion [76-79]. Simple microvoid formation may even lead to blistering of the polymer prior to surface erosion. Evidence of this behavior can be seen in Figure 2. Blistering of structural composites may occur when cracking occurs within the polymer, creating macrovoids in which water accumulates. With surface erosion and cracking, the fiber reinforcement is subsequently attacked, and the whole process is aggravated.

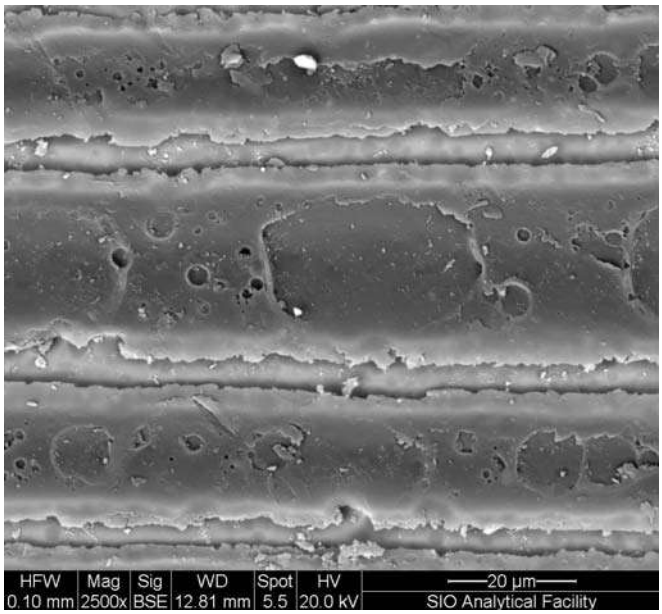

Figure 2. Surface degradation of E-glass/vinyl-ester.
Exposed to 80°C deionized water for 24 weeks.

2.1.2 Definitions of Moisture Transport

The gain and loss of a fluid in a diffusing medium may occur via absorption, adsorption, or desorption. Sorption is a general term used for all these transport mechanisms and is commonly used when the specific mechanism of sorption cannot be identified or isolated. A summary of major points follows below. For a detailed discussion on sorption phenomena, the reader should refer to references [80-83].

Absorption is a physical phenomenon whereby a liquid or vapor *outside* a solid, defined as the *sorbate*, enters into the bulk *solid*, defined as the *sorbent*, from the bulk fluid sorbate [84]. Adsorption occurs when a liquid or vapor outside the solid attaches to the surface of the bulk solid, resulting in an adsorbed phase which is no longer part of the bulk fluid. Physisorption and chemisorption commonly fall under

the umbrella of adsorption, wherein physisorption refers to a weak interaction with the surface and chemisorption considers a strong interaction, similar to chemical bonding [84,85]. Adsorption will not result in physical changes, such as plasticization or swelling [86], which are often seen in material which has absorbed water.

Adsorption is primarily responsible for the uptake of vapors into porous species but is also used to describe vapor sorption by foodstuffs [87,88] and adsorption of fluids to the surfaces of nonporous solids [89]. The adsorbed molecules must be large enough to penetrate the pores as they adsorb to the pore walls [90]. Capillary condensation occurs as the uptake of penetrant continues to increase. Diffusion may sometimes refer to sorption by a porous solid. When fiber/matrix interfaces degrade, wicking along this interface may occur through capillary action, introducing an adsorbed layer of water on surfaces within the bulk composite.

Diffusion of moisture into polymer composites is generally considered an absorption process. However, some diffusion models (i.e., Langmuir diffusion [91,92]) can allow for the physical binding of the water molecules, having entered the bulk material, to the polymer chain. The water molecule may adsorb to the polymer structure in this case, similar to how water may adsorb to a glass or polymer surface.

Desorption describes the loss of penetrant from the solid into the bulk fluid. Desorption can be detected and monitored through negative changes in weight, indicating weight loss, in order to complement positive values for uptake. That is, the concentration of the bulk liquid or gas is lower than the concentration within or on the surface of the solid. For a particular mode of adsorption or absorption, the same

mechanism is assumed to be responsible for the loss of sorbate, thus the same models are employed for uptake and loss of a fluid. However, it should be noted that it is difficult to conclude that the desorption process is a complete reversal of the adsorption or absorption process. Studies show that sorption is not, in fact, a completely reversible process and that the diffusion coefficients, though generally assumed to be a single value for each temperature, may not be identical between uptake and loss of a sorbate [2,26,48,93,94].

Having defined the varying types of sorption, the term "uptake" should be interpreted with care. Moisture "uptake" is sometimes erroneously used when referring to negative desorption weight change values for the sake of simplicity.

2.1.3 States of Water Within a Polymer Network

As water molecules enter a bulk polymer sorbent, those water molecules may exist in two states: free water and bound water [48,92]. Free water is proposed to exist in the free volume of the polymer system while bound water interacts strongly with the polymer network through weak hydrogen bonds [19]. Bound water is assumed to be responsible for swelling by increasing interchain hydrogen bond length as free water travels through pre-existing free volume voids [14,19].

Free volume theory [95] asserts that for a fluid, there is a net available volume between molecules which increases with temperature from an initial value of zero at absolute zero. Subsequent applications of free volume theory to viscoeslastic polymers assume that the viscosity and, consequently, the stiffness of the material are dependent upon the amount of free volume in the material [96]. The presence of a

diluent such as water in a polymer should thereby increase the total free volume of the total system and enhance the mobility of the polymer network [97].

2.2 Immersion vs. Humidity

The saturated state of water vapor, where the vapor pressure e equals the saturation pressure e_s, is thermodynamically distinct from liquid water in that two independent phases of one molecule can exist with equal chemical potentials at equilibrium. Previous studies on composites assume that 100%RH is equivalent to immersion in water in order to obtain isotherms for the material [98,99].

Shroeder's Paradox [100] refers to the discrepancy observed between the fully saturated moisture content of a material after exposure to saturated vapor conditions and immersion in liquid water at a single temperature. Explanations for this paradox vary depending on the material in question. Nafion films are a prominent example for Shroeder's paradox, and previous discussions have justified the behavior with capillary condensation in an assumed porous layer on the Nafion surface [101], as an artifact of measurement techniques [102], or by suggesting there could be multiple solutions to a thermodynamic equation [103].

In the case of water penetration into rubber, it has been theorized that a pressure gradient approaching the surface between liquid and water is responsible for the discrepancy between exposure to saturated vapor and liquid water [93]. An early study on the treatment of rubber suggested that rubber immersed in a water solution will absorb more than that suspended in a saturated vapor above the solution since the rubber will drive to achieve infinite dilution in liquid water [6].

Studies of glass/epoxy composites have noted lower moisture uptake in saturated steam environments when compared to immersion in water at the same temperature [104,105]. Conversely, an investigation of a carbon/epoxy system concluded with a higher moisture uptake in the 95%RH environment than in immersion in water at the same temperature [106].

While LMWS may desorb into humid air, immersion in liquid water allows for leaching of LMWS to form a solution with the bulk liquid. It is also possible for potential leachates to diffuse out of the bulk composite into water droplets formed on the surface in saturated steam environments, leading to higher concentration autocatalytic degradation environments than may occur in immersion environments. Furthermore, as interfacial debonding propagates along a fiber from a transverse surface, capillary avenues form, allowing for the adsorption of water along this interface. Distinct behavior between adsorption of liquid water and water vapor along this capillary interface could represent the work addressing capillary avenues within Nafion films [101].

2.3 A Review on Humidity

In order to fully understand the sorption phenomena of polymer composites exposed to humid environments, it is important to review fundamental definitions employed when considering humidity. Relative humidity (%RH) is the most popular form of reporting humidity values in the atmosphere, but a single relative humidity may represent two drastically different environments at two different temperatures, where the higher temperature moist air has an exponentially greater amount of water

in the air. Despite a strong thermal dependency of the water content in air, isotherms developed by the adsorption community reveal that the relative pressure (or relative humidity, in the case of water vapor) dictates the amount of vapor sorbed by a sorbent [47]. Furthermore, when considering the uptake of moisture in humid environments for design purposes, the abundance of relative humidity data in historical weather records is undeniable.

2.3.1 Definition of Relative Humidity

Relative humidity provides a ratio of the actual amount of water in the air, expressed as a partial pressure e, to the maximum possible amount of water in the air at the same temperature, referred to as the saturation pressure e_s,

$$\%RH = \frac{e}{e_s(T)} \times 100\% . \tag{6}$$

The partial pressure of water in a mixed air environment is experimentally determined while the saturation pressure is determined from available steam tables.

Goff and Gratch [107] determined the expression used in the Smithsonian steam tables which serves as the standard against which all models are compared.

$$\log_{10}\left[e_s(T)\right] = a_0\left(\frac{T_s}{T} - 1\right) + a_1 \log_{10}\left(\frac{T_s}{T}\right) + a_2\left[10^{\,b_0\left(1-\frac{T}{T_s}\right)} - 1\right] + a_3\left[10^{\,b_1\left(\frac{T_s}{T}-1\right)} - 1\right]. \tag{7}$$

$a_0 =$ - 7.90298
$a_1 =$ 5.02808
$a_2 =$ -1.3816×10^{-7}
$a_3 =$ 8.1328×10^{-3}
$b_0 =$ 11.344
$b_1 =$ - 3.49149

where T_s is defined as 373.16 Kelvin, e_s is given in atmospheres, and T is temperature in Kelvin. With the data available in 1946, Goff and Gratch claim $\log_{10} e_s$ in Equation 7 to have an uncertainty of 0.02% and is valid in the range of 0°C to 100°C [107].

The expression developed by Wexler [108] is considered the most accurate to date:

$$\ln\left[e_s(T)\right] = \sum_{i=0}^{6} a_i T^{i-2} + a_7 \ln T \,. \tag{8}$$

$$\begin{aligned} a_0 &= -2.99122729 \times 10^{3} \\ a_1 &= -6.0170128 \times 10^{3} \\ a_2 &= 18.87643854 \\ a_3 &= -0.028354721 \\ a_4 &= 1.7838301 \times 10^{-5} \\ a_5 &= -8.4150417 \times 10^{-10} \\ a_6 &= 4.4412543 \times 10^{-13} \\ a_7 &= 2.858487 \end{aligned}$$

where e_s is given in Pascals, T is temperature in Kelvin based upon the International Practical Temperature Scale of 1968 (IPTS-68). With the data available in 1976, Wexler claimed in Equation 8 are valid for the range of 0°C to 100°C and claims accuracy within 0.907% [108].

The Magnus formula provides a simple expression which tends to fit experimental data with good accuracy.

$$e_s(T) = a \exp\left[\frac{bT}{c+T}\right]. \tag{9}$$

$$\begin{aligned} a &= 6.1121 \\ b &= 17.123 \\ c &= 234.95 \end{aligned}$$

where e_s is given in millibars, T is temperature in degrees Celsius. Coefficients provided in Equation 9 result in uncertainties within 0.15% and are valid over the range of 0°C to 100°C [109].

Equations 7 through 9 are the three most commonly used expressions for the saturation pressure of water vapor over the temperature range 0°C to 100°C. Alternative expressions for $e_s(T)$ are provided in [110-115]. The above equations do not account for large variations to extreme temperatures and pressures and assume that water vapor is isolated rather than present in a water-air mixture. Buck recommends enhancement factors for the conversion of pure water vapor pressure to the vapor pressure of water vapor in a mixture such as air [109]. If e_s is the saturation vapor pressure of pure water and e_s' is the saturation vapor pressure of moist air at some ambient temperature T and pressure P, then the enhancement factor, $f(T,P)$ can be defined as

$$e_s' = f(T,P) \cdot e_s . \tag{10}$$

where Buck [109] provides the enhancement factor as

$$f(T,P) = 1 + a_0 + P\left(a_1 + a_2\left(T + a_3 + a_4 P\right)^2\right). \tag{11}$$

$$\begin{aligned} a_0 &= 4.1 \times 10^{-4} \\ a_1 &= 3.48 \times 10^{-6} \\ a_2 &= 7.4 \times 10^{-10} \\ a_3 &= 30.6 \\ a_4 &= -3.8 \times 10^{-2} \end{aligned}$$

where T is in Celsius and P is in millibars and f will always be greater than 1.

This correction is a weak function of temperature and pressure, so, at standard pressures around sea level, the correction is, at most, around 0.5% ($f(T,P) \approx 1.005$) for

atmospheric temperatures through 100°C [109,110,116], translating to corrections in relative humidity calculations of about 0.4%RH [116]. Most available equations claim to be within a percent accuracy less than the uncertainty inherent in experimental observations of the saturation vapor pressure of pure water [110]. It is thus recommended that, with a maximum accuracy of ± 1.5%RH on modern relative humidity sensors, the Magnus formula provided in Equation 9 should be used void of enhancement factor for the calculation of relative humidity [116].

2.3.2 Definition of Absolute Humidity

Absolute humidity is used to express the density of water vapor in a moist air mixture and can be derived from basic principles [117]. The absolute humidity, d_v, is fundamentally defined as

$$d_v = \frac{m_v}{V}, \tag{12}$$

with m_v as the mass of water vapor in a volume V. If e is the partial pressure of the water vapor, n_v the moles of water vapor, and M_v the molecular weight of water, then the ideal gas law implies

$$d_v = \frac{m_v}{n_v RT/e} = \frac{m_v e}{\frac{m_v}{M_v} RT} = \frac{eM_v}{RT}. \tag{13}$$

Then

$$d_v = \left(217 \frac{\mathrm{g \cdot K}}{\mathrm{m^3 \cdot mb}}\right) \frac{e}{T}. \tag{14}$$

At 20°C, in a pure water vapor environment, a relative humidity of 18%RH correlates to an absolute humidity of about 3 g/m^3, whereas a relative humidity of 99%RH at 80°C correlates to an absolute humidity of about 290 g/m^3.

2.3.3 Dew Point Temperature

The dew point temperature, T_d, is defined as the temperature at which a given ambient pressure would be equal to the saturation pressure for water vapor. Calculation involves determining the inverse of Equations 7, 8, or 9 such that $e_s(T)$ becomes $T_d(e)$. The complex nature of these expressions require that T_d be determined numerically and, so for the sake of simplicity, it is recommended [118] that the inverse of the Mangus formula provided in Equation 9 [109] be used for determination of $T_d(e)$

$$T_d(e) = \frac{c \ln \frac{e}{a}}{b - \ln \frac{e}{a}}. \tag{15}$$

$a =$ 6.1121
$b =$ 17.123
$c =$ 234.95

2.4 Diffusion

Fick's laws provide a theoretical basis for the diffusion of a fluid into a distinct sorbing medium from a higher concentration to a lower concentration. Fick's second law provides for non-steady-state diffusion, where a concentration profile can be investigated via

$$\frac{\partial C}{\partial t} = \nabla \bullet \left[D\left(\vec{\nabla} C\right) \right] \tag{16}$$

where C is the concentration of the sorbate, t is time, and D is the diffusion coefficient. The diffusion coefficient is thus described in units of area per time, describing the rate of diffusion into or out of a sorbent medium.

2.4.1 Major Considerations in Diffusion

Fick's laws most fundamentally require a diffusion coefficient to describe the rate of diffusion and generally require the attainment of an equilibrium content where the rate of uptake slows to zero as equilibrium is approached. These parameters can be affected and described by material characteristics, geometry, processing factors, and even environmental exposures.

2.4.1.1 Diffusion Coefficient

To simplify Equation 16, the diffusion coefficient can be assumed to be independent of concentration and time. Solutions exist for concentration and time dependent diffusion coefficients and are available in [83]. While Fick's second law fundamentally assumes that diffusion into and out of the sorbent are equivalently described by the same diffusion coefficient, this assumption has often been proven invalid [2,26,48,93,94,119,120].

The diffusion coefficient can be determined either by monitoring the concentration profile throughout the volume [121] or via gravimetric measurements. Simple geometries with known solutions to Equation 16 are highly desirable for both methodologies. Tracking the spatial concentration profile over time requires the

destruction of material for each time step. Gravimetric measurements require the weighing of a specimen with known geometry for each time step, allowing for the diffusion of the sorbate into a single sorbent specimen to be monitored over time and providing the total weight change due to uptake or loss of the sorbate rather than a concentration. Ultimately, however, the diffusion coefficient must be calculated according to a theoretical model used to fit experimental data trends.

The thermal dependency of the diffusion coefficient, discussed below, is well known. Numerous studies exist concerning the variability of diffusion coefficient with polymer type [33,35], crosslink density [122], degree of cure [120,123,124], filler type [50,125], and filler amount [75,72,126]. For a multi-phase sorbent such as a filled polymer, the apparent diffusion of the sorbate will depend on the diffusion coefficients of the multiple phases. While a time dependent diffusion coefficient may be considered [119,127], the change in D is more than likely dependent upon a progressing concentration, stress, or reaction front.

2.4.1.1.1 Thermal Dependency of Diffusion Coefficient

It is well known that D is dependent upon temperature and can be described by the Arrhenius relationship

$$D = D_o \exp\left[\frac{-E_a}{RT}\right]. \tag{17}$$

where D_o is the temperature independent empirical constant; E_a, the activation energy; R, the universal gas constant; and T is temperature in Kelvin. The Arrhenius relation can be employed for the thermal dependence of D for any diffusion model, where D_o

and E_a are determined for each model. In the case where an Arrhenius plot of ln$D$ vs. $1/T$ does not result in a linear trend representative of Equation 17, a dual Arrhenius model [128] may be employed where

$$D = D_{o1} \exp\left[\frac{-E_{a1}}{RT}\right] + D_{o2} \exp\left[\frac{-E_{a2}}{RT}\right], \tag{18}$$

where D_{o1}, D_{o2}, E_{a1}, and E_{a2}, are the empirical diffusion coefficients and activations energies of the first and second phases, respectively.

2.4.1.1.2 Geometrical Considerations in Diffusion

For anisotropic substances, the diffusion along the three principal axes will not be identical to that of an isotropic substance with the same geometry. Fick's second law, Equation 16, can be expressed in Cartesian coordinates for an anisotropic substance with diffusion coefficients D_x, D_y, and D_z along the global x, y, and z directions [82]

$$\frac{\partial C}{\partial t} = D_x \frac{\partial^2 C}{\partial x^2} + D_y \frac{\partial^2 C}{\partial y^2} + D_z \frac{\partial^2 C}{\partial z^2}, \tag{19}$$

assuming time and concentration independent diffusion coefficients. Based on heat transfer studies [129], an effective diffusion coefficient can be introduced where

$$\frac{\partial C}{\partial t} = D\left(\frac{\partial^2 C}{\partial \varepsilon^2} + \frac{\partial^2 C}{\partial \eta^2} + \frac{\partial^2 C}{\partial \zeta^2}\right) \tag{20}$$

$$\text{for } \varepsilon = x\sqrt{\frac{D}{D_x}},\ \eta = y\sqrt{\frac{D}{D_y}}, \text{ and } \zeta = z\sqrt{\frac{D}{D_z}}.$$

In the case of non-steady state diffusion into a thin plate with dimensions l, w, and h in the x, y, and z directions, where h is much less than l or w, it can be concluded that [82]

$$\frac{l}{w} = \sqrt{\frac{D_x}{D_y}} \tag{21}$$

since a fundamental assumption of diffusion into a thin plate assumes that diffusion through the six faces do not interfere with one another. A complementary derivation of the effective anisotropic diffusion coefficient D is provided concluding that for a thin plate [98],

$$\frac{\sqrt{D}}{h} = \frac{\sqrt{D_x}}{l} + \frac{\sqrt{D_y}}{w} + \frac{\sqrt{D_z}}{h}. \tag{22}$$

where D_x, D_y, and D_z are dependent upon the orientation of the anisotropic media under consideration.

For an orthorhombic system, as is the case for unidirectional composite laminae, there are three principal diffusivities, D_1, D_2, and D_3, where D_1 is along the fiber axis, D_2 is transverse across the width of the composite, and D_3 is the through thickness diffusivity. Then, after Carslaw and Jaeger [129], the principal diffusivities can be determined by translating from global x-y-z coordinates to local 1-2-3 coordinates, given a fiber orientation described by angles α, β, and γ between the 1 axis and the x, y, and z axes, respectively. In composites, where through thickness properties are very similar to transverse properties across the width, it can be assumed $D_2 = D_3$ [98,129],

$$D_x = D_1 \cos^2 \alpha + D_2 \sin^2 \alpha ,$$

$$D_y = D_1 \cos^2 \beta + D_2 \sin^2 \beta , \tag{23}$$

$$D_z = D_1 \cos^2 \gamma + D_2 \sin^2 \gamma .$$

Shen and Springer proposed a calculation for a composite diffusion coefficient based upon derivations of thermal conductivities [98] given the diffusivities of the resin and fibers, D_r and D_f in a composite with a fiber volume fraction of V_f:

$$D_1 = (1 - V_f) D_r + V_f D_f \tag{24.a}$$

$$D_2 = \left(1 - 2\sqrt{\frac{V_f}{\pi}}\right) D_r + \frac{D_r}{B_D}\left[\pi - \frac{4}{\sqrt{1 - B_D^2 V_f / \pi}} \tan^{-1}\left(\frac{\sqrt{1 - B_D^2 V_f / \pi}}{1 + \sqrt{B_D^2 V_f / \pi}}\right)\right] \tag{24.b}$$

where

$$B_D = 2\left(\frac{D_r}{D_f} - 1\right) \tag{25}$$

For composites where the diffusivity of the fiber is much less than that of the resin, as is often the case in polymer composites, Equation 24 can be reduced for $V_f > 0.785$ to

$$D_1 \cong (1 - V_f) D_r \tag{26.a}$$

$$D_2 \cong \left(1 - 2\sqrt{\frac{V_f}{\pi}}\right) D_r . \tag{26.b}$$

Consequently, Equation 22 can be restated as

$$\frac{\sqrt{D}}{h\sqrt{D_r}} = \frac{\sqrt{1 - V_f \cos^2 \alpha + 2\sqrt{\frac{V_f}{\pi}} \sin^2 \alpha}}{l} + \frac{\sqrt{1 - V_f \cos^2 \beta + 2\sqrt{\frac{V_f}{\pi}} \sin^2 \beta}}{w} + \frac{\sqrt{1 - V_f \cos^2 \gamma + 2\sqrt{\frac{V_f}{\pi}} \sin^2 \gamma}}{h} . \tag{27}$$

For a unidirectional composite with fiber volume greater than 78.5%, the following approximation can be made by reducing Equation 27

$$D \cong D_r h^2 \left[\frac{\sqrt{1-2\sqrt{V_f/\pi}}}{h} + \frac{\sqrt{1-V_f}}{l} + \frac{\sqrt{1-2\sqrt{V_f/\pi}}}{w} \right]^2 \tag{28}$$

While these statements are theoretically available for $V_f > 0.785$, it is important to note that V_f are generally lower than 0.785. Theoretical fiber volume fractions can be calculated as 78.5% for square packing of circular fibers up to 90.7% for hexagonal packing of circular fibers [32]. Unavoidable manufacturing inconsistencies involving fiber alignment, full fiber wet out, and the addition of fillers and fiber sizings or coatings result in V_f typically less than 78.5%.

2.4.1.2 Equilibrium Moisture Content

Isotherms are used to express the maximum moisture content of a sorbing substance as a function of partial pressure [47,81]. Isotherms were developed with adsorption theory [47,81]; and while some have an empirical origin, most have a theoretical basis based upon the adsorption of molecules to a surface. Thermal dependency of maximum moisture content can be introduced through thermal dependency of isotherm coefficients through the implementation of isosteres [84]. While the theoretical bases for isotherms are no longer valid when considering absorption along with adsorption, the availability of these relations allows for immediate implementation of known phenomena.

A series of stylized isotherms are presented in Figure 3. The following is a discussion on isotherms commonly used in the study of moisture sorption of composites. A thorough set of data across relative pressures is hard to find, but available studies indicate that the equilibrium moisture content does not plateau at high relative pressures. Rather, the isotherms may represent curves (a), (c), or (d) in Figure 3. While Langmuir adsorption theory provides a strong foundation for the adsorption field, it will not be addressed here since composites clearly do not experience Langmuir adsorption, described by curve (b) in Figure 3.

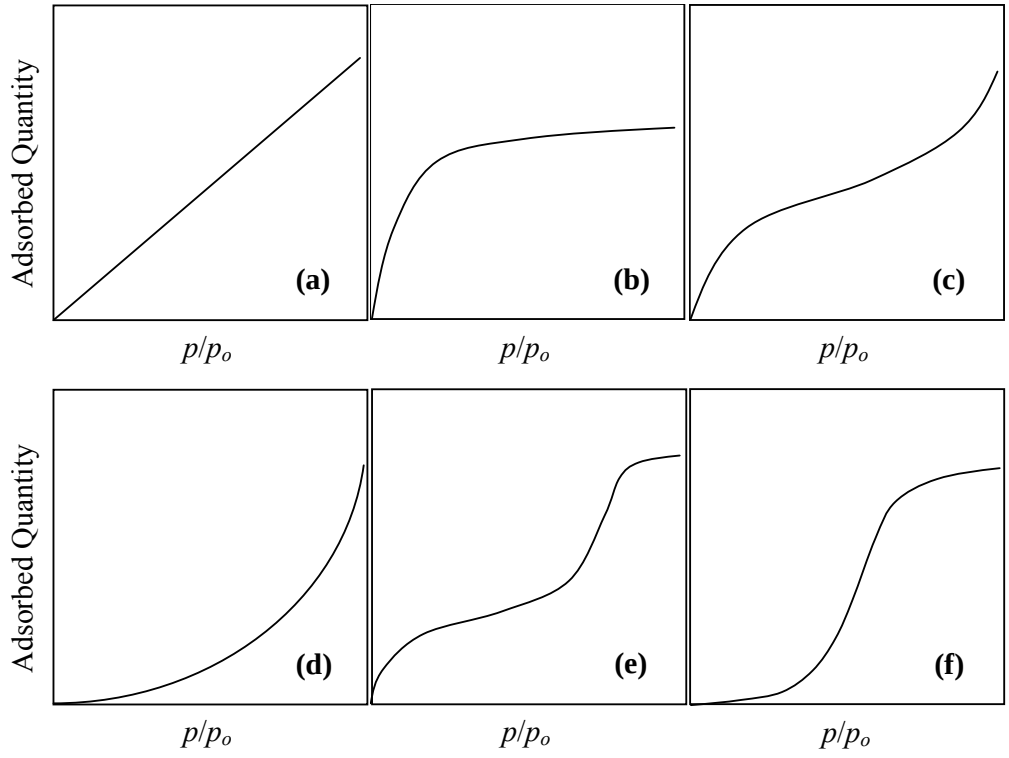

Figure 3. Stylized Isotherms [47,130].
(a) Henry's Law; (b) Langmuir [Brunauer-Emmett-Teller (BET) Type I]; (c) BET Type II; (d) BET Type III; (e) BET Type IV; (f) BET Type V. Partial pressure (p/p_o) is described in terms of vapor pressure p and saturation pressure p_o.

2.4.1.2.1 Henry's Law

At the most fundamental level, it is generally assumed that the amount of sorbate sorbed is directly proportional to the partial pressure which describes the amount of sorbate in the air. In terms of equilibrium moisture content, Henry's Law states

$$M_{\infty} = k(\%RH). \tag{29}$$

where k is known as Henry's Law constant. While the more flexible Freundlich's relation is often implemented in the composites field, results indicate that materials sometimes obey Henry's Law [105,131].

2.4.1.2.2 Freundlich's Relation

Freundlich's relation provides a simple exponential relation using empirical constants a and b:

$$M_{\infty} = a(\%RH)^{b}. \tag{30}$$

For gases, Freundlich's relation can be derived at small vapor pressures using Gibb's equation [133]

$$\Gamma = \frac{-c}{RT} \cdot \frac{d\gamma}{dc}, \tag{31}$$

where Γ is the amount of adsorbed material; c, the surface-active component in solution; R, universal gas constant; T, temperature in Kelvin; and γ, interfacial surface energy.

For a gas, it was proposed [133] that the surface tension of a surface, σ, can be described via the rule of mixtures using the surface tension of the bare surface, σ_0; the

surface tension of the same surface with an adsorbed monomolecular layer, σ_1; and the fraction of surface area with an adsorbed monomolecular layer, θ.

$$\sigma = \sigma_0(1-\theta) + \sigma_1\theta\,, \tag{32}$$

where the adsorbed fraction can be described using the adsorbed quantity using the number of potential locales for adhesion of sorbate (e.g., available oriented surface molecules) [133], N, and the number of vacant adjacent potential adhesion sites, a:

$$\theta = \frac{\Gamma N}{aN_a}\,, \tag{33}$$

where N_A is Avagadro's number. Assuming the interfacial surface tension is equivalent to surface energy, combining Equations 31, 32 and 33 and integrating Equation 31 for c [133] the concentration of the surface-active component in solution,

$$c = K_0\Gamma^{\frac{(\sigma_0-\sigma_1)aN_A}{RTN}}\,, \tag{34}$$

where K_0 is introduced as an integration constant.

While this derivation was executed assuming small concentrations of adsorbate, one can extend the relation for a range of concentrations or partial pressures. Rearranging Equation 34 considering relative humidity $\%RH$ in place of sorbate concentration and equilibrium moisture content M_∞ in place of Γ,

$$M_\infty = K_1(\%RH)^{\frac{RTN}{(\sigma_0-\sigma_1)aN_A}}\,, \tag{35}$$

where the integration constant K_1 and the exponent are analogous to a and b in Equation 30.

Freundlich's equation is widely used in polymer composite research, assuming immersion in liquid water is equivalent to 100%RH, even though the statement is derived for the adsorption of a monomolecular layer. Reported values of *b* for polymer composites range from 1.0 to 4.3 [50,99,105,131,134], despite the observation in the theoretical derivation of Equation 34 that *b* should be less than 1 [133]. That is, where Freundlich's Relation should theoretically represent BET Type I curve, sorption in composites results in a BET Type III isotherm.

2.4.1.2.3 Dual Sorption Theory

Dual Sorption Theory [135,136] accounts for positive deviations from Henry's law by incorporating Langmuir sorption with Henry's Law generally via

$$M_\infty = k(\%RH) + \frac{c(\%RH)}{1 + d(\%RH)}. \tag{36}$$

where *k*, *c*, and *d* can be defined in terms of Henry's law dissolution constant, k_D; the hole affinity constant, *b*; the hole saturation constant, C_H', and the saturation vapor pressure, p_o:

$$\begin{aligned} k &= k_D p_o, \\ c &= C_H' b p_o, \\ d &= b p_o. \end{aligned} \tag{37}$$

Fundamentally, Dual Sorption Theory is based upon the assumption that water enters the sorbent as free water through normal diffusion processes, obeying Henry's Law, but may then become immobilized as bound water at points within the microheterogeneous medium, whereby its equilibrium is described by the Langmuir

isotherm [136]. Additional assumptions are made when considering the kinetic element of Dual Sorption Theory, commonly known as Langmuir diffusion, to be discussed in Section 2.4.2.3.

Equation 36 represents a BET Type II isotherm, seen in Figure 3(c). At sufficiently high and low pressures, the dual sorption isotherm reduces to a linear form where the two linear sections at high and low relative pressures, connected by a nonlinear region, are described by two characteristic slopes. Thermal considerations may be incorporated by using the Arrhenius equation to obtain an enthalpy of dissolution for k_D and an enthalpy of hole filling (a term used to refer to immobilization of sorbate) for b [136].

2.4.1.3 Typical Moisture Sorption Uptake Trends

Dynamic moisture uptake curves, plotted as moisture content as a function of time M_t against $t^{1/2}$, may be as simple as the characteristic Fickian trend, depicted in Figure 4(a), where the initial uptake is linear up to about $0.6M_t/M_\infty$ and concave toward the abscissa as M_t asymptotically approaches the system's equilibrium content, M_∞. Non-Fickian sorption may manifest itself with an initial sigmoidal uptake, two stage phenomena, or other anomalous characteristics as in Figure 4.

Sorption trends which initially demonstrated sorbate uptake may ultimately decrease after a maximum uptake has been reached, such in Figure 4(e), indicating loss of sorbent. It is recommended that when sorption trends indicate degradation, attempts should be made to remove as much sorbate as possible at each measurement in order to identify the amount of material loss experience by the sorbent. Curves with

sudden uptakes after an apparent equilibrium, such as that in Figure 4(f), indicate sorbent breakdown, such as interfacial wicking in composites, which leads to dramatic increases in moisture content.

In the end, several fundamental assumptions must be made about the moisture uptake curves. First and foremost, it is assumed that an increase in weight represents an increase of sorbate population in the sorbent. When sorbate is removed to back-calculate true weight gain after degradation, the weight loss represents the removal of all sorbate and no sorbent. That is, if LMWS are leached into the exposure environment, it is assumed that no further LMWS are leached into the desorption environment. While every attempt is made to purify sorbing species prior to sorbate immersion, it is inevitable that impurities will be present. It is further assumed that impurities, such as metals or salts in solution, do not diffuse into the sorbent. Previous research shows that solutions with ions known to be in solution do absorb into the specimen, though the modes of transport are distinct from that of water molecules [20].

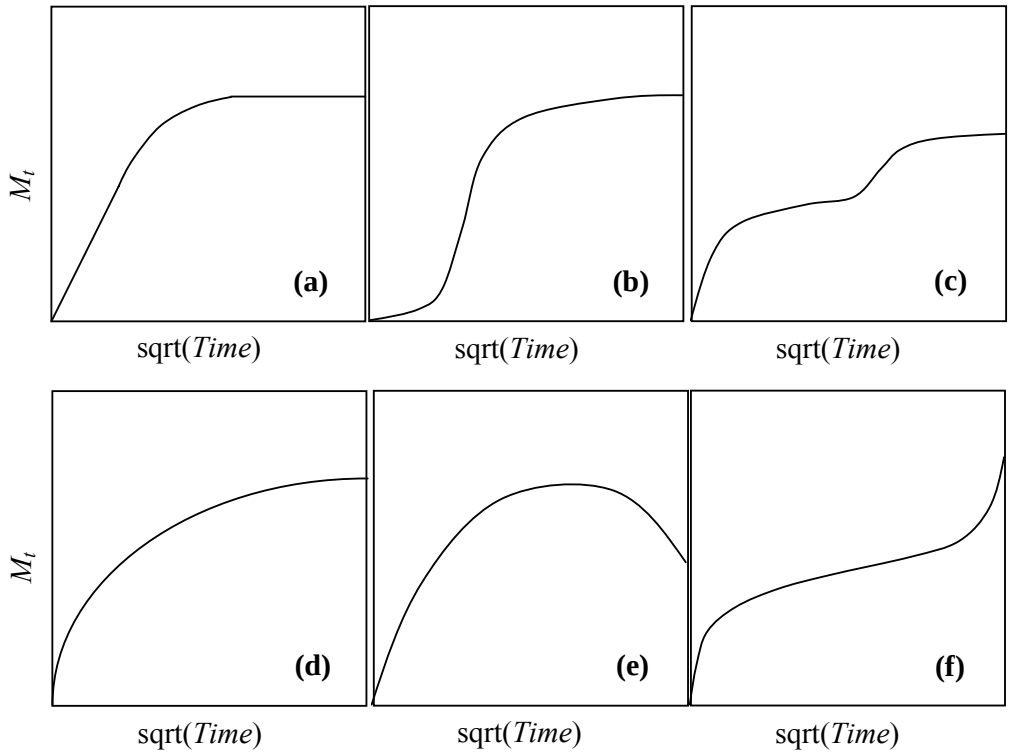

Figure 4. Stylized typical moisture uptake trends after [137].
(a) Fickian; (b), sigmoidal; (c) Two-stage; (d) anomalous;
(e) and (f) trends indicative of degradation.

2.4.2 Diffusion Models

2.4.2.1 Fickian Diffusion Model

2.4.2.1.1 Theoretical Basis for Fickian Diffusion

Fickian diffusion in composites is traditionally treated by considering the one-dimensional case of Fick's second law assuming the diffusion coefficient is concentration independent such that Equation 16 reduces to

$$\frac{\partial C}{\partial t} = D\frac{\partial^2 C}{\partial x^2}. \tag{38}$$

where C is concentration of sorbate per unit sorbent, t is time, x is the distance through the sorbate, and D is the Fickian diffusion coefficient. Fick's laws were developed with fundamental heat transfer equations in mind and, as such, solutions to the plane sheet case are well known [83,129]. In the case of a uniform initial distribution of sorbent, C_0, within a plane sheet with the surfaces kept at a constant concentration, C_1, the concentration distribution, $C(x,t)$, through the thickness of the plate, x, from $-h/2$ to $+h/2$ for a plate thickness h over time, t, is

$$\frac{C(x,t)-C_0}{C_1-C_0}=1-\frac{4}{\pi^2}\sum_{n=0}^{\infty}\frac{(-1)^n}{(2n+1)^2}\exp\left[-\frac{Dt}{h^2}\pi^2(2n+1)^2\right]\cos\left[\frac{(2n+1)\pi x}{h}\right]. \tag{39}$$

for a diffusion coefficient independent of time and position. The total weight change of the substance over time, M_t, is described by integrating $C(x,t)$ over the thickness x from $-h/2$ to $+h/2$ such that

$$M_t=M_\infty\cdot\left\{1-\frac{8}{\pi^2}\sum_{n=0}^{\infty}\frac{1}{(2n+1)^2}\exp\left[-\frac{Dt}{h^2}\pi^2(2n+1)^2\right]\right\}. \tag{40}$$

It is fundamentally assumed that the diffusion mechanisms responsible for diffusion into and out of a material are identical. That is, absorption and desorption diffusion coefficients and sorption trends should be identical, save for the initial and final equilibrium moisture contents. However, this assumption has repeatedly been shown to be invalid when desorption trends do not replicate absorption trends [2,26,48,93,94,119]. An explanation for this discrepancy could be that the sorption process is two phase, where there is some bound water which cannot be removed in the desorption process.

2.4.2.1.2 Treatment of Fickian Diffusion Model

While Crank [83] provided the short time approximation for Equation 40 as

$$M_t = M_\infty \cdot \frac{4\sqrt{Dt}}{h} \cdot \left\{ \frac{1}{\sqrt{\pi}} + 2\sum_{n=1}^{\infty} (-1)^n \, \text{ierfc} \frac{2\sqrt{Dt}}{nh} \right\}, \tag{41}$$

he also suggests that Equation 41 can be approximated as

$$M_t = \frac{4M_\infty}{h} \cdot \sqrt{\frac{Dt}{\pi}} \tag{42}$$

for times through $0.6M_t/M_\infty$ [83,93]. This treatment of approximating Equation 41 as Equation 42 is identical to assuming that, for short times, the plane sheet may be treated as a semi-infinite medium with an initial uniform concentration throughout the sorbent, and a constant uniform concentration at the surface [83,98,129].

Shen and Springer [98] provide an approximation, albeit without reference, which can reduce the computational demands of Equation 40 via

$$M_t \approx M_\infty \cdot \left\{ 1 - \exp\left[-7.3 \left(\frac{Dt}{h^2} \right)^{0.75} \right] \right\}. \tag{43}$$

Diffusion coefficients may be obtained from Equation 42 for short times or from curve fitting Equation 40.

Shen and Springer [98] proposed an accelerated test methodology whereby a value of D is initially approximated, a short time is selected where Equation 42 is valid, and Equation 40 is evaluated to find M_∞, knowing M_t. Then additional times are selected, Equation 40 is evaluated for M_∞, knowing M_t, and D is consequently adjusted such that M_∞ is in good agreement over all time. The authors claim such analysis will

result in values of D and M_∞ for a material without having to perform long-term hot water bath tests.

2.4.2.2 Two Phase Fickian Diffusion

2.4.2.2.1 Theoretical Basis for Two Phase Fickian Diffusion

Maggana and Pissis [138] presented a modified two-phase Fickian model based upon work by Jacob and Jones [139]. Jacobs and Jones introduced a model considering a more dense and a less dense phase, where the moisture uptake is a consequence of two independent diffusion phenomena.

$$\frac{M_t}{M_\infty} = V_d \cdot \left\{1 - \exp\left[-7.3\left(\frac{D_d t}{h^2}\right)^{0.75}\right]\right\} + (1 - V_d) \cdot \left\{1 - \exp\left[-7.3\left(\frac{D_l t}{h^2}\right)^{0.75}\right]\right\} \qquad (44)$$

where V_d is the volume fraction of the more dense phase, D_d is the diffusion coefficient of the more dense phase, and D_l is the diffusion coefficient of the less dense phase.

The model presented in Equation 44 is based upon the fundamental assumption that there are two independent Fickian phases which begin sorption simultaneously [139]. Consequently, there should be two regions of the moisture uptake curve wherein sorption is dominated by the more or less dense phase. The rate of uptake in the early stages of the curve should be additive since both phases are in the early stage. As the less dense phase approaches its equilibrium, the slope of the uptake curve should be characteristic of diffusion in the more dense phase.

Maggana and Pissis generalized the more and less dense phases to two arbitrary independent phases [138]. For these two moisture sorption mechanisms with two maximum moisture contents, M_1 and M_2, and two diffusion coefficients, D_1 and D_2, moisture uptake is described by [138]

$$M_t = M_1 \cdot \left\{ 1 - \frac{8}{\pi^2} \sum_{n=0}^{\infty} \frac{1}{(2n+1)^2} \exp\left[-\frac{D_1 t}{h^2} \pi^2 (2n+1)^2 \right] \right\} + M_2 \cdot \left\{ 1 - \frac{8}{\pi^2} \sum_{n=0}^{\infty} \frac{1}{(2n+1)^2} \exp\left[-\frac{D_2 t}{h^2} \pi^2 (2n+1)^2 \right] \right\}. \quad (45)$$

where

$$M_\infty = M_1 + M_2 . \quad (46)$$

and each diffusion coefficient follows the Arrhenius relation with independent values of D_o and E_a.

Previous research indicates that two phases of water can be observed in a resin exposed to hygothermal environments, where the sorption of Phase I is controlled by the amount of water in the atmosphere and the sorption of Phase II is controlled by temperature and time [38]. Mikols and coworkers present a simplified model accounting for water sorbed into the free volume, described by a maximum moisture content, and for additional water sorbed due to changes in the polymer structure resulting from hygrothermal interactions and changes in free volume [140].

2.4.2.2.2 Treatment of Two Phase Fickian Diffusion

The diffusion coefficients according to Equation 44 may be determined from simple linear curve fits of each phase dominated region. Figure 5 is presented for

clarification of the following discussion. The initial slope of the uptake curve provides the approximate diffusion coefficient, D_x, for the bulk after the traditional Fickian approach [139]

$$\left[\frac{\partial M_t}{\partial \sqrt{t}}\right]_x = \frac{4M_\infty}{h} \cdot \sqrt{\frac{D_x}{\pi}}. \tag{47}$$

However, it should be noted that the initial uptake is actually the summation of the uptake of the two phases. Thus one can state [139]

$$\left[\frac{\partial M_t}{\partial \sqrt{t}}\right]_x = \left[\frac{\partial M_t}{\partial \sqrt{t}}\right]_d + \left[\frac{\partial M_t}{\partial \sqrt{t}}\right]_l. \tag{48}$$

where subscripts *d* and *l* refer to the more and less dense phases.

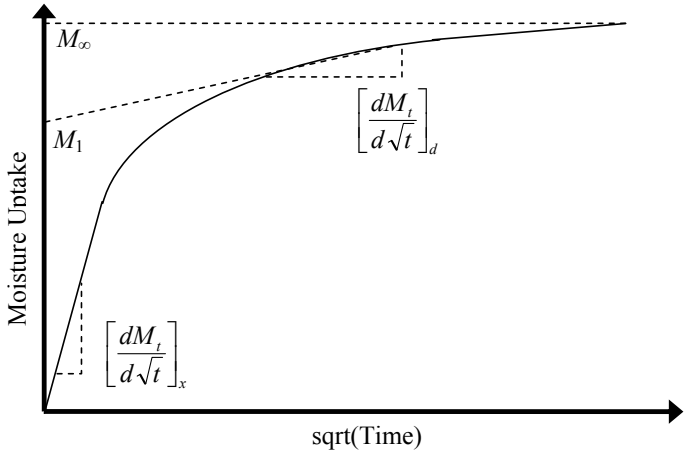

Figure 5. Values for determination of two phase Fickian parameters.

At later times, the slope represents the uptake in the more dense phase as the uptake in the less dense phase approaches equilibrium. By extending a line from the region characterized by sorption of the more dense region to the ordinate axis, the equilibrium content for the less dense phase, M_l, can be determined from the intercept [139], as Figure 5 indicates. Then

$$M_\infty = M_l + M_d \tag{49}$$

allows for the calculation of the corresponding diffusion coefficients after [139]

$$\left[\frac{\partial M_t}{\partial\sqrt{t}}\right]_d = \frac{4M_d}{h}\cdot\sqrt{\frac{D_d}{\pi}}\,. \tag{50.a}$$

$$\left[\frac{\partial M_t}{\partial\sqrt{t}}\right]_l = \frac{4M_l}{h}\cdot\sqrt{\frac{D_l}{\pi}} \tag{50.b}$$

Thus [139]

$$D_d = \pi\left(\frac{h}{4[M_\infty - M_l]}\right)^2\left[\frac{\partial M_t}{\partial\sqrt{t}}\right]_d^2 \tag{51.a}$$

$$D_l = \pi\left(\frac{h}{4M_l}\right)^2\left\{\left[\frac{\partial M_t}{\partial\sqrt{t}}\right]_x - \left[\frac{\partial M_t}{\partial\sqrt{t}}\right]_d\right\}^2. \tag{51.b}$$

It follows from Equations 44 and 45 that the volume fraction of the more and less dense phases can be represented by

$$V_d = \frac{M_d}{M_\infty} \qquad \text{and} \qquad 1 - V_d = \frac{M_l}{M_\infty}\,. \tag{52}$$

However, Jacobs and Jones [139] present a relation for V_d based upon a general expression for thermal conductivity in two component systems having orthorhombic symmetry where

$$V_d = \frac{\left(\frac{D_d}{D_l}+2\right)\left(\frac{D_x}{D_l}-1\right)}{\left(\frac{D_d}{D_l}-1\right)\left(\frac{D_x}{D_l}+2\right)}. \tag{53}$$

Jacobs and Jones admit that the determination of the initial uptake curves may not be so straightforward and, as such, iterations may need to be performed in order to improve the quality of fit [138,139].

Several assumptions can be made when considering the effect of temperature on equilibrium moisture contents. One could consider the case where a material is capable of sorbing a finite amount of sorbate where the volume percentage of one phase of the material would increase with temperature, similar to the model proposed in [140], implying that M_∞ is constant over temperature while V_d varies. Conversely, one could assume that there is no change in the relative volume percentage of either phase but the equilibrium content of each phase of the material increases proportionally with temperature, implying that M_∞ varies with temperature and V_d is constant. In the case of E-glass/vinyl-ester composite, not only is the bulk material heterogeneous, but the vinyl-ester resin matrix itself can be considered a biphasic material where the total moisture content increases with temperature, where the maximum moisture content of those two phases may also vary with temperature at two different rates.

2.4.2.3 Langmuir Diffusion Model

2.4.2.3.1 Theoretical Basis for Langmuir Diffusion

Dual Sorption Theory introduces a model wherein water sorption occurs through the diffusion of free species into the sorbent concurrent with the adsorption of water molecules to the polymer, becoming bound [136]. Carter and Kibler [92] present a non-steady state diffusion model based upon the integration of diffusion and Langmuir adsorption theory [80,91,136].

The following constituent equations as presented in [92] consider two phases of water

$$\frac{dC_D}{dt} = -\frac{dq}{dx} - \sigma \tag{54}$$

Where x is position, t is time, $C_D(x,t)$ is the concentration of the free diffusion phase, $q(x,t)$ is the mass flux of the free phase, and $\sigma(x,t)$ is the rate at which the free phase becomes site bound. It is important to note that only the free phase diffuses, but the free and bound water molecules each have the ability to bind to and to free themselves from the sorbent molecules. Introducing the Langmuir diffusion coefficient, D, the parameters α and β, and the concentration of site bound molecules, $C_S(x,t)$, the following constituent equations can be developed [92]

$$q = -D\frac{dC_D}{dx} \tag{55.a}$$

$$\sigma = \beta C_D - \alpha C_S, \tag{55.b}$$

whereupon [136]

$$\frac{\partial C_D}{\partial t} = D\frac{\partial^2 C_D}{\partial x^2} - \beta C_D + \alpha C_S. \tag{56}$$

The system approaches an equilibrium such that [92,136]

$$\sigma = 0, \qquad \beta C_D = \alpha C_S. \tag{57}$$

That is, α represents the probability that a bound molecule will become free and β, that a mobile molecule will become bound, and the rates of conversion between the two phases will become equivalent as equilibrium approaches. The maximum moisture

content, M_∞, at equilibrium can then be expressed in terms of the equilibrium $C_{D\infty}$ and $C_{S\infty}$:

$$M_\infty = C_{D\infty} + C_{S\infty} = C_{D\infty} + \frac{\beta}{\alpha} C_{D\infty}, \tag{58}$$

Then the moisture content M_t can be expressed as [91,92]

$$M_t = M_\infty \cdot \left\{ 1 - \frac{\beta}{\alpha+\beta}\exp(-\alpha t) - \frac{\alpha}{\alpha+\beta}\exp(-\beta t) \cdot \frac{8}{\pi^2}\sum_{n=0}^{\infty}\frac{1}{(2n+1)^2}\exp\left[-\frac{Dt}{h^2}\pi^2(2n+1)^2\right]\right\}, \tag{59}$$

where t is time, D is the Langmuirian diffusion coefficient, and h is specimen thickness. Carter and Kibler introduced the use of the term κ [92], defined as

$$\kappa = \frac{D\pi^2}{h^2} \tag{60}$$

and state that Equation 59 is valid only for $\alpha,\beta << \kappa$ [92]. Several sources [22,91,105,141] restate Equation 59 without the exp(-βt) term since the rate of conversion between the two phases should be much less than κ:

$$M_t = M_\infty \cdot \left\{ 1 - \frac{\beta}{\alpha+\beta}\exp(-\alpha t) - \frac{\alpha}{\alpha+\beta} \cdot \frac{8}{\pi^2}\sum_{n=0}^{\infty}\frac{1}{(2n+1)^2}\exp\left[-\frac{Dt}{h^2}\pi^2(2n+1)^2\right]\right\}. \tag{61}$$

For short exposure times, where $t \le 0.7/\kappa$, Equation 59 can be expressed as [92]

$$M_t = M_\infty\left[\left(\frac{\alpha}{\alpha+\beta}\right)\cdot\sqrt{\frac{16Dt}{h^2\pi^2}}\right], \qquad t \le 0.7/\kappa. \tag{62}$$

and for long exposure times,

$$M_t = M_\infty\left[1 - \left(\frac{\beta}{\alpha+\beta}\right)\exp(-\alpha t)\right], \qquad t >> 1/\kappa. \tag{63}$$

Pseudo-equilibrium, $M_{ps\infty}$, may be described as

$$M_{ps\infty} = M_{\infty}\left(\frac{\alpha}{\alpha+\beta}\right). \tag{64}$$

This pseudo-equilibrium represents the fraction of mobile water in the sorbent and may become apparent in the form of a plateau at sufficiently high temperatures and sufficiently low specimen thicknesses, where the assumption $\alpha,\beta << \kappa$ becomes more accurate. Figure 6 demonstrates the inherent variability of the pseudo equilibrium plateau as κ ranges from 20α, for which there is no discernable pseudo equilibrium, to 200α, where a pseudo equilibrium is easily detected.

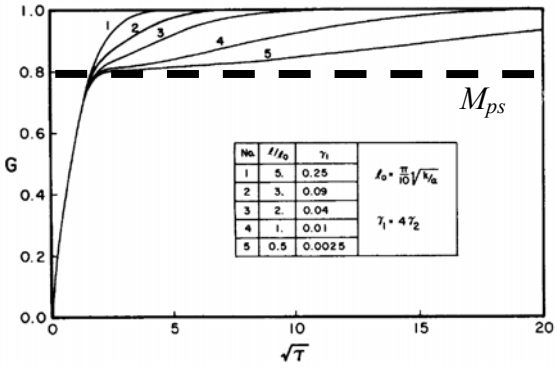

Figure 6. Parametric study [91] of Langmuir diffusion.
$G = M_t/M_{\infty}$ plotted against $\tau = \kappa t$ for $\alpha = 4\beta$.
The value of κ is varied from 20α (Curve 1) to 200α (Curve 5)

2.4.2.3.2 Treatment of Langmuir Diffusion Model

Various basic curve fitting algorithms have been used to obtain values of D, α, β, and sometimes even M_{∞}. One approach begins by selecting a moisture content from an apparent pseudo-equilibrium plateau in the empirical moisture sorption curve to define $M_{ps\infty}$ in order to obtain the ratio of α to $\alpha + \beta$ from Equation 64 [142]. An exponential curve fit was performed according to Equation 63 to obtain β, allowing

for the calculation of α from Equation 64 [142]. The slope of the initial uptake curve of M_t plotted against $t^{1/2}$ for times less than $0.7/\kappa$ was used to determine the diffusion coefficient, D via Equation 62 [142].

Li, Miranda and Sue determine the diffusion coefficient from a curve fit of the simplified solution to Fick's Law, per Equation 40, and constrain D in Equation 59 to this value [143]. M_∞, α, β were then obtained through a curve fitting algorithm. Assuming that $\beta = 0$, would imply that there is no conversion; subsequently, the diffusion coefficient would be equivalent to Fickian diffusion. When $\beta > 0$, water may convert from free to bound water and vise versa, allowing for greater maximum moisture content in the sorbent than in Fickian diffusion.

2.4.2.4 Structural Modification Diffusion Model

2.4.2.4.1 Theoretical Basis for Structural Modification Diffusion

A two stage relaxation model has been presented wherein the first stage is predominantly Fickian diffusion followed by a slow relaxation of the polymer which allows for increased moisture sorption over time [144]. This model amounts to a modified Fickian model with a time dependent maximum moisture content

$$M_t = M_{o\infty} \cdot \left[1 + k\sqrt{t}\right] \cdot \left\{1 - \frac{8}{\pi^2}\sum_{n=0}^{\infty}\frac{1}{(2n+1)^2}\exp\left[-\frac{Dt}{h^2}\pi^2(2n+1)^2\right]\right\}. \qquad (65)$$

where $M_{o\infty}$ is the pseudo-equilibrium moisture content and k is defined as a "relaxation coefficient" [144]. The second phase is characterized by this relaxation whereby the asymptote is an increasing linear function of $t^{1/2}$ rather than a constant M_∞. However,

similar trends have been observed whereby the asymptote is a decreasing linear function of $t^{1/2}$. Decreasing linear asymptotic behavior, where a maximum moisture content is reached and followed by a loss in weight, may indicate sorbent degradation which can be identified by permanent weight loss after redrying. Consequently, k can represent relaxation or degradation phenomena with a simple change in sign and, as such, should be referred to as representative of structural modification rather than a "relaxation coefficient".

2.4.2.4.2 Treatment of Structural Modification Diffusion Model

Determination of $M_{o\infty}$ is not as straightforward as assigning the maximum moisture content. $M_{o\infty}$ represents the equilibrium moisture content for the Fickian component of Equation 65. Consequently, the sorption trend of M_t vs. $t^{1/2}$ should be separated into three sets where Fickian diffusion and structural modification dominate sorption at early and late times, respectively, and the third set represents an intermediate transition region, indicated in Figure 7.

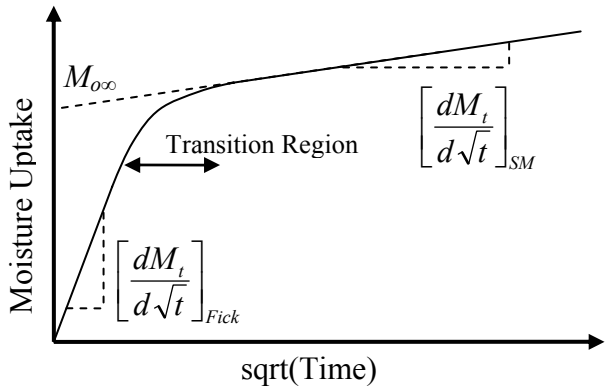

Figure 7. Stylized structural modification uptake trend.

Performing line fits on each of the two sets as in Figure 7 will allow for the determination of $M_{o\infty}$, k and D. The best fit line of the Fickian dominated phase should intercept the origin. The pseudo equilibrium moisture content, $M_{o\infty}$, is determined from the intercept of the best fit line characterizing the gravimetric data dominated by structural modification. With a value of $M_{o\infty}$, D and k can be calculated from the slopes of the corresponding line fits as

$$\left[\frac{\partial M_t}{\partial \sqrt{t}}\right]_{Fick} = \frac{4 M_{o\infty}}{h} \cdot \sqrt{\frac{D}{\pi}} \tag{66.a}$$

$$\left[\frac{\partial M_t}{\partial \sqrt{t}}\right]_{SM} = M_{o\infty} k \,. \tag{66.b}$$

where the subscript SM refers to structural modification.

2.4.2.4.3 Integration of Two-Phase and Structural Modification Models

When considering the two-phase Fickican model, there is an intermediate time from which D_2 can be determined based upon the assumption that the first phase has reached an equilibrium moisture content and the second phase is still in the early stages of sorption. That is, for this intermediate time, Equation 45 can be approximated as

$$M_t \approx M_1 + M_2\left[\frac{4}{h}\sqrt{\frac{D_2 t}{\pi}}\right]. \tag{67}$$

Similarly, the structural modification model can be considered for later time periods, where the Fickian phase has reached its equilibrium moisture content, and the

secondary phase is being modified according to *k*. During this latter period, Equation 65 can be approximated as

$$M_t \approx M_{o\infty} + M_{o\infty}\sqrt{t}\,. \tag{68}$$

From Equations 67 and 68,

$$M_{o\infty} \approx M_1 \tag{69.a}$$

$$M_{o\infty}k \approx \frac{M_2 4}{h}\sqrt{\frac{D_2}{\pi}}\,. \tag{69.b}$$

Using the simplified structural modification model, the diffusion coefficient of the second phase in the dual phase Fickian model can be determined as

$$D_2 \approx \pi\left[\frac{M_{o\infty}kh}{(M_\infty - M_{o\infty})4}\right]^2. \tag{70}$$

Based upon this derivation, it is reasonable to assume that the structural modification facotr *k* is fundamentally related to the Fickian diffusion of a secondary phase. The diffusion within this secondary phase is on such a slow time scale that it may be difficult to identify the secondary equilibrium moisture content in an experimental laboratory time scale.

2.5 Predictive Degradation Models

In developing degradation models, a property, *P*, (e.g., tensile strength, glass transition temperature) is monitored over a period of time with environmental exposure. For the purposed of accelerated testing, these environments are hot water immersion baths, where elevated temperatures accelerate the degradation rate. Constant exposure to hot water baths over a series of temperatures provides an avenue

for the degradation rate to be correlated to temperature and, as such, should allow for the prediction of the degradation rate at ambient temperature. Because the correlation between temperature and degradation rate was established for immersion in water, the rate of degradation at ambient temperature will correlate to the material in constant contact with liquid water.

There are generally two types of degradation models: one which characterizes the time to failure defined by a material property reaching a critical level and one which predicts a property level as a function of time. Because this study concerns materials employed for civil infrastructure, the following discussion will focus on predictive degradation models.

2.5.1 Current Degradation Models

The following summarizes the state of the art in degradation models of fiber reinforced polymer composites.

2.5.1.1 Arrhenius Rate Model

The Arrhenius Rate Model employs the Arrhenius rate equation to describe the rate of degradation of a material property P which is assumed to be proportional to the rate of some reaction [145].

$$\frac{dP}{dt} = A\exp\left[\frac{-E_d}{RT}\right] \tag{71}$$

where A is a pre-exponential constant, E_d is the activation energy for the reaction responsible for degradation, R is the gas constant, T is temperature in Kelvin, and t is time. Furthermore, it is assumed that [145]

$$t(P) \propto \left(\frac{dP}{dt} \right)^{-1}. \tag{72}$$

which would imply

$$\ln t(P) \propto T^{-1} \tag{73}$$

as stated in [145].

The temporal variation of P can be determined as

$$P(t) = B \exp\left[\frac{-E_d}{RT} \right] \ln t + P_o \tag{74}$$

where B is an integration constant and P_0 is the property at time zero. Equation 74 represents the Arrhenius rate degradation model. It has been proposed that the E_d is well represented by the activation energy for the diffusion process [146].

A fundamental assumption of this model states that the rate of degradation is directly related to the rate of a single chemical reaction [145]. It may be possible for a plot of ln $t(P)$ vs. T^{-1} to demonstrate non-linearity, implying that the rate of degradation in the material is controlled by more than one degradation mechanism.

2.5.1.2 Time Temperature Superposition

The Time-Temperature Superposition (TTS) principle is a theoretical model used to describe the time and temperature dependent behavior of material properties for viscoelastic materials [96,147]. Most often, TTS is used for stiffness related properties, but it has also been implemented for time and temperature dependent strength [147,148].

TTS is implemented by shifting a series of curves, obtained at a series of temperatures which describe a material property as a function of time, to form a master curve. The Arrhenius equation can be used in determining the shift factor required to align the degradation trends at a variety of temperatures [148]. When shift factors exhibit non-linear behavior on an Arrhenius plot, it may be appropriate to implement a dual Arrhenius model [128,148]. The material property at a specific time can be determined by referencing the master curve assembled through TTS. One such master curve describes the material property as function of time through an exponential relation where [150,151]

$$\frac{P_\infty - P(t)}{P_\infty - P_0} = \exp\left[\frac{-(t-t_i)^b}{a_T a_M a_C}\right] \tag{75}$$

where P_0 and P_∞ are the initial and final property values; t is time; t_i is the time at which degradation initiates; b is an exponential degradation factor; and a_T, a_M, and a_C are shift factors relating to thermal, mechanical and environmental stress effects, respectively.

Equation 75 was derived on the basis of a failure probability analysis in a degradation study using a Weibull distribution [152,153]. Therefore, the master curve describe by Equation 75 will produce a sigmoidal strength distribution when plotted against time, where there is some induction time required for failure to initiate, followed by a sudden steep drop in property described by b, ending with a gradual final approach to an equilibrium degradation value. Previous studies indicate that the exponential degradation factor b does not change depending on stress histories [153].

2.5.1.3 Crack Propagation Degradation Model

A simple mechanistically based model is presented in the context of GRC accelerated testing wherein the propagation of fiber surface flaws is assumed to be responsible for the degradation of the fiber composite [154]. The theory assumes that the induced stress responsible for propagation of a fiber surface flaw is a function of temperature, the rate of propagation for a surface flaw, da/dt, is proportional to the concentration of hydroxyl ions, C, responsible for hydrolytic attack on glass and the crack propagation rate is described by the Arrhenius equation whereby [154]

$$\frac{da}{dt} = k_C k_T C \exp\left[\frac{-E}{RT}\right] \tag{76}$$

where the terms k_C and k_T relate the proportionality of da/dt to hydroxyl concentration and the proportionality of induced stress to temperature, respectively.

Using the critical stress intensity factor K_{IC} and a geometry factor Y, the strength of a fiber, σ_f, is can be stated using

$$\sigma_f = \frac{K_{IC}}{Y\sqrt{\pi a}}, \tag{77}$$

whereupon the strength of the composite is stated as [154]

$$\sigma = \eta_o \eta_l V_f \sigma_f \tag{78}$$

with η_o and η_l defined as efficiency factors for fiber orientation and length.

Integrating Equation 76 for $a(t)$ and substituting $a(t)$ and Equation 77 into Equation 78, the solution can be normalized to initial values. Consequently,

$$\frac{\sigma(t)}{\sigma_0} = \frac{1}{\sqrt{1+kt}}, \tag{79}$$

where the tensile strength at some time t is σ, and σ_0 is the initial strength. The term k encompasses all proportionality constants, provided on the right hand side of Equation 76, along with the initial flaw size a_o:

$$k = \frac{1}{a_o} k_C k_T C \exp\left[\frac{-E}{RT}\right]. \tag{80}$$

Equation 79 does not allow for a non-zero strength as $t \to \infty$, though such a parameter could be integrated using a form similar to the left hand side of Equation 75.

2.5.1.4 Moisture Dependent Degradation

While temporal degradation models are integral to the design and performance predictions of a material property over time, degradation resulting from exposure to hot water baths is known to be strongly related to the moisture present in the material. Nissan [15] introduced a degradation model integrating the two regimes of moisture degradation where below a critical moisture content, w_c, the moisture forms hydrogen bonds with the polymer network similar to the formation of an adsorption monolayer. Above a critical moisture content, additional water molecules form hydrogen bonds with broken polar bonds and adjacent water molecules. The number of hydrogen bonds established by a single water molecule is described by a cooperative index, *CI*, through the saturation content.

The referenced study addressed the change in Young's modulus with moisture content [15], but the theory could similarly be extended to some arbitrary property *P*.

$$P = P_0 \exp\left[-\frac{1}{3}\cdot\frac{w}{W}\right] \qquad w < w_c \quad (81.a)$$

$$P = P_0 \exp\left[\frac{1}{3}\cdot\frac{w_c}{W}(CI-1)\right]\exp\left[-\frac{CI}{3}\cdot\frac{w}{W}\right] \qquad w > w_c \quad (81.b)$$

where P_0 describes the initial property value, w is the moisture content, and W is the theoretical quantity of water molecules required for each polar group on the sorbent to be in a hydrogen bond with a single water molecule. The critical moisture content, w_c, is theorized to be on the order of the BET monolayer, below which hydrogen bonding with water molecules is sparse, as would be expected in an adsorbed monolayer. Above w_c, water molecules establish hydrogen bonds with neighboring water molecules, leading to a clustering phenomenon.

An alternative study [31] provides a derivation of the property value as a function of moisture content as

$$\frac{P_\infty - P(t)}{P_\infty - P_0} = \exp\left[\frac{-P_\infty}{P_0} M_t\right]. \qquad (82)$$

This equation is based off a fundamental assumption that the degradation of the material property follows an exponential decay with time. However, for a finite equilibrium moisture content, as is commonly observed, the exponential term does not go to zero and, as such, the mathematical statement does not hold, despite its similarity to Equation 81.

2.5.1.5 Multicomponent Degradation

Degradation of fiber reinforced composites is dependent upon the degradation of the constituent elements as well as interfacial adhesion. Heretofore, the degradation models presented are purely empirical and do not address the degradation of the constituent elements. Design of composite structures primarily concerns the tensile modulus and tensile strength. While the tensile modulus does not decrease significantly through exposure to hot water baths, the tensile strength demonstrates severe degradation. Therefore, a degradation model which integrates the degradation of constituent elements to produce the degradation trend of longitudinal tensile strength [155] is extremely useful.

Using the weakest link model with a Weibull distribution for fiber strength, it is possible to consider the longitudinal tensile strength of a composite, σ_{1t}, with a possible debond [155]

$$\sigma_{1t} = \left[\mu\left(\delta + L_d\right)me\right]^{-1/m}, \tag{83}$$

where μ describes the characteristic value of the Weibull distribution, δ is the ineffective length, L_d is the debond length, m is the dispersion of the Weibull distribution, and e is the base of the natural logarithms. The characteristic value of the Weibull distribution is defined as

$$\mu = \frac{1}{L}\left\{\frac{\Gamma\left(1+m^{-1}\right)}{\sigma}\right\}^{-\frac{1}{m}} \tag{84}$$

where σ is the average fiber strength obtained using a gage length of L and Γ is the gamma function. A modified stress corrosion model may be used for calculation of σ in Equation 84 in order to account for zero-stress aging and stress corrosion [155]

$$\sigma\left(t_f, t_a\right) = \left[\frac{t_f}{BS_0^{N-2}\left(1+\alpha t_a\right)^{-\beta(N-2)}}\right]^{-1/N}. \tag{85}$$

where t_f is the time to failure, t_a is the aging time, N is the susceptibility, B is an empirical parameter relating to stress corrosion, and α and β are empirical constants describing zero-stress aging of the fiber. The fiber strength used in the Weibull distribution in Equation 84 can be described assuming that the aging time t_a and the time to failure of the fiber are equivalent. Research has also shown that μ and m may be assumed to be constant [156,157].

The debond length L_d can be described as

$$L_d = \kappa + \lambda \ln t, \tag{86}$$

with empirical parameters κ and λ defined in [155] for an E-glass/epoxy immersed in 95°C water. The ineffective length or stress transfer length is provided as [155,158]

$$\delta = \frac{d_f}{2}\left[\left(\frac{1-\sqrt{V_f}}{\sqrt{V_f}}\right)\left(\frac{E_f}{G_m}\right)\right]^{-1/2} \cosh^{-1}\left[\frac{1+(1-\varphi)^2}{2(1-\varphi)}\right]. \tag{87}$$

where d_f is the fiber diameter, E_f is the fiber modulus, G_m, the matrix shear modulus, and φ is the stress intensity factor defined as the ratio of the stress from the end of the ineffective length δ away from the broken end of the fiber to a point far away from the break. For an arbitrary stress development of φ=0.9, the $\cosh^{-1}$ term simplifies to 2.302.

The fiber volume fraction and fiber modulus can be assumed constant with environmental exposure. G_m, can be described using glass transitions temperatures [155]

$$G_m = G_{m\infty}\sqrt{\frac{T_{gw} - T}{T_{gd} - T_0}} \tag{88}$$

with the long term matrix shear modulus $G_{m\infty}$, wet and dry glass transition temperature T_{gw} and T_{gd}, temperature of exposure T, and empirically determined reference temperature T_0. While expressions are available for the variability of T_{gw} as a function of moisture content, direct measurement of T_{gw} would be recommended.

This model does have some drawbacks. Equation 86 assumes that interfacial debonding initiates immediately. In reality, interfacial degradation is dependent upon the progression of the diffusion front. It may be possible to implement a time shift factor to account for delayed initiation of interfacial debonding. Furthermore, the debond length L_d is about 1000 times larger than the ineffective length δ, indicating that Equation 83 is highly dependent upon Equation 86.

At the most fundamental level, the model presented here does not allow for acceleration factors. Rigorous implementation of this model in multiple environments would require isolated degradation studies of the fiber and neat matrix in the environments which correspond to the exposure conditions for the composite. The factors provided with Equation 86 are derived for a specific environment and will not apply to accelerated testing performed in humid environments or at alternative temperatures of immersion.

2.5.1.6 Metric Based Numerical Analysis

One degradation model takes into account the various mechanisms responsible for composite degradation and incorporates them into metric based analysis [159]. While this model may be applied to space environments to account for reactions such as oxidation which can result in crosslinking or charring, the model can also be simplified to address exposure to moist environments at elevated temperatures, where hydrolysis can occur.

The change of a property P can be characterized by the progression of metric α_i from 0 to 1, describing the progression of a chemical reaction i from the initial state ($\alpha_i = 0$) to the conclusion of the reaction ($\alpha_i = 1$) [159]. Chemical reactions may include oxidative crosslinking, mass loss reactions, hydrolysis, or post-cure [159]. For each metric, the change in material properties from P_0 can be related to the degradation state as [159]

$$\frac{P}{P_0} = \sqrt{\frac{T_g - T}{T_g - T_o}}\left(1 + p\alpha_i{}^q\right) \tag{89}$$

where P_0 is the initial property value, T_g is the glass transition temperature, T is the temperature of exposure, T_o is a reference temperature, and p and q are empirical parameters.

For a chemical reaction α_i, the progress of the reaction can be described in terms of the rate of reaction k_i, activation energy E_i, and concentration of diffusing substance c_s using empirical parameters n_i and m_i [159]

$$\frac{\partial \alpha_i}{\partial t} = k_i \left(1-\alpha_i\right)^{n_i} c_s^{\,m_{si}} \exp\left(\frac{-E_i}{RT}\right). \tag{90}$$

The mechanistic model presented here is intended to be considered through numerical analysis and, heretofore, has been primarily implemented for high temperature exposures where oxidation is a primary concern [159,160].

2.5.1.7 Equivalent Temperature

Because in-service environments are inherently dynamic, a time variant model must be able to account for variant temperature. The concept of equivalent temperature is introduced [161] through a degradation model which assumes that for a particular temperature, the degradation rate is a constant

$$\frac{dP}{dt} = A\exp\left[\frac{-E}{RT(t)}\right] \qquad P = \int_0^t A\exp\left[\frac{-E}{RT(t')}\right]dt' + P_0 \tag{91}$$

Then some equivalent temperature, T^*, is introduced such that

$$\exp\left[\frac{-E}{RT^*}\right]t = \int_0^t \exp\left[\frac{-E}{RT(t')}\right]dt', \tag{92}$$

implying

$$T^* = \frac{-E}{R\cdot\ln\left(\frac{1}{t}\int_0^t \exp\left[\frac{-E}{RT(t')}\right]dt'\right)}. \tag{93}$$

Simplifications may be made, assuming the temperature varies periodically [161].

Using the equivalent temperature, it can be shown that the average temperature of a region can be inadequate to describe the degradation of a polymer [161], as

described through a degradation rate model. This discrepancy can be less than 1°C for some tropical or equatorial climates in comparison to 10°C for extreme climates [161].

2.5.2 Degradation Models Integrating Exposure to Relative Humidity

The models presented in Section 2.5.1 are empirically based upon exposure to aggressive environments at elevated temperatures and have primarily been employed for use with accelerated testing in hot water baths. Environmental degradation models have been developed to predict changes in properties after exposure to an environment with varying temperature, relative humidity [162-165]. These models also take ultraviolet (UV) exposure into account since their purpose is to predict the performance a material property with exposure to in-service outdoor environments. Hygrothermal exposure is well known to accelerate UV degradation of polymer materials [166,167]. While UV exposure is an important factor for environmental degradation studies, composites used in civil infrastructure are most often used outside of direct sunlight.

2.5.2.1 Exponential Humidity Term

The rate of degradation of material performance has been described by an extension of the Eyring model for temperature incorporating a second stress, identified as relative humidity [162]. The change in performance is stated as [162]

$$\frac{dP}{dt} = A\left[T(t)\right]^{-B} \exp\left[\frac{-E}{RT(t)}\right] \exp\left[\%RH(t)\cdot\left(C+\frac{D}{T(t)}\right)\right] I_{UV}(t), \tag{94}$$

where I_{UV} is the ultraviolet irradiance defined in [162] and *A, B*, *C*, and *D* are empirical parameters. A simplified form based upon the Arrhenius equation removes the temperature dependency in the exponential humidity term [163]

$$\frac{dP}{dt} = A\exp\left[\frac{-E}{RT(t)}\right]\exp\left[B\cdot\%RH(t)\right]I_{UV}(t), \tag{95}$$

where *A* and *B* are empirical parameters. For constant environmental conditions,

$$P(t) - P_0 = A\exp\left[\frac{-E}{RT}\right]\exp\left[B\cdot\%RH\right]I_{UV}t\,, \tag{96}$$

where P_0 is the property at time zero. In the absence of UV exposure, the irradiance term may be absorbed into the pre-exponential factor *A*.

While this model does allow for time dependent environmental exposure, for static conditions, it assumes the rate of degradation is constant with time. The degradation of structural composite properties is well known to slow over time.

2.5.2.2 Power Law Humidity Term

An existing model [164,165] describes the time for a polymer to reach a specific property level, τ, as

$$\tau = A\exp\left[\frac{E}{RT}\right](\%RH)^{-c}\,{I_{UV}}^{-1}, \tag{97}$$

where *A* and *c* are empirical constants, *E* is the activation energy for the thermal process, and I_{UV} is the irradiation dose of ultraviolet light below 400nm. This model is fundamentally similar to the Arrhenius model introduced in Section 2.5.1.1. The pre-logarithmic term in Equation 74 could be considered equivalent to $1/\tau$ in Equation 97.

2.5.3 Summary of Degradation Models

Existing predictive degradation models range in complexity from a simple one parameter empirical statement in the Arrhenius rate degradation model to a complex numerical metric based analysis. Most degradation models presented in Section 2.5 assume that the Arrhenius model holds, just as for diffusion.

2.6 Research Goals

It is the main goal of this research to establish a sound understanding of the degradation mechanisms experienced by a model E-glass/vinyl-ester composite exposed to humid environments and to compare these modes of degradation to those which result from water immersion. The property of main concern here is the longitudinal tensile strength of a model E-glass/vinyl-ester pultruded composite. Complementary short beam shear and DMTA testing shall be performed to provide insight as to the modes of degradation occurring in the polymer matrix and interphase. Gravimetric studies will be conducted in order to understand the modes of sorption in all humid and immersion environments for all specimen types. The results from this study should help to understand the mechanisms of sorption and degradation in order to contribute to the development of predictive degradation models for composites which incorporate humidity as a degradation factor.

2.7 References

1. Antoon, M.K. and J.L. Koenig. "The structure and moisture stability of the matrix phase in glass-reinforced epoxy composites." *Journal of Macromolecular Science – Reviews in Macromolecular Chemistry and Physics*. Vol. C19, No. 1 (1980) 135-173.

2. Mijovic, J. and K.-F. Lin. "The Effect of Hygrothermal Fatigue on Physical/Mechanical Properties and Morphology of Neat Epoxy Resin and Graphite/Epoxy Composite." *Journal of Applied Polymer Science*. Vol. 30, No. 6 (1985) 2527-2549.

3. Wood, C.A. and W.L. Bradley. "Determination of the Effect of Seawater on the Interfacial Strength of an Interlayer E-glass/Graphite/Epoxy Composite by *In Situ* Observation of Transverse Cracking in an Environmental SEM." *Composites Science and Technology*. Vol. 57, No. 8 (1997) 1033-1043.

4. Bunker, B.C. "Molecular mechanisms for corrosion of silica and silicate glasses." *Journal of Non-Crystalline Solids*. Vol. 179 (1994) 300-308.

5. Ishida, H. and J.L. Koenig. "The Reinforcement Mechanism of Fiber-Glass Reinforced Plastics under Wet Conditions: A Review." *Polymer Engineering and Science*. Vol. 18, No. 2 (1978) 128-145.

6. Lowry, H.H. and G.T. Kohman. "The mechanism of the absorption of water by rubber." *Journal of Physical Chemistry*. Vol. 31, No. 1 (1927) 23-57.

7. Adams, R.D. and M.M. Singh. "The dynamic properties of fiber-reinforced polymers exposed to hot, wet conditions." *Composites Science and Technology*. Vol. 56 (1996) 977-997.

8. Lee, M.C. and N.A. Peppas. "Water transport in epoxy resins." *Prog. Polym. Sci.* Vol. 18 (1993) 947-961.

9. Selzer, R. and K. Friedrich. "Mechanical properties and failure behavior of carbon fibre-reinforced polymer composites under the influence of moisture." *Coposites Part A*. Vol. 28A. (1997) 595-604.

10. Wright, W.W. "The effect of diffusion of water into epoxy resins and their carbon-fiber reinforced composites." *Composites*. (1981) 201-205.

11. Auad, M.L., M. Aranguren, and J. Borrajo. "Epoxy-Basted Divynyl Ester Resin/Styrene Copolymers: Composition Dependence of the Mechanical and Thermal Properties." *J. of Applied Polymer Science.* Vol. 66 (1997) 1059-1066.

12. Apicella, A., C. Migliaresi, L. Nicolais, L. Iaccarino, and S. Roccotelli. "The water ging of unsaturated polyester-based composites: influence of resin chemical structure." *Composites*. Vol. 14, No. 4 (1983) 387-392.

13. Penczek, P., J. Sodhi, and R. Ostrysz. "Unsaturated Ester Resins." *Journal of Applied Polymer Science*. Vol. 101 (2006) 2627-2631.

14. Kwei, T.K. "Strength of Epoxy Polymers. I. Effect of Chemical Structure and Environmental Conditions." *J. of Applied Polymer Science*. Vol. 10 (1966) 1647-1655.

15. Nissan, A.H. "H-Bond Dissociation in Hydrogen Bond Dominated Solids." *Macromolecules*. Vol. 9, No. 5 (1976) 840-850.

16. Mijovic, J. and H. Zhang. "Molecular Dynamics Simulation Study of Motions and Interactions of Water in a Polymer Network." *Journal of Physical Chemistry B*. Vol. 108, No. 8 (2004) 2557-2563.

17. Abusafieh, A. and S.R. Kalidindi. "Effect of water Absorption on the Izod Impact Energy of Crosslinked Poly(Methyl Methacrylate-Acrylic Acid) and Their Composites." *Polymer Composites*. Vol. 19, No. 1 (1998) 23-30.

18. Chiang, M.Y.M. and M. Fernandez-Garcia. "Relation of Swelling and Tg Depression to the Apparent Free Volume of a Particle-Filled, Epoxy-Based Adhesive." *J. of Applied Polymer Science*. Vol. 87 (2003) 1436-1444.

19. Adamson, M.J. "Thermal expansion and swelling of epoxy resin used in graphite/epoxy composite materials." *J. of Materials Science*. Vol. 15 (1980) 1736-1745.

20. Chin, J.W., K. Aouadi, M.R. Haight, W.L. Hughes, and T. Nguyen. "Effects of Water, Salt Solution and Simulated Concrete Pre Solution on the Properties of Composite Matrix Resins Used in Civil Engineering Applications." *Polymer Composites*. Vol. 22, No. 2 (2001) 282-297.

21. Chu, W. and W. M. Karbhari. "Effect of Water Sorption on Performance of Pultruded E-Glass/Vinylester Composites." *Journal of Materials in Civil Engineering*. Vol. 17, No. 1 (2005) 63-71.

22. Ghorbel, I. and D. Valentin. "Hydrothermal Effects on the Physico-Chemical Properties of Pure and Glass Fiber Reinforced Polyester and Vinylester Resins." *Polymer Composites*. Vol. 14, No. 4 (1993) 324-334.

23. Fraga, A.N., V.A. Alvarez, A. Vazquez, and O. de la Osa. "Relationship Between Dynamic Mechanical Properties and Water Absorption of Unsaturated Polyester and Vinyl Ester Glass Fiber Composites." *J. of Composite Materials.* Vol. 37, No. 17 (2003) 1553-1573.

24. DeNeve, B. and M.E.R. Shanahan. "Water Absorption by an epoxy resin and its effect on the mechanical properties and infra-red spectra." *Polymer*. Vol. 34, No. 24 (1993) 5099-5105.

25. Antoon, M.K., J.L. Koenig, and T. Serafini. "Fourier-Transform Infrared Study of the Reversible Interaction of Water and a Crosslinked Epoxy Matrix." *Journal of Polymer Science*. Vol. 19 (1981) 1567-1575.

26. Cotugno, S., D. Larobina, G. Mesitieri, P. Musto, and G. Ragosta. "A novel spectroscopic approach to investigate transport processes in polymers: the case of water-epoxy interaction." *Polymer*. Vol. 42 (2001) 6431-6438.

27. L.E. Nielsen "Crosslinking: Effect on Physical Properties of Polymers." *J. Macromol. Scie. – Revs. Macromol. Chem.* Vol. C3, No. 1 (1969) 69-103.

28. Barton, J.M. and D.C.L. Greenfield. "The Use of Dynamic Mechanical Methods to Study the Effect of Absorbed Water on Temperature-dependent Properties of an Epoxy Resin-Carbon Fiber Composite." *Bristh Polymer Journal.* Vol. 18, No. 1 (1986) 51-56.

29. Rodriguez, E., M. Larranaga, I. Mondragon, and A. Vazquez. "Relationship between the Network Morphology and Properties of Commercial Vinyl Ester Resins." *J. of Applied Polymer Science*. Vol. 100 (2006) 3895-3903.

30. Scott, T.F., W.D. Cook, J.S. Forsythe. "Kinetics and network structure of thermally cured vinyl ester resins." *European Polymer Journal.* Vol. 38, No. 4 (2002) 705-716.

31. Papanicolaou, G.C., T.V. Kosmidou, A.S. Vatalis, and C.G. Delides. "Water Absorption Mechanism and Some Anomolous Effects on the Mechanical and Viscoelastic Behavior of an Epoxy System." *Journal of Applied Polymer Science*. Vol. 99 (2006) 1328-1339.

32. Kaw, A.K. *Mechanics of Composite Materials.* CRC Press: New York, 1997.

33. Lee, S.-B., T.J. Rockett, and R.D. Hoffman. "Interactions of water with unsaturated polyester, vinyl ester and acrylic resins." *Polymer*. Vol. 33, No. 17 (1992) 3691-3697.

34. Karbhari, V.M. "Dynamic Mechanical Analysis of the Effect of Water on E-Glass/Vinylester Composites." *Journal of Reinforced Plastics and Composites*. Vol. 25, No. 6 (1996) 631-644.

35. Abeysinghe, H.P., W. Edwards, G. Pritchard, and G.J. Swampillai. "Degradation of crosslinked resins in water and electrolyte solutions." *Polymer*. Vol. 23 (1982) 1785-1790.

36. Ishai, O. "Environmental Effects on Deformation, Strength, and Degradation of Unidirectional Glass-Fiber Reinforced Plastics. II. Experimental Study." *Polymer Engineering and Science*. Vol. 15, No. 7 (1975) 491-499.

37. Morii, T., H. Hamada, Z. Maekawa, T. Tanimoto, T. Hirano, and K. Kiyosumi. "Weight change mechanism of randomly oriented CFRP panel immersed in hot water." *Composite Structures*. Vol. 23 (1993) 95-100.

38. Zhou, J. and J.P. Lucas. "Hygrothermal effects of epoxy resin. Part II: variations of glass transition temperature." *Polymer*. Vol. 40, No. 20 (1999) 5513-5522.

39. Nogueira, P. C. Ramirez, A. Torres, et al. "Effect of Water Sorption on the Structure and Mechanical Properties of an Epoxy Resin System." *Journal of Applied Polymer Science*. Vol. 80 (2001) 71-80.

40. Wedgewood, A.R., J.C. Seferis, and T.R. Beck. "Transport and Related Properties of Paint Films. II. Dynamic Mechanical Properties and Humidity Effects." *Journal of Applied Polymer Science*. Vol. 30 (1985) 111-133.

41. Xian, G. and V.M. Karbhari. "Segmental relaxation of water-aged ambient cured epoxy." *Polymer Degradation and Stability*. Vol. 92, No. 9 (2007) 1650-1659.

42. Mijovic, J. and K.-F. Lin. "Time-Dependent Changes in Morphology of Neat and Reinforced Epoxy Resins Part I. Neat Epoxies." *Journal of Applied Polymer Science*. Vol. 32 (1986) 3211-3227.

43. Leveque, D., A. Schieffer, A. Mavel, and J-F. Maire. "Analysis of how thermal aging affects the long-term mechanical behavior and strength of polymer-matrix composites." *Composites Science and Technology*. Vol. 65 (2005) 395-401.

44. Kong, E.S.W. and M.J. Adamson. "Effect of physical ageing on moisture sorption of amine-cured epoxies." *Polymer Communications*. Vol. 24 (1983) 171-173.

45. Zimm, B.H. and J.L. Lundberg. "Sorption of vapors by high polymers." *Journal of Physical Chemistry*. Vol. 60, No. 4 (1956) 425-428.

46. Starkweather, H.W. "Clustering of water in polymers." *Journal of Polymer Science Part B – Polymer Letters*. Vol. 1, No. 3 (1963) 133-138.

47. van der Wel, G.K. and O.C.G. Adan. "Moisture in organic coatings – a review." *Progress in Organic Coatings*. Vol. 37, No. 1-2 (1999) 1-14.

48. Zhou, J. and J.P. Lucas. "Hygrothermal effects of epoxy resin. Part I: the nature of water in epoxy." *Polymer*. Vol. 40, No. 20 (1999) 5505-5512.

49. Karad, S. and F.R. Jones. "Mechanisms of moisture absorption by cyanate ester modified epoxy resin matrices: the clustering of water molecules." *Polymer*. Vol. 46, No. 8 (2005) 2732-2738.

50. DeIasi, R. and J.B. Whiteside. "Effect of Moisture on Epoxy Resins and Composites." *Advanced Composite Materials – Environmental Effects, ASTM STP 658*. J.R. Vinson, Ed. American Society for Testing and Materials (1978) 2-20.

51. Weitsman, Y.J. and Y.-J. Guo. "A correlation between fluid-induced damage and anomalous fluid sorption in polymeric composites." *Composites Science and Technology*. Vol. 62 (2002) 889-908.

52. Bascom, W.D. "Water at the Interface." *Journal of Adhesion.* Vol. 2 (1970) 161-183.

53. Michalske, T.A. and S.W. Freiman. "A molecular interpretation of stress corrosion in silica." *Nature*. Vol. 295 (1982) 511-512.

54. Michalske, T.A. and S.W. Freiman. "A Molecular Mechanism for Stress Corrosion in Vitreous Silica." *Journal of the American Ceramic Society*. Vol. 66, No. 4 (1983) 284-288.

55. Matthewson, M.J. and C.R. Kurkjian. "Environmental Effects on the Static Fatigue of Silica Optical Fiber." *Journal of the American Ceramic Society*. Vol. 71, No. 3 (1988) 177-183.

56. Schutte, C.L. "Environmental durability of glass-fiber composites." *Materials Science and Engineering*. Vol. R13 (1994) 265-234.

57. France, P.W., W.J. Duncam, D.J. Smith, and K.J. Beales. "Strength and fatigue of multicomponent optical glass fibers." *Journal of Materials Science*. Vol. 18 (1983) 785-792.

58. Shibata, S., S. Takahashi, S. Mitachi, and M. Yasu. "Strength of Multi-Component Glass Fibers." *Journal of Non-Crystalline Solids*. Vol. 43 (1981) 79-90.

59. Wiederhorn, S.M. "Influence of Water Vapor on Crack Propagation in Soda-Lime Glass." *Journal of the American Ceramic Society*. Vol. 50, No. 8 (1967) 407-414.

60. Schmitz, G.K. and A.G. Metcalfe. "Stress corrosion of E-glass fibers." *I&EC Product Research and Development*. Vol. 5, No. 1 (1966) 1-8.

61. Zhu, T., J. Li, X. Lin, and S. Yip. "Stress-dependent molecular pathways of silica-water reaction." *Journal of the Mechanics and Physics of Solids*. Vol. 53 (2005) 1597-1623.

62. Bando, Y., S. Ito, and M. Tomozawa. "Direct Observation of Crack Tip Geometry of SiO_2 Glass by High-Resolution Electron Microscopy." *Journal of the American Ceramic Society*. Vol. 67, No. 3 (1984) C36-C37.

63. Kurkjian, C.R., J.T. Krause, and U.C. Paek. "Tensile strength characteristics of 'perfect' silica fibers." *Journal de Physique*. Vol. C9 (1982) C9-585-586.

64. Armstrong, J.L., M.J. Matthewson, and C.R. Kurkjian. "Humidity Dependence of the Fatigue of High-Strength Silica Optical Fibers." *Journal of the American Ceramic Society*. Vol. 83, No. 12 (2000) 3100-3108.

65. Browning, C.E. "The Mechanisms of Elevated Temperature Property Losses in High Performance Structural Epoxy Resin Matrix Materials After Exposures to High Humidity Environments." *Polymer Engineering and Science*. Vol. 18, No. 1 (1978) 16-24.

66. Upadhyay, P.C., G.S. Gupta, and D.W. Lyons. "Plastic Deformation of Fiber Coating in Polymer Matrix Composites under Hygrothermal Loading." *Journal of Reinforced Plastics and Composites*. Vol. 18, No. 11 (1999) 985-1010.

67. Liao, K. and Y.-M. Tan. "Influence of moisture-induced stress on in situ fiber strength degradation of unidirectional polymer composite." *Composites: Part B*. Vol. 32 (2001) 365-370.

68. Aktas, L, Y.K. Hamidi, and M.C. Altan. "Combined Edge and Anisotropy Effects on Fickian Mass Diffusion in Polymer Composites." *Journal of Engineering Materials and Technology*. Vol. 126 (2004) 427-435.

69. Dewimille, B. and A.R. Bunsell. "The modeling of hydrothermal aging in glass fibre reinforced epoxy composites." *Journal of Physics D – Applied Physics*. Vol. 15, No. 10. (1982) 2079-2091.

70. Arvanitopoulos, C.D. and J.L. Koenig. "FT-IR Microspectroscopic Investigation of the Interphase of Epoxy Resin-Glass Fiber-Reinforced Composites." *Applied Spectroscopy*. Vol. 50, No. 1 (1996) 1-10.

71. Jensen, R.E., C.E. Johnson, and T.C. Ward. "Investigation of a Waterborne Epoxy for E-glass Composites." *Journal of Polymer Science: Part B: Polymer Physics*. Vol. 38 (2000) 2351-2365.

72. Lekatou, A. Faidi, S.E., D. Ghiaoui, S.B. Lyon, and R.C. Newman. "Effect of water and its activity on transport properties of glass/epoxy particulate composites." *Composites Part A*. Vol. 28A (1997) 223-236.

73. Dufresne, A. and C. Lacabanne. "Thermo-stimulated creep analysis on the effect of water in glass bead-reinforced composites." *Polymer*. Vol. 36, No. 23 (1995) 4417-4424.

74. Arvanitopoulos, C.D. and J.L. Koenig. "Infrared Spectral Imaging of the Interphase of Epoxy-Glass Fiber-Reinforced Composites under Wet Conditions." *Applied Spectroscopy*. Vol. 50, No. 1 (1996) 11-18.

75. Aktas, L., Y. Hamidi, M.C. Altan. "Effect of Moisture on the Mechanical Properties of Resin Transfer Molded Composites – Part I: Absorption." *Journal of Materials Processing & Manufacturing Science*. Vol. 10 (2002) 239-254.

76. Göpferich, A. "Mechanisms of polymer degradation and erosion." *Biomaterials*. Vol. 17 (1996) 103-114.

77. Göpferich, A. "Erosion of composite polymer matrices." *Biomaterials*. Vol. 18 (1997) 397-403.

78. von Burkersroda, F., L. Schedl, and A. Göpferich. "Why degradable polymers undergo surface erosion or bulk erosion." *Biomaterials*. Vol. 23 (2002) 4221-4231.

79. Lyu, S., R. Sparer, and D. Untereker. "Analytical Solutions to Mathematical Models of the Surface and Bulk Erosion of Solid Polymers." *Journal of Polymer Science: Part B: Polymer Physics*. Vol. 43 (2005) 383-397.

80. Brunauer, S. *Physical Adsorption of Gases and Vapors.* Oxford University Press: Princeton, N.J. (1945)

81. Tvardosvskiy, A.V. *Interface science and technology: Vol 13 Sorbent Deformation*. Elsevier: San Francisco, CA (2007).

82. Jost, W. *Diffusion in solids liquids, gases*. Academic Press Inc.: New York (1960).

83. Crank, J. *The Mathematics of Diffusion*. Oxford University Press: New York (1970).

84. Ponec, V., Z. Knor, and S. Černy. *Adsorption on Solids*. Butterworth & Co.: Toronto, 1974.

85. Clunie, J.S. and B.T. Ingram. "Adsorption of non-ionic surfactants." *Adsorption from Solution at the Solid/Liquid Interface*. G.D. Parfitt and C.H. Rochester, eds. Academic Press: San Diego, 1983.

86. Chin, J.W., T. Nguyen, K. Aouadi. "Sorption and Diffusion of Water, Salt Water, and Concrete pore Solution in Composite Matrices." *Journal of Applied Polymer Science*. Vol. 71 (1999) 483-492.

87. Beristain, C.I., H.S. Garcia, and E. Azuara. "Enthalpy-Entropy Compensation in Food Vapor Adsorption." *Journal of Food Engineering*. Vol. 30, No. 3-4 (1996) 405-415.

88. Toğrul, H. and N. Arslan. "Moisture Sorption Behavior and Thermodynamic Characteristics of Rice stored in a Chamber under Controlled Humidity." *Biosystems Engineering*. Vol. 95, No. 2 (2006) 181-195.

89. Brunauer, S., J. Skalny, and E.E. Bodor. "Adsorption on Nonporous Solids." *Journal of Colloid and Interface Science*. Vol. 30, No. 4 (1969) 546-552.

90. Hagymassy, J., S. Brunauer, and R.S. Mikhail. "Pore Structure Analysis by Water Vapor Adsorption, I. *t*-Curves for Water Vapor." *Journal of Colloid and Interface Science*. Vol. 29, No. 3 (1969) 485-491.

91. Gurtin, M.E. and C. Yamoti. "On a Model for Two Phase Diffusion in Composite Materials." *Journal of Composite Materials.* Vol. 13 (1979) 126-130.

92. Carter, H.G. and K.G Kibler. "Langmuir-Type Model for Anomalous Moisture Diffusion in Composite Resins." *Journal of Composite Materials.* Vol. 12 (1978) 118-131.

93. van Amerongen, G.J. "Diffusion in Elastomers." *Rubber Chemistry and Technology*. Vol. 37, No. 5 (1964) 1065-1152.

94. Weinmüller, C., C. Langel, F. Fornasiero, C.J. Radke, and J.M. Prausnitz. "Sorption kinetics and equilibrium uptake for water vapor in soft-contact-lens hydrogels." *Journal of Biomedical Materials Research Part A*. Vol. 77A, No.2 (2006) 230-241.

95. Doolittle, A.K and D.B. Doolittle. "Studies in Newtonian Flow. V. Further Verification of the free-Space Viscocity Equation." *Journal of Applied Physics*. Vol. 28, No. 8 (1957) 901-905.

96. Williams, M.L., R.F. Landel, and J.D. Ferry. "The Temperature Dependence of Relaxation Mechanisms in Amorphous Polymers and Other Glass-forming Liquids." *Journal of the American Chemical Society*. Vol. 77 (1955) 3701-3707.

97. Kelley, F.N. and F. Bueche. "Viscosity and Glass Temperature Relations for Polymer-Diluent Systems." *Journal of Polymer Science*. Vol. L (1961) 549-556.

98. Shen, C.H. and G.S. Springer. "Moisture Absorption and Desopriton of Composite Materials." *Journal of Composite Materials*. Vol. 10 (1976) 2-20.

99. McKague, E.L., J.D. Reynolds, and J.E. Halkias. "Swelling and Glass Transition Relations for Epoxy Matrix Material in Humid Environments." *Journal of Applied Polymer Science*. Vol. 22 (1978) 1643-1654.

100. von Schroeder, P. "Über Erstarrungs- und Quellungserscheinungen von Gelatine." *Zeritschrift für Physicalisch Chemie*. Vol. 45, No. 1 (1903) 75-117.

101. Choi, P. and R. Datta. "Sorption in Proton-Exchange Membranes: An Explanation of Schroeder's Paradox." *Journal of the Electrochemical Society*. Vol. 150, No. 12 (2003) E601-E607.

102. Onishi, L.M., J.M. Prausnitz, and J. Newman. "Water-Nafion Equilibria. Absence of Schroeder's Paradox" *J. Phys. Chem. B*. Vol. 111 (2007) 10166-10173.

103. Vallieres, C., D. Winkelmann, D. Roizard, E. Favre, P. Scharfer, and M. Kind. "On Schroeder's Paradox." *Journal of Membrand Science*. Vol. 278, No 1-2 (2006) 357-364.

104. Harper, J.F. and M. Naeem. "A comparative study of the effect of moisture absorption on the mechanical properties of glass fibre reinforced plastics." *Proceedings of the Third International Conference on Composite Interfaces.* H. Ishida, Ed. (1990) 801-808.

105. Bonniau, P. and A.R. Bunsell. "A Comparative Study of Water Absorption Theories Applied to Glass Epoxy Composites." *Journal of Composite Materials*. Vol. 15 (1981) 272-293.

106. Choi, H.S., K.J. Ahn, J.-D. Nam, and H.J. Chun. "Hygroscopic aspects of epoxy/carbon fiber composite laminates in aircraft environments." *Composites Part A*. Vol. 32 (2001) 709-720.

107. Goff, J.A. and S. Gratch. "Low-pressure properties of water from -160-212F." *Trans. Amer. Soc. Heat. Vent. Eng.* Vol. 52 (1946) 95-122.

108. Wexler, A. "Vapor Pressure Formulation for Water in Range 0 to 100°C. A Revision." *Journal of Research of the National Bureau of Standards—A. Physics and Chemistry*. Vol. 80A, No. 5 and 6. (1976) 775-785.

109. Buck, A.L. "New equations for computing vapor-pressure and enhancement factor." *Journal of Applied Meteorology*. Vol. 20, No. 12 (1981) 1527-1532.

110. Gibbins, C.J. "A survey and comparison of relationships for the determination of the saturation vapor-pressure over plane surfaces of pure water and of pure ice." *Annales Geophysicae*. Vol. 8, No. 12 (1990) 859-885.

111. Gueymard, C. "Assessment of the accuracy and computing speed of simplified saturation vapor equations using a new reference dataset." *Journal of Applied Meteorology*. Vol. 32 (1993) 1294-1300.

112. Sargent, G.P. "Computation of vapour pressure, dew-point and relative humidity from dry- and wet-bulb temperatures." *Meteorological Magazine*. Vol. 109 (1980) 238-246.

113. Alduchov, O.A. and R.E. Eskridge. "Improved Magnus Form Approximation of Saturation Vapor Pressure." *Journal of Applied Meteorology*. Vol. 35, No. 4 (1996) 601-609.

114. Lowe, P.R. "An Approximating Polynomial for the Computation of Saturation Vapor Pressure." *Journal of Applied Meteorology*. Vol. 16 (1977) 100-103.

115. Abbott, P.F. and R.C. Tabony. "The estimation of humidity parameters." *Meteorological Magazine*. Vol. 114 (1985) 49-56.

116. Lovell-Smith, J.W. and H. Pearson. "On the concept of relative humidity." *Institute of Physics Publishing*. Vol. 43, No. 1 (2006) 129-134.

117. Harrison, L.P. "Fundamental Concepts and Definitions Relating to Humidity" in *Humidity and Moisture: Measurement and Control in Science and Industry*. Vol. 3. eds, A. Wexler and W.A. Wildhack. (1963) 3-249.

118. Lawrence, M.G. "The Relationship between Relative Humidity and the Dewpoint Temperature in Moist Air: A Simple Conversion and Applications." *Bulletin of the American Meteorological Society*. Vol. 86, No. 2 (2005) 225-233.

119. Whitney, J.M. and C.E. Browning. "Some Anomalies Associated with Moisture Diffusion in Epoxy Matrix Composite Materials." *Advanced Composite Materials – Environmental Effects, ASTM STP 658*. J.R. Vinson, Ed., American Society for Testing and Materials (1978) 43-60.

120. Shirrell, C.D. "Diffusion of water Vapor in Graphite/Epoxy Composites." *Advanced Composite Materials—Environmental Effects*. ASTM STP 658. J.R. Vinson, Ed. American Society for Testing and Materials. (1978) 21-42.

121. Marshall, J.M., G.P. Marshall, and R.F. Pinzelli. "The Diffusion of Liquids Into Resins and Composites." *Polymer Composites*. Vol. 3, No. 3 (1982) 131-137.

122. Diamant, Y., G. Marom, and L.J. Broutman. "The Effect of Network Structure on Moisture Absorptoin of Epoxy Resins." *Journal of Applied Polymer Science*. Vol. 26 (1981) 3015-3025.

123. Karad, S.K., D. Attwood, and F.R. Jones. "Moisture Absorption by Cyanate Ester Modified Epoxy Resin Matrices. Part IV: Effect of Curing Scheules." *Polymer Composites*. Vol. 24, No. 4 (2003) 567-576.

124. Gupta, V.B., L.T. Drzal, and M.J. Rich. "The Physical Basis of Moisture Transport in a Cured Epoxy Resin System." *J. of Applied Polymer Science*. Vol. 30 (1985) 4467-4493.

125. Kumosa, L., B. Benedikt, D. Armentrout, and M. Kumosa. "Moisture absorption properties of unidirectional glass/polymer composites used in composite (non-ceramic) insulators." *Composites Part A*. Vol. 35 (2004) 1049-1063.

126. Aronhime, M.T., S. Neumann, and G. Marom. "The anisotropic diffusion of water in Kevlar-epoxy composites." *Journal of Materials Science*. Vol. 22 (1987) 2435-2446.

127. Roy, S., W.X. Xu, S.J. Park, and K.M. Liechti. "Anoalous Moisture Diffusion in Viscoelastic Polymers: Modeling and Testing." *Journal of Applied Mechanics*. Vol. 67 (2000) 391-396.

128. Celina, M., K.T. Gillen, and R.A. Assink. "Accelerated aging and lifetime prediction: Review of non-Arrhenius behavior due to two competing processes." *Polymer Degradation and Stability*. Vol. 90 (2005) 395-404.

129. Carslaw, H.S. and J.C. Jaeger. *Conduction of Heat in Solids*. 2nd ed. Oxford University Press: New York, 1959.

130. Brunauer, S., L.S. Deming, W.E. Deming, and E. Teller. "On a Theory of the van der Waals adsorption of Gases." *Journal of the American Chemistry Society*. Vol. 62 (1940) 1723-1732.

131. Loos, A.C. and G.S. Springer. "Moisture Absorption of Graphite-Epoxy Composites Immersed in Liquids and in Humid Air." *Journal of Composite Materials*. Vol. 13 (1979) 131-147.

132. Toth, J. "State equations of the solid-gas interface layers." *Acta Chmica Academiae Scientiarum Hungaricae*. Vol. 69, No. 3 (1971) 311-328.

133. Henry, D.C. "A Kinetic Theory of Adsorption." *Philosophical Magazine*. Vol. 44, No. 262 (1922) 689-705.

134. Verghese, K.N.E., M.D. Hayes, K. Garcia, C. Carrier, J. Wood, J.R. Riffle, and J.J. Lesko. "Influence of Matrix Chemistry on the Short Term, Hydrothermal Aging of Vinyl Ester Matrix and Composites under Both Isothermal and Thermal Spiking Conditions." *Journal of Composite Materials*. Vol. 33, No. 20 (1999) 1918-1938.

135. Barrer, R.M., J.A. Barrie, and J. Slater. "Sorption and Diffusion in Ethyl Cellulose. Part III: Comparison between Ethyl Cellulose and Rubber." *Journal of Polymer Science*. Vol. 27 (1958) 177-197.

136. Vieth, W.R., J.M. Howell, and J.H. Hsieh. "Dual Sorption Theory." *Journal of Membrane Science*. Vol. 1 (1976) 117-220.

137. Weitsman, Y.J. "Anomalous fluid sorption in polymeric composites and its relation to fluid-induced damage." *Composites: Part A*. Vol. 37 (2006) 617-623.

138. Maggana, C. and P. Pissis. "Water sorption and Diffusion Studies in an Epoxy Resin System." *J. of Polymer Science*. Vol. 37 (1999) 1165-1182.

139. Jacobs, P.M. and F.R. Jones. "Diffusion of moisture into two-phase polymers. Part 1." *Journal of Materials Science*. Vol. 24 (1989) 2331-2336.

140. Mikols, W.J., J.C. Seferis, A. Apicella, and L. Nicolais. "Evaluation of Structural Changes in Epoxy Systems by Moisture Sorption-Desorption and Dynamic Mechanical Studies." *Polymer Composites.* Vol. 3, No. 3 (1982) 118-124.

141. Glaskova, T.I., R.M. Guedes, J.J. Morais, and A.N. Aniskevich. "A comparative analysis of moisture transport models as applied to an epoxy binder." *Mechanis of Composite Materials*. Vol. 43, No. 4 (2007) 377-388

142. Popineau, S., C. Rondeau-Mouro, C. Sulpice-Gaillet, and M.E.R. Shanahan. "Free/bound water absorption in an epoxy adhesive." *Polymer*. Vol. 46 (2005) 10733-10740.

143. Li, Y., J. Miranda, H.-J. Sue. "Hygrothermal diffusion behavior in bismaleimide resin." *Polymer*. Vol. 42 (2001) 7791-7799.

144. Bao, L.-R., A.F. Yee, and C.Y.-C. Lee. "Moisture absorption and hygrothermal aging in a bismaleimide resin." *Polymer*. Vol. 42 (2001) 7327-7333.

145. Litherland, K.L., D.R. Oakley, and B.A. Proctor. "The use of accelerated ageing procedures to predict the long term strength of GRC composites." *Cement and Concrete Research*. Vol. 11 (1981) 455-466.

146. Phani, K.K., and N.R. Bose. "Temperature Dependence of Hydrothermal Ageing of CSM-Laminate During Water Immersion." *Composites Science and Technology*. Vol. 29 (1987) 79-87.

147. Wineman, A.S. and K.R. Rajagopal. *Mechanical Response of Polymers: An Introduction*. Cambridge University Press: New York, 2000.

148. Nakada, M., Y. Miyano, M. Kinoshita, R. Koga, T. Okuya, and R. Muki. "Time-Temperature Dependence of Tensile Strength of Unidirectional CRFP." *Journal of Composite Materials*. Vol. 36, No. 22 (2002) 2567-2581.

149. Fujieda, H. N. Sekine, M. Nakada, Y. Himano, A. Kiraishi, and S.W. Tsai. "Applicability of Time-Temperature-Water Absorption Suspterposition Principle for Flexural Strength of CFRP Laminates." *JSME International Journal Series A*. Vol. 46, No. 3 (2003) 467-472.

150. Kaelble, D.H., P.J. Dynes, and E.H. Cirlin. "Interfacial Bonding and Environmental Stability of Polymer Matrix Composites." *Journal of Adhesion*. Vol. 6 (1974) 23-48.

151. Phani, K.K. and N.R. Bose. "Hydrothermal ageing of CSM-laminate during water immersion – an acousto-ultrasonic study." *Journal of Materials Science*. Vol. 21 (1986) 3633-3637.

152. Halpin, J.C. and H.W. Polley. "Observations on the Fracture of Viscoelastic Bodies." *Journal of Composite Materials*. Vol. 1 (1967) 64-81.

153. Halpin, J.C., J.R. Kopf, and W. Goldberg. "Time Dependent Static Strength and Reliability for Composites." *Journal of Composite Materials*. Vol. 4 (1970) 461-474.

154. Purnell, P., N.R. Short, and C.L. Page. "A static fatigue model for the durability of glass fibre reinforced cement." *Journal of Materials Science*. Vol. 26 (2001) 5385-5390.

155. Barbero, E.J. and T.M. Damiani. "Phenomenological Prediction of tensile Strength of E-glass Composites." *Journal of Reinforced Plastics and Composites*. Vol. 22, No. 4 (2003) 373-394.

156. Gao, S.L., E. Maeder, A. Abdkader, and P. Offermann. "Environmental resistance and mechanical performance of alkali-resistant glass fibers with surface sizings." *Jounral of Non-Crystalline Solids*. Vol. 325 (2003) 230-241.

157. Brown, E.N., A.K. Davis, K.D. Jonnalagadda, and N.R. Sottos. "Effect of surface treatment on the hydrolytic stability of E-glass fiber bundle tensile strength." *Composites Science and Technology*. Vol. 65 (2005) 129-136.

158. Beltzer, A.I., M. Piau, and Y. Weitsman. "Note on the ineffective length of a fiber." *Mechanics of Materials*. Vol. 13, No. 4 (1992) 285-294.

159. McManus, H.L., B.J. Foch, and R.A. Cunningham. "Mechanism-Based Modeling of Long-Term Degradation." *Journal of Composites Technology & Research*. Vol. 22, No. 3 (2000) 146-152.

160. McManus, H.L. and C.C. Chamis. "Stress and Damage in Polymer Matrix Composite Materials Due to Material Degradation at High Temperatures." *NASA Technical Memorandum 4682*, January 1996.

161. Purnell, P. "Interpretation of climatic temperature variations for accelerated ageing models." *Journal of Materials Science*. Vol. 39 (2004) 113-118.

162. Jorgensen, G.J., H.M. Kim, and T.J. Wendelin. "Durability studies of solar reflector materials exposed to environmental stresses." *Durability testing of Nonmetallic*

Materials, ASTM STP 1294. R.J. Herling, Ed., American Society for Testing and Materials, 1996.

163. Jorgensen, G.J. "A Phenomenological Approach to Obtaining Correlations between Accelerated and Outdoor Exposure Test Results for Organic Materials." *Journal of Testing and Evaluation*. Vol. 32, No. 6 (2000) 494-499.

164. Minsker, K.S., S.V. Kolesov, and G.E. Zaikov. *Degradation and stabilization of vinyl chloride-based polymer*. Permagon Press, Inc.: New York, 1988.

165. White, J.R. and A. Turnbull. "Weathering of polymers: mechanisms of degradation and stabilization, testing strategies and modeling." *Journal of Materials Science*. Vol. 29 (1994) 584-613.

166. Fedor, G.R. and P.J. Brennan. "Comparison between natural weathering and fluorescent UV exposures: UVA-340 Lamp Test Results." *Durability Testing of Nonmetallic Materials, ASTM STP 1294*. R.J. Herling, Ed., American Society for Testing and Materials, 1996.

167. Nguyen, T., J. Martin, E. Byrd, and N. Embree. "Relating Laboratory and Outdoor Exposure of Coatings: II. Effects of Relative Humidity on Photodegradation and the Apparent Quantum Yield of Acrylic-Melamine Coatings." *Journal of Coatings Technology*. Vol. 74, No. 932 (2002) 65-80.

3. Materials and Experimental Procedure

3.1 Material Description

The material system under investigation is a pultruded unidirectional E-glass/vinyl-ester composite composed of a bisphenol-epoxy vinyl-ester resin (Reichhold, DION VER 9102) matrix with unidirectional single-end E-glass fibers (PPG 113Y). The composite system was fabricated by Glasforms, Inc. While most process parameters were considered proprietary, it was communicated that the speed of the pultrusion line was 91 cm/min, the die temperature was in the range of 120°C, and no post-cure was performed. Fiber volume fraction was determined to be 68% from burn-off testing, and the glass transition temperature, T_g, was 117°C as determined using dynamic mechanical thermal analysis (DMTA) with the three-point bending fixture in the transverse mode. The degradation temperature as determined from thermogravimetric analysis (TGA) was 415°C.

The nominal width and thickness of the as-received material were 100 mm and 1.36 mm, respectively. Four specimen sizes, provided in Table 2, were selected for tension, short beam shear (SBS), DMTA, and gravimetric observations according to ASTM specifications, as noted in Section 3.3.

Longitudinal tensile testing was executed in order to determine longitudinal tensile parameters used in composite design. While SBS testing is primarily used to determine the inter-laminar shear strength (ILSS) of a composite laminate, SBS testing

was executed to gain an understanding of the performance of the fiber/matrix bond in the monolayer pultruded composite under consideration.

Specimens were cut to size using a diamond wet saw and were finished by wet sanding all cut edges with 320 grit silicon carbide polishing paper. Samples were labeled prior to environmental exposure for purposes of identification.

Table 2. Nominal Specimen Dimensions. Nominal thickness is 1.36 mm.

Specimen Type	Longitudinal (mm)	Transverse (mm)
SBS	11	5
DMTA	10	35
Gravimetric (Moisture)	25.4	25.4
Tension	254	25.4

3.2 Environmental Conditions

It was the main goal of this research to gain a fundamental understanding of the synergistic mechanisms of degradation in a composite exposed to humid environments and to compare them to the mechanisms of degradation resulting from immersion in deionized water. To accomplish this task, sixteen static environments, including immersion in deionized water and humid air, were selected for the current investigation. Environments were labeled according to Table 3. The notation provided in Table 3 will be used throughout the following chapters. Temperatures were controlled to within ± 3°C and relative humidities were controlled within ± 5%RH.

Specimens were immersed in deionized water at four temperatures (20°C, 40°C, 60°C, 80°C) and exposed to three relative humidities (18%RH, 50%RH, 99%RH) at the lower three temperatures (20°C, 40°C, 60°C).

The three lower temperatures of immersion (20°C, 40°C, and 60°C) were selected to complement accelerated hot water immersion studies available in the literature [1-7]. A fourth temperature of immersion at 80°C was added to complement the lower exposures. The four 99%RH environments were selected in order to compare exposure to immersion in liquid water and exposure to high humidity environments. 18%RH and 50%RH were selected as the low and medium humidities so that the changes in material properties with exposure could be extended over a wide, distributed range of humidity.

Table 3. Environmental Conditions.
* 2A refers to ambient laboratory conditions.

Environment	Temperature (°C)	Relative Humidity	Immersion
2L	20	18%	-
2M	20	50%	-
2H	20	99%	-
2I	20	-	Immersion
4L	40	18%	-
4M	40	50%	-
4H	40	99%	-
4I	40	-	Immersion
6L	60	18%	-
6M	60	50%	-
6X	60	75%	-
6H	60	99%	-
6I	60	-	Immersion
8H	80	99%	-
8I	80	-	Immersion
2A*	Ambient (~20)	Ambient (~30%)	-

A fourth relative humidity (75%RH) was added several months after the initiation of the test program after observing that material properties were similar between sets exposed to 18%RH and 50%RH at a single temperature and between sets exposed to 99%RH and immersion at a single temperature. The 75%RH environment

at 60°C (6X) provided a link between distinct behaviors observed at lower and higher humidities. Similarly, a set exposed to 80°C at 99%RH (8H) was later added to complement immersion data. While it would have been preferable to include additional 75%RH environments, material availability limited additional environments to just two (6X, 8H) where the size and number of sets were also smaller than those tested in the other 14 environments.

99%RH high humidity environments (2H, 4H, 6H, 8H) were established by suspending specimens over deionized water at specified temperatures. Environmental chambers were used to establish environments 2L, 2M, 4L, 4M, 6L, 6M, 6X for the specified temperatures and humidities. Ambient conditions (2A) refer to ambient laboratory conditions of 20°C and 30%RH.

With the exception of material exposed to 2A, all specimens were pre-conditioned at 40°C, 18%RH for six weeks in order to remove any moisture present while minimizing post-cure and embrittlement. Samples were removed at specified intervals for testing, whereupon half of each set was tested immediately after environmental exposure (referred to as “Wet”), and the remaining half were post-conditioned for another six weeks at 40°C at 18%RH prior to testing (referred to as “Dry”). Specimens exposed to ambient conditions (2A) were tested in the as-received form without pre-conditioning or post-conditioning in order to monitor the material properties of the unexposed material.

3.3 Test Program

Specimens were cut according to Table 2 for tension, SBS, and DMTA testing. Gravimetric observations were made on all four specimen types in order to gain an understanding of how moisture uptake behaved differently in the same material between specimen sizes. Tensile tests were conducted to monitor the longitudinal tensile properties used in composite design, while SBS and DMTA tests provided insight into the performance of the matrix and interphase.

With the exception of three environmental conditions, all tests were performed after 12, 24, 36, 48, 72, and 96 weeks exposure. The three environmental conditions 2A, 6X, and 8H were added late in the test program and so results are report through 72 weeks only. Due to a shortage of material, tensile testing of 6X and 8H was not performed at 24 and 36 weeks.

3.3.1 Gravimetric Observations

All samples were weighed prior to pre-conditioning, exposure, testing, and post-conditioning. Specimens were removed from each environment and allowed to equilibrate to room temperature, until cool to the touch, prior to all weight measurements. Wet samples from high humidity and immersion environments were wiped dry with paper towel prior to weighing. Measurements were taken on a balance with resolution of 10^{-5} g. Weights were recorded after readings held for an audible five second count, with the exception of specimens exposed to 8H and 8I. The prominent wicking effect experienced by samples exposed to 8H and 8I resulted in unstable readings in ambient environments due to immediate evaporation of water

which had wicked along degraded interfaces. Therefore, "Wet" weights for highly degraded specimens were recorded at the first sign of stability in the balance reading. Gravimetric observations were made at 1 hr, 2 hr, 4 hr, 6 hr, 9 hr, 24 hr, 48 hr, 72 hr, 1 wk, 2 wk, 4 wk, 6 wk, 8 wk, 10 wk, 12 wk, 15 wk, 18 wk, 24 wk, 36 wk, 48 wk, 60 wk, 72 wk, and 96 wk.

3.3.2 Mechanical Testing

Longitudinal tensile properties were monitored with environmental exposure to provide information as to how the ingress of moisture affects design properties dominated by the fiber and interphase. Tensile testing was performed according to ASTM-D3039 with a crosshead speed of 2 mm/min in order to obtain longitudinal tensile modulus, strength, and failure strain. The tensile modulus was calculated using stresses and strains at 0.05% and 0.2%.

Short beam shear strengths were monitored in order to understand the effect of moisture on the matrix and interphase dominated SBS strengths. Short beam shear testing was performed in the longitudinal direction according to ASTM-D2344 using a span of 6.35 mm. The SBS setup did not allow for a span less than 6.35 mm, despite the recommendation of ASTM-D2344 to use a span four times the specimen thickness, which is 5.44 mm here. In order to avoid compression failure of the SBS specimen, a larger specimen size than is recommended by ASTM-D2344 was used with the available SBS setup with verification by previous work on the same material system.

3.3.3 Dynamic Mechanical Thermal Analysis

Dynamic Mechanical Thermal Analysis (DMTA) was conducted according to ASTM-E1640 as a complementary test to the mechanical SBS test in order to provide information on changes in the polymer structure and interphase. The composite was tested in the three-point bending setup with a 28 mm span, loading the transverse axis, where material properties are matrix dominated. Testing was performed at a frequency of 1 Hz and with a heating rate of 4°C/min between 20°C and 200°C. The glass transition temperature was selected using the tanδ peak height and the E" peak height. A detailed comparison of these results is presented in Section 6.2.2.

3.4 References

1. Bonniau, P. and A.R. Bunsell. "A Comparative Study of Water Absorption Theories Applied to Glass Epoxy Composites." *Journal of Composite Materials.* Vol. 15 (1981) 272-293.

2. Ghorbel, I. and D. Valentin. "Hydrothermal Effects on the Physio-Chemical Properties of Pure and Glass Fiber Reinforced Polyester and Vinylester Resins." *Polymer Composites*. Vol. 14, No. 4 (1993) 324-334.

3. Chin, J., K. Aouadi, and T. Nguyen. "Effects of Environmental Exposure on Fiber-Reinfoced Plastic (FRP) Materials Used in Construction." *Journal of Composites Technology & Research*. Vol. 19, No. 4 (1997) 205-213.

4. Karbhari, V.M. and S. Zhang. "E-Glass/Vinylester Composites in Aqueous Environments – I: Experimental Results." *Applied Composite Materials.* Vol. 10 (2003) 19-48.

5. Chu, W. and V.M. Karbhari. "Effect of Water Sorption of Performance of Pultruded E-Glass/Vinylester Composites." *Journal of Materials in Civil Engineering.* Vol. 17, No. 1 (2005) 63-71.

6. Xian, G. and V.M. Karbhari. "DMTA Based Investigation of Hygrothermal Ageing of an Epoxy System Used in Rehabilitation." *Journal of Applied Polymer Science*. Vol. 104 (2007) 1084-1094.

7. Helbling, C. and V.M. Karbhari. "Investigation of the Sorption and Tensile Response of Pultruded E-Glass/Vinylester Composites Subjected to Hygrothermal Exposure and Sustained Strain." *Journal of Reinforced Plastics and Composites*. Vol. 27, No. 6 (2008) 613-638.

4. Gravimetric Results

4.1 Overview

Gravimetric trends monitoring the weight change of a material over time allow for the interpretation of diffusion phenomena through the application of diffusion models. Knowledge of the process of water sorption in a polymer composite provides for an understanding of physical processes which occur as the water and constituent elements interact. For instance, gravimetric trends may reveal concentration driven diffusion profiles or physical relaxation of the polymer. Additionally, thermal effects can be investigated through the implementation of diffusion models on sorption trends, where activation energies may shed insight as to the physical processes responsible for changes in the polymer composite.

Where weight loss may occur, monitoring the weight of the composite with environmental exposure also allows for the identification of leaching of low molecular weight species (LMWS) or for the identification of severe material degradation. Severe degradation may be indicated by sudden weight gains, where wicking along interfaces may occur or by gradual weight loss where degraded material leaches into the surrounding environment more quickly that water sorbs into the bulk composite. Irreversible degradation may be identified through weight changes alone in these cases.

When considering the uptake of water in material exposed to humid air and liquid water, it is assumed that the only sorbing substance is water molecules. The

apparent moisture content at some time t, M_t, is calculated using the initial weight after pre-conditioning W_0 and the "wet" weight after environmental exposure W_w

$$M_t = \frac{W_w - W_0}{W_0} \times 100\% . \quad (1)$$

After reconditioning at 40°C and 18%RH for 6 weeks, a "dry" weight W_d is obtained where the difference between wet and dry weight reveals the actual amount of water sorbed. Where $W_d < W_0$, it is clear that the composite has degraded enough such that material has been lost to the surrounding environment. In aggressive environments, hydrolysis will result in the production of LMWS due to the degradation of the vinyl-ester polymer network, interphase, and fiber reinforcement. It is assumed that loss of degraded material occurs during environmental exposure and that post-conditioning drives out water molecules only. The adjusted moisture content $M_{t,a}$ can be defined as

$$M_{t,a} = \frac{W_w - W_d}{W_0} \times 100\% . \quad (2)$$

Because $W_d < W_0$ was observed only in material exposed to some 99%RH and immersion environments, adjusted moisture uptake will be used for gravimetric data resulting from exposure to these conditions only.

The following presents moisture uptake trends with a discussion of apparent sorption phenomena and degradation mechanisms. These effects are considered for all four specimen sizes defined in Section 3.1. Table 4 reviews the dimensions of the exposed specimens. Experimental data is considered with several diffusion models in order to shed light on the mechanisms responsible for changes in material properties.

These mechanisms may change depending on the temperature and water content of the environment. Activations energies are determined for diffusion coefficients of the Fickian and structural modification models, where the diffusion coefficient demonstrated a thermal dependency.

Table 4. Nominal specimen dimensions. Nominal thickness is 1.36 mm.

Specimen Type	Longitudinal (mm)	Transverse (mm)
SBS	11	5
DMTA	10	35
Gravimetric (Moisture)	25.4	25.4
Tension	254	25.4

4.2 Classification of Uptake Trends

Figure 8 summarizes possible four typical uptake trends (a-d) discussed in Section 2.4.1.3 and presents four additional trends (e-h) which were observed in this study. Uptake trends may be described as Fickian, Figure 8(a); two-stage, Figure 8(b); and anomalous, Figure 8(c). Trends may also indicate degradation, Figure 8(d), where degraded material may be lost at a greater rate than water was sorbed. Severe degradation indicated by dramatic increases in moisture content, introduced in Section 2.4.1.3 is not included in Figure 8 since this behavior was not observed in this study. Exposure to two environments resulted in two-stage sorption followed by indications of degradation, Figure 8(e). At medium humidities, initial linear uptake was observed, followed by a gradual increasing or decreasing trend or both, as depicted in Figure 8(f), (g), and (h). An increasing trend, Figure 8(f), indicates possible structural relaxation phenomena where once saturation of the material occurs, the water molecules which interrupt inter-chain hydrogen bonding allow for relaxation of the

polymer structure, where additional water may sorb into the structure. Conversely, a decreasing trend, Figure 8(g), may occur after an apparent saturation content, where it is possible that loss of residual LMWS may occur at a much slower rate than the uptake of water. A combination of these effects may be described by a hybridization of these gradual increases or decreases in moisture content, Figure 8(h).

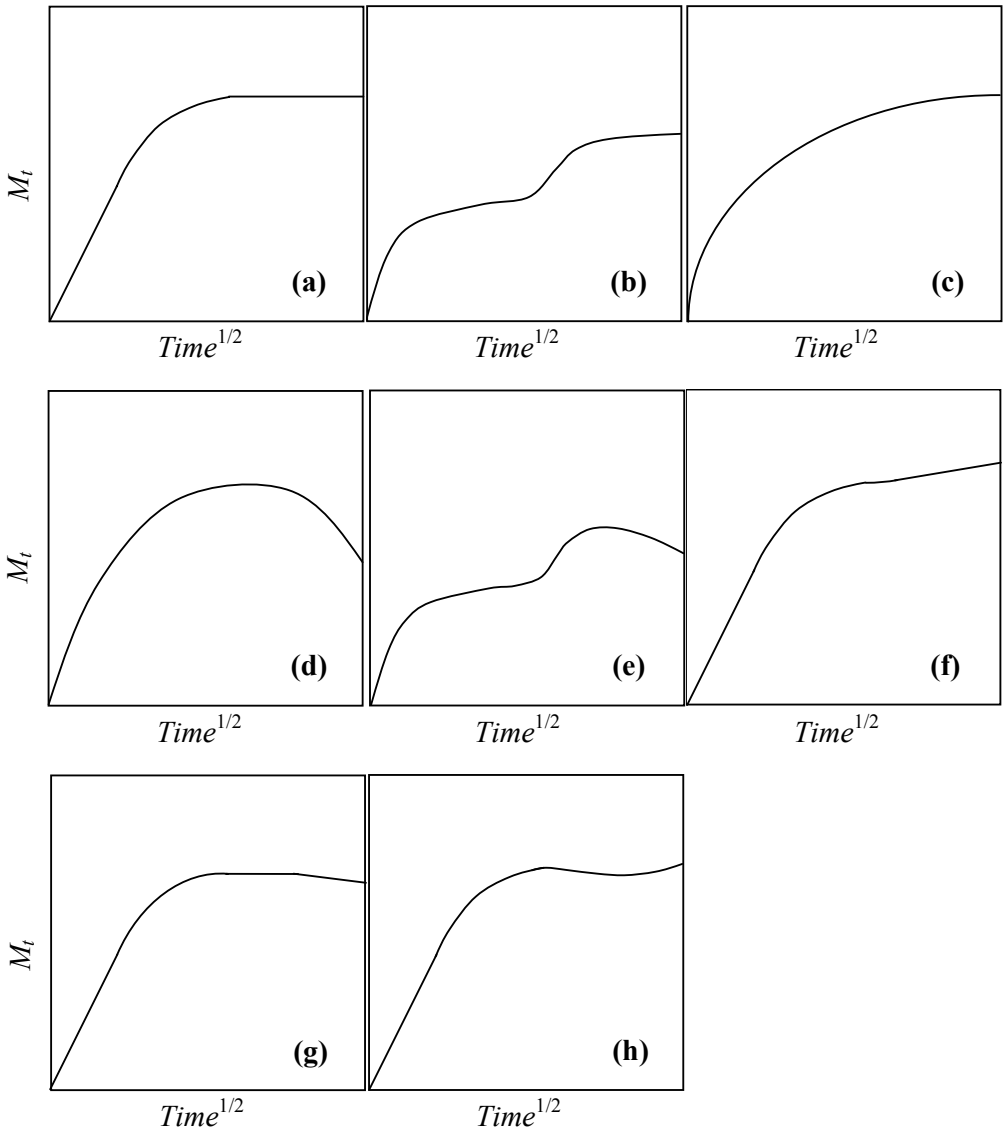

Figure 8. Stylized typical moisture uptake trends.
(a) Fickian; (b) two-stage; (c) anomalous; (d) indicative of degradation; (e) two-stage with indications of degradation; (f), (g), and (h) indicative of structural modification.

Table 5 provides a summary of the types of uptake curves observed after exposure to the 15 environments, excluding ambient conditions. Table 5 also addresses the differences between moisture trends which may occur in material exposed to a single environment where the four specimen sizes did not all demonstrate the same behavior.

Table 5. Characterization of apparent uptake trends for all specimen sizes. RH = Relative Humidity; Imm. = Immersion.

Environ.	Temp (°C)	RH	Imm.	SBS	DMTA	Moisture	Tension
2L	20	18%RH	—	c	c	c	e
4L	40	18%RH	—	c	c	c	c
6L	60	18%RH	—	c	c	c	e
2M	20	50%RH	—	a	a	a	a
4M	40	50%RH	—	f	f	f	f
6M	60	50%RH	—	h	h	h	h
6X	60	75%RH	—	g	g	g	a
2H	20	99%RH	—	c	c	c	b
4H	40	99%RH	—	c	c	c	c
6H	60	99%RH	—	e	b	b	c
8H	80	99%RH	—	d	d	d	c
2I	20	—	I	c	c	c	c
4I	40	—	I	c	c	c	c
6I	60	—	I	e	b	e	e
8I	80	—	I	d	d	d	d

Representative trends for moisture and tensile specimens exposed to 18%RH are presented in Figure 9 and Figure 10, respectively. Material exposed to 60°C at low humidity (18%RH) demonstrated weight loss in all material sizes, reflected by $M_t < 0$. The decrease in weight occurred after material pre-conditioned at 40°C and 18%RH was exposed to the same humidity at a higher temperature, indicating either that pre-conditioning did not remove all residual moisture or that exposure to this higher temperature resulted in a loss of LMWS such as styrene.

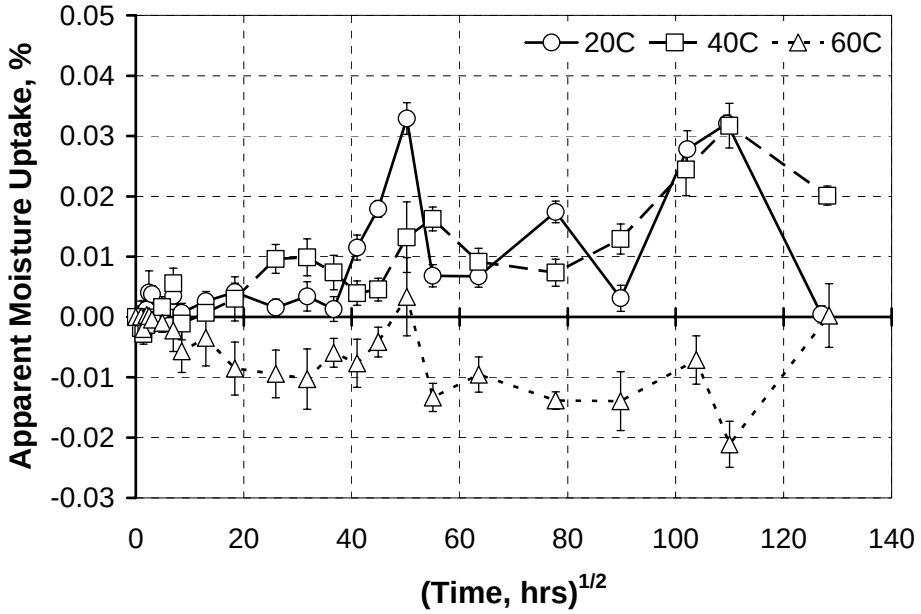

Figure 9. Moisture uptake trends for moisture specimens exposed to 18%RH. Error bars indicate standard deviations.

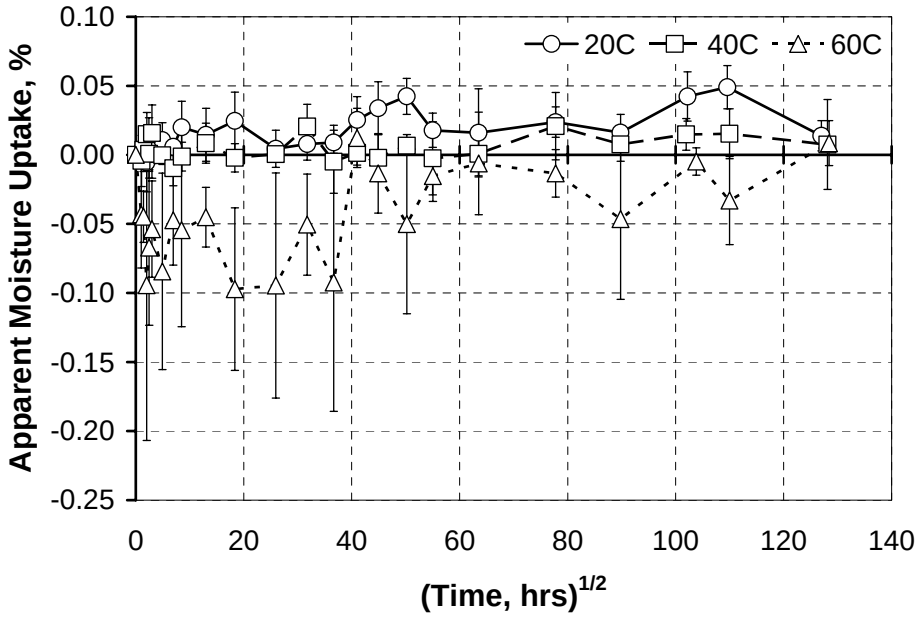

Figure 10. Moisture uptake trends for tensile specimens exposed to 18%RH. Error bars indicate standard deviations.

It was interesting to note that the weight loss was most pronounced for the tensile specimens, the largest specimens exposed. After the first twelve weeks of exposure to 18%RH at 60°C, there was a gradual increase in M_t such that M_t was less than but within scatter range of $M_t = 0$. These results indicate that it is possible that after initial desorption, the dry polymer network relaxed, allowing for subsequent uptake of water molecules. The trends for the three smaller specimens exposed to 18%RH at 60°C were well represented by the sorption trend in Figure 9, which depicts the sorption of the moisture specimens, illustrating a general trend of weight loss over 96 weeks exposure.

For all temperatures of exposure at 18%RH, the maximum moisture content M_{max} was greatest for the tensile specimens. The larger value of M_{max} for the tensile specimens is likely a consequence of the larger surface area of tensile specimens which allows for greater adsorption in these humid environments. While the longitudinal diffusion coefficient for composites has been observed to be greater than the transverse diffusion coefficient [1,2], the domination of through thickness diffusion implies that the rate of sorption, described by Fick's second law, is not affected by the competing flux in other directions. Therefore, where desorption occurs, the sorbate may more readily exit in the transverse direction. Similarly, where uptake occurs, the sorption of water in the fiber direction will result in a longer time to equilibrium since the longitudinal direction is much larger.

The slower rate of diffusion in tensile specimens is exhibited in material exposed to 50%RH when comparing uptake in moisture specimens, shown in Figure

11, to that in tensile specimens, shown in Figure 12. Exposure to 50%RH at 20°C demonstrates Fickian behavior where the initial uptake is linear and after about 12 weeks (45 $hr^{1/2}$) M_t hovers about an apparent equilibrium. M_t after 12 weeks most represents an asymptote in tensile specimens. Sorption in SBS specimens is presented in Figure 13 where it can be seen that M_t trends are more erratic, despite similarity to overall sorption trends for all other specimen sizes. Figure 11 through Figure 14 are presented with similar scales so that the trends can be directly compared with one another.

Exposure to 50%RH at 40°C results in a pseudo-equilibrium for all moisture specimens at approximately 6 weeks (32 $hr^{1/2}$). The moisture uptake trend of DMTA specimens closely represents that of moisture specimens where the main difference between the two curves is that M_t for DMTA specimens at any time is less than that of moisture specimens. A pseudo-equilibrium can also be detected for SBS uptake trends at about 6 weeks (32 $hr^{1/2}$) for the 40°C exposure at 50%RH, after which there is a gradual steady increase in M_t. Before 6 weeks, however, SBS specimens appear to experience a sudden uptake at 2 weeks (18 $hr^{1/2}$) which does not occur in an y other specimen size. Because SBS specimens are just 5 mm wide and because a roving of glass fiber is generally less than 5 mm wide, SBS specimens may not provide a representative unit cell of the bulk pultruded material. Rather, the more erratic behavior could be a result of measurements which are made on specimens which are more heterogeneous than larger specimens which are at least 5 times wider than SBS specimens.

Tensile specimens take approximately 15 weeks (50 $hr^{1/2}$) to reach pseudo-equilibrium, which is longer than the three smaller specimens exposed to the same environment of 50%RH at 40°C. This longer time is expected since the apparent diffusion coefficient for tensile specimens is expected to be the lowest of all sizes, as indicated by Equation 22 in Section 2.4.1.1.2. All material exposed to 50%RH at 40°C demonstrate a pseudo-equilibrium, though the time to reach this level may vary depending on specimen size. After this pseudo-equilibrium there is a steady increase in M_t for all specimen sizes, indicating a possible relaxation of the polymer which would allow for greater moisture sorption with time.

At 60°C in 50%RH, a pseudo-equilibrium can be identified at about 6 weeks (32 $hr^{1/2}$) in all specimens, as shown in Figure 11 through Figure 13. After reaching this pseudo-equilibrium, moisture and DMTA specimens show a slight decrease in M_t, followed by a subsequent gradual weight gain, as seen in Figure 14. Similar to results from 40°C at 50%RH, the uptake trend of DMTA specimens represents that of moisture specimens closely, where the magnitude of M_t is consistently less for DMTA specimens. Again, the moisture sorption trend of SBS specimens is less smooth than for moisture and DMTA specimens. The scatter in M_t measurements is also higher for the smallest specimen size than for moisture and DMTA specimens. While a pseudo-equilibrium can be identified for SBS specimens around 6 weeks, no consistent increase or decrease can be distinguished thereafter.

The uptake in tensile specimens exposed to 50%RH at 60°C demonstrates a gradual increase in Mt after pseudo-equilibrium, indicating polymer relaxation similar

to that which occurs at late times in moisture and DMTA specimens exposed to the same environment and in material exposed to 50%RH at 40°C. However, the relaxation in 60°C appears to be less than that occurring in 40°C at the same humidity. Exposure to 60°C results in a stiffer polymer network than exposure to 40°C does, reflected by increases in T_g to be discussed in Section 6.2.2.1, so the polymer may not relax as readily in the presence of water at a higher temperature of exposure. Moisture sorption trends in moisture and DMTA specimens reveal competing mechanisms are responsible for weight changes. These mechanisms include water sorption, loss of LMWS, and polymer relaxation. Exposure to 18%RH at 60°C indicates that weight loss is most rapid for tensile specimens, so it would be expected that leaching of LMWS would not be detected after pseudo-equilibrium in tensile specimens.

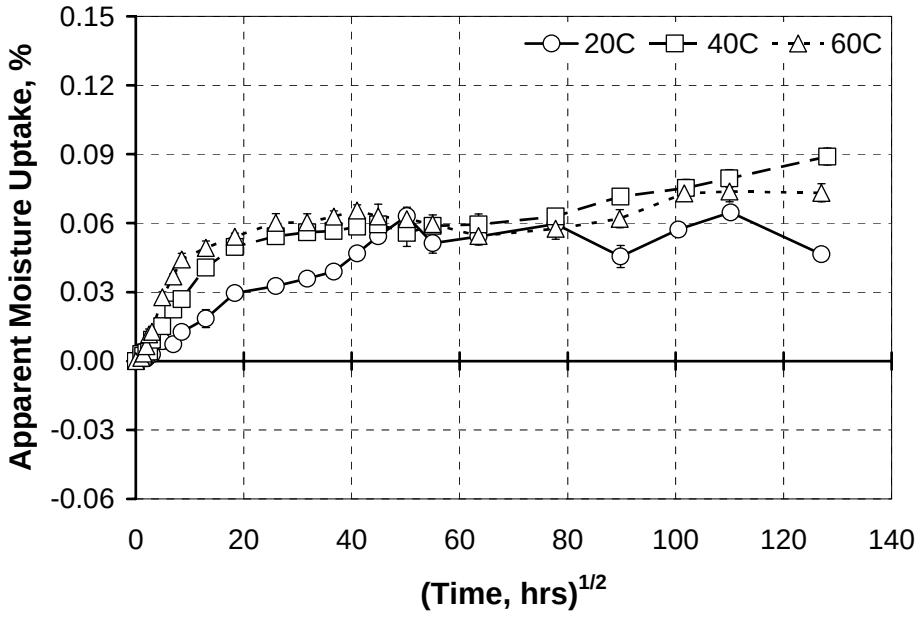

Figure 11. Moisture uptake trends for moisture specimens exposed to 50%RH. Scale selected to allow for direct comparison of 50%RH gravimetric trends. Error bars indicate standard deviations.

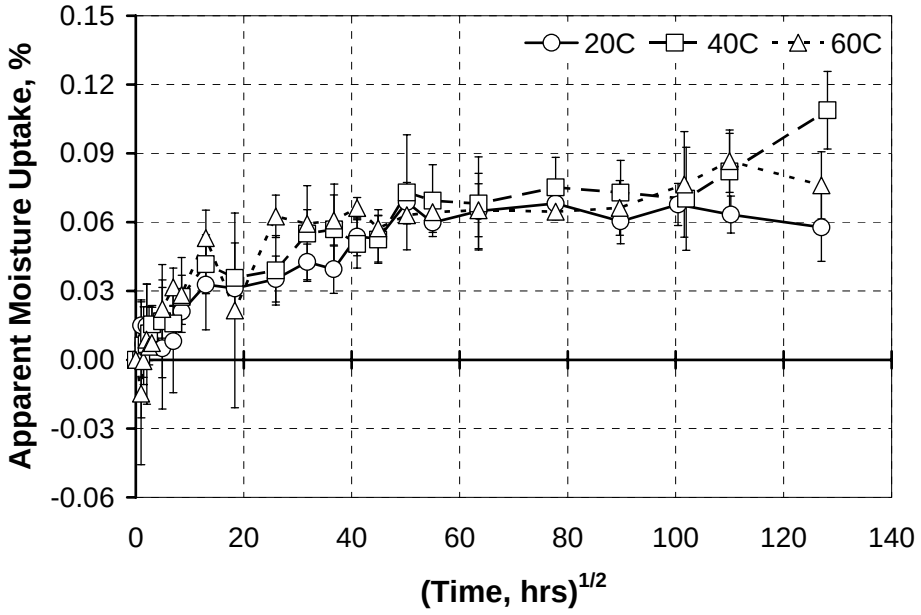

Figure 12. Moisture uptake trends for tensile specimens exposed to 50%RH. Scale selected to allow for direct comparison of 50%RH gravimetric trends. Error bars indicate standard deviations.

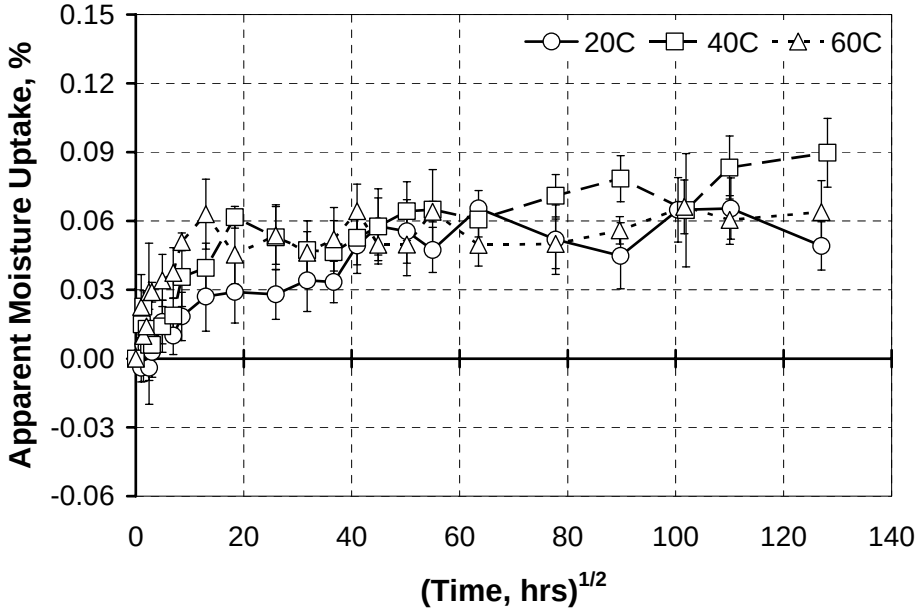

Figure 13. Moisture uptake trends for SBS specimens exposed to 50%RH. Scale selected to allow for direct comparison of 50%RH gravimetric trends. Error bars indicate standard deviations.

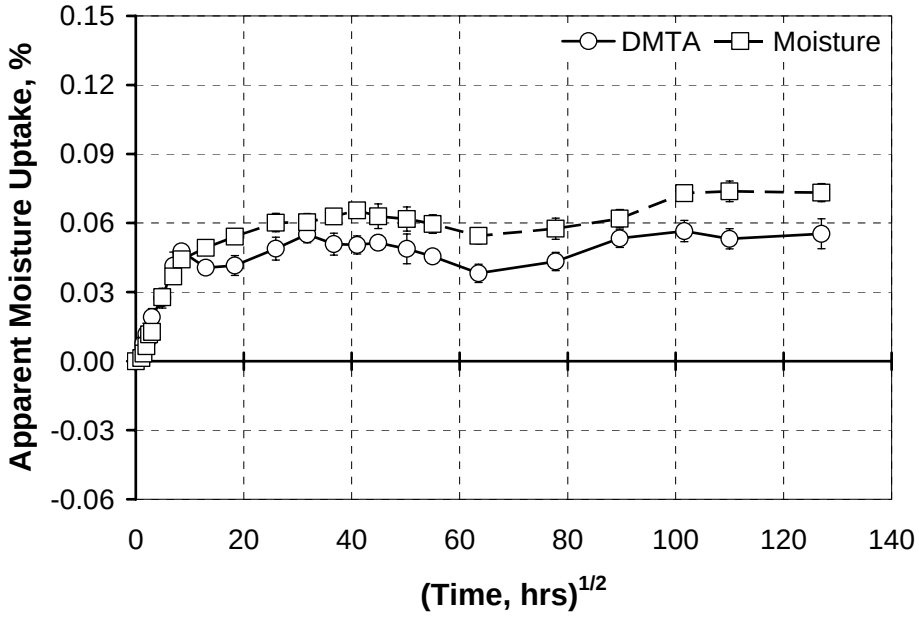

Figure 14. Moisture uptake trends for DMTA and moisture specimens exposed to 50%RH at 60°C. Scale selected to allow for direct comparison of 50%RH gravimetric trends. Error bars indicate standard deviations.

Similarly, material exposed to 75%RH at 60°C shows varying behavior depending on size, as shown in Figure 15 and Figure 16. Again DMTA specimens demonstrate sorption behavior which closely resembles that of moisture specimens. However, after about 2 weeks (18 $hr^{1/2}$) DMTA specimens exhibit weight loss, possibly due to leaching of LMWS while the larger moisture specimens indicate slight polymer relaxation at early times followed by a slight decrease in weight. Tensile specimens exhibit Fickian diffusion, as seen in Figure 16. It is possible that the leaching of LMWS and polymer relaxation, seen in material exposed to 60°C at 50%RH, complete with the moisture sorption such that no definitive net uptake or loss is seen after 8 weeks (37 $hr^{1/2}$). Again, SBS specimens show high scatter, but a general decrease in M_t can be observed after about 10 weeks (41 $hr^{1/2}$), as seen in

Figure 16. These results indicate that for 75%RH at 60°C, possible leaching is greater for smaller specimens, where it may be easier for LMWS to exit the material from the center of the specimen. Leaching could not be identified in tensile specimens. It may be that leaching is so quick that it cannot be detected before equilibrium is reached. This conclusion, while supported by 18%RH gravimetric trends, is in contrast to the weight loss detected in the 75%RH environment after reaching pseudo-equilibrium which is decreases in magnitude for larger specimens.

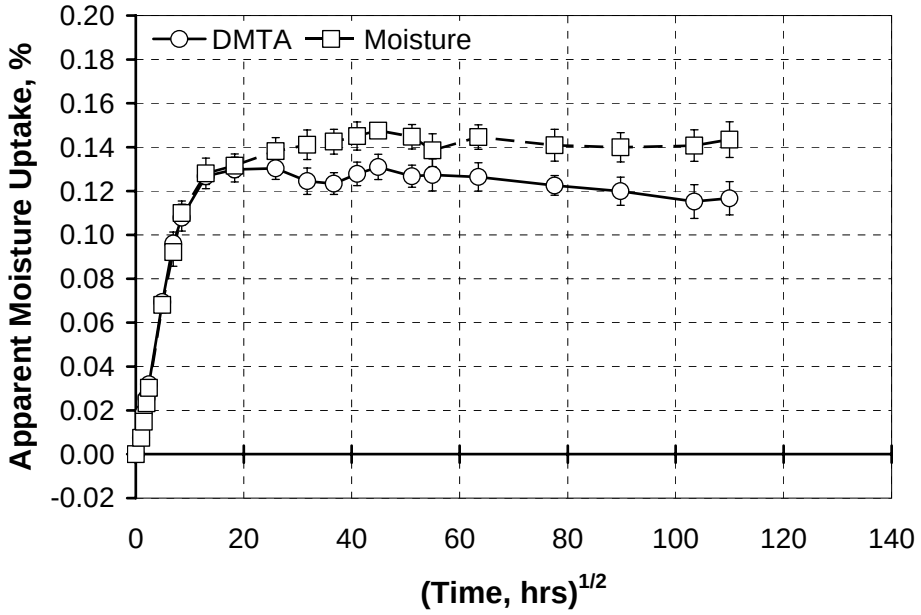

Figure 15. Moisture uptake trends for DMTA and moisture specimens exposed to 75%RH at 60°C. Scale selected to allow for direct comparison of 75 %RH gravimetric trends. Error bars indicate standard deviations.

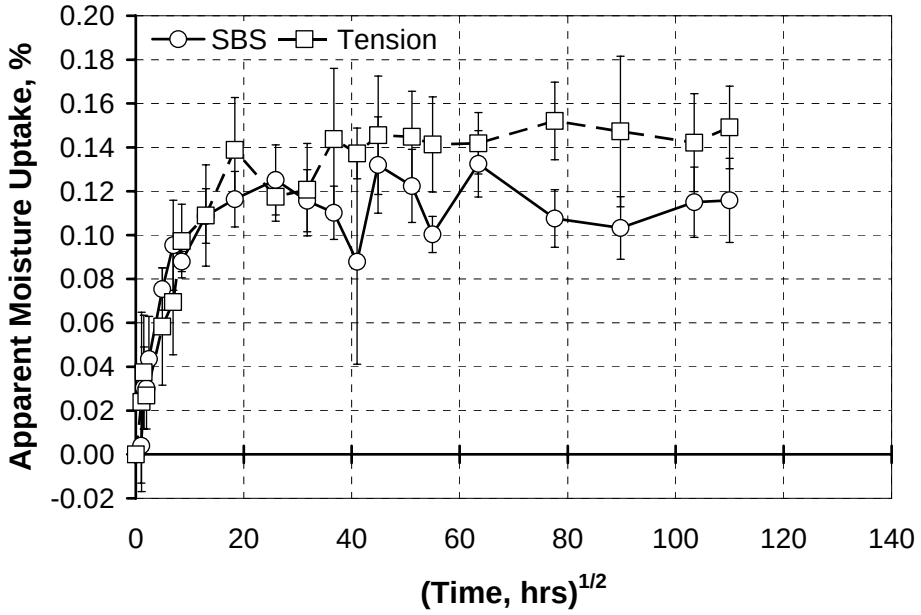

Figure 16. Moisture uptake trends for SBS and tensile specimens exposed to 75%RH at 60°C. Scale selected to allow for direct comparison of 75 %RH gravimetric trends. Error bars indicate standard deviations.

Exposure to 20°C and 40°C in 99%RH and water immersion resulted in anomalous moisture uptake trends for all specimen sizes. Representative moisture uptake trends are presented in Figure 17. The non-linearity of the entire curve reveals non-Fickian behavior with continual moisture uptake. Exposure to 99%RH and immersion at 60°C resulted in initial anomalous behavior with a sharp uptake in moisture content between 18 and 24 weeks (55 and 63 $hr^{1/2}$), illustrating two-stage moisture sorption, as shown in Figure 18 and Figure 19.

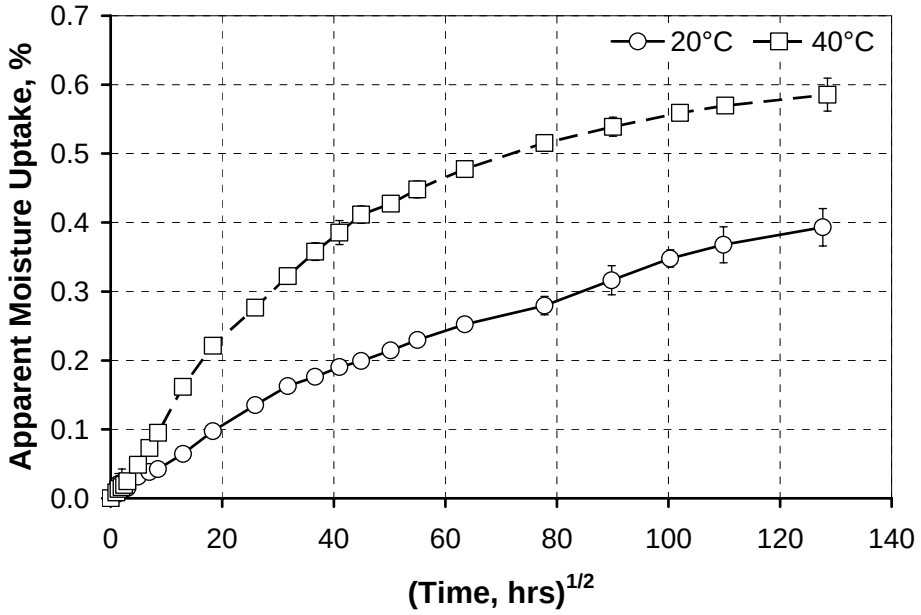

Figure 17. Moisture uptake trends for moisture specimens exposed to immersion at 20°C and 40°C. Error bars indicate standard deviations.

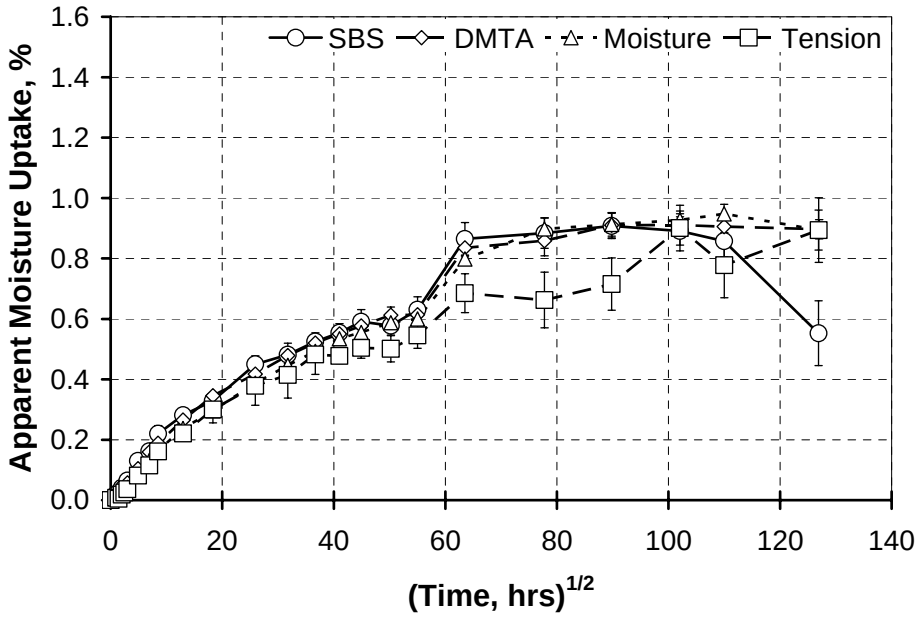

Figure 18. Apparent moisture uptake trends for material exposed for 60°C at 99%RH. Error bars indicate standard deviations.

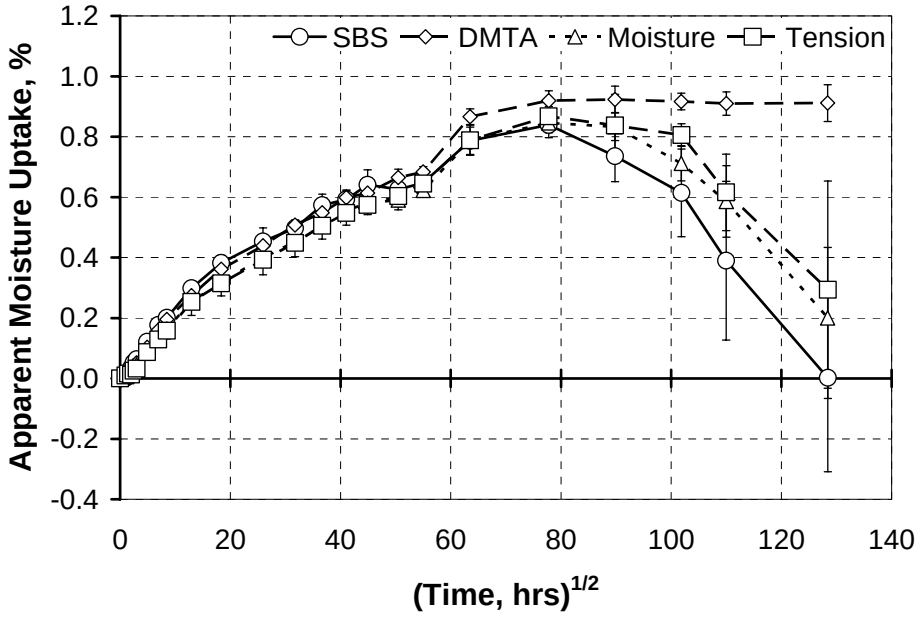

Figure 19. Apparent moisture uptake trends for material exposed for 60°C immersion. Error bars indicate standard deviations.

After exposure to 99%RH at 60°C, two-stage sorption is not obvious in the gravimetric trend of tensile specimens alone. There is a spike between 18 and 24 weeks which could be interpreted as an indication of the second stage of sorption using evidence from sorption trends for smaller specimens. However, tensile specimens exposed to liquid water at the same temperature clearly demonstrate two-stage sorption.

In the case of 99%RH exposure at 60°C, loss of degraded material is observed in SBS specimens only while exposure to 60°C water immersion reveals weight loss in SBS, moisture, and tensile specimens. In 99%RH, leaching is likely to occur as degraded material desorbs into water condensed on the composite surface. For smaller specimens, these droplets may coalesce to form a film which will produce a greater area of contact between liquid water and the composite, allowing for greater leaching.

SBS specimens are the only ones to demonstrate weight loss in 99%RH at 60°C, as expected. Leaching from material exposed to 99%RH at 80°C also demonstrates this same behavior where the weight loss increases with decreasing specimen size, as shown in Figure 20. Exposure to 99%RH and immersion at 80°C results in gravimetric trends indicative of material degradation for all specimen sizes.

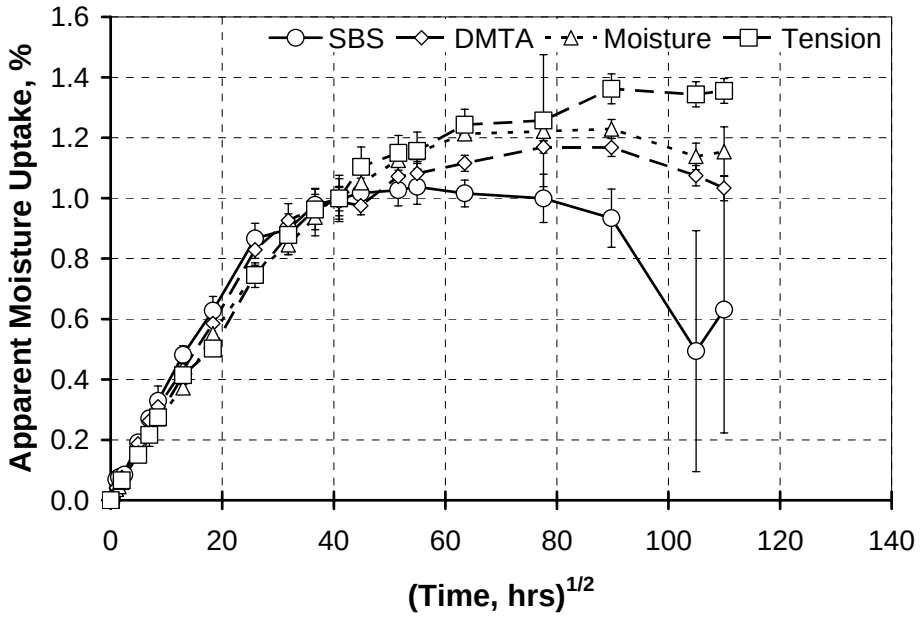

Figure 20. Apparent moisture uptake trends for material exposed for 80°C at 99%RH. Error bars indicate standard deviations.

DMTA specimens do not reveal significant degradation in immersion at 60°C, as shown in Figure 19, and indicate a delayed onset of degradation for immersion at 80°C. This effect is a direct consequence of the fact that while moisture specimens were immersed in water resting loosely in polypropylene racks, DMTA specimens were exposed in punctured polyethylene bags. Similar to SBS specimens, the degraded material produced in moisture specimens was more readily leached out into the surrounding liquid medium. Consequently, the relative volume available for

uptake of water is increased, the effects of hydrolysis are aggravated, and more degraded material is leached out. While degraded material produced in DMTA specimens immersed in water do leach out into the surrounding water, as indicated by $W_d < W_0$, the weight loss is not as dramatic as specimens immersed loosely.

4.3 Maximum Moisture Content

Table 6 presents a summary of the maximum observed apparent moisture contents, M_{max}, for all specimen sizes in all environments. The maximum moisture content tends to increase with temperature for each humidity condition except 50%RH. At 18%RH, the composite loses weight, indicating loss of residual moisture not removed after preconditioning for 6 weeks in 18%RH at 40°C. That is, the mechanism responsible for weight change in 60°C is distinct from the moisture uptake seen for lower temperatures at the same humidity, as discussed in the previous section. Similarly, the lower M_{max} for 60°C at 50%RH is indicative of a loss of residual LMWS after initial uptake of water in the humid environment. Relaxation of the polymer in 40°C and 50%RH allows for greater moisture uptake not seen at the lower temperature of exposure at 20°C.

It is worth noting that M_{max} for DMTA species exposed to immersion environments at 60°C and 80°C are greater than other specimen sizes. Because the DMTA specimens were immersed in polyethylene bags, it is possible that the diffusion of degraded species out of the bulk material was hindered by the film. While holes in the bags allowed water to flow in and out, the movement of water around the specimens in the bags was likely much less than around those specimens immersed

freely in the liquid water, resulting in lesser weight loss of degraded material from DMTA specimens.

Table 6. Maximum apparent moisture content (%) for all specimen sizes. Brackets indicate standard deviations.

Env.	SBS	DMTA	Moisture	Tension
2L	0.0404 [0.0124]	0.0309 [0.0022]	0.0329 [0.0026]	0.0490 [0.0156]
4L	0.0458 [0.0275]	0.0147 [0.0087]	0.0317 [0.0037]	0.0208 [0.0244]
6L	-0.0246 [0.0091]	-0.0363 [0.0080]	-0.0211 [0.0038]	-0.0972 [0.0588]
2M	0.0655 [0.0078]	0.0614 [0.0060]	0.0647 [0.0019]	0.0687 [0.0086]
4M	0.0897 [0.0150]	0.0798 [0.0043]	0.0890 [0.0037]	0.1088 [0.0169]
6M	0.0662 [0.0117]	0.0565 [0.0047]	0.0738 [0.0045]	0.0866 [0.0136]
6X	0.1325 [0.0151]	0.1310 [0.0058]	0.1475 [0.0032]	0.1521 [0.0177]
2H	0.3636 [0.0244]	0.2312 [0.0090]	0.2688 [0.0156]	0.2899 [0.0140]
4H	0.7320 [0.0256]	0.7003 [0.0315]	0.6658 [0.0275]	0.5198 [0.0483]
6H	0.9076 [0.0419]	0.9103 [0.0374]	0.9481 [0.0310]	0.9007 [0.0757]
8H	1.0376 [0.0582]	1.1690 [0.0199]	1.2288 [0.0317]	1.3616 [0.0496]
2I	0.4426 [0.0319]	0.4834 [0.0276]	0.3932 [0.0271]	0.3725 [0.0333]
4I	0.6823 [0.0487]	0.7121 [0.0162]	0.5856 [0.0239]	0.6042 [0.0315]
6I	0.8388 [0.0421]	0.9235 [0.0437]	0.8455 [0.0327]	0.8675 [0.0326]
8I	0.8432 [0.0415]	1.0796 [0.0533]	0.9983 [0.0661]	0.9896 [0.1102]

Table 7 presents maximum adjusted moisture contents for material exposed to 99%RH and immersion environments. Exposure to 99%RH at 20°C for 96 weeks did not result in any weight loss, so no adjusted moisture content is reported. Only the smaller SBS and DMTA specimens exposed to 99%RH at 40°C and immersion at 20°C experienced weight loss. There was no statistically significant weight loss after redrying in gravimetric and tensile specimens exposed to 99%RH at 40°C and immersion at 20°C. Standard deviations reported in Table 7 are the largest standard deviation of the wet or dry set. The high scatter reported for material exposed to 80°C immersion is a consequence of unstable readings due to immediate evaporation of water from the highly degraded material, as discussed in Section 3.2.1. The errors

were especially high for tension samples exposed to 80°C immersion since the large surface area of these specimens allowed for more wicking.

Table 7. Maximum adjusted moisture content (%) for sets experiencing weight loss. Brackets indicate standard deviations.

Env.	SBS	DMTA	Gravimetric	Tension
4H	0.7579 [0.0256]	0.7046 [0.0315]	—	—
6H	1.0364 [0.0524]	1.0582 [0.0603]	1.0156 [0.0310]	0.9152 [0.1067]
8H	1.3621 [0.0800]	1.4477 [0.0300]	1.4675 [0.0317]	1.5289 [0.0496]
2I	0.5046 [0.0319]	0.5009 [0.0276]	—	—
4I	0.7599 [0.0494]	0.7336 [0.0162]	0.7081 [0.0239]	0.6674 [0.0315]
6I	1.0963 [0.3310]	1.0515 [0.0388]	1.0445 [0.2330]	0.9932 [0.1100]
8I	1.3440 [0.5238]	1.3930 [0.1211]	1.8119 [0.5905]	2.2638 [1.4956]

4.3.1 Effect of Specimen Size on Maximum Moisture Content

Apparent M_{max} value for 20°C, 40°C, and 60°C indicate a general decreasing trend with increasing size while material exposed to 80°C appears to sorb more water in larger specimens. When compared to unexposed material in Figure 21 and Figure 22, scanning electron microscopy reveals severe interfacial degradation and surface erosion in material exposed to 80°C, shown in Figure 23 and Figure 24.

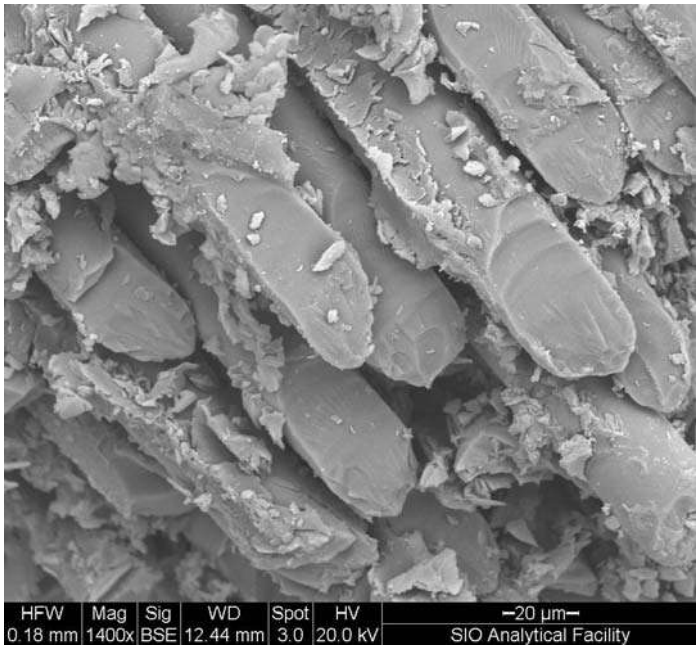

Figure 21. SEM of unexposed failed tensile specimen.

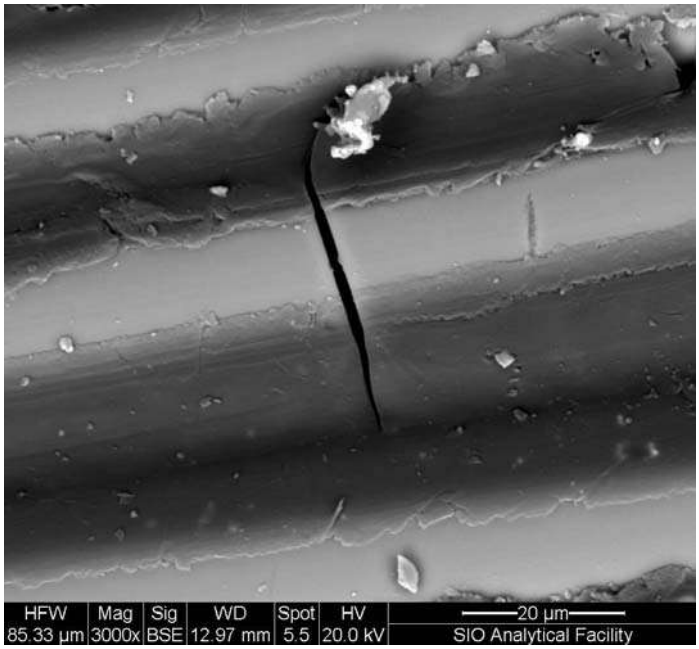

Figure 22. SEM of surface of unexposed failed tensile specimen. Fiber fracture is attributed to tensile failure during tensile testing.

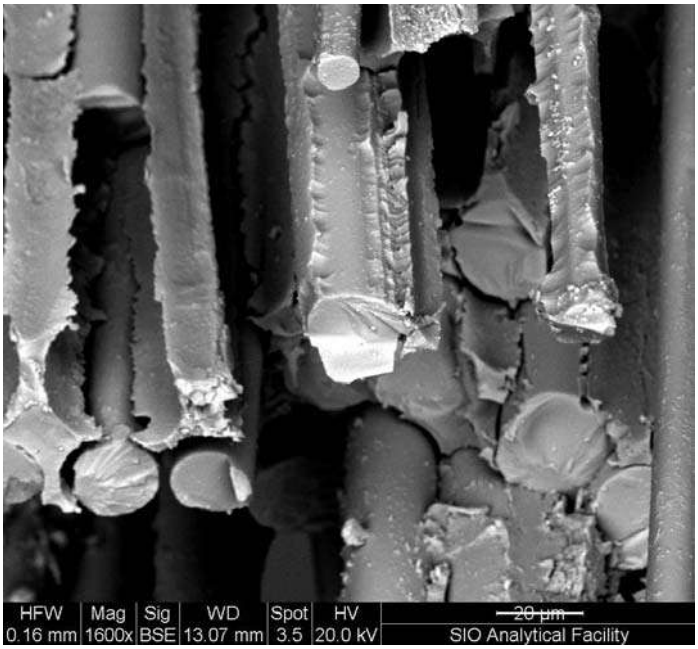

Figure 23. SEM of failed tensile specimen exposed to 80°C immersion for 72 weeks.

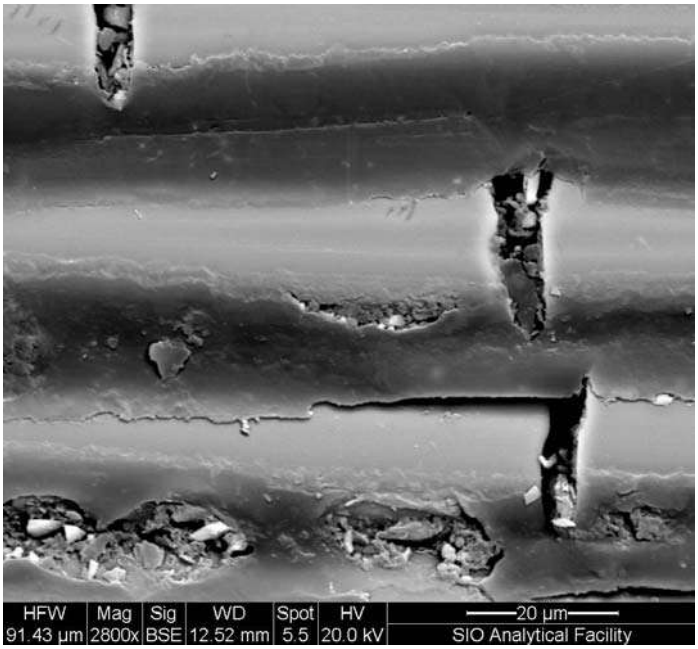

Figure 24. SEM of surface of moisture specimen exposed to 80°C immersion for 12 weeks.
Fiber failure is attributed to stress corrosion cracking.
No mechanical testing was performed on this specimen.

While thin surface layers of polymer resin above the glass fiber do no appear to be present prior to environmental exposure, as seen in Figure 22, the resin rich areas apparent in Figure 24 reveal polymer matrix degradation and loss. It appears that particulate matter is present in these voids formed in resin rich areas, possibly contributing to or aggravating polymer degradation. The fiber failure in Figure 21, Figure 22, and Figure 23 is attributed to tensile failure since material investigated in those three micrographs were all removed from failed tensile specimens. The material investigated for Figure 24 was a gravimetric specimen which was not mechanically tested. Stress corrosion cracking of the fiber such as that seen in Figure 24 is also visible on the surface of untested material which has been exposed to lower temperatures of immersion for less time.

In the vicinity of the fiber fracture in Figure 24, an interphasial debond, about 40 μm in length, can be identified, whereas unexposed material does not reveal significant interfacial debonding even after tensile testing and failure, as seen in Figure 21 and Figure 22. Interphasial degradation can be identified around glass fibers in exposed material tested to failure in tension where fiber failure has occurred with minimal damage to the surrounding polymer matrix. This material degradation allows for wicking which will be more prominent in larger specimens with greater surface area, evidenced by greater values of M_{max}.

Below 80°C, tensile specimens consistently indicate the lowest M_{max}. However, because larger composite specimens will have lower apparent diffusion

coefficients, it is expected that the larger specimens will have lower moisture content, even at large times [1].

4.3.2 Isotherms

An isotherm can be developed for each temperature by plotting M_{max} against partial pressure, e/e_s or p/p_o. Figure 25 presents isotherms for gravimetric specimens. It is clear from Figure 25 that the material follows a Brunauer-Emmett-Teller (BET) Type III isotherm, introduced in Section 2.4.1.2. Consequently, neither Henry's Law nor Dual Sorption Theory can apply, and Freundlich's Relation is employed after

$$M_\infty = a\left(\frac{\%RH}{100\%}\right)^b . \tag{3}$$

A summary of a and b values is presented in Table 8. Values for 80°C are not provided since there was only one humid environment at 80°C. It is clear from Table 7 and Table 8 that Freundlich's relation underestimates M_{max} at 99%RH.

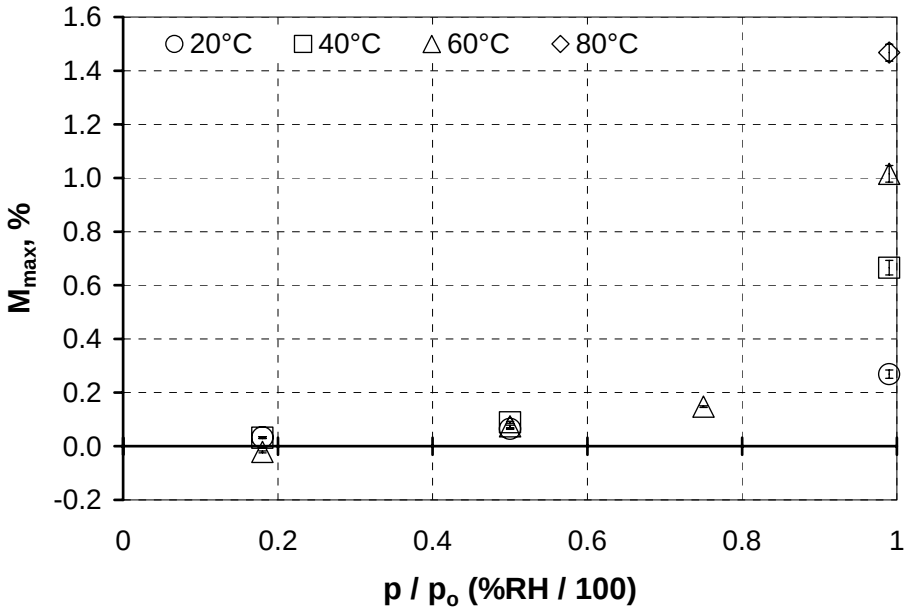

Figure 25. Isotherm for moisture specimens.
Adjusted M_{max} used where applicable.
Error bars indicate standard deviations.

Table 8. Parameters for Freundlich's Relation.

Temp	SBS		DMTA		Gravimetric		Tension	
(°C)	*a* (%)	*b*	*a* (%)	*b*	*a* (%)	*b*	*a* (%)	*b*
20	0.265	1.2	0.191	1.1	0.216	1.2	0.220	1.0
40	0.517	1.6	0.563	2.2	0.496	1.7	0.475	1.9
60	0.746	3.9	0.813	4.1	0.752	3.7	0.682	3.3

4.4 Diffusion Model Results

The following section summarizes results for diffusion models applied to gravimetric observations for moisture specimens. Adjusted moisture data were only considered for 99%RH at 60°C and 80°C and for immersion at 40°C, 60°C, and 80°C, per Table 7. In order to address thermal trends for each diffusion mechanism, apparent moisture data for 20°C and 40°C at 99%RH and 20°C immersion were

analyzed to complement adjusted data at other temperatures. Diffusion model results for all specimen sizes are available in Appendix A.

4.4.1 Fickian Diffusion

Sorption behavior of this E-glass/vinyl-ester composite system reasonably represents Fickian diffusion for 50%RH and 75%RH exposures. However, sorption trends for material exposed to 99%RH and immersion demonstrate non-Fickian behavior. For $M_t < 0.6M_{max}$ prior to weight loss of degraded species, the uptake curves are non-linear at all temperatures, as depicted in Figure 26.

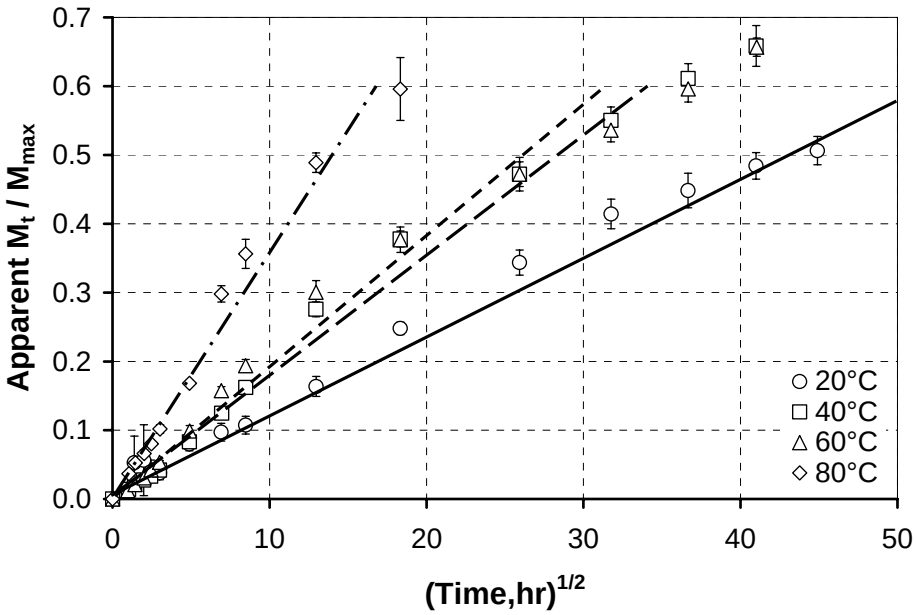

Figure 26. Initial apparent moisture sorption trend for immersion environments.
——: 20°C, — —: 40°C, - -: 60°C, — - —: 80°C
Error bars indicate standard deviations.

Nonetheless, the Fickian diffusion model was used to obtain Fickian diffusion coefficients for all environmental exposures. Two approaches were used: the first using apparent moisture trends and the second using adjusted moisture trends in order

to account for degradation. When using apparent data, the maximum weight gain for each environment was used as M_∞, assuming that each environment has a distinct maximum moisture content which is characterized by humidity and temperature. The second approach assumes that M_∞ is independent of temperature and can be detected through adjusted moisture uptake data, which accounts for loss of degradation products.

Diffusion coefficients were calculated according to Equation 42 in Section 2.4.2.1.2. Table 9 and Table 10 summarize the equilibrium content, M_∞, and Fickian diffusion coefficient, D, for apparent and adjusted moisture uptake trends, respectively. Experimental and theoretical values are compared in Figure 27 through Figure 32 using Equation 40 in Section 2.4.2.1.1 summed through $n = 50$.

Table 9. Fickian diffusion parameters using apparent moisture trends.

Env.	M_∞ (%)	D (10^{-8} mm^2/s)
2 L	0.033	0.46
4 L	0.032	0.28
6 L	-0.014	8.64
2 M	0.057	5.89
4 M	0.060	26.8
6 M	0.074	48.7
6 X	0.148	78.7
2 H	0.269	2.19
4 H	0.666	2.28
6 H	0.894	2.50
8 H	1.229	6.07
2 I	0.393	1.35
4 I	0.586	3.40
6 I	0.846	3.97
8 I	0.998	12.8

Table 10. Fickian diffusion parameters using adjusted moisture trends.

Env.	M_∞ (%)	D (10^{-8} mm^2/s)
2H	1.468	0.032
4H	1.468	0.170
6H	1.468	0.846
8H	1.468	3.74
2I	2.068	0.031
4I	2.068	0.102
6I	2.068	0.259
8I	2.068	0.990

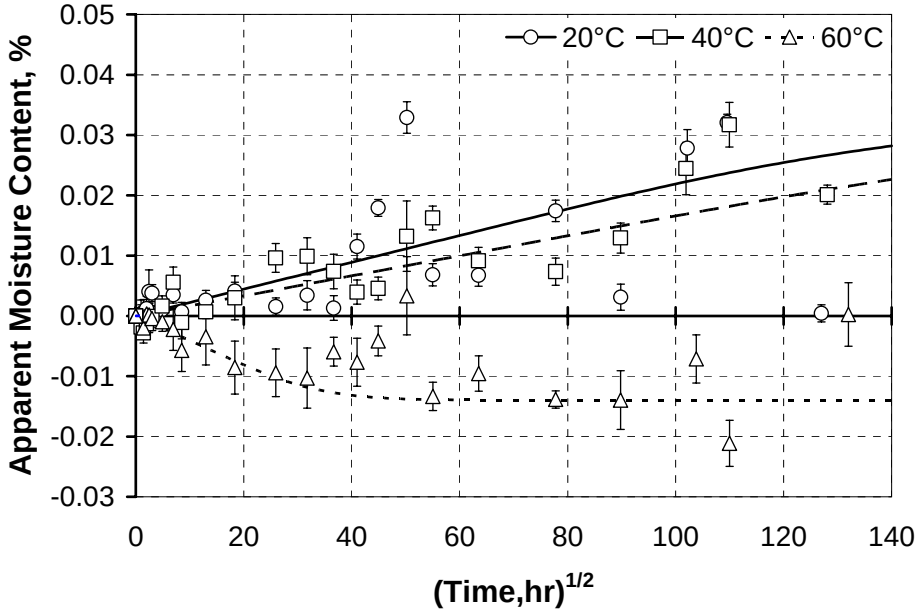

Figure 27. Comparison of apparent experimental moisture uptake trends to theoretical Fickian diffusion model for 18%RH exposures. Error bars indicate standard deviations.

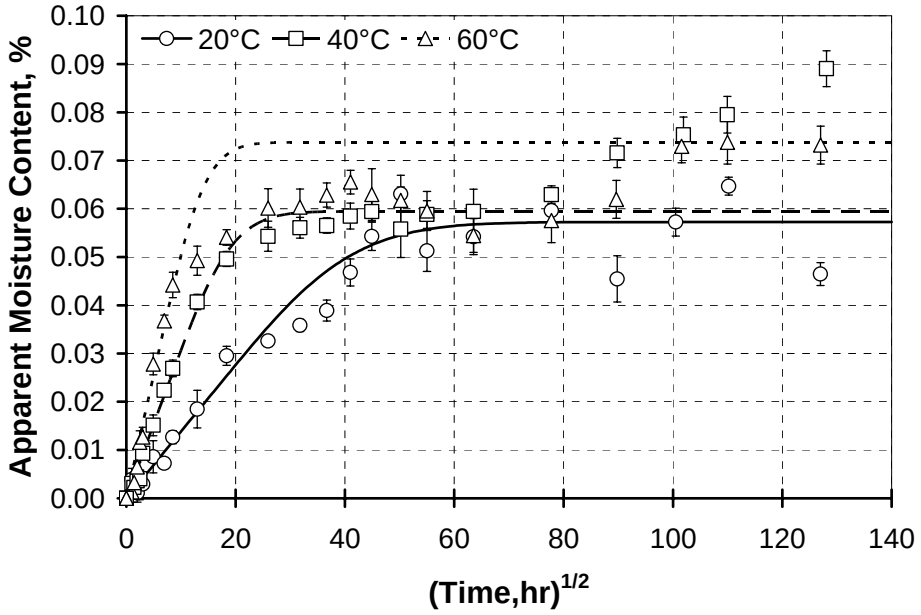

Figure 28. Comparison of apparent experimental moisture uptake trends to theoretical Fickian diffusion model for 50%RH exposures. Error bars indicate standard deviations.

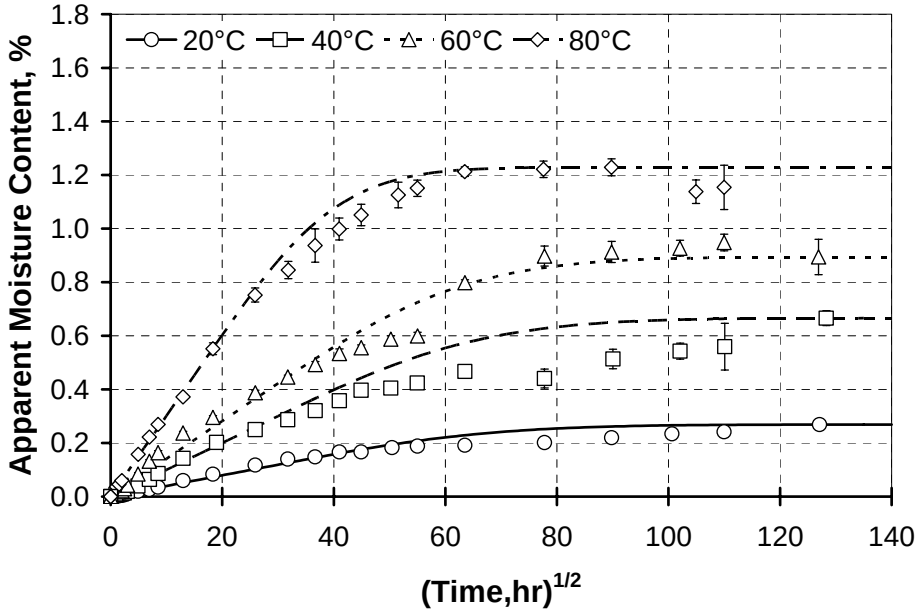

Figure 29. Comparison of apparent experimental moisture uptake trends to theoretical Fickian diffusion model for 99%RH exposures. Error bars indicate standard deviations.

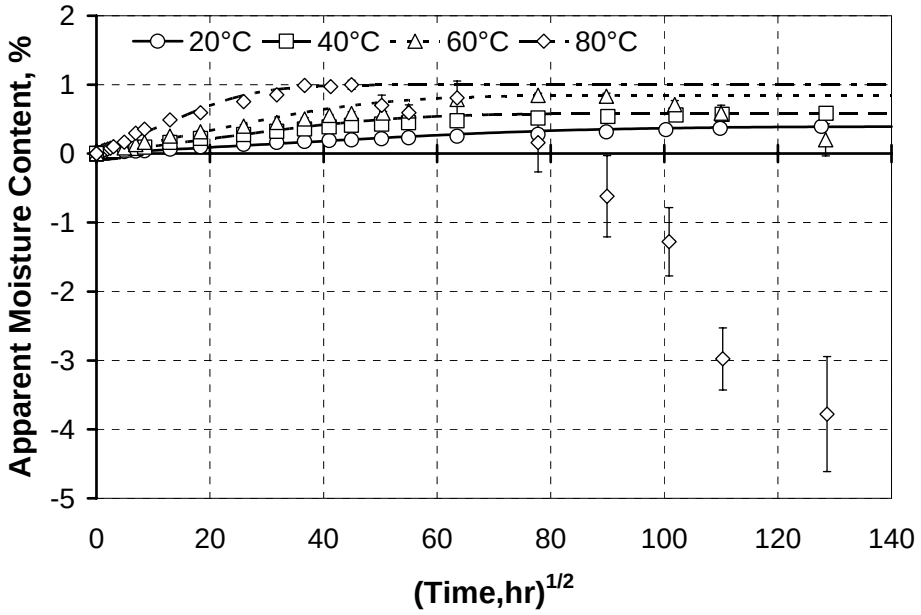

Figure 30. Comparison of apparent experimental moisture uptake trends to theoretical Fickian diffusion model for immersion exposures. Error bars indicate standard deviations.

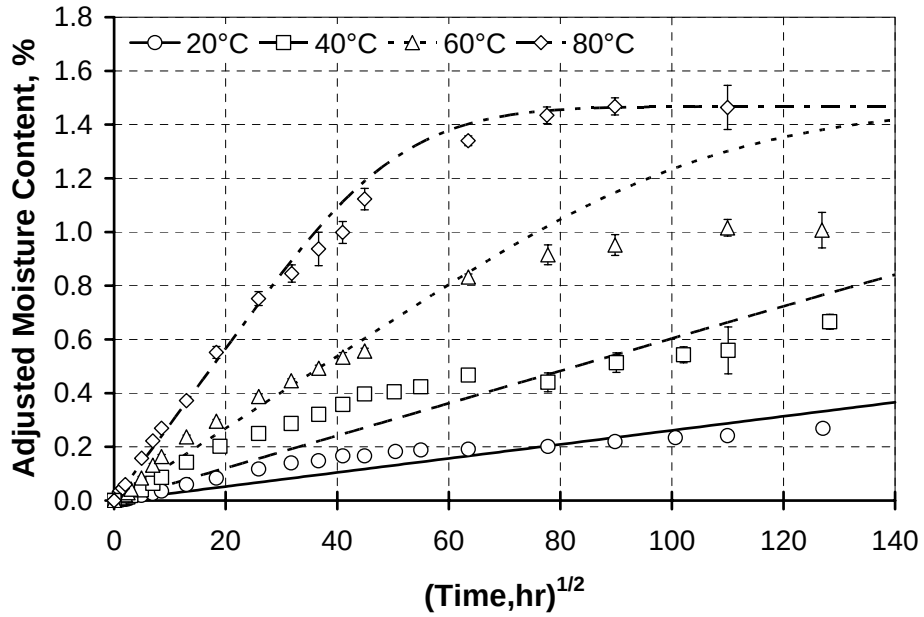

Figure 31. Comparison of adjusted experimental moisture uptake trends to theoretical Fickian diffusion model for 99%RH exposures. Error bars indicate standard deviations.

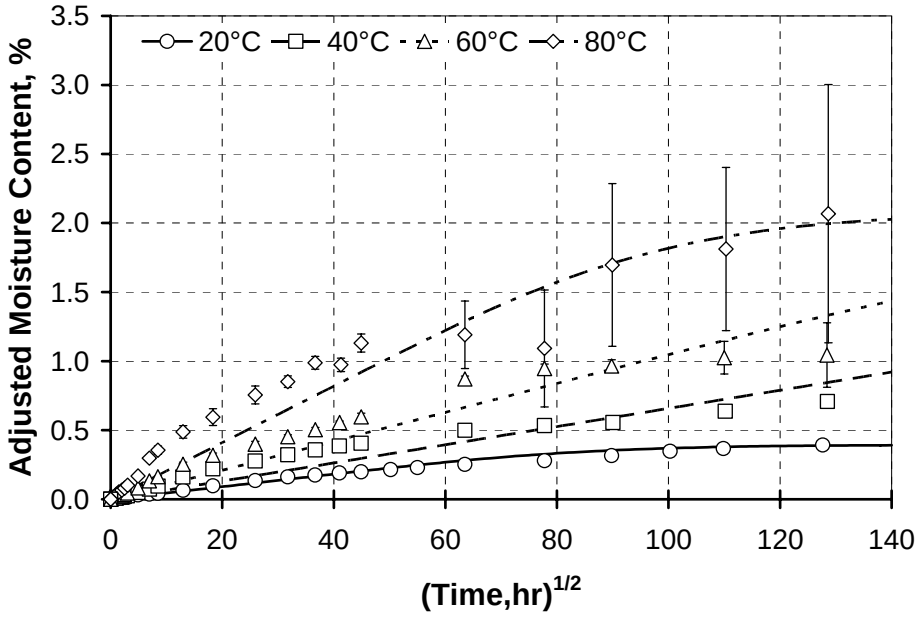

Figure 32. Comparison of adjusted experimental moisture uptake trends to theoretical Fickian diffusion model for immersion exposures. Error bars indicate standard deviations.

4.4.1.1 18%RH Results

Employing the Fickian diffusion model assumes that there is an initial linear uptake region to $0.6M_{\infty}$. However, the extreme sensitivity of the composite to moisture in dry environments resulted in gravimetric trends with high scatter at all temperatures. The high diffusion coefficient at 60°C reflects the quick desorption of residual species, possibly residual LMWS or water molecules not removed through pre-conditioning, indicating that it is possible that the pre-conditioning process did not remove all water. At lower temperatures, a gradual increase in moisture content occurs over the 96 weeks of exposure, as seen in Figure 27. Around 18 weeks, there is a spike in moisture content both at 20°C and 40°C, with a larger spike occurring at

20°C. Figure 27 further indicates the similarity in gravimetric trends at these two temperatures, reflected by their similar M_∞ and D in Table 9.

4.4.1.2 50%RH Results

The diffusion coefficient for 50%RH at 40°C was calculated using an apparent equilibrium content which was less than the maximum observed moisture content. It is clear from Figure 12 and Figure 28 that from about 24 weeks on, non-Fickian diffusion occurs, as noted in Table 5. Consequently, M_∞ was selected to be the apparent equilibrium of about 0.06%, per Table 9. Results for Fickian diffusion calculations are very reasonable for 50%RH. In order to gauge goodness of fit, the correlation coefficient was calculated to compare experimental and predicted values, where 0 indicates a poor fit and 1 indicates a perfect fit. For 50%RH Fickian results, the correlation coefficient is 0.978, 0.960, and 0.977 for 20°C, 40°C, and 60°C results, respectively.

4.4.1.3 75%RH Results

Fickian diffusion models well the moisture uptake trend experienced by the E-glass/vinyl-ester composite in 75%RH at 60°C, where there is a clear linear initial trend and M_t approaches an equilibrium content through 96 weeks exposure. The correlation coefficient for predictions according to Fickian diffusion is 0.997 for the 60°C exposure at 75%RH, which is better than any goodness of fit for 50%RH exposure.

4.4.1.4 99%RH and Immersion Results

In order to accommodate leaching of degraded species, adjusted moisture contents were used in an alternative methodology for fitting the Fickian model. Because knowledge of the dry weight provided for calculation of the water content in material where severe degradation occurred, it was assumed that the apparent M_{max} was valid for all temperatures, as shown in Table 10.

4.4.1.4.1 Apparent Uptake Trends

Diffusion coefficients for apparent uptake trends are greater for immersion environments than for 99%RH. These higher D are a direct consequence of the lower M_∞ for immersion environments. The loss of degraded material in liquid water environments results in lower maximum moisture contents. Consequently, D will be larger, even for similar initial moisture uptake trends since the moisture uptake will approach equilibrium sooner. Claiming M_∞ as the maximum moisture content is based upon the assumption that Fickian diffusion dominates prior to weight loss revealed by a decrease in moisture content. Then the Fickian diffusion in 99%RH extends through a longer period of time to higher moisture contents, where the Fickian diffusion process is slower.

4.4.1.4.2 Adjusted Uptake Trends

Diffusion coefficients obtained using adjusted moisture uptake trends are higher for 99%RH environments than for immersion, but this result is also related to the lower equilibrium moisture content, which is 30% less at 99%RH than for

immersion. Because the material is not capable of holding as much water in a steam environment, it reaches equilibrium more quickly, reflected by the higher *D*.

4.4.1.5 Activation Energies

Figure 33 presents Arrhenius plots of ln*D* vs. 1000/*T*. Table 11 summarizes the activation energies determined for the Fickian diffusion model. Activation energies calculated for the Fickian diffusion coefficients demonstrate a decreasing trend with increasing relative humidity. These decreasing E_a values indicate that less energy is required to activate the diffusion process with increasing humidity.

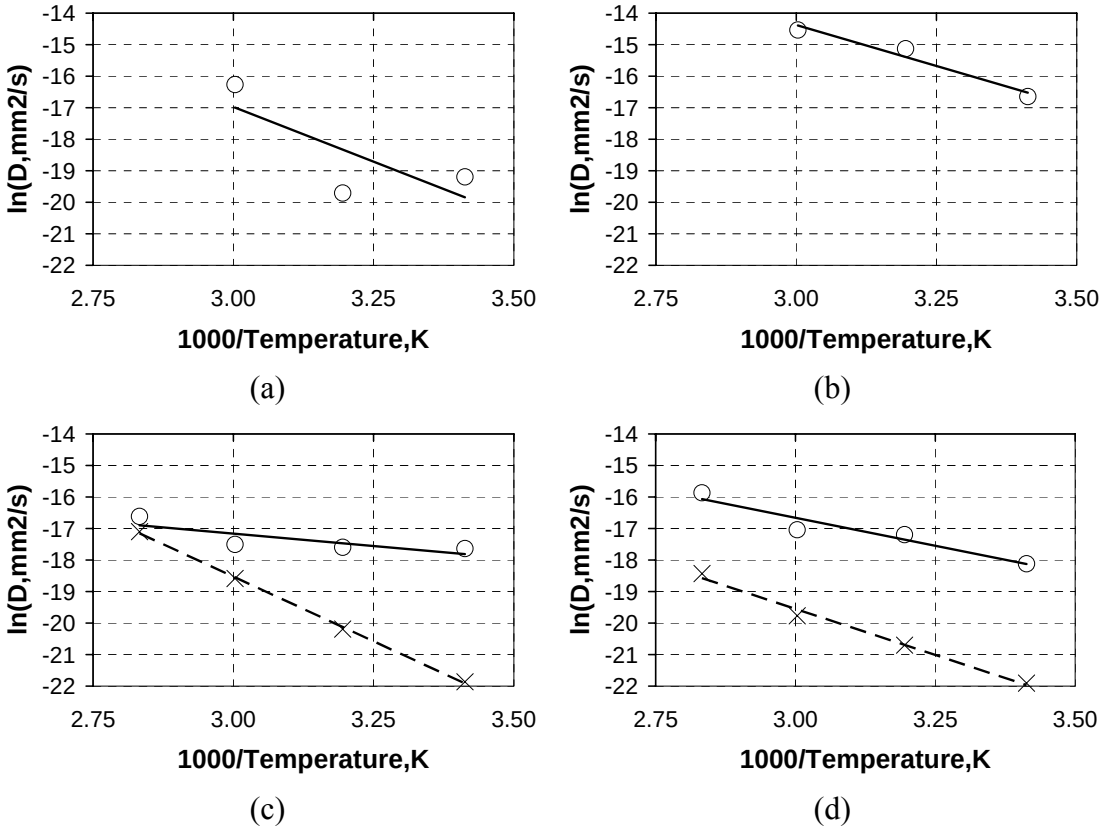

Figure 33. Arrhenius plots for Fickian diffusion coefficient.
(a) 18%RH, (b) 50%RH, (c) 99%RH, (d) immersion; ○: apparent, ×: adjusted.

Table 11. Activation energies for Fickian diffusion coefficients.

E_a (kJ/mol)	Apparent	Adjusted
18%RH	58	—
50%RH	43	—
99%RH	13	68
Immersion	30	49

The activation energy for diffusion coefficients calculated using apparent moisture contents for liquid water environmental exposures is greater than for 99%RH, indicating that more energy is required for moisture in the liquid phase to diffuse into the composite. Because the degradation of the composite is included in apparent moisture sorption trends, it is expected that the activation energy for D calculated using apparent uptake trends is higher since the activation energy must also account for the activation energy of alternative mechanisms of mass transport. Otherwise, the trend of decreasing E_a with increasing environmental moisture would indicate that less energy should be required for diffusion of the liquid phase.

Conversely, when the moisture content is assumed to be uniform across temperature but distinct between 99%RH and immersion, as is the case when considering adjusted moisture uptake trends, less energy is required to activate the diffusion process in the liquid environment. The moisture contents used here, $M_{t,a}$, account for mass loss due to degradation and so indicate that less energy is required when the composite is exposed to the liquid phase of water.

It is possible that as the environment transitions from liquid water to high water vapor content to low water vapor content the activation energy allows for the head of adsorption. While adsorption is effectively instantaneous, as water molecules

diffuse into the bulk sorbent, adsorbed molecules are expected to diffuse into the bulk solid, so sorbate must continually adhere to the composite surface.

4.4.2 Two Phase Fickian Diffusion

Two phase Fickian diffusion was employed according to the methodology presented in Section 2.4.2.2. In the case of apparent moisture trends indicative of degradation, it was necessary to use a value other than M_{max} for calculation of diffusion parameters. Because the degradation is responsible for removing material after sorption by the first phase, it must follow that $M_2 < 0$ and $M_1 > M_{max}$. Consequently, for these degradation trends the *minimum* moisture content observed after M_{max} was used for M_∞ rather than M_{max}, as suggested in [3]. This methodology was used for immersion exposures at 60°C and 80°C only.

Diffusion coefficients were calculated according to Equation 51 in Section 2.4.2.2.2. Table 12 and Table 13 present the moisture contents, M_1 and M_2, and diffusion coefficients, D_1 and D_2, for the two phase Fickian diffusion model for apparent and adjusted moisture uptake trends, respectively. Experimental and theoretical values are compared in Figure 34 through Figure 39 using Equation 45 in Section 2.4.2.2.1 summed through $n = 50$.

Table 12. Two phase Fickian diffusion parameters using apparent moisture trends.

Env.	M_1 (%)	M_2 (%)	D_1 (10^{-8} mm^2/s)	D_2 (10^{-8} mm^2/s)
2L	0.017	0.016	2.54	0.014
4L	0.009	0.031	59.7	0.366
6L	- 0.005	- 0.016	14.8	0.076
2M	0.054	0.011	7.79	0.0004
4M	0.040	0.049	44.2	0.533
6M	0.053	0.021	79.0	0.536
6X	0.145	0.003	81.6	0.973
2H	0.123	0.145	7.39	0.577
4H	0.257	0.409	8.41	0.511
6H	0.754	0.194	4.92	0.601
8H	1.449	- 0.220	5.75	1.58
2I	0.187	0.206	3.93	0.625
4I	0.413	0.173	5.20	0.649
6I	2.374	- 3.019	1.79	0.307
8I	5.868	-10.645	3.59	0.502

Table 13. Two phase Fickian diffusion parameters using adjusted moisture trends.

Env.	M_1 (%)	M_2 (%)	D_1 (10^{-8} mm^2/s)	D_2 (10^{-8} mm^2/s)
6H	0.685	0.331	5.09	0.709
8H	1.212	0.256	5.24	0.979
4I	0.281	0.428	6.59	0.585
6I	0.359	0.685	8.84	0.809
8I	0.494	1.574	20.2	0.568

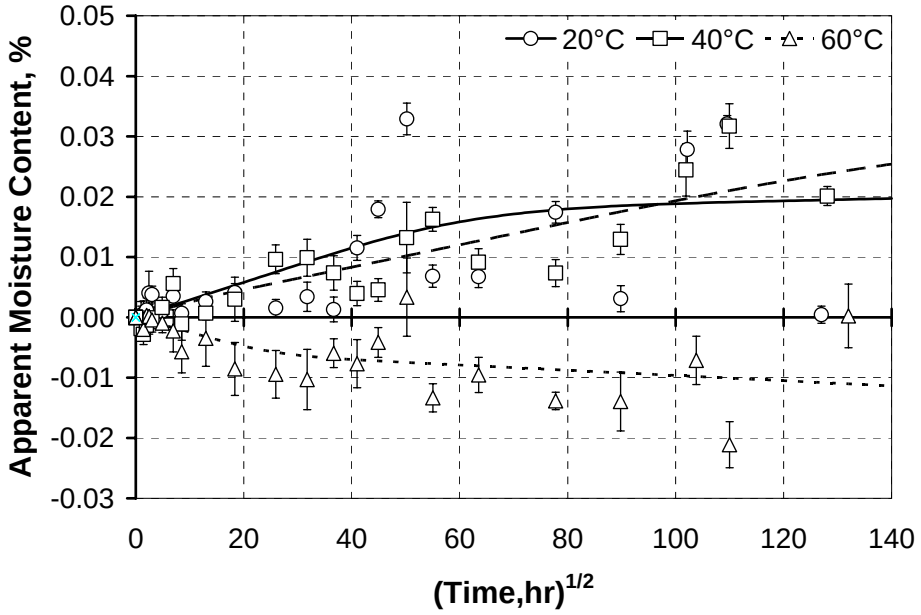

Figure 34. Comparison of apparent experimental moisture uptake trends to theoretical two phase Fickian model for 18%RH environments. Error bars indicate standard deviations.

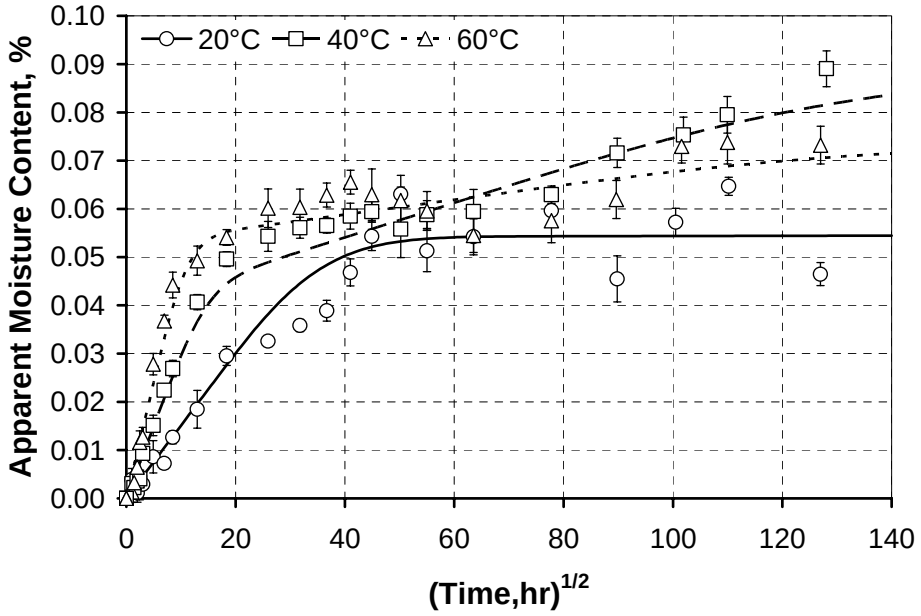

Figure 35. Comparison of apparent experimental moisture uptake trends to theoretical two phase Fickian model for 50%RH environments. Error bars indicate standard deviations.

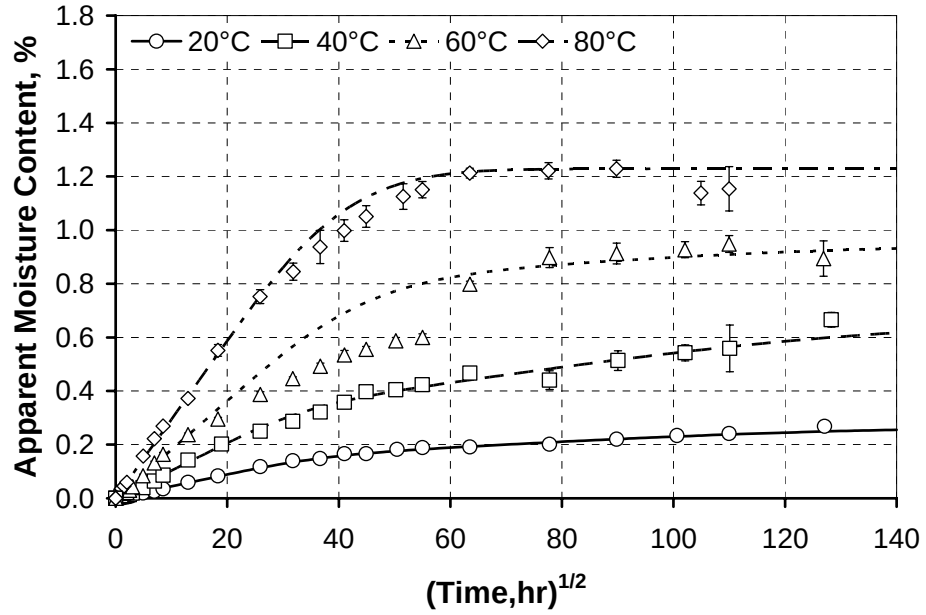

Figure 36. Comparison of apparent experimental moisture uptake trends to theoretical two phase Fickian model for 99%RH environments. Error bars indicate standard deviations.

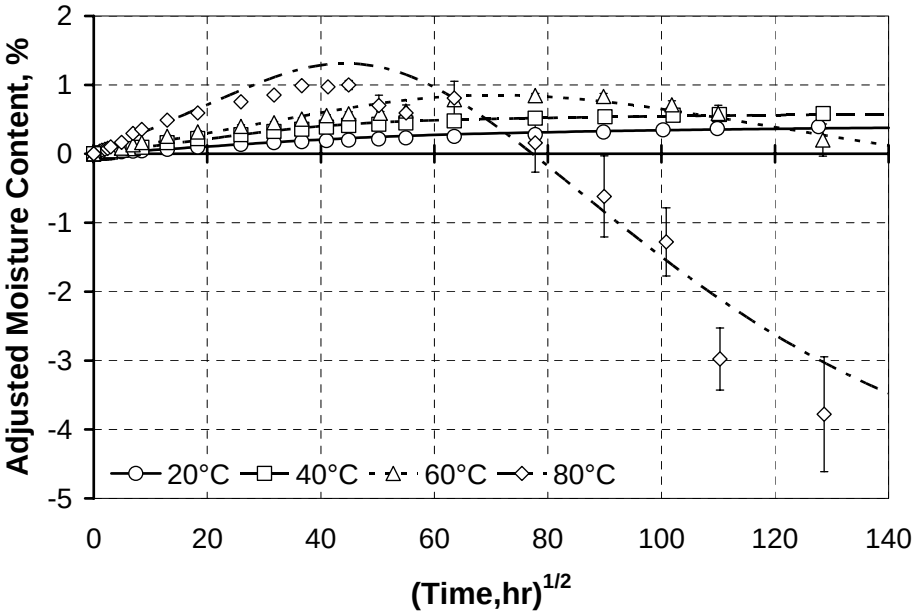

Figure 37. Comparison of apparent experimental moisture uptake trends to theoretical two phase Fickian model for immersion environments. Error bars indicate standard deviations.

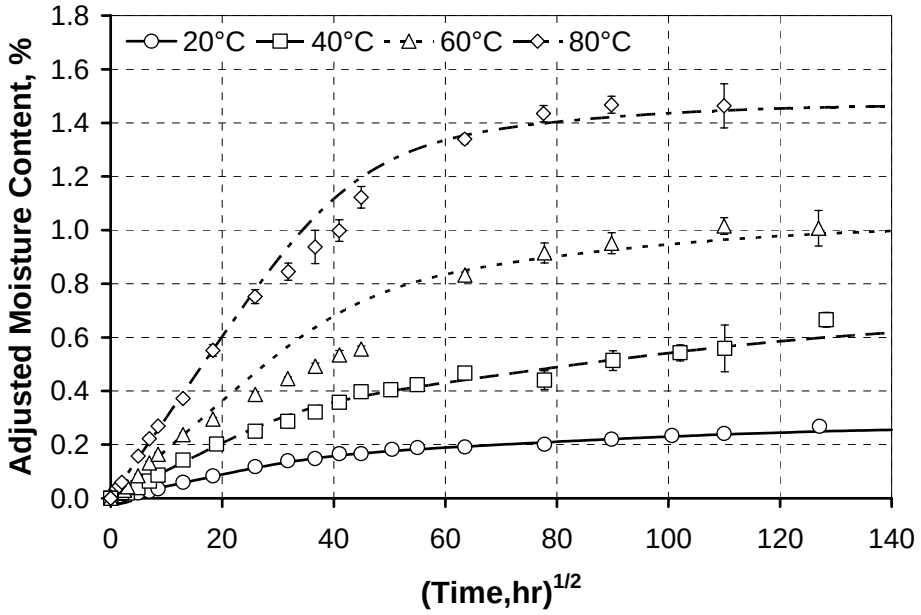

Figure 38. Comparison of adjusted experimental moisture uptake trends to theoretical two phase Fickian model for 99%RH environments. Error bars indicate standard deviations.

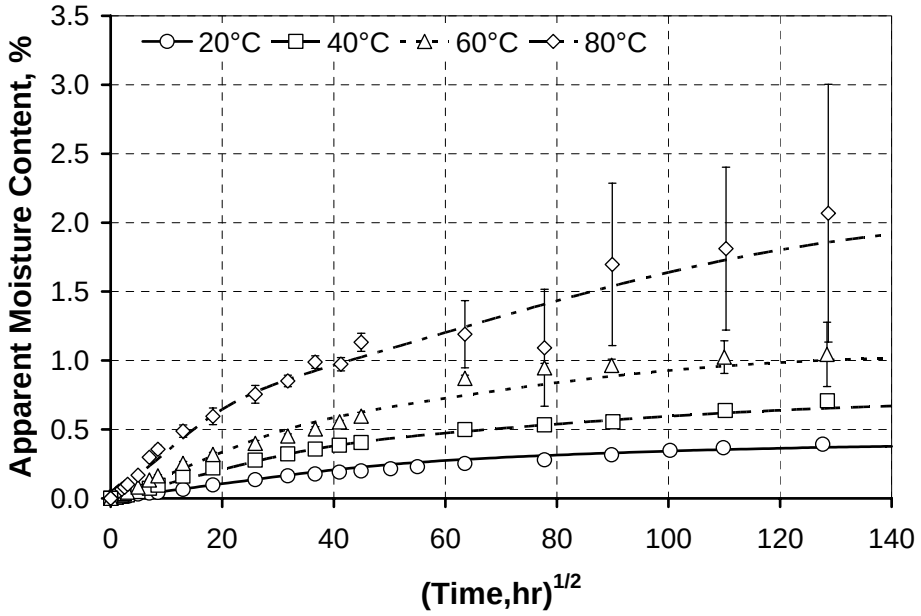

Figure 39. Comparison of adjusted experimental moisture uptake trends to theoretical two phase Fickian model for immersion environments. Error bars indicate standard deviations.

A major difficulty arises when attempting to determine two phase Fickian diffusion parameters for 99%RH and immersion environments with data through 96 weeks. The two phase Fickian model fundamentally assumes that available moisture trends demonstrate regions dominated by each of the two phases. However, for lower temperatures, 20°C and 40°C, in 99%RH and immersion, it is highly likely that only the first phase dominates in the first 96 weeks of exposure. Results for 60°C and 80°C indicate that M_1 is at least 0.7 %, and 40°C immersion gravimetric data indicate a maximum experimental moisture content of around 0.6 % to 0.7 % for moisture specimens, noted in Table 6 and Table 7. While it is possible that M_1 is lower at these lower temperatures, it is more likely that the first phase has not yet reached equilibrium.

While the two phase Fickian model appears to fit data well, the diffusion coefficients do not demonstrate a thermal trend at humidities other than 50%RH. At low humidity, the sensitive nature of the sorbent to moisture results in erratic behavior which makes it difficult to isolate distinct regions dominated by sorption of the two phases. Calculations of goodness of fit reflect the high scatter which make calculation of the diffusion parameters difficult.

The two phase Fickian model results in correlation coefficients which range from 0.975 to 0.999 for apparent moisture trends resulting from exposures to 50%RH and above. Correlation coefficients for 18%RH two phase Fickian curve fits are 0.610, 0.885, and 0.621 for 20°C, 40°C, and 60°C, respectively. Adjusted moisture trends produce correlation coefficients ranging from 0.979 to 0.994, though the

adjusted moisture trend for 60°C immersion produced a correlation coefficient of 0.884. In general, it can be concluded that the two phase Fickian model appears to fit data well, except for low humidity exposures.

For apparent trends obtained from 99%RH and immersion exposures, the diffusion coefficients and M_1 values are greater for 40°C than for 20°C; and these values are also greater for 80°C than for 60°C. However, the diffusion coefficients are generally lower for 60°C and 80°C than for 20°C and 40°C. Adjusted data reflect a slightly different trend for immersion, with D_1 demonstrating clear thermal activation. D_2 for adjusted immersion data shows a general decreasing trend with temperature while M_2 increases with temperature. These results indicate that the polymer structure may relax, allowing for greater moisture sorption, while uptake of the water molecules are hindered by greater movement and interaction with the polymer network.

4.4.3 Langmuir Diffusion

Table 14 and Table 15 present the equilibrium moisture content M_∞, diffusion coefficient D, and probabilities of conversion α and β for the Langmuir diffusion model presented in Section 2.4.2.3 for apparent and adjusted moisture uptake trends, respectively. It is again stated that α and β describe the probability that a bound water molecule will convert to free water and vice versa. Parameters were determined according to the methodology presented in [4] using Equations 62 and 63 in Section 2.4.2.3.1, where α and $\beta / (\alpha+\beta)$ are found from a long term exponential curve fit and D is found from a short term linear fit. Experimental and theoretical values are

compared in Figure 40 through Figure 45 using Equation 59 in Section 2.4.2.3.1 summed through $n = 50$.

Table 14. Langmuir diffusion parameters using apparent moisture trends.

Env.	M_∞ (%)	D (10^{-6} mm^2/s)	α (10^{-8} s^{-1})	β (10^{-8} s^{-1})
2L	0.033	2.73	2.60	12.8
4L	0.032	0.03	2.50	19.7
6L	- 0.021	0.54	1.42	3.58
2M	0.065	0.22	0.71	0.16
4M	0.089	0.98	2.92	2.37
6M	0.074	1.58	4.72	1.62
6X	0.148	1.99	- 0.75	- 0.02
2H	0.269	0.23	3.40	2.92
4H	0.666	0.22	2.51	2.37
6H	0.948	2.04	10.3	42.0
8H	1.229	2.50	23.3	59.5
2I	0.393	1.76	5.21	15.6
4I	0.586	0.37	6.60	6.88
6I	0.845	0.13	- 0.78	- 0.15
8I	0.998	0.53	- 6.42	- 1.31

Table 15. Langmuir diffusion parameters using adjusted moisture trends.

Env.	M_∞ (%)	D (10^{-6} mm^2/s)	α (10^{-8} s^{-1})	β (10^{-8} s^{-1})
4H	1.468	0.20	0.49	1.53
6H	1.468	0.29	1.38	2.01
8H	1.468	2.62	15.9	53.1
2I	2.068	0.30	0.21	2.17
4I	2.068	0.22	0.36	1.53
6I	2.068	0.31	0.78	1.96
8I	2.068	0.82	3.76	8.04

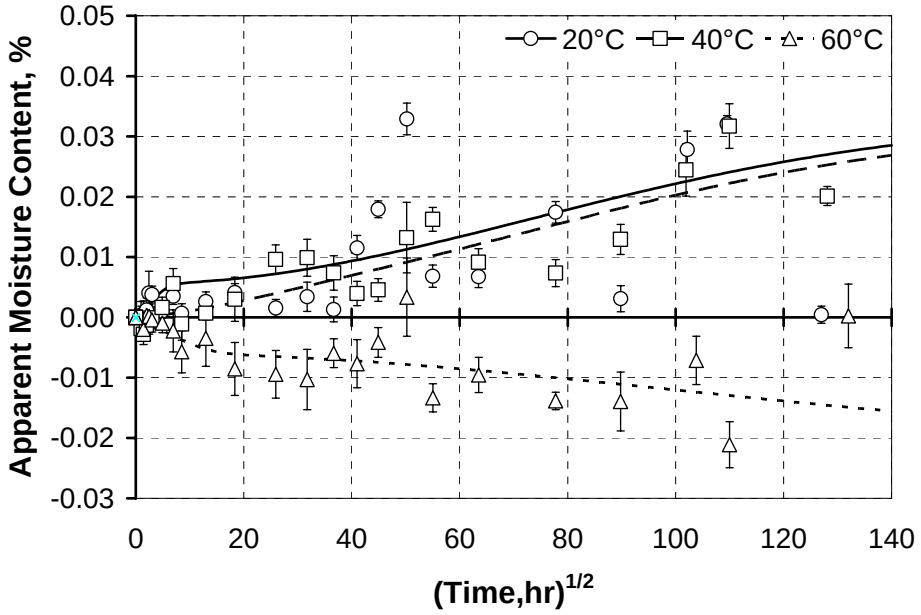

Figure 40. Comparison of apparent experimental moisture uptake trends to theoretical Langmuir model for 18%RH environments. Error bars indicate standard deviations.

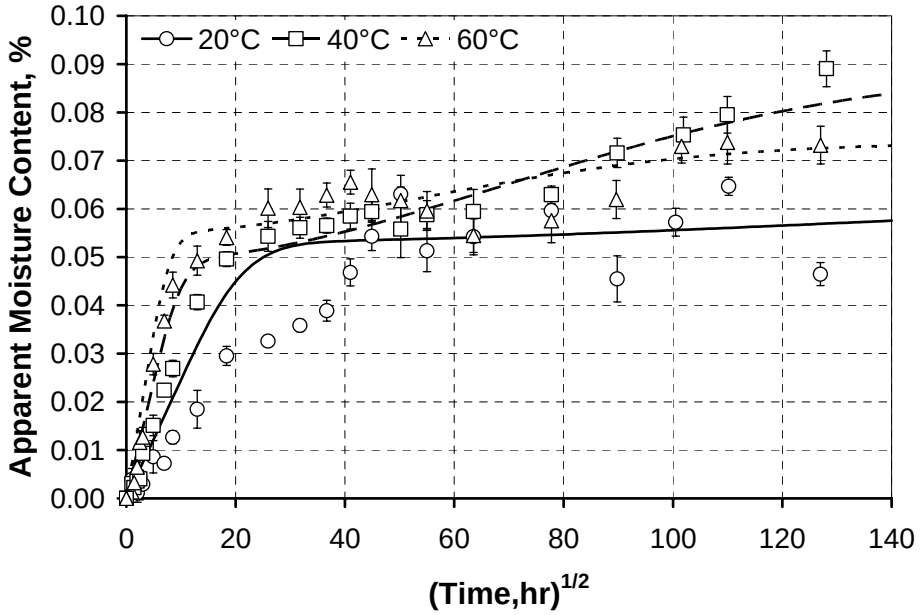

Figure 41. Comparison of apparent experimental moisture uptake trends to theoretical Langmuir model for 50%RH environments. Error bars indicate standard deviations.

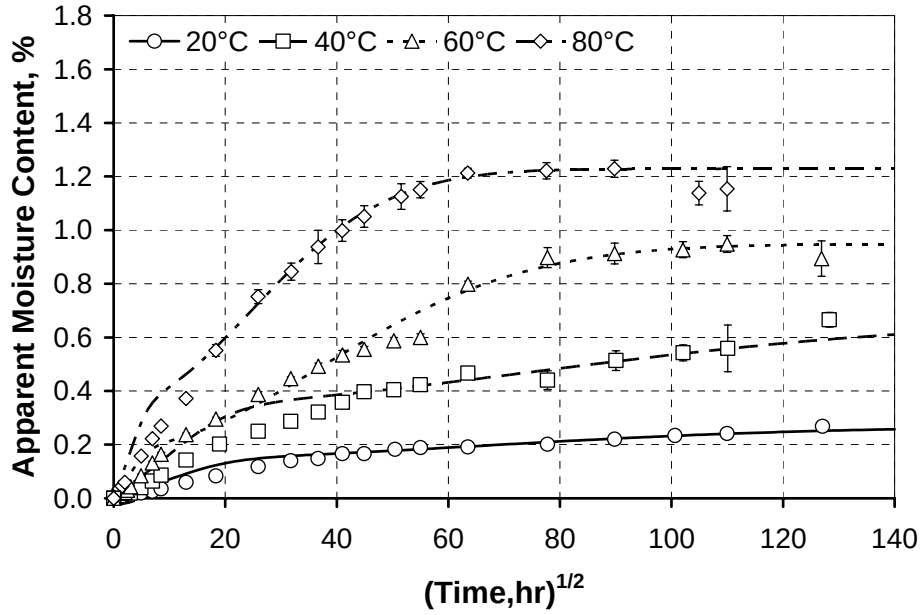

Figure 42. Comparison of apparent experimental moisture uptake trends to theoretical Langmuir model for 99%RH environments. Error bars indicate standard deviations.

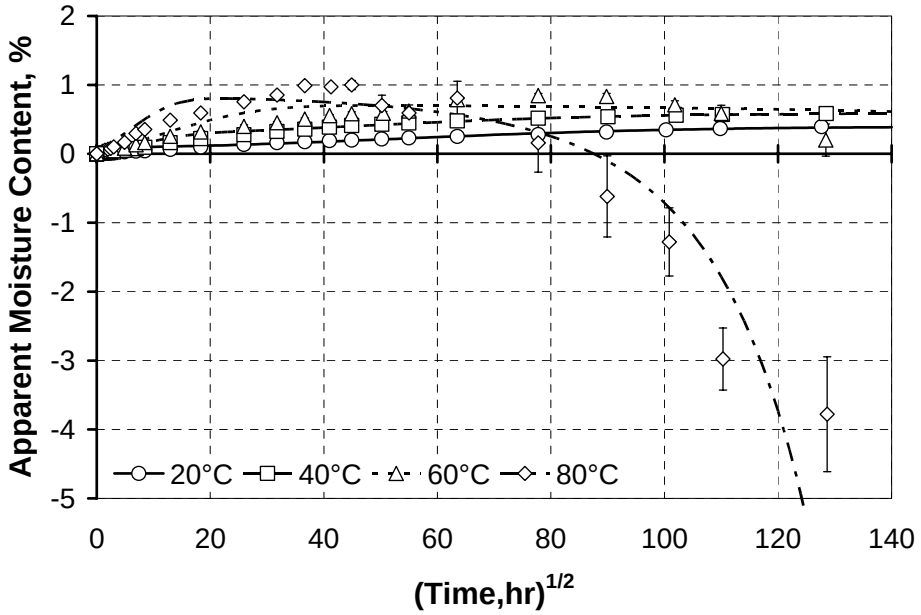

Figure 43. Comparison of apparent experimental moisture uptake trends to theoretical Langmuir model for immersion environments. Error bars indicate standard deviations.

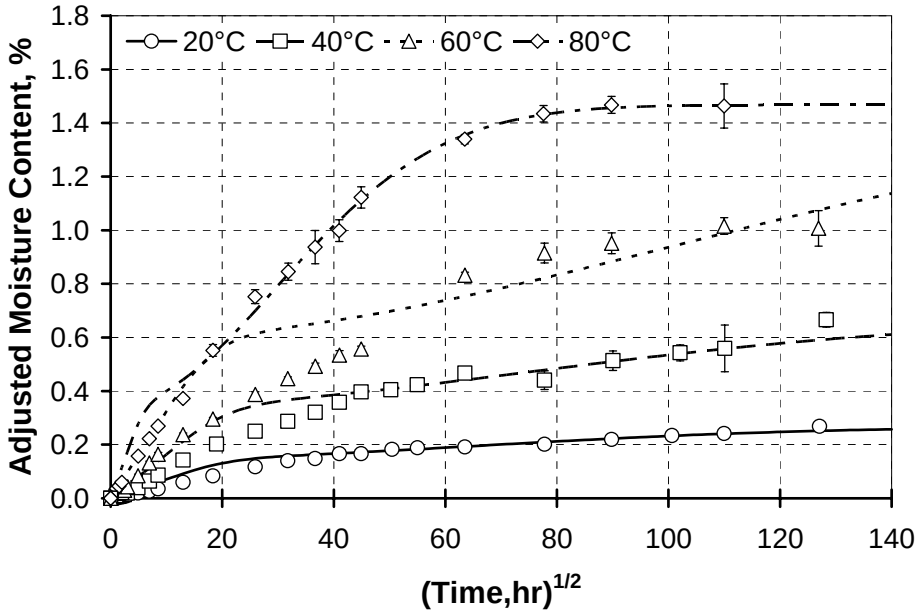

Figure 44. Comparison of adjusted experimental moisture uptake trends to theoretical Langmuir model for 99%RH environments. Error bars indicate standard deviations.

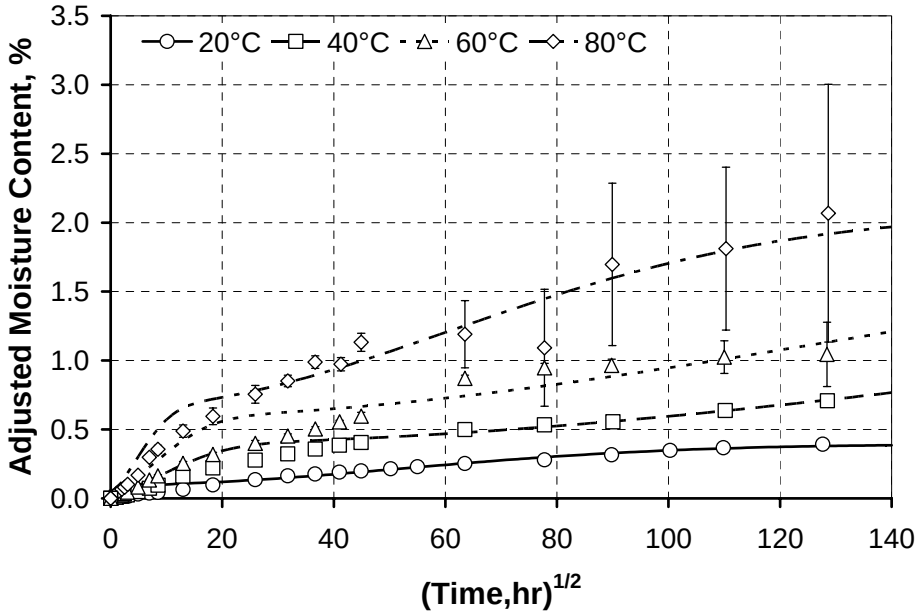

Figure 45. Comparison of adjusted experimental moisture uptake trends to theoretical Langmuir model for immersion environments. Error bars indicate standard deviations.

Negative values of α and β were produced in environments where decreases in M_t occurred after M_{max} was reached. For apparent moisture trends indicating weight loss after reaching M_{max}, the Langmuir diffusion model is not appropriate since α and β describe probabilities of conversion between the free and bound state of water [4]. Probabilities must be positive. The Langmuir diffusion model does not account for loss of free or bound water or degraded material to the exposure environment.

While the diffusion coefficients produced were reasonable [5], no consistent thermal trend could be established for D. Interestingly, the thermal trend detected in α and β represent that established in [5], where the rates of conversion show a thermal trend for 20°C, 60°, and 80°C, but α and β are smallest for 40°C. This trend is also shown in 99%RH and immersion environments. It is possible that severe degradation occurring at 60°C and 80°C, indicated by permanent losses in SBS strength and the glassy modulus, is responsible for inconsistent results at higher temperatures.

For adjusted moisture uptake trends, where $M_{t,a}$ represents the amount of water sorbed by accounting for loss of degraded species, $\beta > \alpha$ indicates that once a water molecule diffuses into the sorbent, it is more likely that that molecule will become bound to sorbent structure. This trend is also seen in apparent trends at higher temperatures with 99%RH, where degradation is less severe than immersion. At 50%RH, however, it is less likely that a molecule will become bound; rather, it is more likely that a water molecule will transition from free to bound, as indicated by $\alpha > \beta$.

4.4.4 Structural Modification Diffusion

Table 16 and Table 17 present the pseudo-equilibrium content, $M_{o\infty}$; diffusion coefficient, D; and structural modification factor, k, for the structural modification model, according to Equation 66 in Section 2.4.2.4.2, for apparent and adjusted moisture uptake trends, respectively. Experimental and theoretical values are compared in Figure 46 through Figure 51 using Equation 65 in Section 2.4.2.4.1 summed through $n = 50$.

Table 16. Structural modification diffusion parameters using apparent moisture trends.

Env.	$M_{o\infty}$ (%)	D (10^{-7} mm^2/s)	k (10^{-4} s$^{-0.5}$)
2L	0.017	0.22	-0.18
4L	0.001	1.48	34.7
6L	-0.005	2.19	1.36
2M	0.054	0.78	0.01
4M	0.042	5.02	1.30
6M	0.053	8.43	0.49
6X	0.145	8.13	-0.03
2H	0.097	2.06	2.29
4H	0.250	1.62	1.99
6H	0.754	0.52	0.33
8H	1.342	0.49	-0.21
2I	0.187	0.82	1.45
4I	0.413	0.68	0.56
6I	2.374	0.040	-1.17
8I	5.869	0.037	-2.13

Table 17. Structural modification diffusion parameters using adjusted moisture trends.

Env.	$M_{o\infty}$ (%)	D (10^{-7} mm^2/s)	k (10^{-4} s$^{-0.5}$)
6H	0.685	0.71	0.67
8H	1.212	0.62	0.35
4I	0.281	1.68	1.93
6I	0.359	2.20	2.85
8I	0.494	4.75	3.98

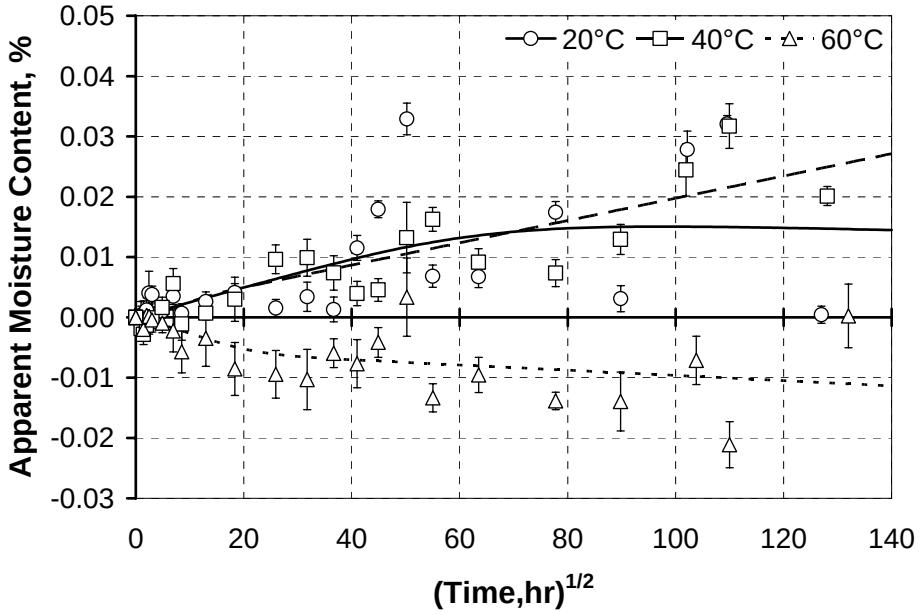

Figure 46. Comparison of apparent experimental moisture uptake trends to theoretical structural modification model for 18%RH environments. Error bars indicate standard deviations.

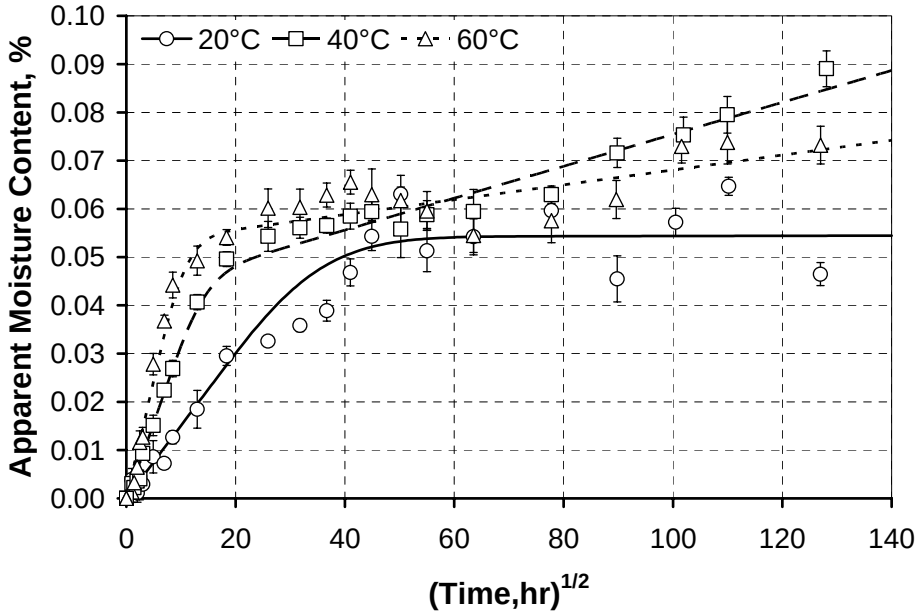

Figure 47. Comparison of apparent experimental moisture uptake trends to theoretical structural modification model for 50%RH environments. Error bars indicate standard deviations.

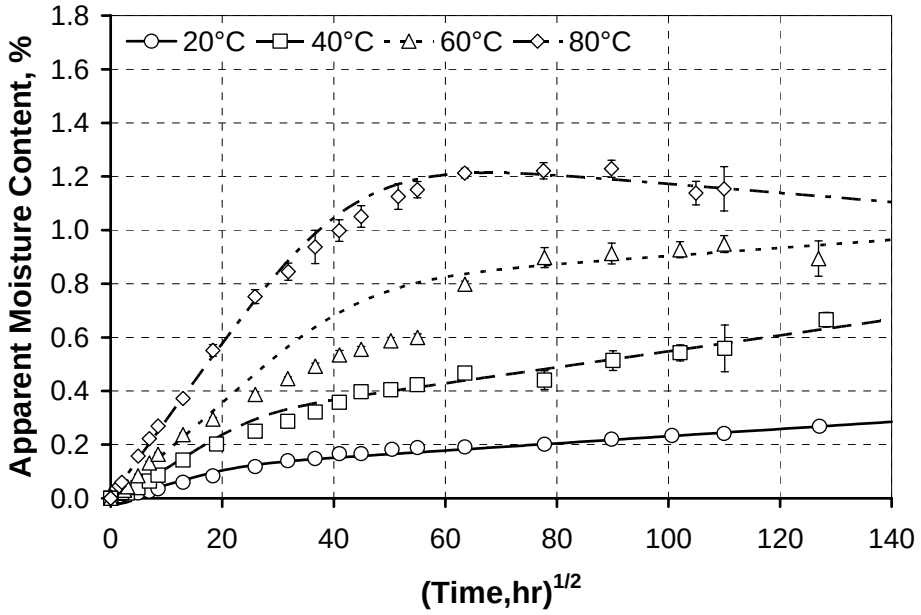

Figure 48. Comparison of apparent experimental moisture uptake trends to theoretical structural modification model for 99%RH environments. Error bars indicate standard deviations.

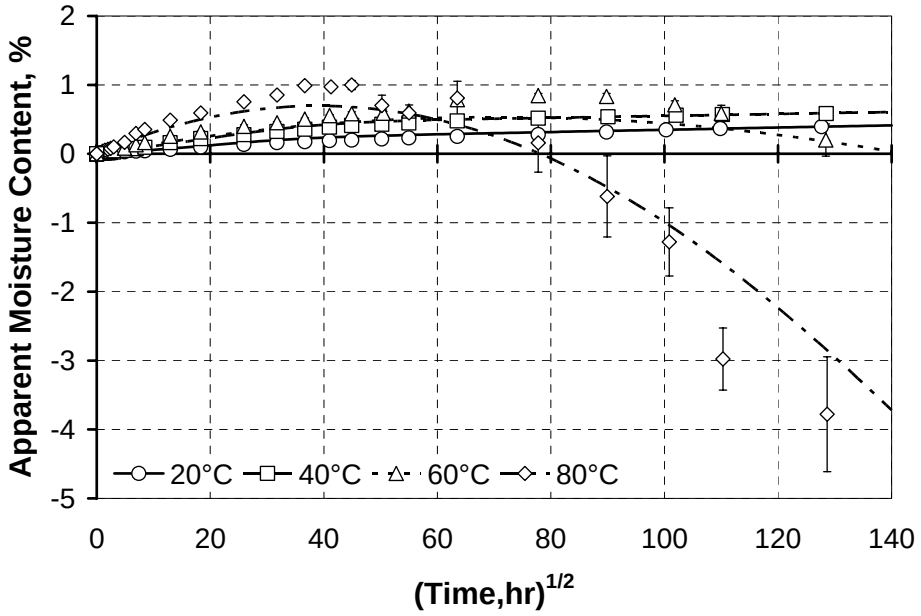

Figure 49. Comparison of apparent experimental moisture uptake trends to theoretical structural modification model for immersion environments. Error bars indicate standard deviations.

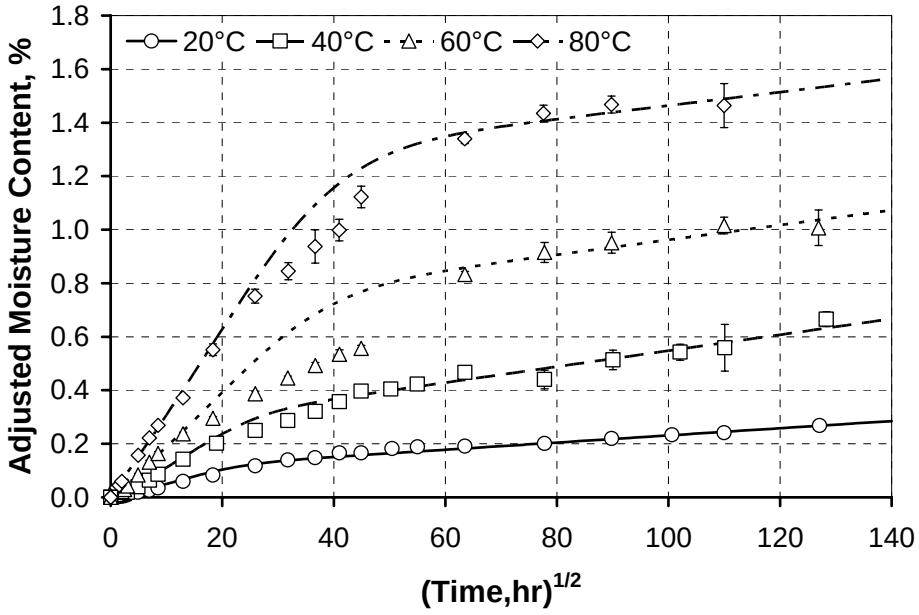

Figure 50. Comparison of adjusted experimental moisture uptake trends to theoretical structural modification model for 99%RH environments. Error bars indicate standard deviations.

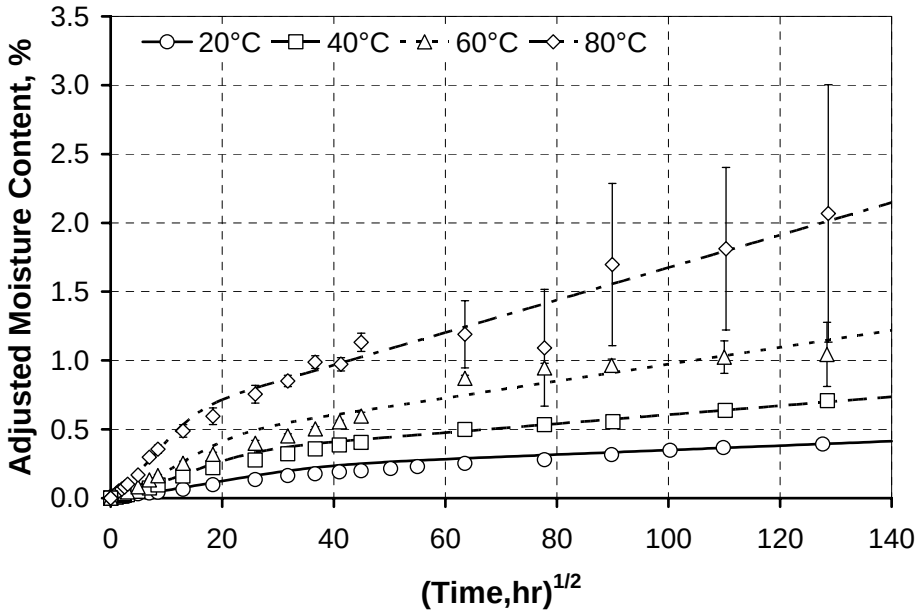

Figure 51. Comparison of adjusted experimental moisture uptake trends to theoretical structural modification model for immersion environments. Error bars indicate standard deviations.

4.4.4.1 18%RH Results

Diffusion parameters at 18%RH may be a bit deceiving. The $M_{o\infty}$ value at 18%RH for all temperatures is on the order of a standard deviation of a single M_t data point. However, the thermal trend in $M_{o\infty}$ reflects the general trend that some weight gain occurs at 20°C and that weight loss beyond initial pre-conditioning occurs in 60°C. Weight loss would therefore imply a different mechanism is responsible for structural modification at 60°C. It is possible that residual LMWS are lost in the 60°C low humidity environment after which weight gain may occur, reflected by the low, positive value of k. Exposure to 18%RH at 40°C should not result in significant weight change since the material was pre-conditioned at 40°C and 18%RH prior to all environmental exposures. In fact, over the first 72 hours of exposure, the apparent moisture "uptake" is less than zero, implying that weight loss occurred at early time past the 6 weeks pre-conditioning. Over the next two years, significant structural modification occurred where M_t increased from -0.003 [0.002] % at 72 hrs to 0.032 [0.004] % at 72 weeks. While these moisture contents are very low, it is possible that, similar to 60°C exposure, 40°C results in relaxation of the polymer, allowing for more water molecules to ingress. At 20°C, the structural modification is less, as would be expected since higher temperatures result in greater polymer chain mobility.

4.4.4.2 50%RH Results

At 50%RH, $M_{o\infty}$ increases from 18%RH, while k decreases. The diffusion coefficient D, describing the Fickian dominated component of the structural modification model, increases with temperature, as would be expected. Again, the

most significant structural modification occurs at 40°C, reflected by the *k* values in Table 16. Pseudo-equilibrium contents are within a standard deviation of one another, again following Fickian dominated diffusion at early times. It is possible that at 60°C desorption of LMWS occurs gradually over two years. It is further possible that residual LMWS such as styrene slowly polymerize over the first 10 weeks (41 $hr^{1/2}$) of exposure to elevated temperature, after which residual volatiles leach out over the next 14 weeks. From 24 weeks through 96 weeks (64 through 127 $hr^{1/2}$), it appears that polymer relaxation occurs as the moisture content gradually increases. If the same $M_{o\infty}$ value of 0.053 % is used, the polymer relaxation which occurs from 24 weeks on would be reflected in a *k* of 1.12×10^{-4} $s^{-0.5}$ at 60°C, on the same order of 40°C. Similarly, in 50%RH at 40°C, the gravimetric trend appears to hold an equilibrium moisture content from about 4 weeks through 24 weeks. However, after 24 weeks, the moisture content shows a clear increasing trend, reflecting polymer relaxation, allowing from additional moisture uptake.

While there is evidence for desorption of LMWS at 60°C both at 18%RH and 50%RH, there is no evidence for desorption at 40°C. A greater presence of LMWS would imply that there are more free ends to polymer chains, allowing for more hydrogen bonds which would result in greater polymer relaxation. At 60°C, residual post-cure and loss of LMWS would result in a tighter polymer network, after which polymer relaxation could occur but the polymer network would still have less mobility at exposure to 60°C.

4.4.4.3 75%RH Results

Exposure to 75%RH at 60°C results in a diffusion coefficient about the same as 50%RH, despite distinct $M_{o\infty}$ values. It can be theorized that diffusion coefficients at the same temperature and different humidities would identical, as these results imply. However, D as determined from apparent moisture uptake values for 60°C at 99%RH and immersion are, respectively, 40 and 200 times less than those D determined for the lower humidities at the same temperature. It is possible that these much lower values of D for apparent trends are a consequence of the larger values of $M_{o\infty}$ which must be larger than equilibrium in order to account for degradation. Analysis of adjusted moisture uptake trends results in diffusion coefficients which are about 10 to 50 times smaller at 99%RH and immersion, respectively, when compared to D for 50%RH and 75%%RH at the same temperature, as seen in Table 16.

Looking at the structural modification parameter for apparent trends at 60°C, a clear decreasing trend appears with increasing environmental moisture content, where k ranges from 1.36×10^{-4} $s^{-0.5}$ at 18%RH to -1.17×10^{-4} $s^{-0.5}$ in immersion, as shown in Table 16. Desorption of LMWS would occur sooner and faster in drier environments, allowing for polymer relaxation to occur at earlier times, reflected by greater values in k. In 99%RH and immersion at 60°C, the water content in the composite after 96 weeks is up near 1 %, compared to 0.07 % and 0.14 % in 50%RH and 75%RH, respectively. Prolonged exposure with high water content at elevated temperatures provides significant time for relaxation, hydrolysis, and desorption of degraded species to occur. The weight loss due to desorption of degraded species into 60°C

high humidity and immersion environments is reflected by the negative *k*. More aggressive degradation and weight loss at 80°C is reflected by even larger values of *k*.

4.4.4.4 99%RH and Immersion Results

In 99%RH and immersion environments, the diffusion coefficient demonstrates a decreasing trend with increasing temperature, contrary to expectations. It is possible that these results indicate a dominance of structural modification over Fickian diffusion in 99%RH and immersion environments. Competing mechanisms of structural modification, such as polymer relaxation, desorption of residual LMWS, and leaching of degradation products, dominate over absorption of water molecules. The relative dominance of these competing mechanisms are further reflected in the thermal trend of structural modification parameters, which decrease from positive to negative values with increasing temperature, as noted in Table 16.

Model parameters for adjusted moisture trends in Table 17 should be considered along with results for 99%RH exposure at 20°C and 40°C and immersion at 20°C. At 99%RH, the pseudo-equilibrium content increases with temperature, indicating higher temperatures provide a greater capacity for moisture uptake. However, *D* and *k* still demonstrate a decreasing trend with increasing temperature at 99%RH. Together, it can be concluded that while the capacity for moisture uptake increases with temperature, the rates of change within the polymer structure are inhibited by increasing temperature in this humid environment.

Conversely, *D* and *k* for immersion environments tend to increase with temperature, while $M_{o\infty}$ levels are significantly lower. The higher diffusion

coefficients imply that pseudo-equilibrium is reached within days, resulting in structural modification which is responsible for moisture uptake for a greater portion of the exposure time. These results indicate that increasing temperature not only speeds up the rate of diffusion, but it is also responsible for increasing relaxation of the polymer. Considering adjusted values rather than apparent values inherently ignores competing degradation mechanisms, other than possible wicking, by considering the moisture uptake alone.

4.4.4.5 Activation Energies

Figure 52 presents Arrhenius plots of diffusion coefficients versus temperature. Table 18 summarizes the activation energies determined for the structural modification model.

While apparent gravimetric data for 50%RH results in a reasonable activation energy for the structural modification diffusion coefficient, the negative values for 99%RH and immersion environments are counterintuitive. The diffusion coefficient is generally found to increase with temperature, indicating an endothermic process. Table 18 indicates, however, that the diffusion process in 99%RH is an exothermic process, where the diffusion and relaxation processes slow with increasing temperature, while the pseudo-equilibrium content increases greatly with temperature. That is, the temperature alters the structure of the material, providing greater capacity while the process becomes more tortuous for the diffusing molecules. It is possible that water in its vapor state is less favorable to entering the composite material than in the liquid state. While degradation occurs in high humidity environments, as

evidenced by weight loss after redrying, this weight loss is more severe in immersion environments.

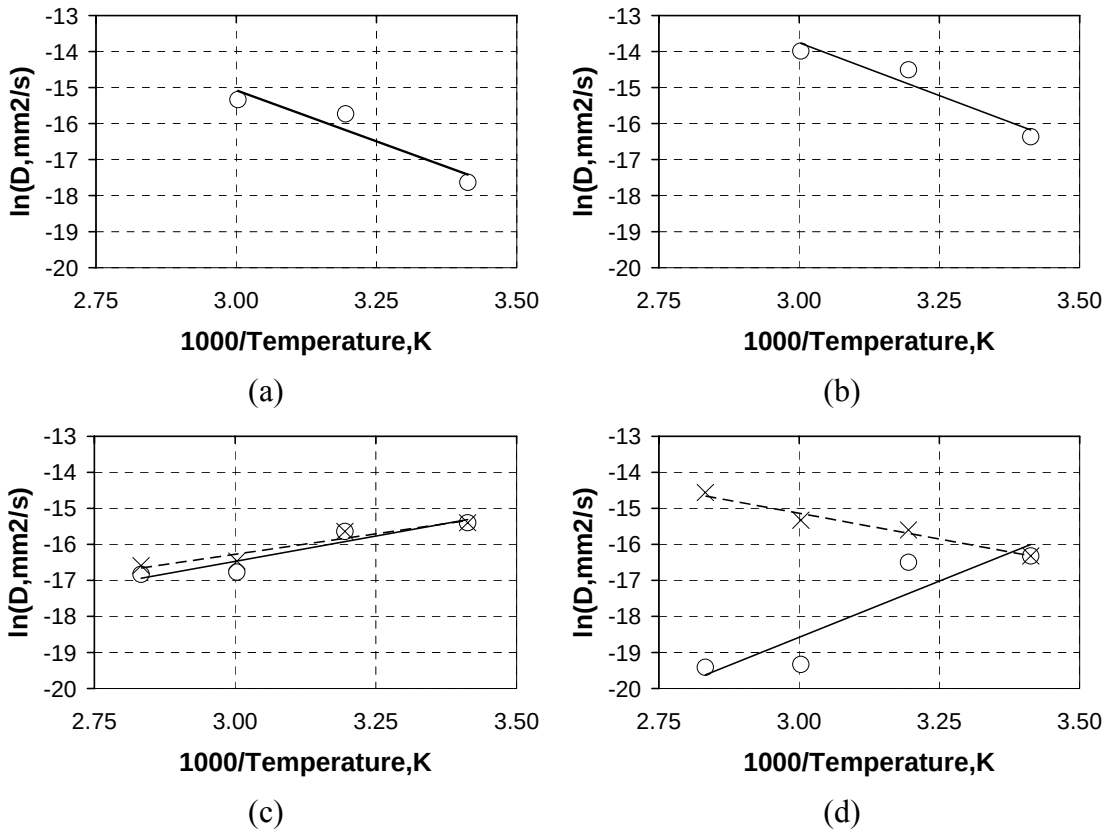

Figure 52. Arrhenius plots for structural modification diffusion coefficient. (a) 18%RH, (b) 50%RH, (c) 99%RH, (d) immersion; ○: apparent, ×: adjusted.

Table 18. Activation energies for structural modification diffusion coefficients.

E_a (kJ/mol)	Apparent	Adjusted
18%RH	47	—
50%RH	49	—
99%RH	-23	-19
Immersion	-52	24

For immersion environments, the degradation evidenced by apparent moisture sorption is so severe that the structural modification process dominates early on.

Consequently, the diffusion process is inhibited by the overwhelmingly favorable structural modification as temperature increases.

Conversely, the degradation and loss of material in the immersion environment may allow for faster diffusion of water, even at early times. The removal of degraded species in the liquid water alters the polymer structure such that diffusion of water is greatly enabled through an increase in available free volume. Consequently, the Fickian dominated diffusion process in immersion environments is a thermally activated process, contrary to the case of 99%RH.

4.5 Directional Diffusion Coefficients

With diffusion coefficients for multiple specimen sizes of a unidirectional composite, it is possible to compare the longitudinal and transverse diffusion coefficients [6]. Recall that for anisotropic Fickian Diffusion, where D_x, D_y, and D_z are the diffusion coefficients in a material with respective dimensions of l, w, and h [6],

$$\frac{\sqrt{D}}{h} = \frac{\sqrt{D_x}}{l} + \frac{\sqrt{D_y}}{w} + \frac{\sqrt{D_z}}{h}. \tag{3}$$

For a unidirectional composite with a longitudinal direction of length l, it can be assumed that $D_x = D_{\parallel}$ and $D_y = D_z = D_{\perp}$ where $D_{\parallel}$ and $D_{\perp}$ are diffusion coefficients in the longitudinal and transverse directions, respectively.

$$\sqrt{D} = \frac{h}{l}\sqrt{D_{\parallel}} + \left(1 + \frac{h}{w}\right)\sqrt{D_{\perp}}. \tag{4}$$

Using multiple linear regression analysis with Equation 4, $D_{\|}$ and $D_{\perp}$ were calculated from Fickian diffusion, presented in Appendix A.1, results and are presented in Table 19 and Table 20. In some cases, denoted by * in Table 19, the values of $D_{\|}^{0.5}$ were less than zero, indicating that the analysis is not valid for those experimentally determined D. Figure 53 compares the predicted and experimental D using Equation 4 with values provided in Table 19 and Table 20.

Table 19. Longitudinal and transverse D for apparent moisture trends. Using Fickian D. * $D_{\|}^{0.5} < 0$

Env.	$D_{\|}$ (10^{-8} mm^2/s)	$D_{\perp}$ (10^{-8} mm^2/s)	$D_{\|} / D_{\perp}$
2L	203 *	5.56	36.6
4L	13.7 *	1.59	8.3
6L	5.63 *	35.3	0.2
2M	25.3	6.63	3.8
4M	0.02	14.5	0.001
6M	2015	18.2	111
6X	791	54.9	14.4
2H	15.3	2.00	7.7
4H	0.02	2.58	0.007
6H	26.5	5.67	4.7
8H	78.7	4.31	18.3
2I	1.07 *	1.58	0.7
4I	0.24	2.88	0.1
6I	30.4	5.58	5.4
8I	43.2	14.8	2.9

Table 20. Longitudinal and transverse D for adjusted moisture trends..

Env.	$D_{\|}$ (10^{-8} mm^2/s)	$D_{\perp}$ (10^{-8} mm^2/s)	$D_{\|} / D_{\perp}$
2H	0.00002	0.03	0.001
4H	1.43	0.12	12.2
6H	13.0	0.38	34.2
8H	25.6	3.14	8.2
2I	0.48	0.02	24.7
4I	1.15	0.06	18.1
6I	11.7	0.14	83.3
8I	86.7	0.61	142.7

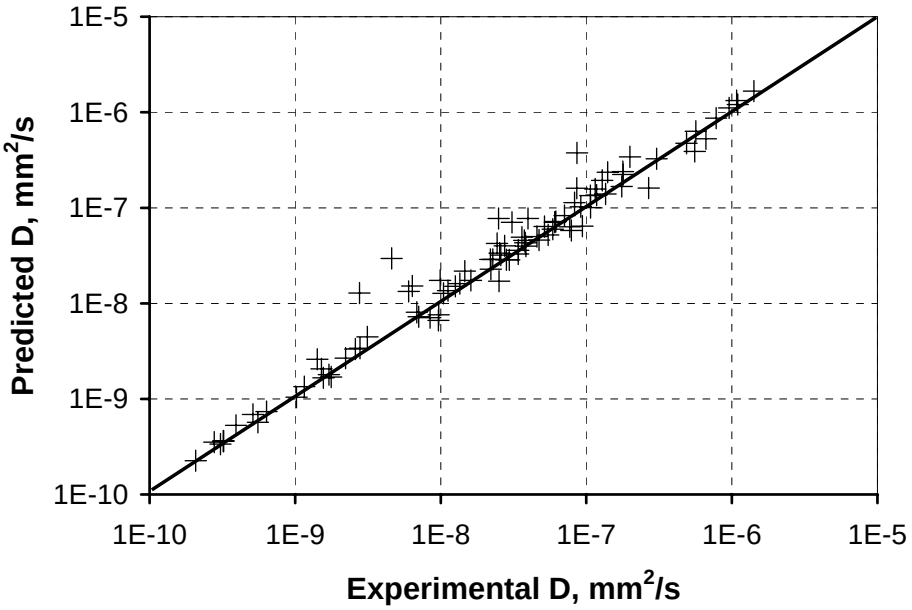

Figure 53. Comparison of predicted and experimental D accounting for size. Using Fickian results. Line indicates equal values.

The values of $D_{\parallel} / D_{\perp}$ obtained using apparent moisture trends range from 0.001 to 111 and do not indicate a trend with temperature. Values of $D_{\parallel} / D_{\perp}$ determined from adjusted moisture trends, where loss of degraded material is accounted for, do not indicate a thermal trend either. However, they do consistently indicate that longitudinal diffusion is greater than transverse. The severe degradation observed in material exposed to immersion at 60°C and 80°C are likely responsible for the high $D_{\parallel}$ indicated by adjusted moisture trends. These high $D_{\parallel}$ may indicate wicking along degraded interfaces such as those illustrated in Figure 23 and Figure 24. At 80°C, the weight loss due to degradation was less severe in 99%RH than in immersion, indicating that the diffusion along degraded interphasial avenues should be

less. This proposition is confirmed by the lower value of $D_{\|}$ at 80°C, though no other adjusted result demonstrates this trend.

4.6 References

1. Aktas, L, Y.K. Hamidi, and M.C. Altan. "Combined Edge and Anisotropy Effects on Fickian Mass Diffusion in Polymer Composites." *Journal of Engineering Materials and Technology*. Vol. 126 (2004) 427-435.

2. Dewimille, B. and A.R. Bunsell. "The modeling of hydrothermal aging in glass fibre reinforced epoxy composites." *Journal of Physics D – Applied Physics*. Vol. 15, No. 10. (1982) 2079-2091.

3. Jacobs, P.M. and F.R. Jones. "Diffusion of moisture into two-phase polymers. Part 1." *Journal of Materials Science*. Vol. 24 (1989) 2331-2336.

4. Carter, H.G. and K.G Kibler. "Langmuir-Type Model for Anomalous Moisture Diffusion in Composite Resins." *Journal of Composite Materials.* Vol. 12 (1978) 118-131

5. Bonniau, P. and A.R. Bunsell. "A Comparative Study of Water Absorption Theories Applied to Glass Epoxy Composites." *Journal of Composite Materials*. Vol. 15 (1981) 272-293.

6. Shen, C.H. and G.S. Springer. "Moisture Absorption and Desopriton of Composite Materials." *Journal of Composite Materials*. Vol. 10 (1976) 2-20.

5. Mechanical Characterization

5.1 Tensile Testing

Longitudinal tensile testing was executed in order to determine longitudinal tensile parameters used in composite design. Initial tensile properties are presented in Table 21. The average and standard deviation for pre-conditioned material was obtained from tensile testing of 69 specimens pre-conditioned at 40°C and 18%RH for 6 weeks. Material exposed to 40°C at 18%RH was also tested in sets of 5 after another 6, 12, 18, 24, 30, 36, 42, 48, 54, 72, 78, 96, and 102 weeks of exposure, providing an additional 65 tests. The baseline average and standard deviation were calculated using results from a total 134 tensile tests of material exposed to 40°C at 18%RH.

Table 21. Initial tensile properties.
Brackets indicate standard deviations.

	As-Received	Pre-conditioned	Baseline
Strength (MPa)	1141 [31]	1109 [46]	1119 [44]
Modulus (GPa)	49.4 [1.8]	53.8 [3.2]	52.5 [3.1]
Failure Strain (%)	1.92 [0.06]	1.71 [0.13]	1.79 [0.13]

Exposure to 18%RH at 40°C results in embrittlement after the removal of water, as indicated by increased tensile modulus and decreased tensile strength and failure strain. Both as-received and pre-conditioned longitudinal tensile specimens demonstrated a brooming mode of failure, as depicted in Figure 54.

Previous work on the hygrothermal degradation of the tensile strength of a glass/vinylester system has revealed similar irreversible degradation [1,2].

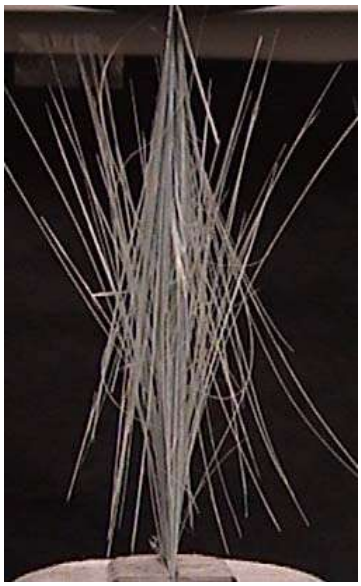

Figure 54. Brooming failure of tensile specimen.

Tensile results for all environmental exposures can be found in Appendix B.1. The resulting trends can be classified into three groups. Tensile properties of material exposed to 18%RH and 50%RH did not change significantly, though subtle increases in strength and strain can be detected. Exposure to 99%RH and immersion in deionized water resulted in severe degradation of tensile properties. Exposure to 75%RH at 60°C resulted in decreased tensile properties which were less significant than that which occurred in material exposed to 99%RH and immersion environments but more significant than that which occurred after exposure to 50%RH. Redrying of material exposed to 75%RH at 60°C resulted in recovery of tensile properties such that the dry values were within baseline scatter. The following discussion has been broken up into three sections where the effect of (i) 18%RH and 50%RH, (ii) 75%RH, and (iii) 99%RH and immersion are discussed in detail.

5.1.1 Low and Medium Humidity Tensile Results

For material exposed to 18%RH and 50%RH environments at all temperatures, the tensile strength remains within scatter bounds of the initial pre-conditioned value over an exposure period of 96 weeks. A brooming failure mode was observed in all sets tested.

Figure 55 provides the tensile strength of the composite after exposure to 18%RH for 72 weeks. For exposure to low humidity, no significant changes in strength values were observed between wet and dry testing. The tensile strength of material exposed to 18%RH at 40°C appears to increase some, though the wet and dry values are both within initial baseline scatter. However, baseline values were calculated using tensile results for pre-conditioned material along with results from material exposed to 40°C and 18%RH for all exposure times. Therefore, this apparent increase in strength reflects the scatter inherent in the baseline set.

Figure 56 provides the longitudinal tensile strength after exposure to 50%RH for 72 weeks. After post-conditioning of material exposed to 50%RH, the average dry tensile strength is consistently greater than the average wet tensile strength. However, after the removal of water, the dry tensile strengths are generally still within initial scatter range. These results indicate that the removal of water contents between 0.05% and 0.1%, resulting from exposure to 50%RH, slightly increases the tensile strength of the composite.

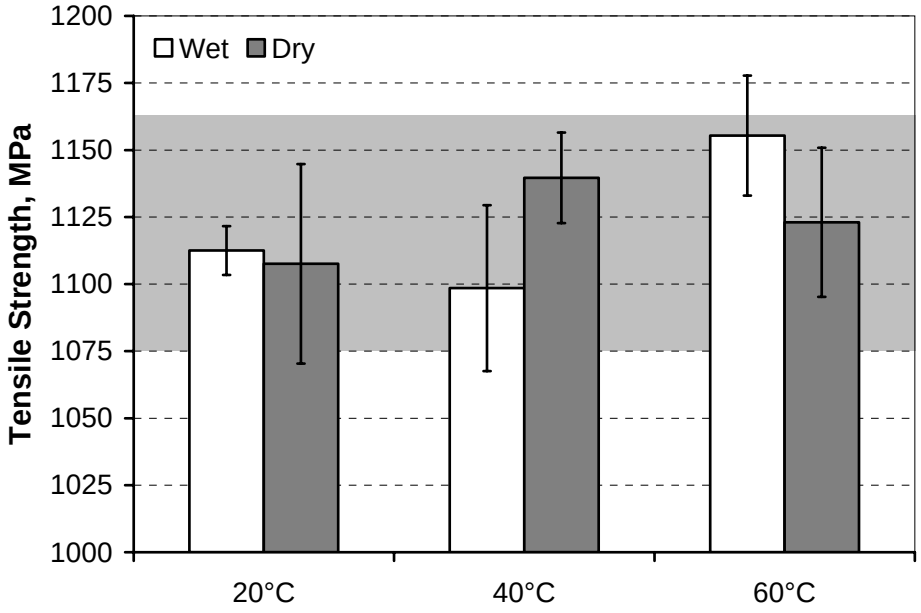

Figure 55. Tensile strength after exposure 18%RH for 72 wks. Shaded region indicates baseline average and standard deviation. Error bars indicate standard deviations.

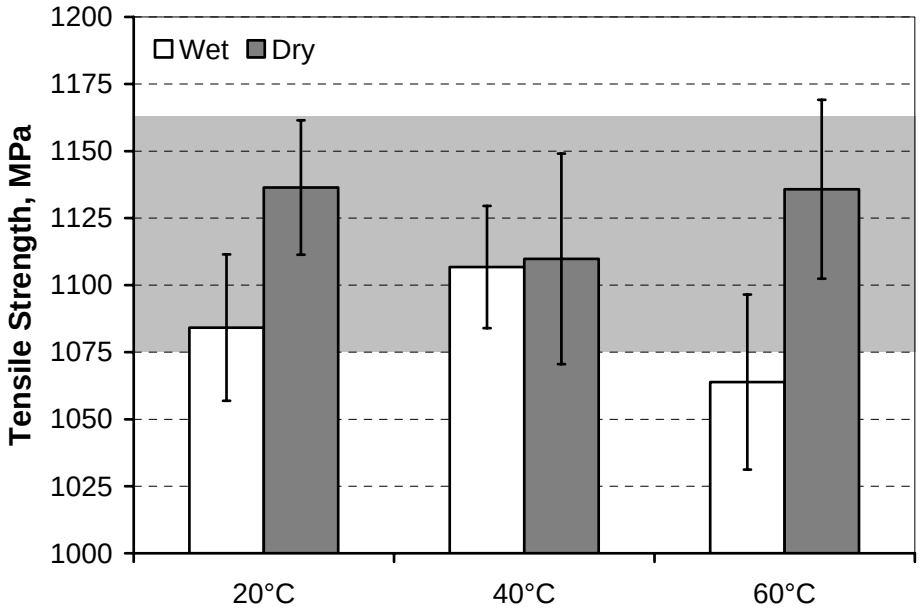

Figure 56. Tensile strength after exposure to 50%RH for 72 wks. Shaded region indicates baseline average and standard deviation. Error bars indicate standard deviations.

The observed decrease in tensile modulus resulting from exposure to low and medium humidity environments is similarly insignificant for both wet and dry sets. It is interesting to note that the average tensile modulus does increase after exposure to 18%RH and 50%RH at 20°C and 50%RH at 40°C for 12 weeks prior to a subsequent decrease, as depicted in Figure 57 and Figure 58. The average tensile modulus is otherwise lower than the baseline through two years for all environmental exposures.

There is an observable increase in the average failure strain of material exposed to low and medium humidity environments, depicted in Figure 59 and Figure 60, although minimal. The average dry failure strain tends to be greater than the wet, though the scatter in the baseline and concerned wet and dry sets is high. For instance, the difference between wet and dry strains tends to be less than the standard deviation of the baseline set.

In summary, material exposed to 18%RH and 50%RH demonstrates consistent, albeit subtle, increases in tensile strength and failure strain, seen in Figure 61 and Figure 62, while the tensile modulus decreases slightly but remains within initial scatter.

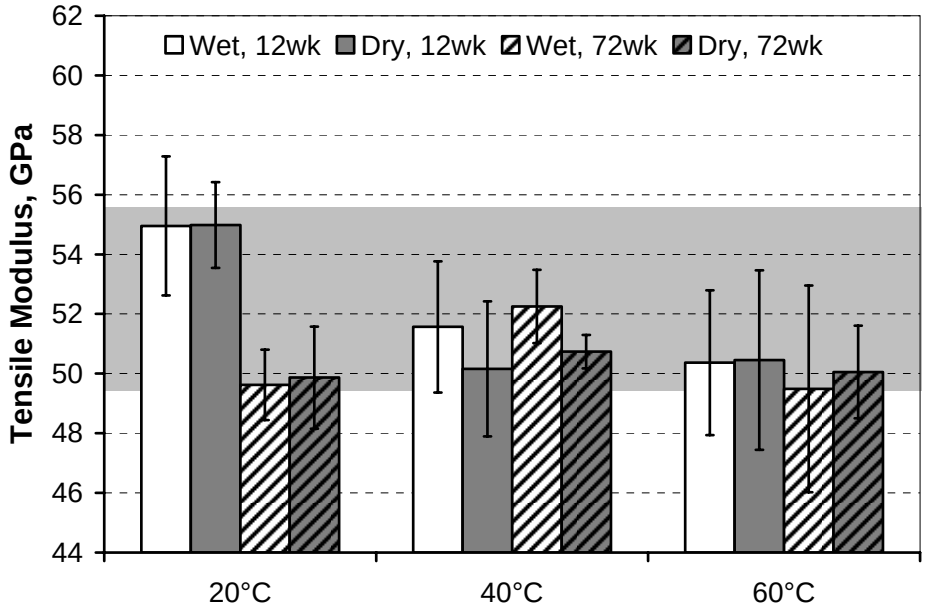

Figure 57. Tensile modulus after exposure to 18%RH for 12 and 72 wks. Shaded region indicates baseline average and standard deviation. Error bars indicate standard deviations.

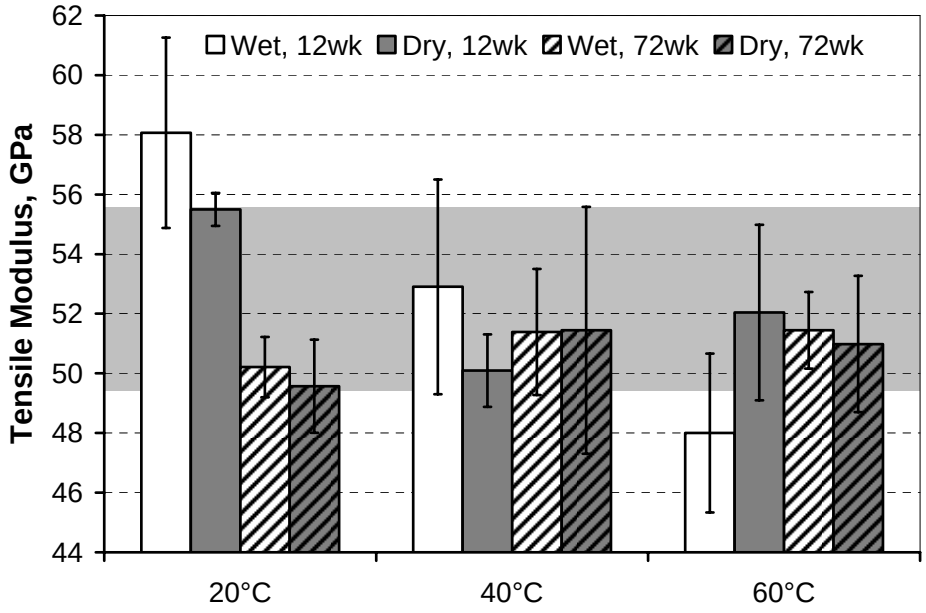

Figure 58. Tensile modulus after exposure to 50%RH for 12 and 72 wks. Shaded region indicates baseline average and standard deviation. Error bars indicate standard deviations.

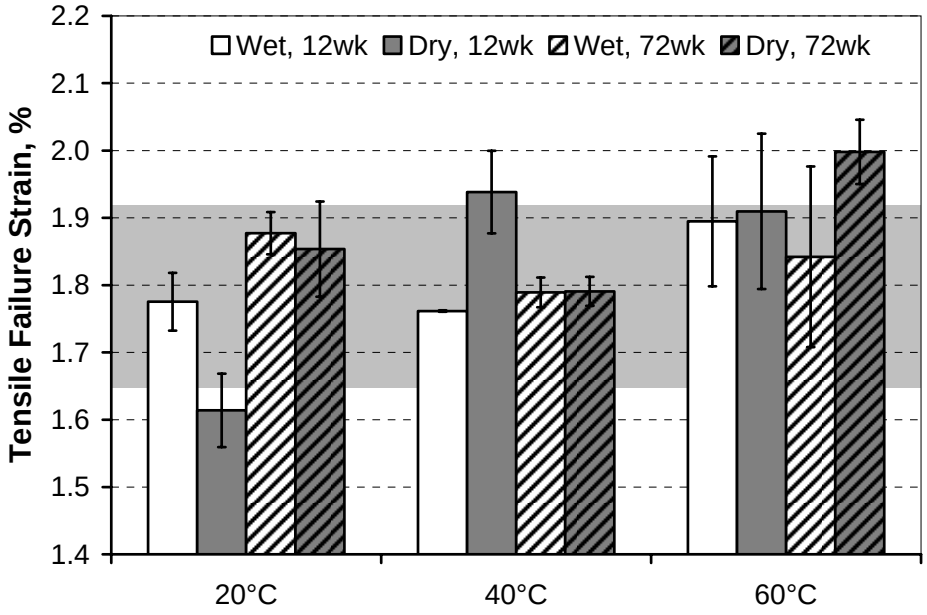

Figure 59. Tensile failure strain after exposure to 18%RH for 72 weeks. Shaded region indicates baseline average and standard deviation. Error bars indicate standard deviations.

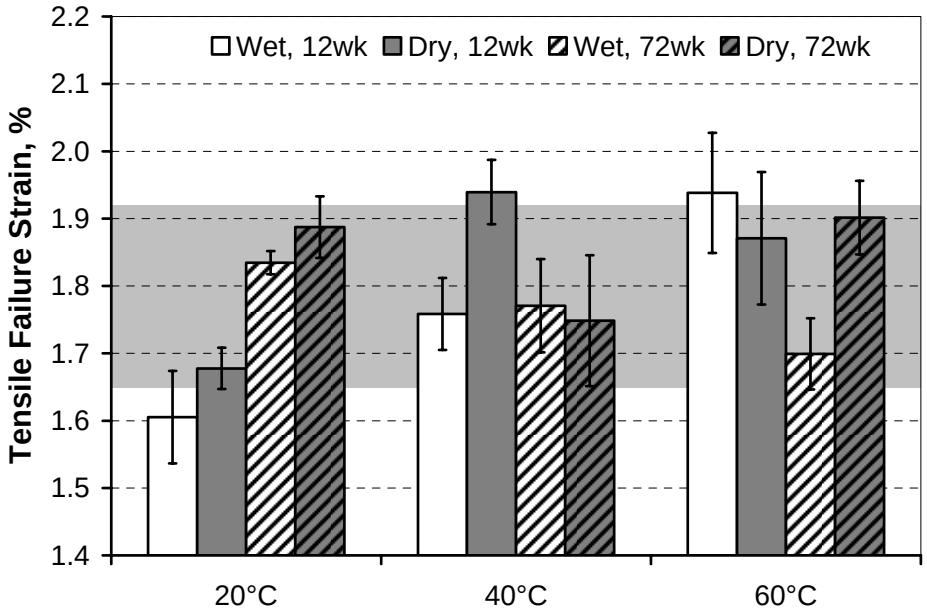

Figure 60. Tensile failure strain after exposure to 50%RH for 72 weeks. Shaded region indicates baseline average and standard deviation. Error bars indicate standard deviations.

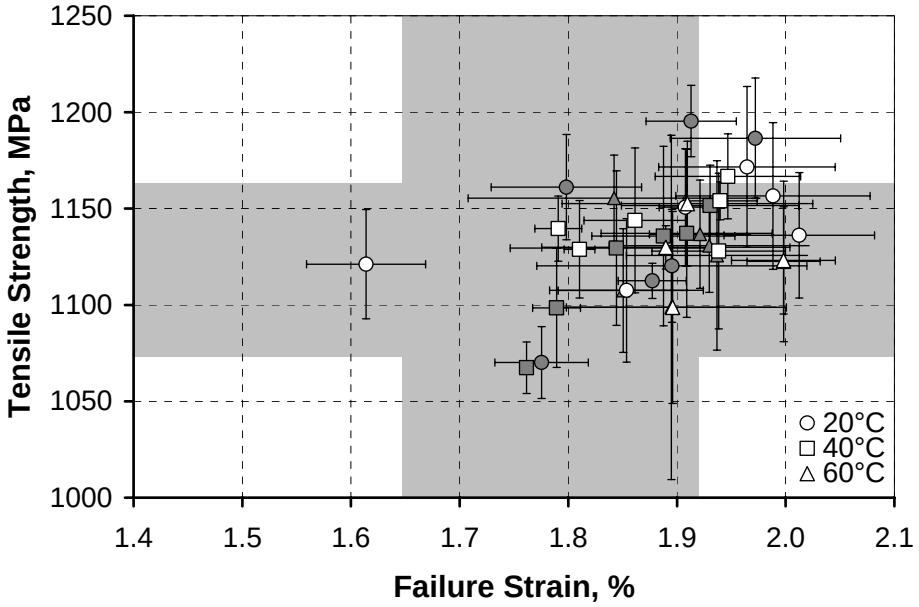

Figure 61. Tensile strength and failure strain after exposure to 18%RH. Closed: wet, open: dry. Shaded region indicates baseline averages and standard deviations. Error bars indicate standard deviations.

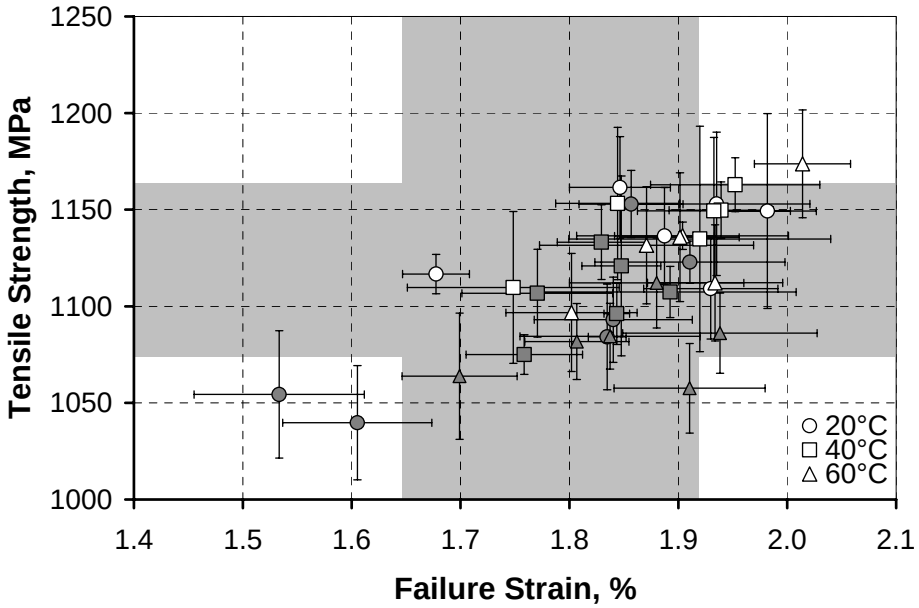

Figure 62. Tensile strength and failure strain after exposure to 50%RH. Closed: wet, Open: dry. Shaded region indicates baseline averages and standard deviations. Error bars indicate standard deviations.

5.1.2 75%RH Tensile Results

Exposure to 75%RH at 60°C (6X) resulted in a partly reversible decrease in tensile strength, similar to but more severe than that observed in material exposed to 50%RH at the same temperature (6M), as seen in Figure 63. While exposure to 50%RH at 60°C results in a relatively constant wet tensile strength, ranging from a low of 1058 [23] MPa at 24 weeks to a high of 1112 [23] MPa at 48 weeks, the wet tensile strength of material exposed to 75%RH at 60°C demonstrates a steady decreasing trend with time.

If recovery is defined as

$$\%\text{Recovery} = \frac{P_d - P_w}{P_0 - P_w} \times 100\%, \quad (1)$$

where P_d, P_w, and P_0 are the average dry, wet, and initial property values, it can be concluded that post-conditioning of material exposed to 75%RH at 60°C leads to a 61%, 72%, and 35% recovery in tensile strength at 12, 48, and 72 weeks, while redrying of material exposed to 50%RH at 60°C generally leads to increases in tensile strength above baseline values. These results indicate that there is some progression of irreversible degradation with time resulting from exposure to 75%RH but not 50%RH.

Figure 64 presents the wet tensile strength for each individual specimen exposed to 75%RH plotted against the apparent moisture content of each specimen. The apparent moisture content is calculated from wet and initial weights, using Equation 1 from Section 4.1. Figure 64 indicates that there is no clear relation of moisture content to tensile strength. Rather the degradation mechanism responsible

for reversible deterioration of the tensile strength is a function of time. The progression of decreasing tensile strength and strength recovery could therefore be a consequence of progressive interfacial debonding or polymer breakdown. Increases in the tanδ peak height obtained from Dynamic Mechanical Thermal Analysis (DMTA) for material exposed to 60°C, discussed in Section 6.2.3.2, indicates that there is some progression of interfacial debonding or a chemical reaction leading to a decrease in crosslink density or a combination of both. A discussion on crosslink density can be found in Section 6.2.4.

Because tensile strength is highly dependent upon interfacial and polymer strength, the breakdown of these component strengths would lead to a decrease in longitudinal composite strength. The discussion in Section 6.2.4 addresses the partially reversible nature of these changes in crosslink density and tanδ peak height. Furthermore, DMTA results reveal that there is some plasticization within the polymer matrix or interphase, reflected by an increase in glass transition temperature T_g and tanδ peak height after redrying. A partially reversible decrease in crosslink density and the occurrence of plasticization would indicate a reversible decrease in polymer strength which would be reflected in the composite tensile strength.

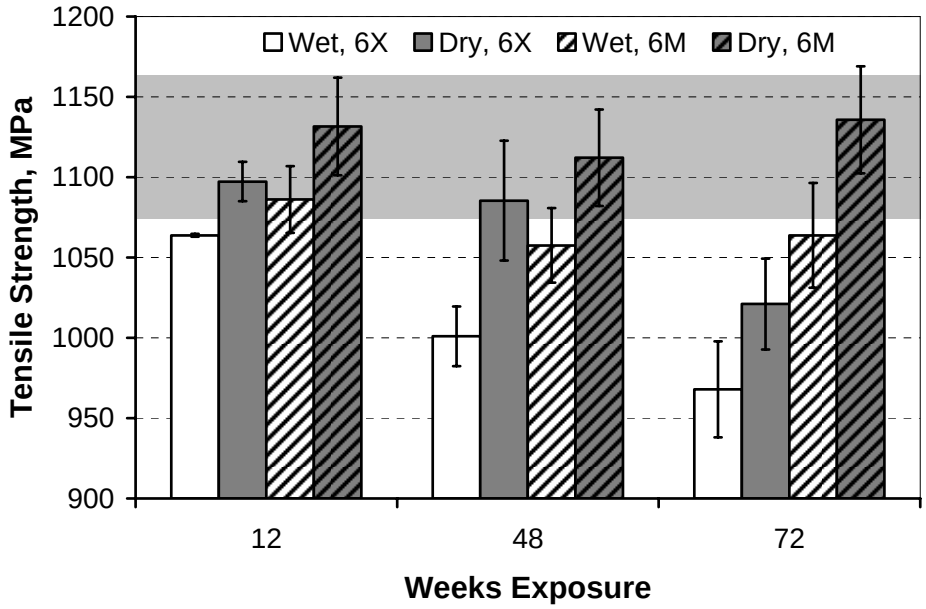

Figure 63. Tensile strength after exposure to 75%RH and 50%RH at 60°C. Shaded region indicates baseline average and standard deviation. Error bars indicate standard deviations.

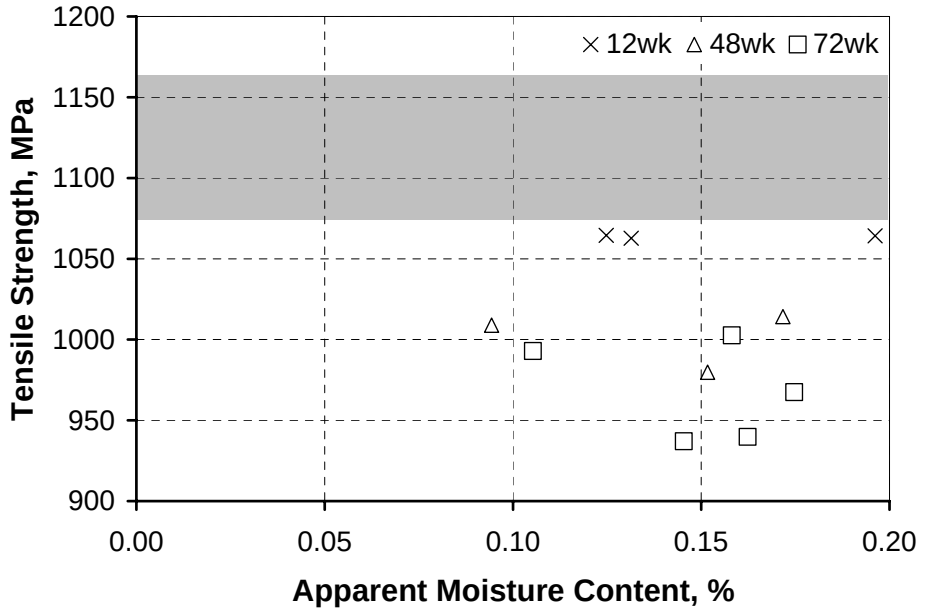

Figure 64. Wet tensile strength of material exposed to 75% at 60°C. Shaded region indicates baseline average and standard deviation.

In the first 12 weeks of exposure to 75%RH at 60°C, the tensile modulus experienced a sharp decrease of 12.4% from 53.8 [3.2] GPa to 47.1 [1.8] GPa, as shown in Figure 65. Post-conditioning material exposed for 12 weeks resulted in a subsequent increase of 8.3% to 51.0 [2.0] GPa, where the dry modulus is within initial scatter bounds. After 12 weeks, however, the wet and dry moduli steadily increase to where they are each within initial scatter bounds. An investigation of the wet tensile modulus as a function of moisture content for each specimen, shown in Figure 66, indicates that there does not appear to be a direct dependence on moisture content. Again, a progressive trend can be identified with time as the tensile modulus increases with time of exposure, independent of moisture content.

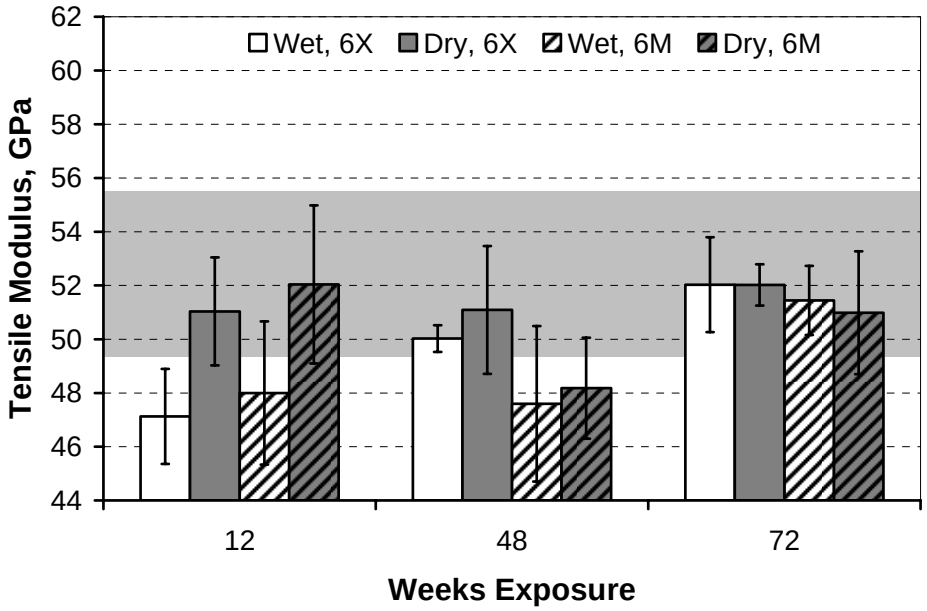

Figure 65. Tensile modulus after exposure to 75%RH and 50%RH at 60°C.
Shaded region indicates baseline average and standard deviation.
Error bars indicate standard deviations.

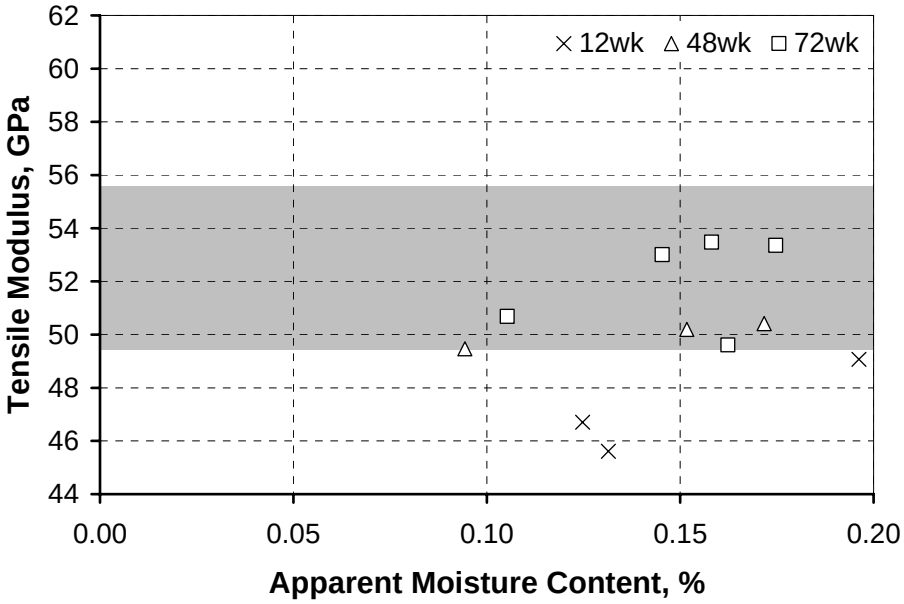

Figure 66. Wet tensile modulus of material exposed to 75% at 60°C. Shaded region indicates baseline average and standard deviation.

The tensile strain, presented in Figure 67, does not change until after 12 weeks of exposure to 75%RH at 60°C. After the first 12 weeks, a marked decrease in the average wet tensile failure strain occurs, whereupon the failure strain increases after redrying. Loading curves, provided in Figure 68 and Figure 69, indicates that wet material experiences a stiffening effect starting at a strain of about 0.8 %. This onset of stiffening is later than that for pre-conditioned material, in which stiffening appears to initiate at a strain of about 0.5 %. A secondary modulus may be defined as the modulus calculated from stresses and strains between 1.25 % and 1.4 %. Table 22 provides a summary of secondary moduli for material exposed to 60°C at 50%RH and 75%RH for 48 weeks. It is clear that the stiffening effect is more significant after exposure to 75%RH than for 50%RH, and this late stiffening is partly responsible for a decrease in failure strain.

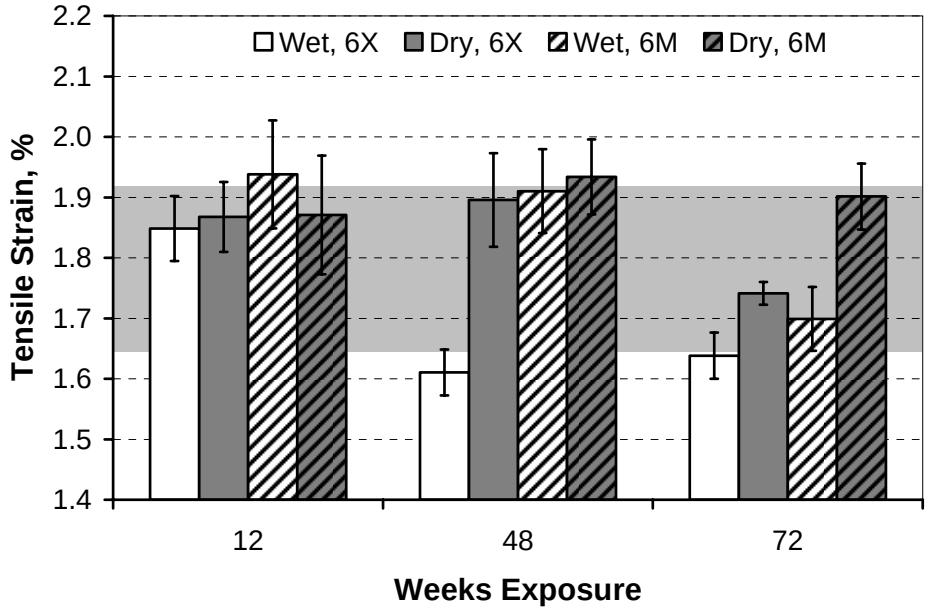

Figure 67. Tensile failure strain after exposure to 75%RH and 50%RH at 60°C.
Shaded region indicates baseline average and standard deviation.
Error bars indicate standard deviations.

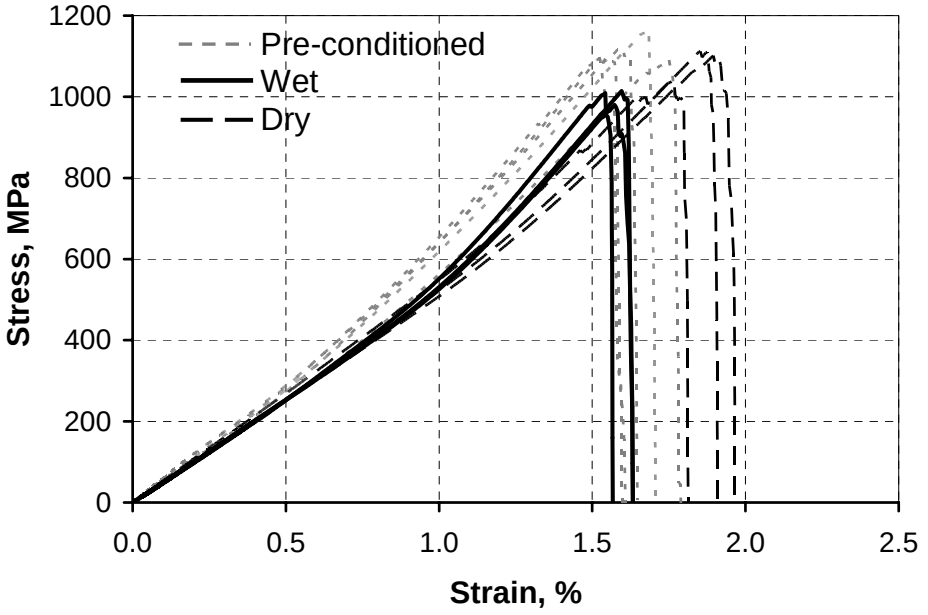

Figure 68. Loading curves of material exposed to 75%RH at 60°C for 48 weeks.
Five loading curves are presented for the pre-conditioned set.
Three loading curves for both sets of exposed material are presented.

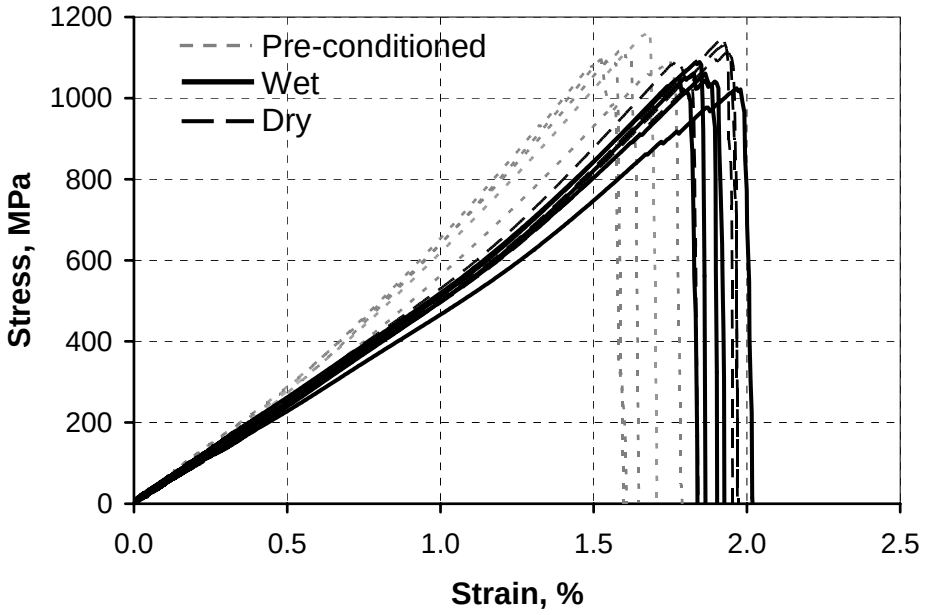

Figure 69. Loading curves of material exposed to 50%RH at 60°C for 48 weeks. Five loading curves are for each set.

Table 22. Secondary moduli for material exposed to 50%RH and 75%RH at 60°C for 48 weeks. Brackets indicate standard deviations.

	50%RH	75%RH	Baseline
Wet	67.5 [2.9]	86.9 [4.6]	78.9 [7.0]
Dry	71.3 [3.9]	69.0 [4.0]	

Similar to the tensile strength and tensile modulus, the secondary modulus appears to be independent of moisture content, as seen in Figure 70. Nonetheless, it is clear that the presence of moisture in the material leads to a stiffening effect which can be reversed after the removal of water. The plasticization effect detected through DMTA tests, which will be discussed in Section 6.2.2.2 and 6.2.3.2, is more pronounced after exposure to 75%RH than after exposure to 50%RH. With the plasticized matrix, the fiber reinforcement may align at higher strains, leading to a higher secondary modulus. While the tensile strength and modulus demonstrate a

clear trend with time, the results presented in Figure 70 do not indicate any clear temporal trend in secondary modulus.

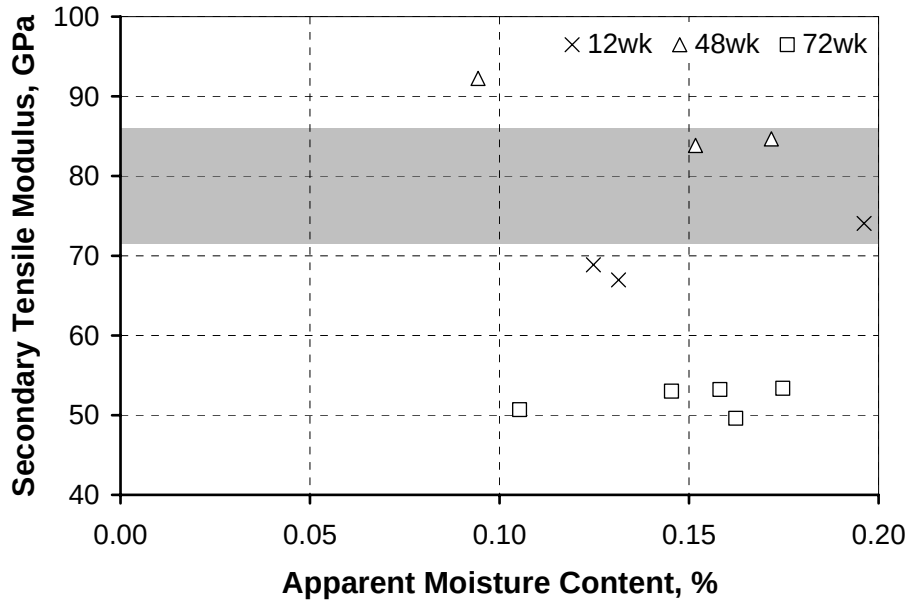

Figure 70. Wet secondary modulus of material exposed to 75% at 60°C. Shaded region indicates baseline average and standard deviation.

5.1.3 High Humidity and Immersion Tensile Results

Degradation of tensile properties after exposure to 99%RH and immersion environments is more severe than any resulting from less aggressive environments and, at elevated temperatures, is irreversible. Only material exposed to room temperature 99%RH and immersion demonstrated a complete regain of tensile strength after post-conditioning, as seen in Figure 71 through Figure 74.

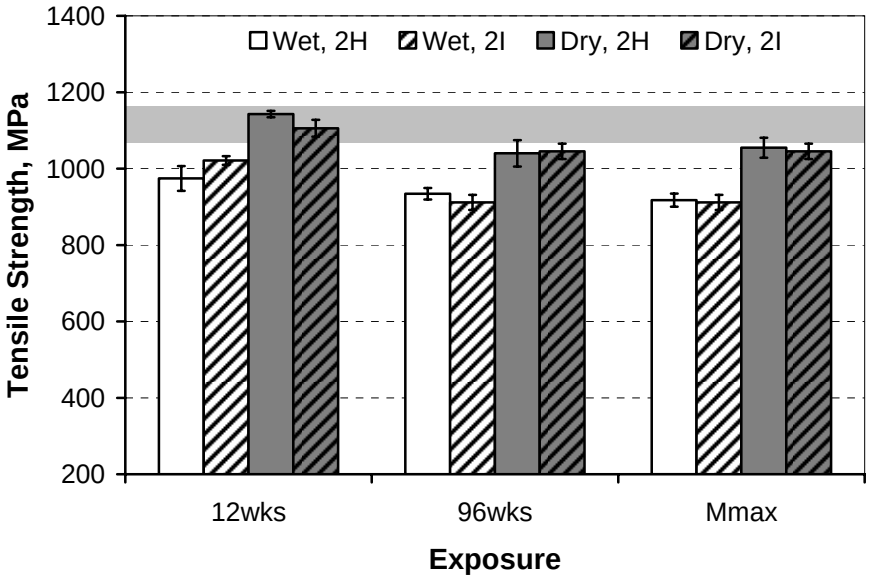

Figure 71. Tensile strength after exposure to 99%RH and immersion at 20°C. H = 99%RH, I = Immersion. M_{max} is maximum apparent moisture content. Shaded region indicates baseline average and standard deviation. Error bars indicate standard deviations.

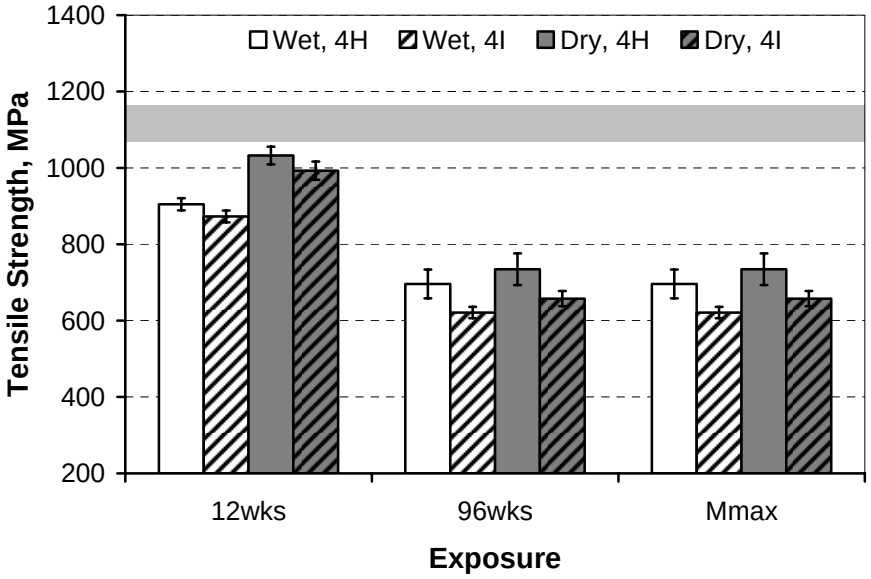

Figure 72. Tensile strength after exposure to 99%RH and immersion at 40°C. H = 99%RH, I = Immersion. M_{max} is maximum apparent moisture content. Shaded region indicates baseline average and standard deviation. Error bars indicate standard deviations.

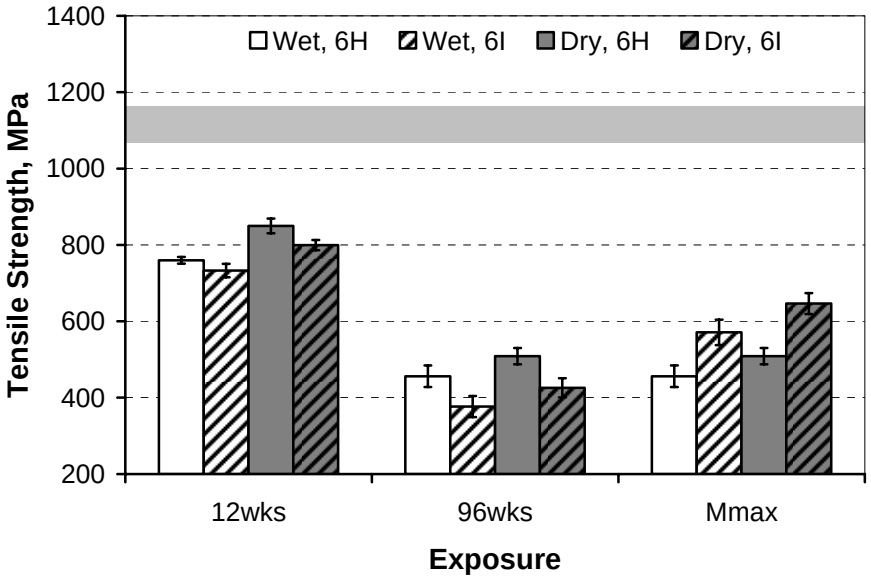

Figure 73. Tensile strength after exposure to 99%RH and immersion at 80°C. H = 99%RH, I = Immersion. M_{max} is maximum apparent moisture content. Shaded region indicates baseline average and standard deviation. Error bars indicate standard deviations.

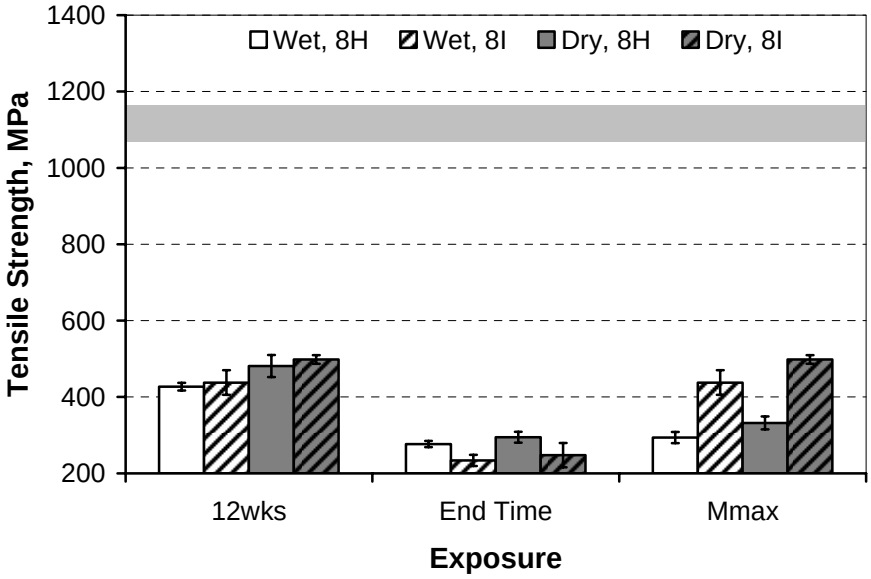

Figure 74. Tensile strength after exposure to 99%RH and immersion at 80°C. H = 99%RH, I = Immersion. M_{max} is maximum apparent moisture content. The end time for all sets was 96 weeks except for 80°C, 99%RH (8H), which was tested through 72 weeks only. Shaded region indicates baseline average and standard deviation. Error bars indicate standard deviations.

All saturated environments demonstrate some recovery in tensile strength, though the regain decreases with increasing temperature of exposure. Using the definition of recovery provided in Equation 1 in Section 5.1.2, Table 23 summarizes the maximum recovery observed over 96 weeks of exposure and the recovery at the end of testing at 96 weeks. Recovery values greater than 100% indicate a material which experienced an increase in tensile strength above the baseline average after uptake and removal of water. These increased strengths are within initial scatter.

Table 23. Recovery of tensile strength after exposure to saturated environments. End time is 96 weeks for all sets except for 80°C, 99%RH (8H), which was tested through 72 weeks only. Brackets indicate standard deviations.

	Maximum Recovery		**Recovery at End Time**	
Environ.	**Maximum Recovery**	**Dry Tensile Strength (MPa)**	**Recovery at End Time**	**Dry Tensile Strength (MPa)**
Baseline	—	1119 [44]	—	1119 [44]
2H	128%	1161 [34]	57%	1040 [34]
2I	127%	1155 [44]	64%	1045 [20]
4H	60%	1032 [23]	9%	735 [42]
4I	49%	993 [24]	7%	658 [20]
6H	25%	850 [19]	8%	509 [21]
6I	17%	800 [13]	7%	426 [25]
8H	8%	481 [29]	5%	332 [17]
8I	9%	498 [11]	2%	248 [32]

Except for material exposed to 20°C in 99%RH and immersion, the maximum recovery in tensile strength occurred at 12 weeks. For material exposed to 20°C at 99%RH and 20°C immersion, the maximum recovery occurred at 36 weeks and 24 weeks, respectively. Through 48 weeks, however, the dry tensile strength is within initial scatter for material exposed to saturated environments at 20°C. After 48 weeks, the tensile strength of material exposed to 20°C in 99%RH and immersion demonstrates irreversible degradation. Even at room temperature in high moisture

content environments, there is a progression from reversible to irreversible degradation concurrent with plasticization.

After 12 weeks of exposure, the increasing irreversibility of material degradation resulting from exposure to 99%RH and immersion environments at elevated temperatures is obvious and already shows a dependency on temperature. After 96 weeks of exposure, while the dry tensile strength is higher for after exposure to 40°C than for 60°C, the recovery is about the same.

While the average tensile strength after exposure to 80°C immersion increases after redrying, at every time step except for 12 weeks, the scatter of the wet and dry sets are such that the two sets overlap, as demonstrated in Figure 75. Even with the overlap in scatter, there is a small recovery in tensile strength, possibly due to the reversal of plasticization in the resin matrix.

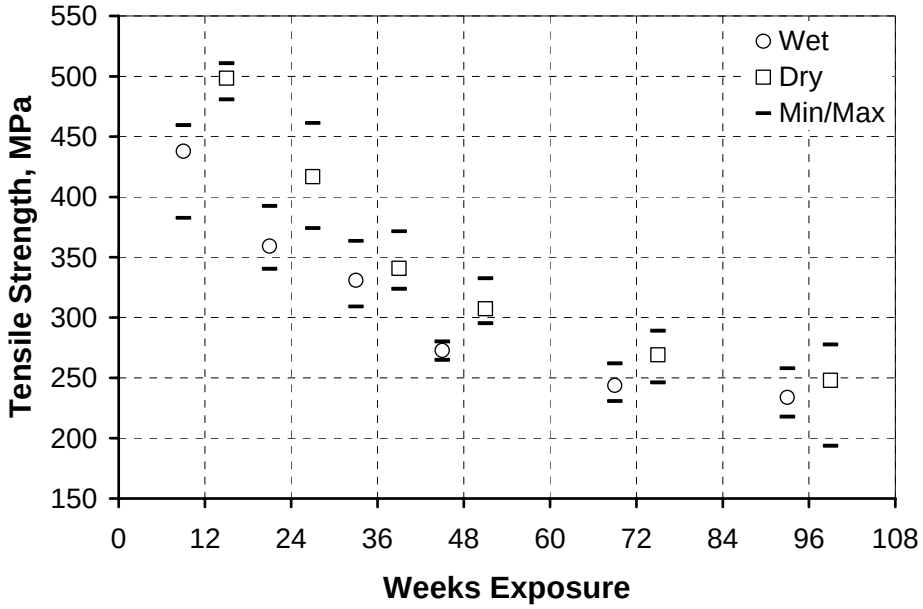

Figure 75. Tensile strength of material exposed to immersion at 80°C. Values plotted are the average, minimum and maximum for each set of 5 tests. Each time step is offset by 3 weeks for clarity.

The failure mode transitions from primarily a longitudinal splitting failure, as after exposure to 99%RH and immersion environments at 20°C, to a surface separation failure. The surface separation failure is characterized by surface layers failing in tension and separating from the inner thickness, which fails in longitudinal splitting. Because the inner thickness is much less than the total composite thickness, the surface sections constrain the longitudinal splitting failure within, as depicted in Figure 76. Increasing exposure time, temperature of exposure and moisture content leads to increasing width in surface separation sections, indicating that tensile strength of the surface layer decreases with time and moisture content.

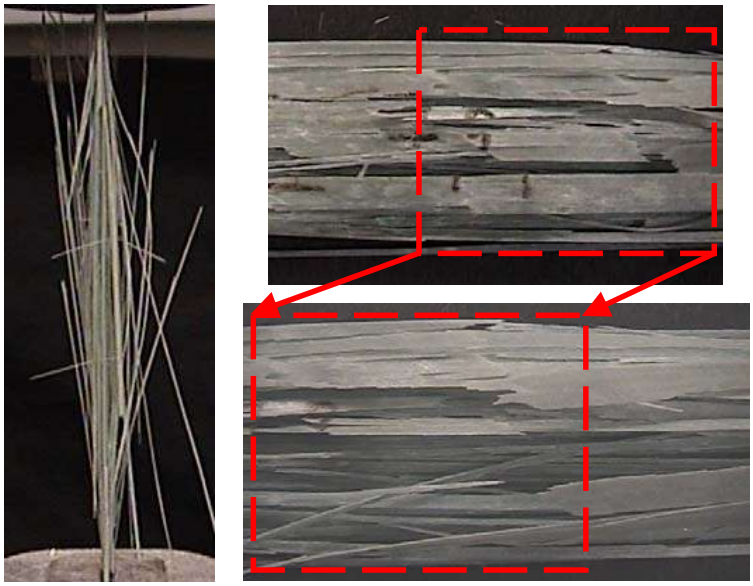

(a) (b)

Figure 76. Surface separation failure mode of tensile specimen. Material exposed to 60°C immersion for 24 weeks. (a) Side view, (b) view of surface. Boxed area identifies same location on single specimen with and without surface removed to reveal sub-surface longitudinal splitting.

Scanning electron microscopy further corroborates the development of failure mode in tensile specimens, where significant decreases in interfacial adhesion are

observed. Figure 77 indicates good fiber/matrix adhesion in failed pre-conditioned tensile specimens. In contrast, Figure 78 reveals interfacial debonding on the inner surface of one of these sections which failed in tension on the specimen surface and separated from the inner thickness.

In Figure 77, where fibers have pulled out from the bulk material, matrix remains adhered to the fiber surface. The failure of the polymer matrix appears to be brittle in nature. Longitudinal matrix splitting can also be identified in Figure 77. In Figure 78, fiber pullout occurs with little or no matrix adhered to the surface. There are long sections of resin matrix on the failure surface where fiber failure occurred with little damage to the matrix, leaving only the concave resin surface, indicating loss of fiber/matrix adhesion. Polymer matrix failure appears to be more ductile in the wet material presented in Figure 78.

Figure 79 depicts two characteristic features of these debonding areas. Region I in Figure 79 is a smooth surface which could represent a void formed between the fiber and matrix. Such smooth, defined surfaces are not seen in unexposed failed tensile specimens, so it is reasonable to conclude that Region I indicates interfacial debonding. Region II represents a general loss of fiber/matrix adhesion with localized polymer failures where adhesion was better. Sub-micron pitting can also be identified in Region II and on the surfaces adjacent to the labeled areas. The localized failures tend to be less than 3 μm. There is strong evidence that these areas of localized polymer failure occur where there is kaolin filler. Kaolin clay is a filler commonly used in pultrusion and has also been identified at pitting sites on the glass fiber. The

effect of kaolin on glass fiber composite degradation will be addressed further in Section 5.3.

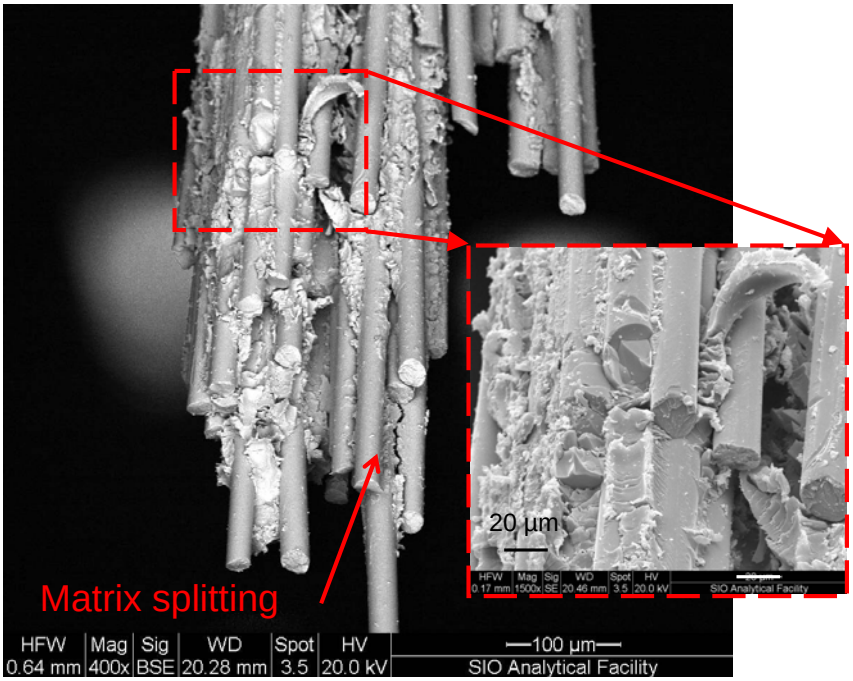

Figure 77. SEM of tensile failure of as-received material.

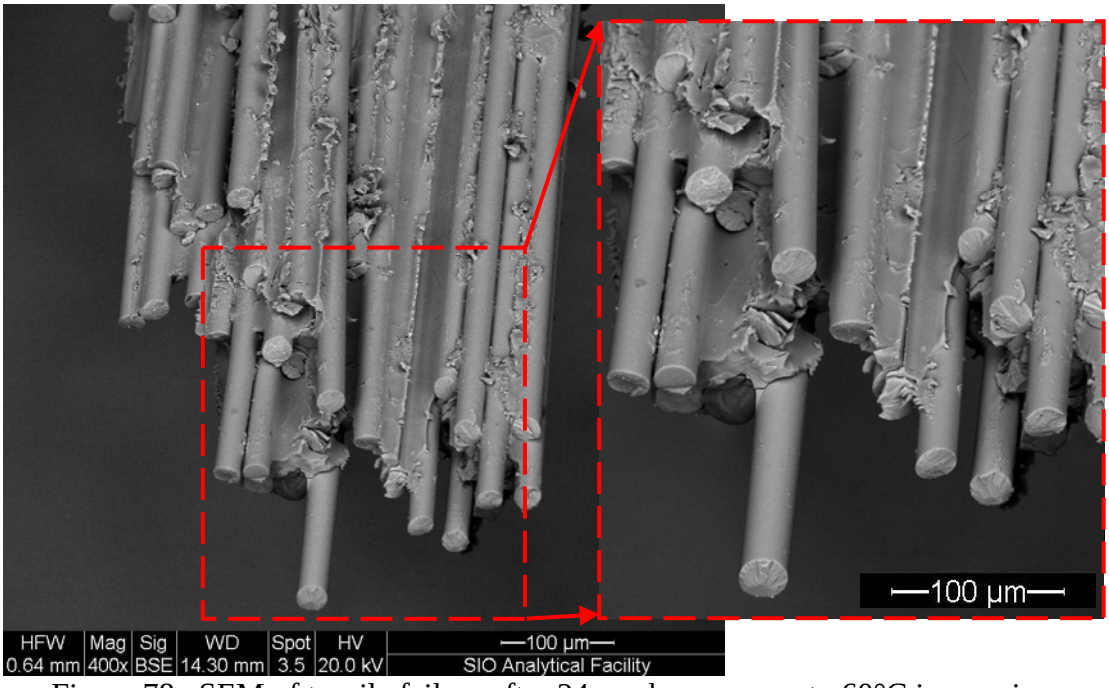

Figure 78. SEM of tensile failure after 24 weeks exposure to 60°C immersion.

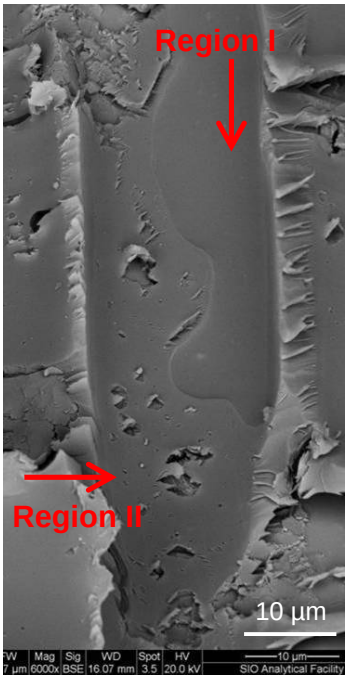

Figure 79. SEM of tensile failure after 24 weeks exposure to 60°C immersion.

Increasing moisture content clearly has a detrimental effect on the tensile strength of the E-glass/vinyl-ester composite under consideration here. Figure 80 presents the wet tensile strength as a function of the adjusted moisture content in the tensile specimen, where the adjusted moisture content uses the wet, dry, and initial weights, defined as W_w , W_d, and W_0, respectively, to account for leaching of degraded material into the exposure environment:

$$M_{t,a} = \frac{W_w - W_d}{W_0} \times 100\% . \qquad (2)$$

Figure 80 demonstrates that for material with similar moisture contents exposed to 99%RH and immersion at the same temperature, the wet tensile strength resulting from exposure to 99%RH is less than that resulting from immersion. Because it takes a longer period of time to reach a particular moisture content in 99%RH than in

immersion, it would be expected that time aggravates the degradation resulting from moisture uptake. Redrying of the material demonstrates some recovery in tensile strength, as seen in Figure 81; however, as the wet tensile strength decreases, the recovery after redrying also decreases. The irreversible degradation occurring at higher moisture contents, seen in Figure 80, becomes more severe as its influence on the tensile strength increases.

The tensile modulus demonstrated a general decreasing trend with moisture content in material exposed to 99%RH and immersion, but the exposed values were generally within initial scatter, as seen in Figure 82 through Figure 85. It is expected that the tensile modulus would decrease with increasing moisture, as the polymer resin plasticizes.

For all 99%RH and immersion environments, the change in tensile modulus from wet to dry is on the order of a standard deviation. However, removal of water from material exposed to 99%RH and immersion at 20°C, 40°C, and 60°C does consistently result in stiffening of the composite for all conditions except 99%RH at 60°C, where no clear trend could be identified.

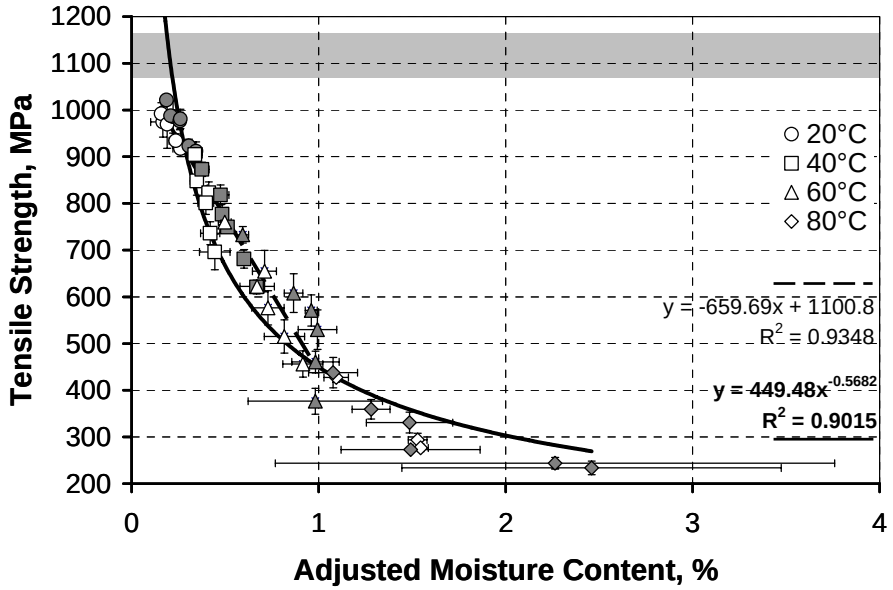

Figure 80. Wet tensile strength as a function of adjusted moisture content for 99%RH and immersion exposures. Open: 99%RH, closed: immersion. Linear fit was performed for $M_{t,a} < 1\%$. Power fit was performed for all $M_{t,a}$. Shaded region indicates baseline average and standard deviation. Error bars indicate standard deviation.

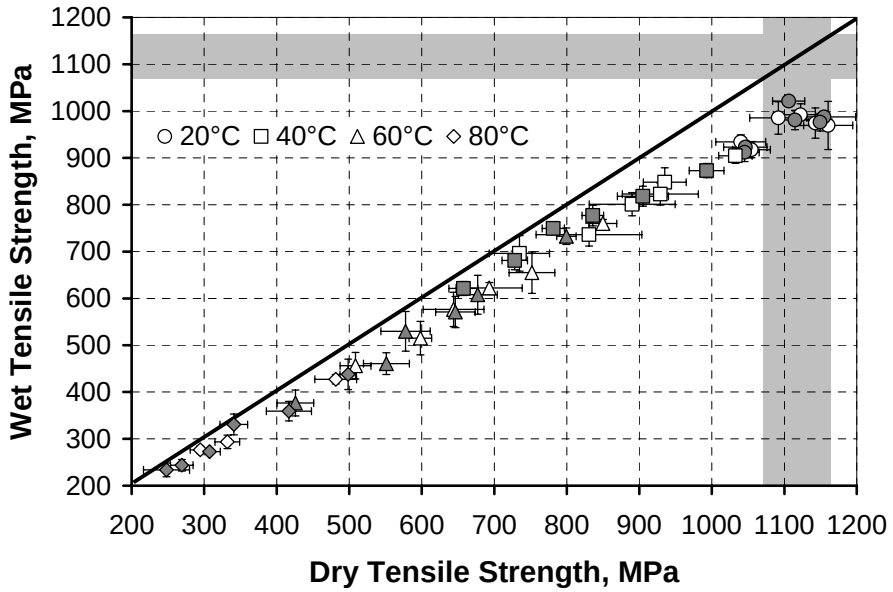

Figure 81. Wet and dry tensile strengths for 99%RH and immersion exposures. Open: 99%RH, closed: immersion. The solid line indicates no recovery in tensile strength after post-conditioning. Shaded region indicates baseline average and standard deviation. Error bars indicate standard deviations.

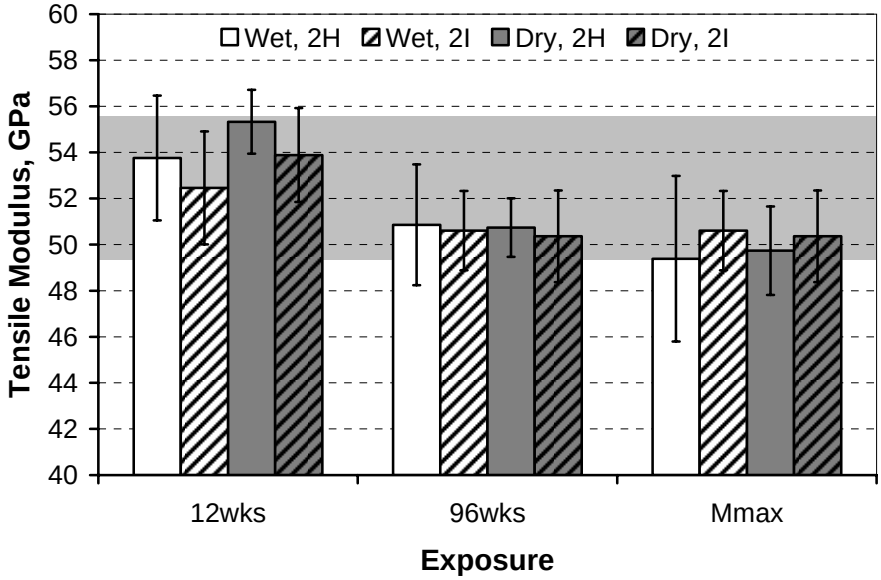

Figure 82. Tensile modulus after exposure to 99%RH and immersion at 20°C. H = 99%RH, I = Immersion. M_{max} is maximum apparent moisture content. Shaded region indicates baseline average and standard deviation. Error bars indicate standard deviations.

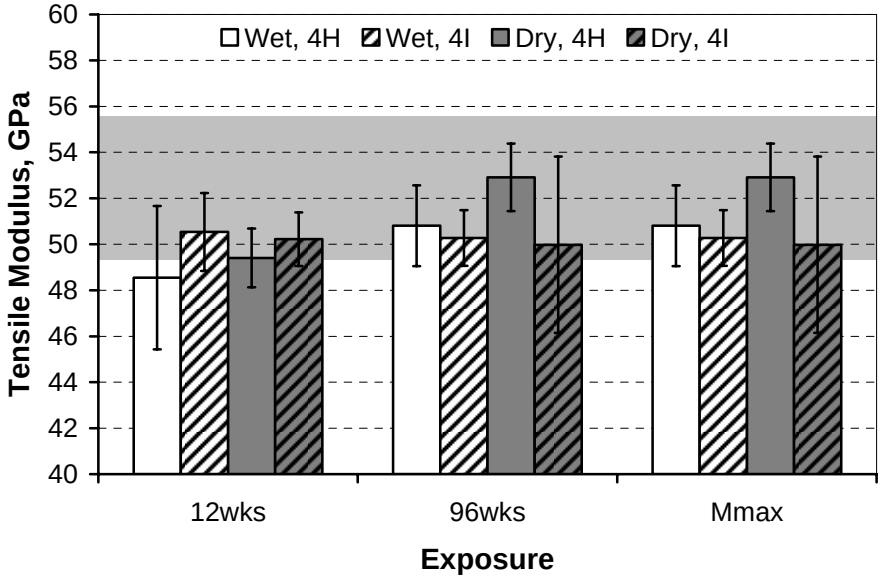

Figure 83. Tensile modulus after exposure to 99%RH and immersion at 40°C. H = 99%RH, I = Immersion. M_{max} is maximum apparent moisture content. Shaded region indicates baseline average and standard deviation. Error bars indicate standard deviations.

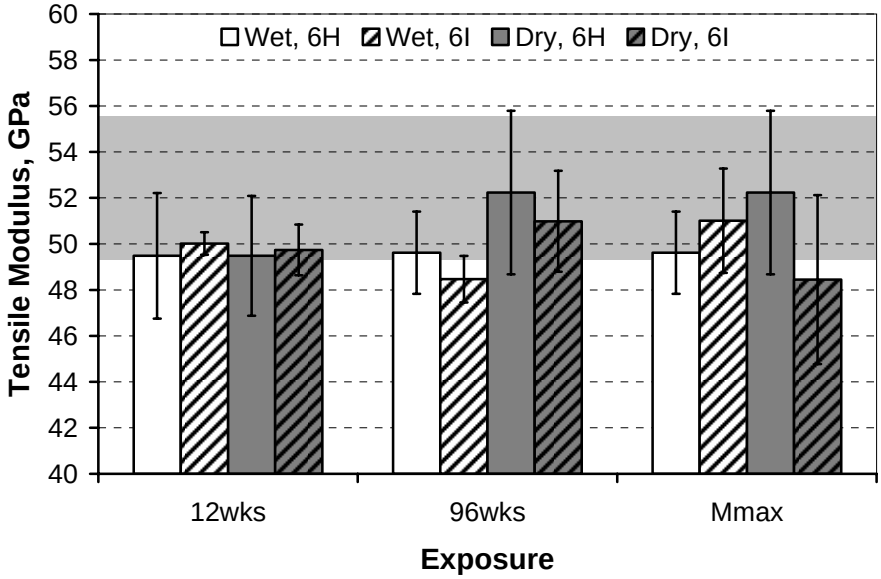

Figure 84. Tensile modulus after exposure to 99%RH and immersion at 60°C. H = 99%RH, I = Immersion. M_{max} is maximum apparent moisture content. Shaded region indicates baseline average and standard deviation. Error bars indicate standard deviations.

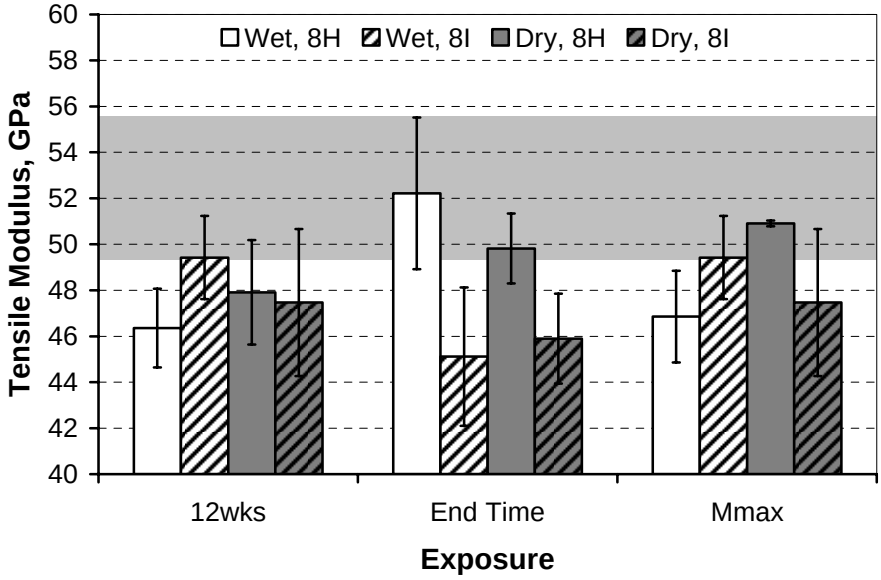

Figure 85. Tensile modulus after exposure to 99%RH and immersion at 80°C. H = 99%RH, I = Immersion. M_{max} is maximum apparent moisture content. The end time for all sets was 96 weeks except for 80°C, 99%RH (8H), which was tested through 72 weeks only. Shaded region indicates baseline average and standard deviation. Error bars indicate standard deviations.

Exposure to 99%RH and immersion at 80°C leads to degradation of the tensile modulus, as shown in Figure 85 and Figure 86, likely due to degradation and weakening of the fiber as well as the polymer matrix. Redrying of material exposed to 80°C immersion leads to a decrease in tensile modulus. DMTA results, which will discussed in Section 6.2.2.3, reveal significant plasticization of the polymer matrix, where the dry glass transition temperature increases by ~20°C after the removal of water. A plasticized matrix will not only increase the load in the fibers, reflecting a higher longitudinal modulus, but it will also allow for fiber alignment at small loads, further increasing the longitudinal modulus when compared to dry modulus values. It is also possible that a severe loss of fiber/matrix adhesion allows for increasing sensitivity to matrix plasticization. In less severe environments, where fiber/matrix adhesion may be greater, it is possible that the modulus is more dependent upon the performance of the system as a whole, including the stress transfer between less degraded fiber and matrix.

The decrease in longitudinal tensile failure strain after exposure to 99%RH and immersion environments represents a trend similar to that seen in the degradation of tensile strength. However, Figure 87 and Figure 88 indicate that, as tensile properties degrade, the tensile strength experiences a greater loss than the tensile strain.

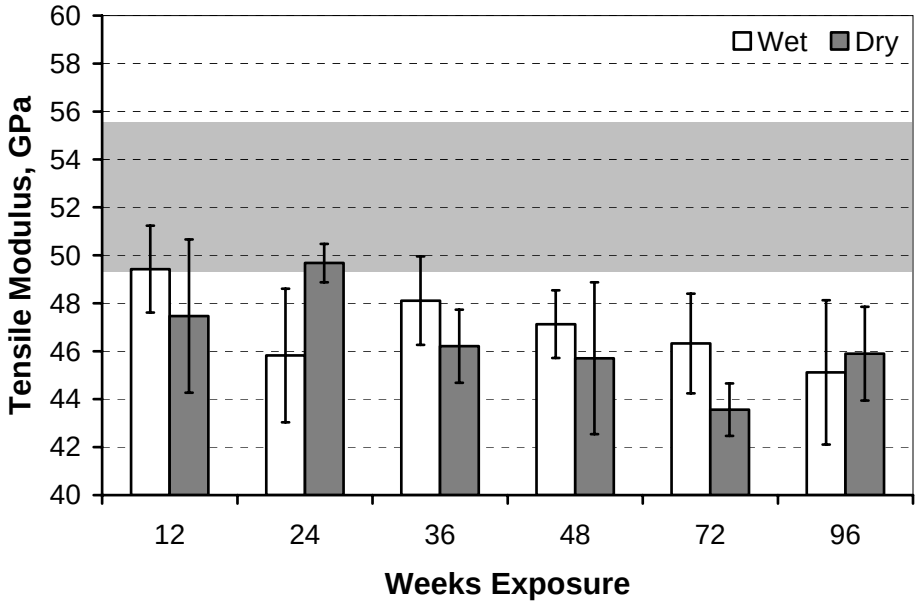

Figure 86. Tensile modulus after exposure to 80°C immersion. Shaded region indicates baseline average and standard deviation. Error bars indicate standard deviations.

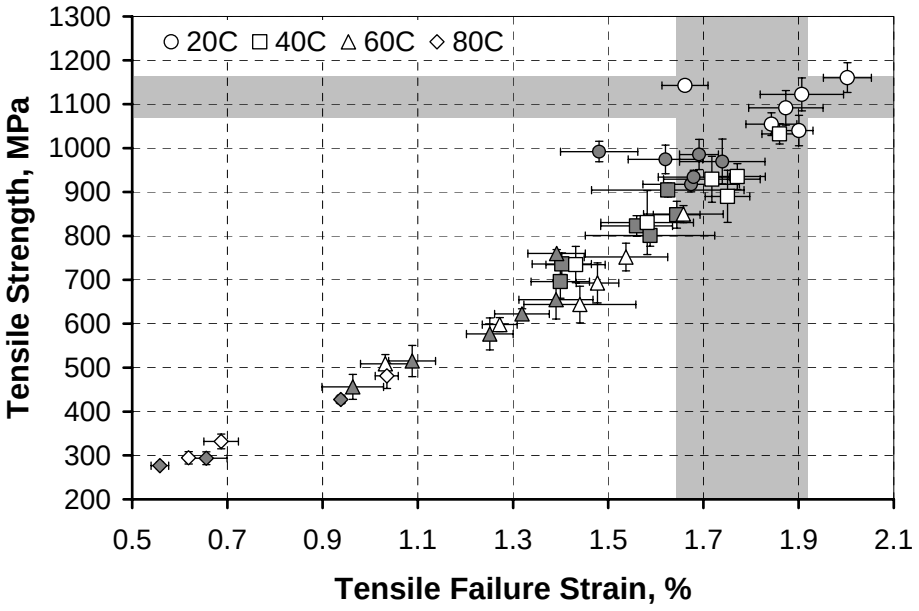

Figure 87. Tensile stress and strain after exposure to 99%RH. Closed: wet, open: dry. Shaded region indicates baseline average and standard deviation. Error bars indicate standard deviations.

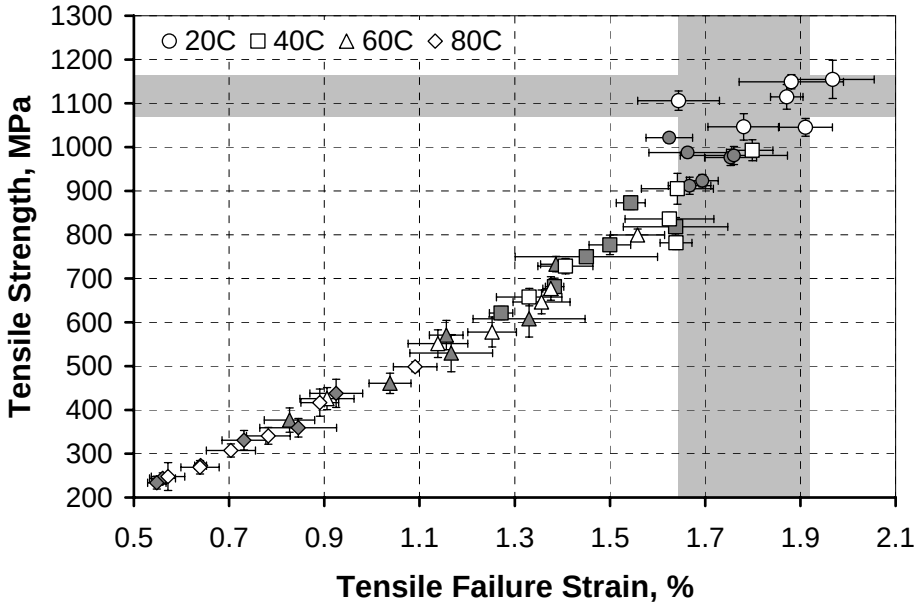

Figure 88. Tensile stress and strain after immersion.
Closed: wet, open: dry. Shaded region indicates baseline average and standard deviation. Error bars indicate standard deviations.

Exposure to 99%RH and immersion at 20°C results in a loss of wet tensile strength with no significant change in failure strain. Redrying material exposed to 20°C results in a return of tensile strength to initial values along with an increase in tensile strain, seen in Figure 87 and Figure 88. Removal of the water in material exposed to 99%RH at 40°C results in a full regain of tensile failure strain despite a permanent decrease in tensile strength.

These changes in failure strain and strength can be related to the secondary modulus, introduced in Section 5.1.2. Figure 89 presents a summary of moduli after exposure to 99%RH and immersion at 20°C and 40°C for 96 weeks. Secondary moduli are not provided for 60°C and 80°C exposures since the exposed material failed prior to the onset of a second modulus. Exposure to high humidity and

immersion at 20°C and 40°C results in a secondary modulus less than the initial baseline value, 78.9 [7.0] GPa. Thus it is possible for tensile specimens with these lower secondary moduli to achieve higher strains even where tensile strength has been lost. Figure 87 and Figure 88 show that material exposed to 99%RH and immersion at 20°C and 40°C have been observed to return to failure strains within baseline scatter after post-conditioning. It is possible that, in the case of these exposures, tensile failure is dominated by the maximum fiber strain. Interfacial degradation may be responsible for these losses in secondary modulus and ultimate strength.

While the tensile modulus at early loading does not demonstrate a dramatic dependence upon moisture content, Figure 90 indicates the secondary modulus clearly decreases with increasing moisture content. Thus, while the plasticizing effect may not manifest itself at low loads, plasticization appears to influence the modulus at higher loads, leading to higher failure strains. SEM investigations provided no evidence of fiber degradation after exposure to 20°C and 40°C, supporting the theory that failure after these exposures is dictated by fiber strain. At higher temperatures, pitting of fibers, such as that shown in Figure 91, results in severely degraded fiber strengths, leading to lower composite strengths and strains.

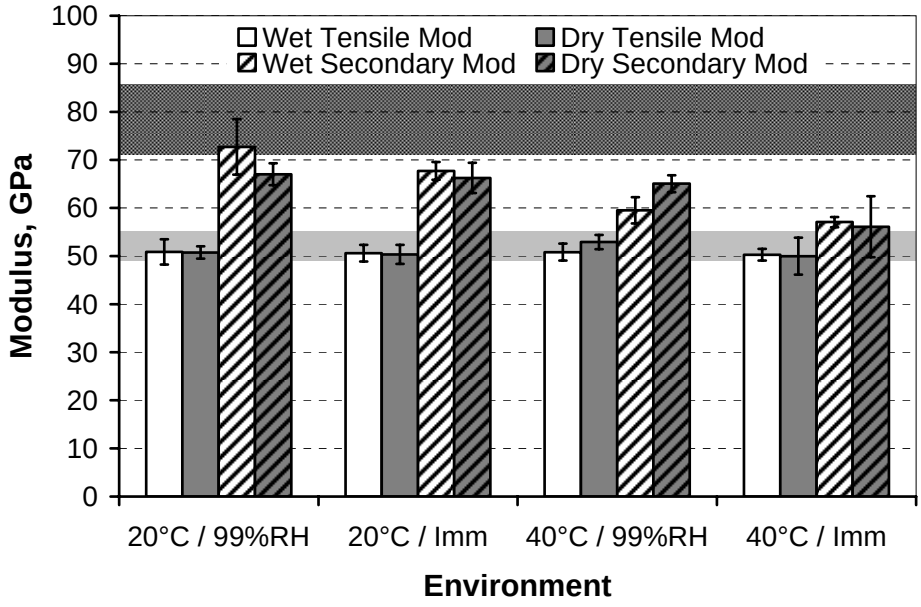

Figure 89. Tensile modulus and secondary modulus after exposure to 99%RH and immersion (Imm) at 20°C and 40°C for 96 weeks. Shaded region indicates baseline average and standard deviation for tensile modulus (light) and secondary modulus (dark). Error bars indicate standard deviations.

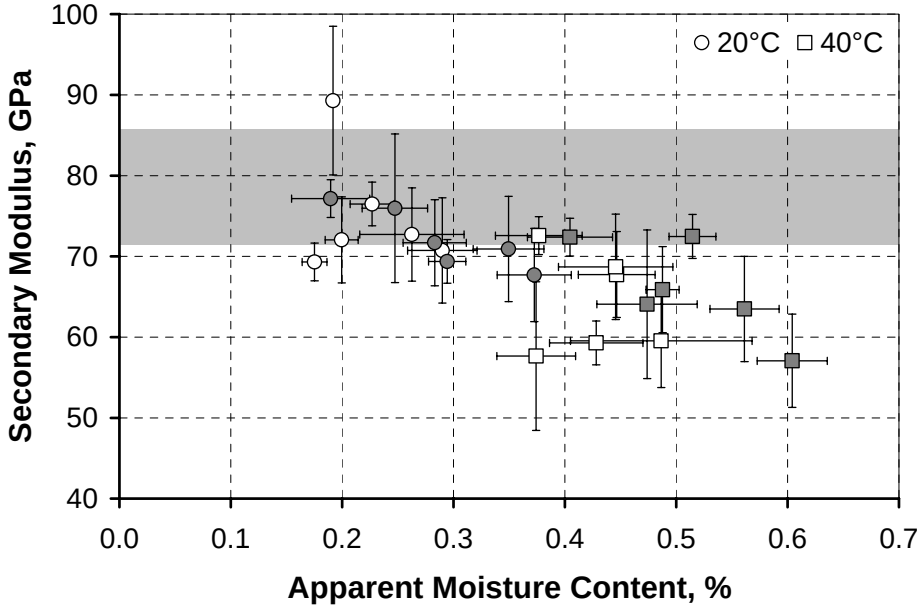

Figure 90. Secondary modulus after exposure to 99%RH and immersion at 20°C and 40°C. Open: 99%RH, closed: immersion. Shaded region indicates baseline average and standard deviation. Error bars indicate standard deviations.

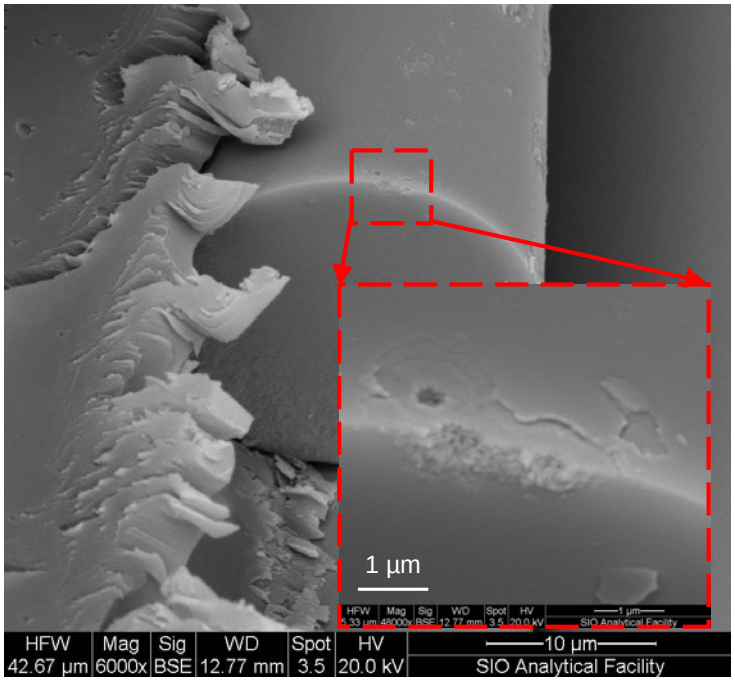

Figure 91. SEM of fiber pitting in tensile specimen. Exposed to 80°C immersion for 72 weeks.

5.2 Short Beam Shear Testing

SBS testing was executed to gain an understanding of the performance of the fiber/matrix bond in the monolayer pultruded composite under consideration. Initial short beam shear (SBS) strengths are presented in Table 24. The average and standard deviation for pre-conditioned material was obtained from SBS tests of 70 specimens pre-conditioned at 40°C and 18%RH for 6 weeks. Material exposed to 40°C at 18%RH was also tested in sets of 5 after another 6, 12, 18, 24, 30, 36, 42, 48, 54, 72, 78, 96, and 102 weeks of exposure, providing an additional 65 tests. The baseline average and standard deviation were calculated using results from a total 135 SBS tests of material exposed to 40°C at 18%RH. Exposure to 18%RH at 40°C results in

slight strengthening after the removal of water, possibly due to embrittlement, as seen in pre-conditioned tensile data.

Table 24. Initial short beam shear strength.
Brackets indicate standard deviations.

	SBS Strength
As-Received	66.6 [0.7]
Pre-Conditioned	71.2 [2.2]
Baseline	71.9 [2.2]

ASTM-D2344 states that a true short beam shear strength may only be considered for specimens which fail in shear. It is also possible for specimens to fail in crushing and bending. Bending was the only alternative failure mode detected and occurred only in highly degraded specimens. Here, short beam shear strengths are presented regardless of failure mode. Short beam shear data for all environments, times, wet, and dry sets can be found in Appendix B.2.

5.2.1 Low and Medium Humidity Short Beam Shear Results

While tensile properties do not demonstrate any significant change, short beam shear testing of material exposed to 18%RH and 50%RH at elevated temperatures reveals increased strengths, as seen in Figure 92 and Figure 93. Room temperature exposures at 18%RH and 50%RH demonstrate a slight decrease in SBS strength, although these values are within initial scatter.

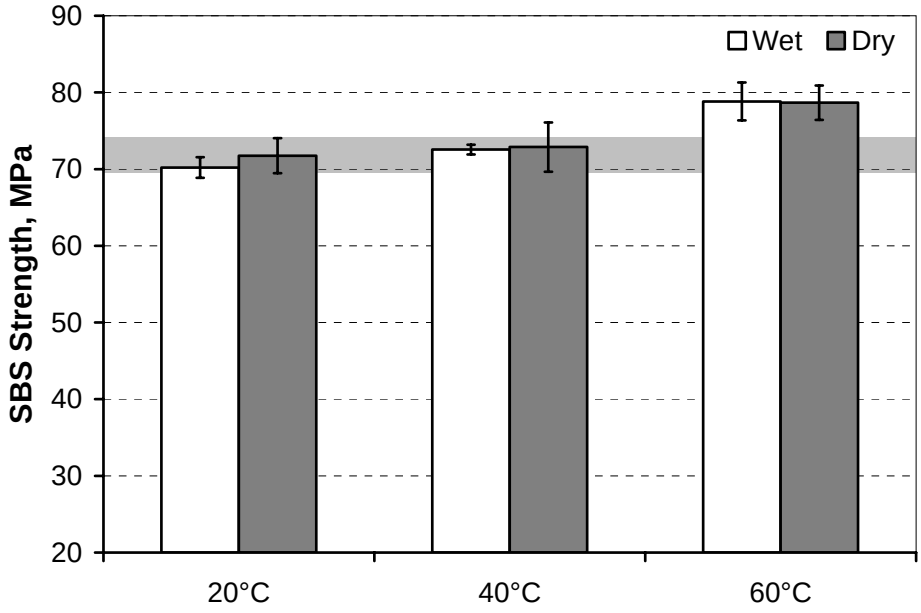

Figure 92. SBS strength after exposure to 18%RH for 96 wks.
Shaded region indicates baseline average and standard deviation.
Error bars indicate standard deviations.

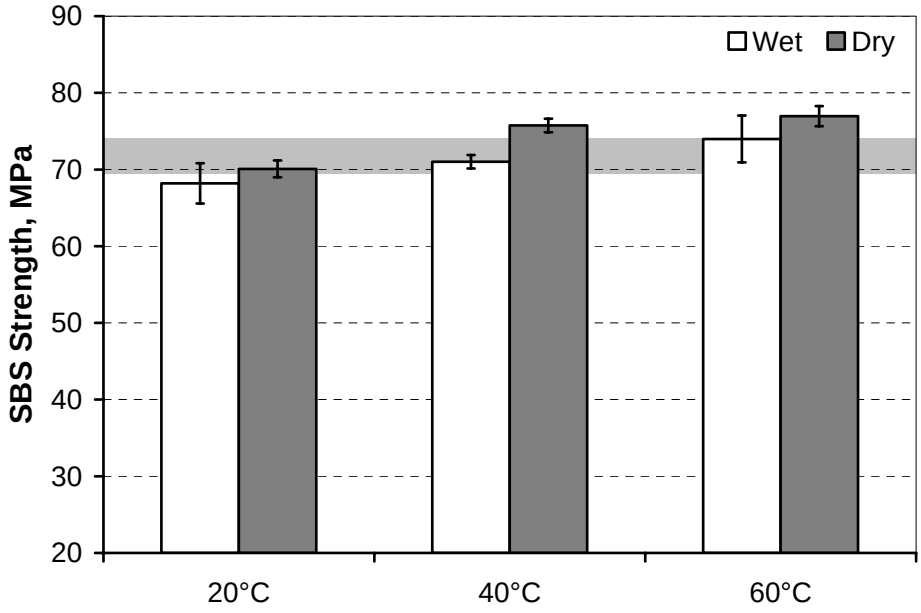

Figure 93. SBS strength after exposure to 50%RH for 96 wks.
Shaded region indicates baseline average and standard deviation.
Error bars indicate standard deviations.

The lowest wet SBS strength observed was produced after exposure to 50%RH 20°C, where the SBS strengths over 96 weeks of exposure ranged from a minimum of 66.5 [2.3] MPa at 36 weeks to a maximum of 69.5 [1.1] MPa at 48 weeks. The highest wet SBS strength was produced after exposure to 18%RH at 60°C, with SBS strengths ranging from 75.0 [1.7] MPa at 36 weeks to 78.8 [2.5] MPa at 96 weeks. When material is exposed to 50%RH, the SBS strength increases after the sorbed water is removed. Thus, the plasticizing effect of water becomes obvious even at such low water contents of 0.05 % to 0.1 %. At low humidity, 18%RH, in elevated temperatures the SBS strengths consistently increase with temperature. Removal of water after exposure to 50%RH at elevated temperatures reveals an increase in SBS strength over the baseline value.

It is possible that a post-cure effect or loss of low molecular weight species (LMWS) lead to the strengthening effect detected through increases in SBS strengths, and this effect is amplified at higher temperatures. The presence of water decreases the SBS strength, regardless of temperature, indicating plasticization. If the SBS test is taken to reflect the relative interfacial strength of a composite, this clear sensitivity of SBS strength to even small quantities of moisture demonstrates the high sensitivity of the interphase in this E-glass/vinyl-ester composite. It is also possible that the SBS strength reflects plasticization or embrittlement of the matrix, which may fail in shear.

5.2.2 75%RH Short Beam Shear Results

SBS testing reveal that exposure to 75%RH at 60°C results in a wet SBS strength which is just below baseline scatter, as seen in Figure 94. Redrying increases

the SBS strength to above or within initial scatter. Figure 94 compares SBS results after exposure to 75%RH and 50%RH, demonstrating that the removal of water leads to a greater increase of SBS strength for material exposed to 75%RH, while the dry SBS strengths are greater for material exposed to 50%RH.

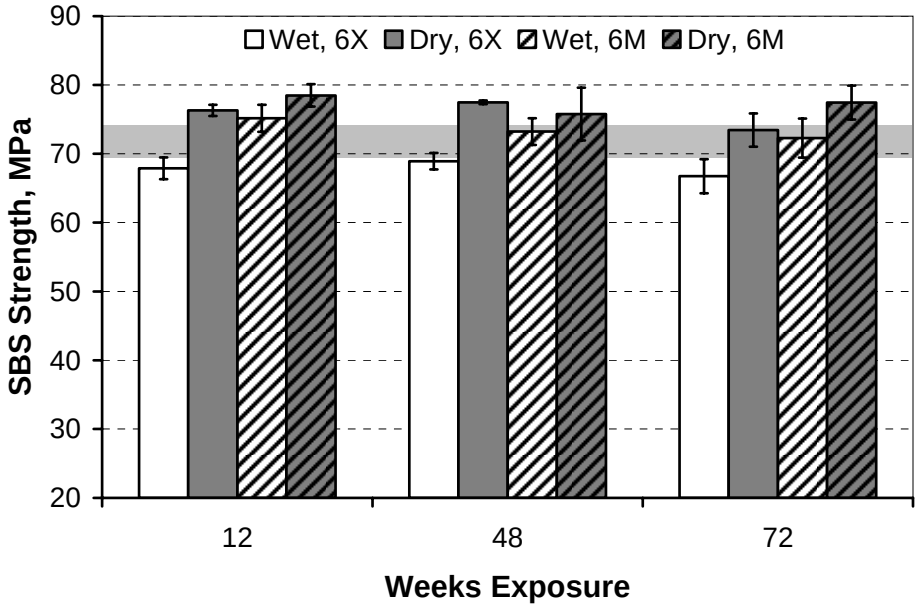

Figure 94. SBS strengths after exposure to 50%RH and 75%RH at 60°C. Shaded region indicates baseline average and standard deviation. Error bars indicate standard deviations.

Increasing moisture contents, resulting from exposure to increased relative humidity at one temperature of exposure, result in decreased SBS strengths both before and after the removal of any sorbed water, as seen in Figure 95 and Figure 96. That is, the presence of water negatively affects interfacial adhesion and matrix shear strength, as monitored through SBS testing, and higher water contents result in increasingly permanent degradation even if combined with strengthening due to post-cure or loss of LMWS at elevated temperatures.

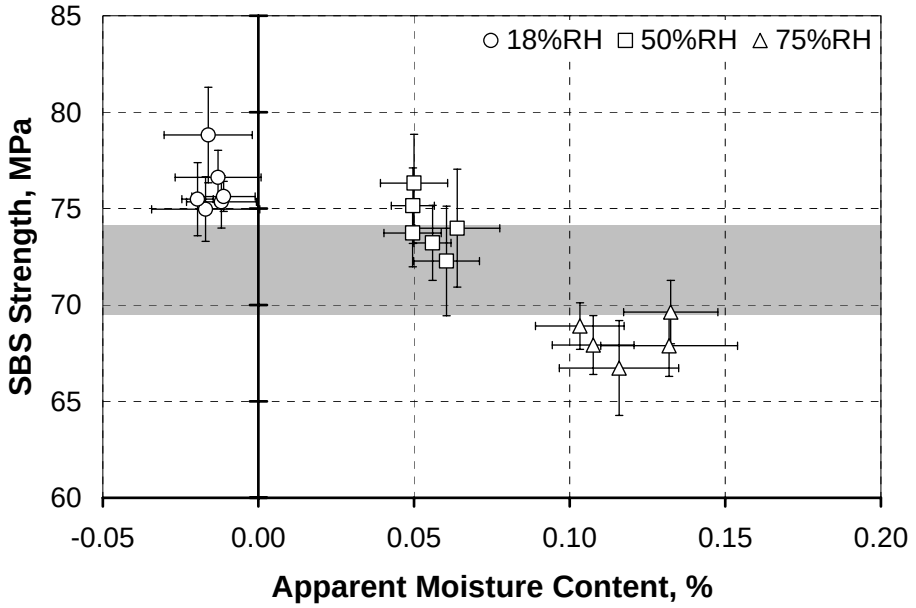

Figure 95. Wet SBS strength and apparent moisture content after exposure to 60°C.
Shaded region indicates baseline average and standard deviation.
Error bars indicate standard deviations.

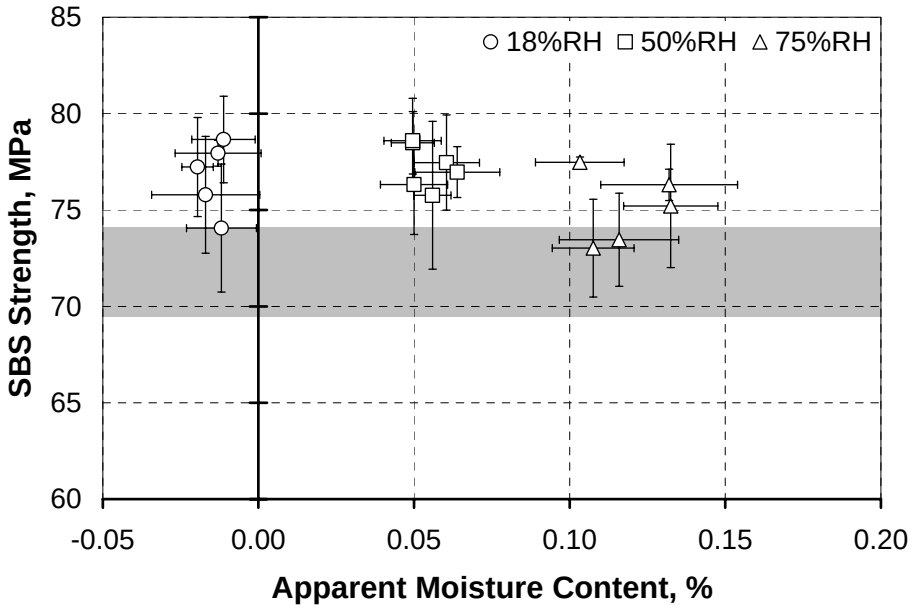

Figure 96. Dry SBS strength and apparent moisture content after exposure to 60°C.
Shaded region indicates baseline average and standard deviation.
Error bars indicate standard deviations.

5.2.3 High Humidity and Immersion Short Beam Shear Results

The reversible plasticizing effect becomes most evident at higher moisture contents which result from exposure to 99%RH and water immersion. For a particular moisture content, while there is no significant difference between the effects of 99%RH and immersion exposures, as seen in Figure 97, there is a thermal effect. The wet SBS strength for material exposed to 20°C saturated environments of 99%RH and immersion is consistently lower than the SBS strength for material exposed to 99%RH and immersion at 40°C, indicating that the strengthening effect, which may result from post-cure or leaching of LMWS, is one of several competing mechanisms responsible for changes in SBS strength.

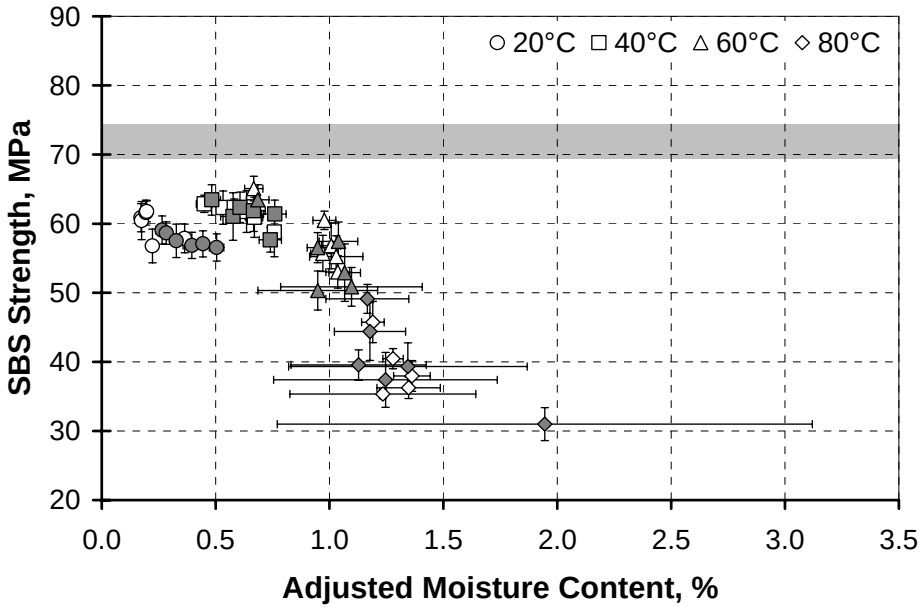

Figure 97. Wet SBS strength after exposure to saturated environments. Open: 99%RH, closed: immersion. Shaded region indicates baseline average and standard deviation. Error bars indicate standard deviations.

Table 25 and Table 26 present the SBS results after 12, 24, and 96 weeks of exposure. Material exposed to 60°C immersion and 99%RH for 12 weeks demonstrated full recovery in SBS strength after post-conditioning. The dry SBS strength in material exposed to these 60°C conditions for 12 weeks indicates a strengthening effect similar to that seen in material exposed to 60°C at lower humidities and all 40°C conditions. Exposure to 99%RH and immersion at 20°C results in a plasticization effect revealed by the full recovery in SBS strength after post-conditioning without a strengthening effect seen at elevated temperatures. After 12 weeks in these 60°C immersion and 99%RH, the dry SBS strength is lower than the baseline value, indicating that the onset of irreversible degradation occurs between 12 and 24 weeks. Gravimetric results for material exposed to 99%RH and immersion at 60°C reveal a sharp increase in moisture uptake between 18 and 24 weeks of exposure which was discussed in Section 4.2. The degradation revealed by SBS testing in material exposed to 80°C is irreversible from at least 12 weeks.

Table 27 and Table 28 provide the differences between wet and dry SBS strengths for 99%RH and immersion exposures. This set of data indicates that the removal of water from material exposed to 99%RH and immersion conditions results in an increase in SBS strength ranging from 6.5 [2.8] MPa to 16.2 [2.8] MPa, with no clear indication of how elevated temperature affects regain. Hydrogen bonds formed by the water molecules with the polymeric interphase will result in plasticization leading to decreased interfacial strength. Hydrogen bonds formed by water molecules

with the polymer itself will decrease the shear modulus and strength even while the presence of water promotes crosslinking, increasing the same constituent strengths.

Table 25. SBS strength after exposure to 99%RH.
* 80°C, 99%RH was tested through 72 weeks only; 72 week results reported here.
Brackets indicate standard deviations.

	Wet			Dry		
Time (wk)	12	24	96*	12	24	96*
20°C	60.9 [2.0]	60.4 [2.8]	57.9 [2.1]	72.9 [2.0]	68.9 [2.6]	69.0 [1.3]
40°C	62.9 [1.3]	62.3 [2.4]	58.8 [3.6]	73.6 [1.1]	74.6 [1.4]	70.9 [2.1]
60°C	65.1 [1.8]	55.7 [2.6]	55.2 [3.0]	75.8 [0.7]	65.8 [3.5]	62.8 [2.6]
80°C	45.8 [3.0]	40.5 [1.5]	35.4 [0.7]	54.9 [2.5]	47.0 [2.8]	41.9 [1.2]

Table 26. SBS strength after immersion in water.
Brackets indicate standard deviations.

	Wet			Dry		
Time (wk)	12	24	96	12	24	96
20°C	59.1 [2.0]	58.6 [1.6]	57.5 [2.0]	71.3 [2.2]	71.5 [0.7]	69.5 [1.7]
40°C	63.4 [2.2]	61.0 [3.4]	61.4 [2.2]	74.5 [1.1]	73.6 [1.3]	73.6 [1.3]
60°C	63.4 [2.2]	56.5 [2.2]	50.9 [2.8]	74.4 [4.7]	65.1 [4.7]	60.0 [2.9]
80°C	49.1 [2.1]	44.4 [4.2]	31.0 [2.4]	57.0 [3.8]	54.2 [3.5]	40.0 [1.7]

Table 27. Difference between wet and dry SBS strengths for 99%RH.
* 80°C, 99%RH was tested through 72 weeks only.
Brackets indicate maximum standard deviation between wet and dry sets.

Time (wk)	20°C	40°C	60°C	80°C
12	12.1 [2.1]	10.8 [1.3]	10.7 [1.8]	9.2 [3.0]
24	8.4 [2.8]	12.3 [1.3]	10.1 [3.5]	6.5 [2.8]
36	8.7 [2.0]	10.2 [1.9]	5.4 [2.1]	7.4 [2.2]
48	9.8 [1.5]	8.5 [3.0]	9.2 [3.5]	9.5 [1.8]
72	14.2 [3.0]	10.4 [3.1]	14.5 [2.3]	6.5 [1.2]
* 96	11.1 [2.1]	12.1 [3.6]	7.6 [3.0]	—

Table 28. Difference between wet and dry SBS strengths for immersion.
Brackets indicate maximum standard deviation between wet and dry sets.

Time (wk)	20°C	40°C	60°C	80°C
12	12.2 [2.2]	11.0 [2.2]	10.9 [4.7]	7.9 [3.8]
24	12.8 [1.6]	12.6 [3.4]	8.6 [4.7]	9.8 [4.2]
36	13.3 [2.4]	11.2 [3.2]	12.4 [4.2]	12.3 [2.2]
48	14.5 [1.9]	11.1 [3.0]	8.8 [3.1]	7.3 [3.4]
72	13.3 [1.9]	15.1 [1.8]	16.2 [2.8]	7.5 [4.0]
96	13.0 [2.0]	12.2 [2.0]	9.2 [2.9]	9.0 [2.4]

Through 96 weeks of exposure to 40°C immersion and 99%RH, post-conditioning results in full recovery of the SBS strength to the high end of the initial scatter range. DMTA tests reveal a dry T_g which is 3°C to 9°C greater than the initial baseline average for material exposed to the same exposure conditions, indicating a tightening of the polymer network which could be inferred from SBS strengths which are also above the baseline value.

DMTA testing also reveals that an irreversible increase in tanδ peak height occurs after exposure to 60°C and 80°C exposures of 99%RH and immersion, indicating significant loss of interfacial adhesion [3]. These results will be addressed further in Section 6.2.3.3. Furthermore, a transition in SBS failure mode for these degraded specimens from shear to flexure indicates clear degradation of the fiber reinforcement which was indicated by concurrent irreversible decreases in tensile failure strain.

The increase in SBS strength after post-conditioning does not appear to depend on time or, consequently, moisture content, as seen in Table 27 and Table 28. Figure 98 provides the dry SBS strength plotted against weight loss, W_l, after redrying where W_l is defined using the weight prior to exposure W_0 and the weight after exposure and subsequent pre-conditioning W_d

$$W_l = \frac{W_d - W_0}{W_0} \times 100\% \quad (3)$$

.

Figure 98 indicates that irreversible degradation of SBS strength occurs where weight loss after post-conditioning exceeds 0.1 %, indicating severe degradation of the constituent materials.

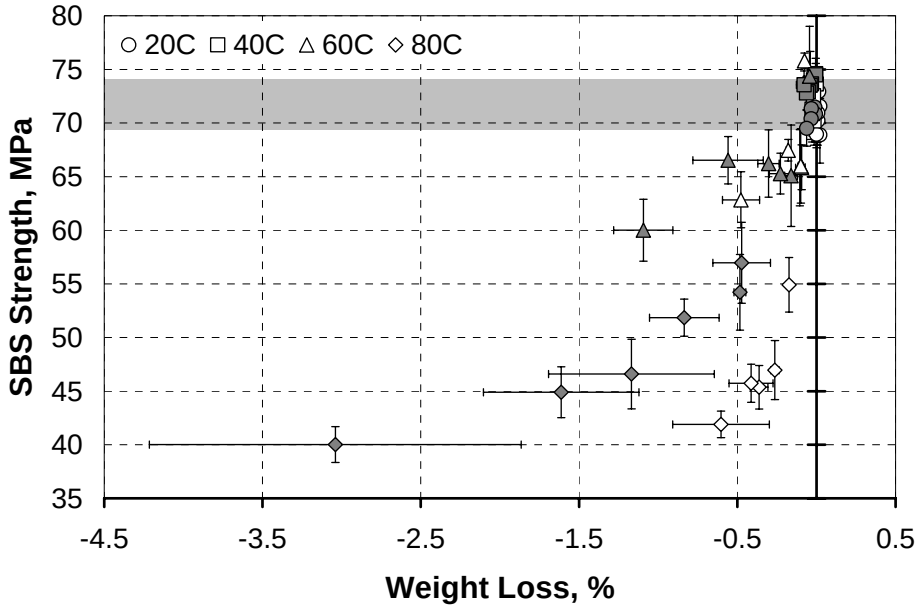

Figure 98. Dry SBS strength and weight loss after redrying.
Open: 99%RH, closed: immersion. Shaded region indicates baseline average and standard deviation. Error bars indicate standard deviations.

Material exposed to saturated environments at 80°C demonstrate extreme degradation, where the loss in dry SBS strength is already 14.3 [3.8] MPa for immersion and 16.3 [2.6] MPa for 99%RH after 12 weeks and reaches up to 31 [1.7] MPa loss after 72 weeks in 99%RH and 96 weeks in immersion . The increase in SBS strength after redrying by material exposed to saturated conditions at 80°C tends to be less than that of other saturated environments, as seen in Table 27 and Table 28, possibly because of weakened fiber strength.

5.3 Effect of Kaolin Filler

Evidence was presented earlier in Section 5.1.3 that kaolin clay filler, commonly used in pultrusion, may contribute to the degradation of material properties.

Kaolin is a hydrous alumina silicate clay, $Al_2O_3 \cdot 2SiO_2 \cdot 2H_2O$ which is primarily mined from hydrothermal deposits [4]. Pure kaolinite composes 50-99% of kaolin clay and is characterized by a pseudohexagonal plate structure which forms a layered crystal through hydrogen bonding [4].

Scanning electron microscopy of failed tensile specimens tested after 72 weeks exposure to 80°C immersion are shown in , where pitting has occurred in the vicinity of a filler particle. Electron Dispersive X-Ray Spectroscopy (EDX) results, presented in Figure 100 and Figure 101, confirm that a layered structure identified in specimens exposed to 80°C immersion for 72 weeks has a high concentration of aluminum and silicon but low concentrations of carbon and calcium. The oxygen peak was not as strong as the aluminum and silicon peaks, but did conclusively indicate that oxygen is present in higher concentrations where there is filler and less so in the polymer and fiber. These results indicate that the filler is, in fact, kaolin clay and not calcium carbonate $CaCO_3$, another common filler used in pultrusion.

Tensile testing of material exposed to 80°C resulted in fiber failure at pitting sites, shown in Figure 102 through Figure 104. SEM analysis consistently revealed kaolin filler particles were located at pitting sites where fiber failure occured. It can be inferred that kaolin acts as an initiator for pitting of glass fiber in this pultruded composite. While kaolin clay is known to slow the diffusion of water into and the degradation of composite materials when compared to unfilled or calcium carbonate filled glass fiber composites [5], kaolin does appear to aggravate the fiber pitting process.

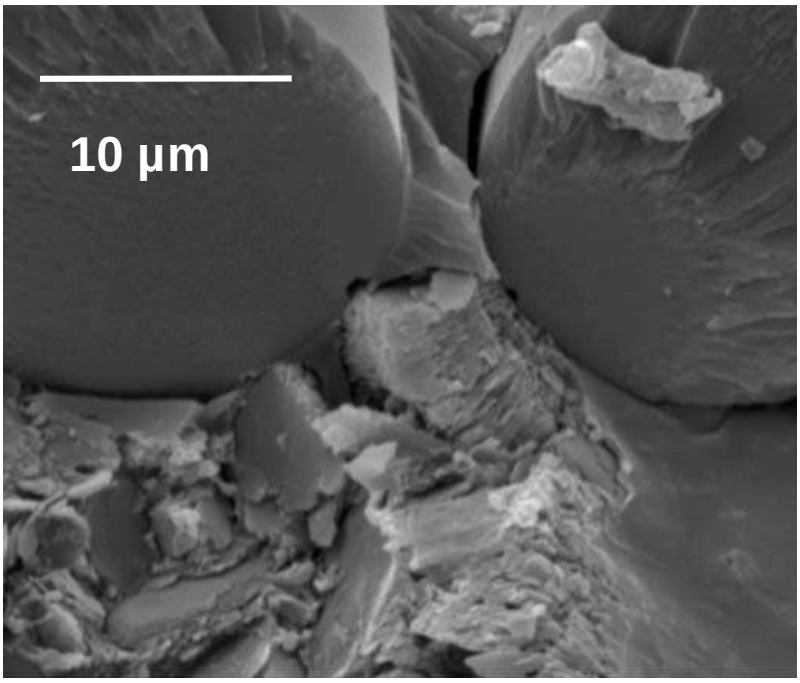

Figure 99. SEM micrograph of area used for EDX dot map.
Failed tensile specimen exposed to 80°C immersion for 72 weeks.

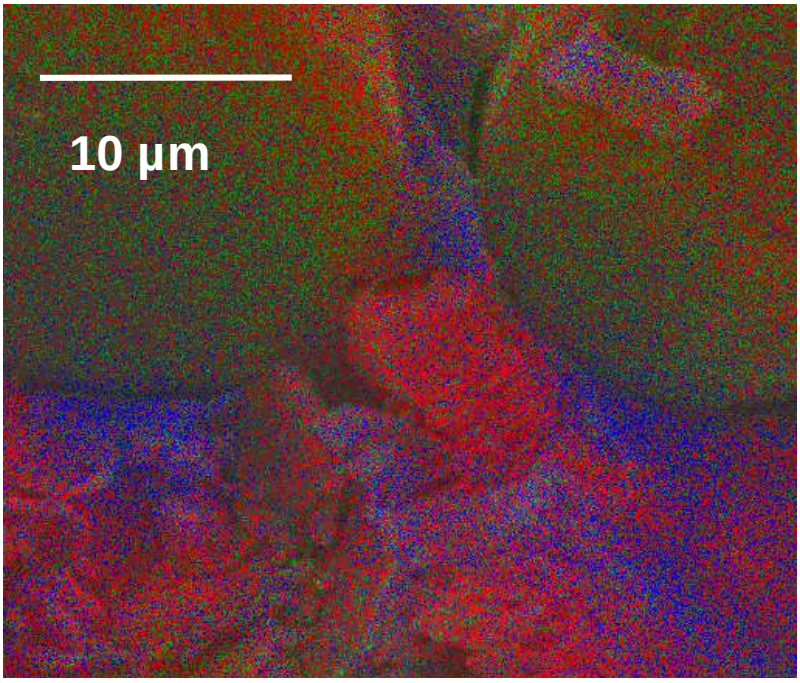

Figure 100. Color coded dot map of EDX results corresponding to Figure 99.
Failed tensile specimen exposed to 80°C immersion for 72 weeks.
Key to colors in dot map: Green: Calcium, Blue: Carbon, Red: Silicon.

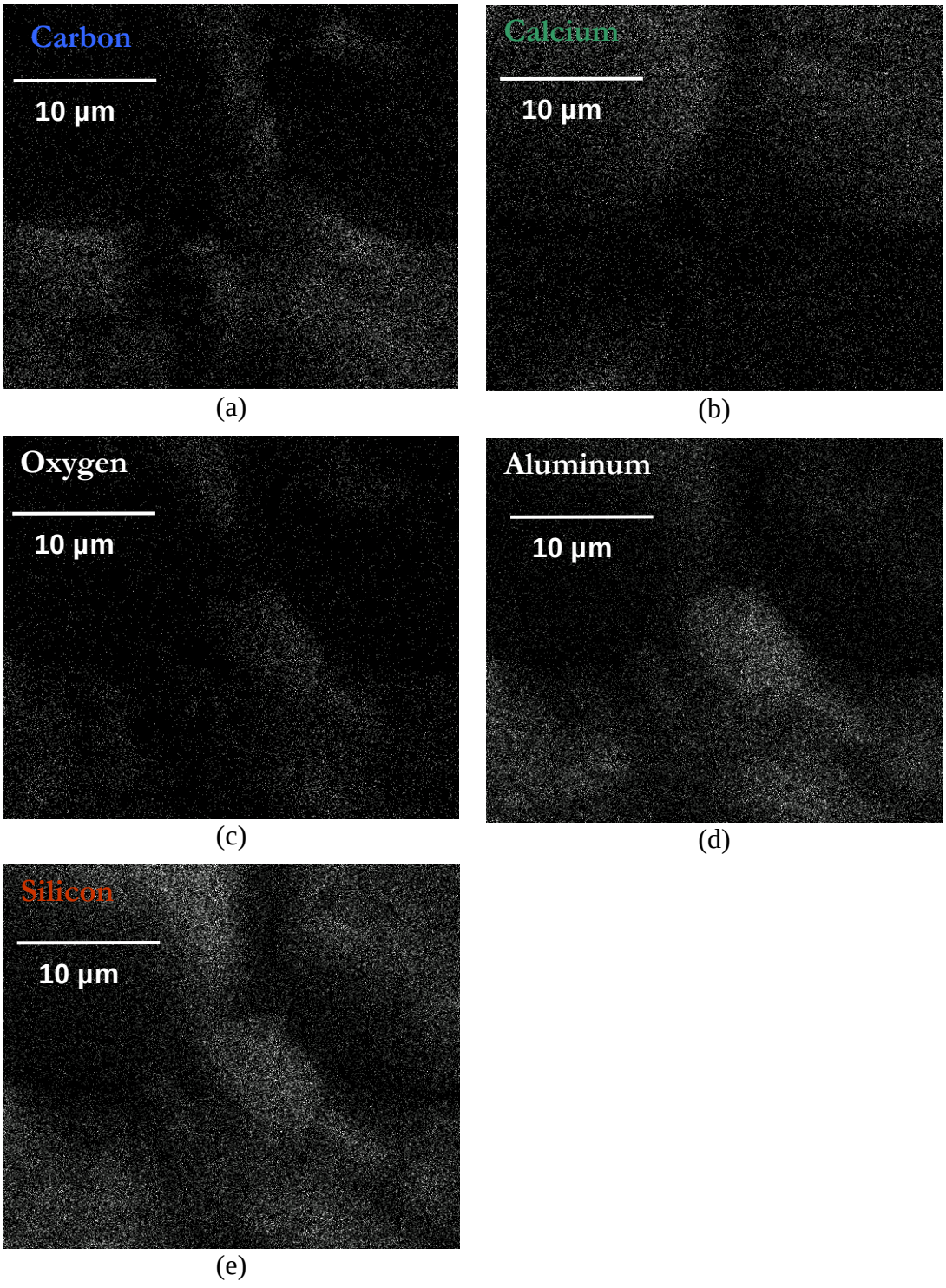

Figure 101. Elemental breakdown of EDX dot map corresponding to Figure 99. Failed tensile specimen exposed to 80°C immersion for 72 weeks. (a) Carbon, (b) calcium, (c) oxygen, (d) aluminum, (e) silicon.

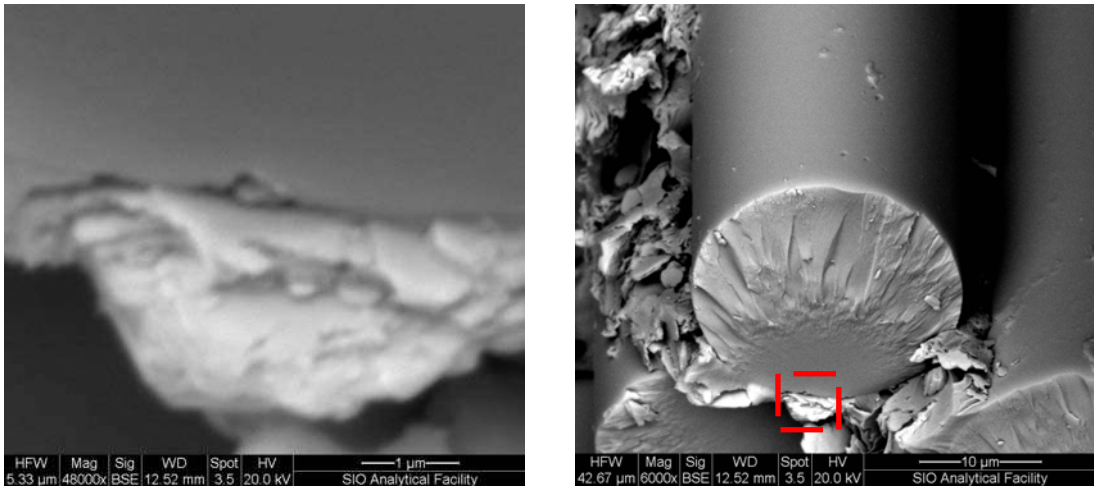

(a) (b)

Figure 102. SEM micrograph of fiber pitting occurring next to kaolin. Failed tensile specimen exposed to 80°C immersion for 72 weeks. (a) is higher magnification of boxed area in (b).

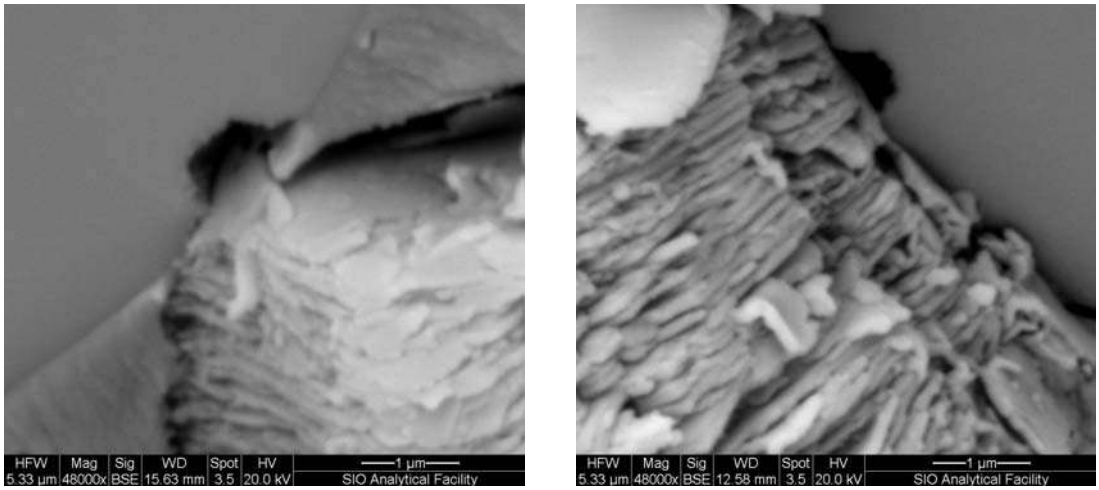

(a) (b)

Figure 103. SEM micrograph of fiber pitting occurring next to kaolin. Failed tensile specimen exposed to 80°C immersion for 72 weeks. Image of pitting in fibers at (a) left and (b) right in Figure 99.

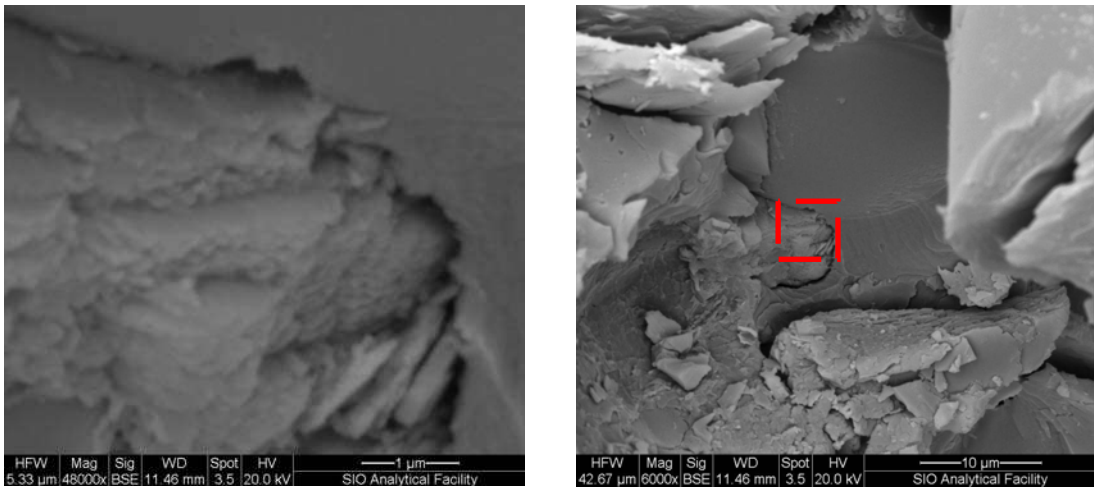

(a) (b)

Figure 104. SEM micrograph of fiber pitting occurring next to kaolin. Failed tensile specimen exposed to 80°C immersion for 72 weeks. (a) is higher magnification of boxed area in (b).

Because the plate-like kaolin crystalline structure is established through hydrogen bonding, it would be expected that water molecules would be attracted to these filler particles. The attraction of water molecules to kaolin slows the diffusion of water through the bulk composite, but it will also establish local sites with high water concentrations. When kaolin is located near the surface of a glass fiber, it is then expected that pitting will be localized in the vicinity of clay filler particles. While clay filler may be viewed to slow the degradation of glass fiber composites, there is cause for concern in that it may aggravate the fiber pitting process. The localized pitting may have occurred at scratches on the fiber surface which were created through frictional contact between the filler and fiber during the manufacturing process or it may be possible that the particles establish a high energy surface site by introducing heterogeneities on the fiber surface. In either case, the fluctuations in surface energy would be established in the presence of kaolin, leading to pitting at these locations [6].

It may also be possible that there is some dissolution of aluminum and silicon into the polymer matrix from the glass fiber. It has been established that glass fiber should exhibit dissolution of silica with pitting [7]. Furthermore, it has also been claimed that hydrolytic degradation of the glass fiber results from ion exchange reactions and contributes to local alkalinity [8]. Interestingly, kaolin is known to only react with strong acids and bases and to demonstrate ion exchange reactions [4]. Therefore the reactivity of kaolin and the glass fiber could act synergistically to further aggravate degradation.

It should also be recalled that E-glass fiber is known to have a chemical makeup which consists of Al_2O_3 along with several other metal oxides [9]. It has been posed that water preferentially adsorbs to the heterogeneous surface sites characterized by metal oxides in E-glass fibers [9], which may lead to localized degradation. It may be possible that the metal-oxide surface heterogeneities together with the alumina present in kaolin contribute to high surface energies where pitting is very likely. In either of these cases pitting of the fiber may lead to dissolution of silicon or aluminum which may form a dissolution locally in the vicinity of kaolin filler particles. Therefore, high temperatures and moisture contents should lead not only fiber pitting but also to greater degradation localized around kaolin filler.

Kaolin was identified earlier in Section 5.1.3 underneath sites of localized polymer failure in specimens which also demonstrated poor interfacial adhesion. The micrograph presented in Figure 79 which depicted poor fiber/matrix adhesion is presented again in Figure 105. A closer look at one of the localized failure sites

reveals a layered structure underneath representing that of kaolin. Figure 105, Figure 103(a), and Figure 104(b) all indicate that the kaolin filler particle may experience debonding along its own interface after immersion in deionized water. Again, because water would be attracted to the kaolin filler, it may be expected that localized debonding occurs at the filler interface. Debonding would then result in greater moisture sorption in the immediate vicinity of the filler particle, leading to possible microcracking, microvoid formation, or polymer degradation. The resin surface at the failed fiber/resin interface in Figure 105 shows some similarity to the failed fiber/resin interface shown in Figure 106 and Figure 107 and on the right side of Figure 99.

In summary, kaolin may slow the initial degradation of a glass reinforced composite. The hydrophilic nature of kaolin clay may ultimately lead to more severe degradation over the decades long service life of a civil structure.

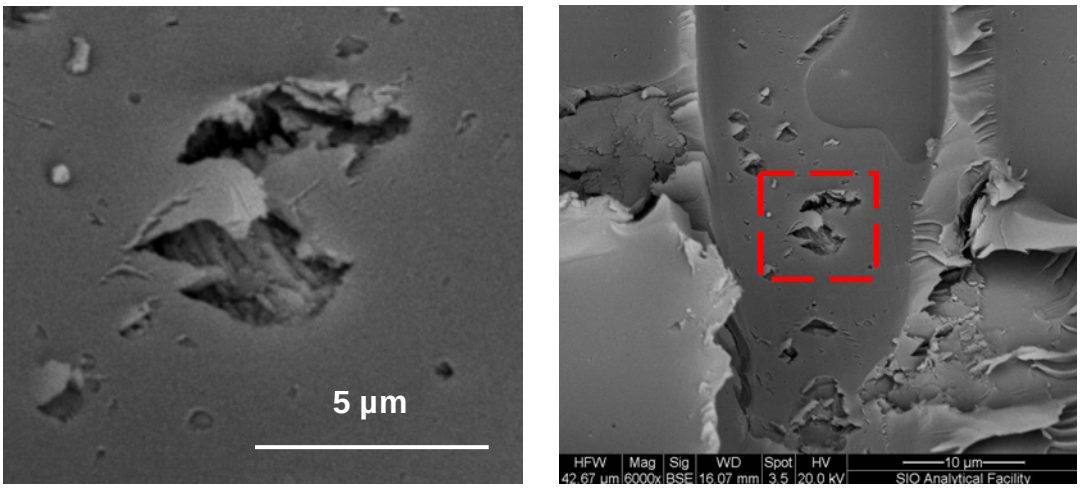

(a) (b)

Figure 105. SEM micrograph of failed tensile specimen revealing kaolin filler. Material exposed to 60°C immersion for 24 weeks.
(a) is higher magnification of boxed area in (b).

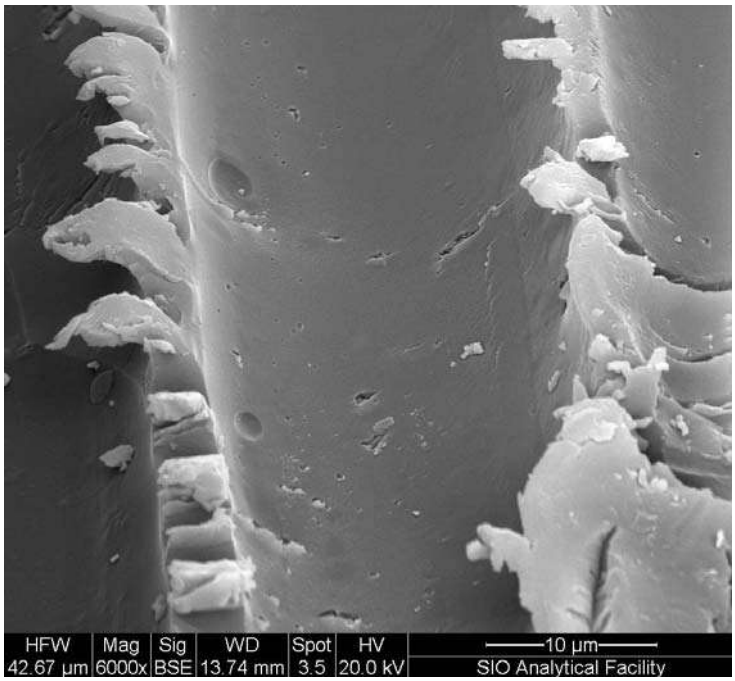

Figure 106. SEM micrograph of failed tensile specimen exposed to 60°C immersion for 24 weeks, indicating weakened polymer at fiber/matrix interface.

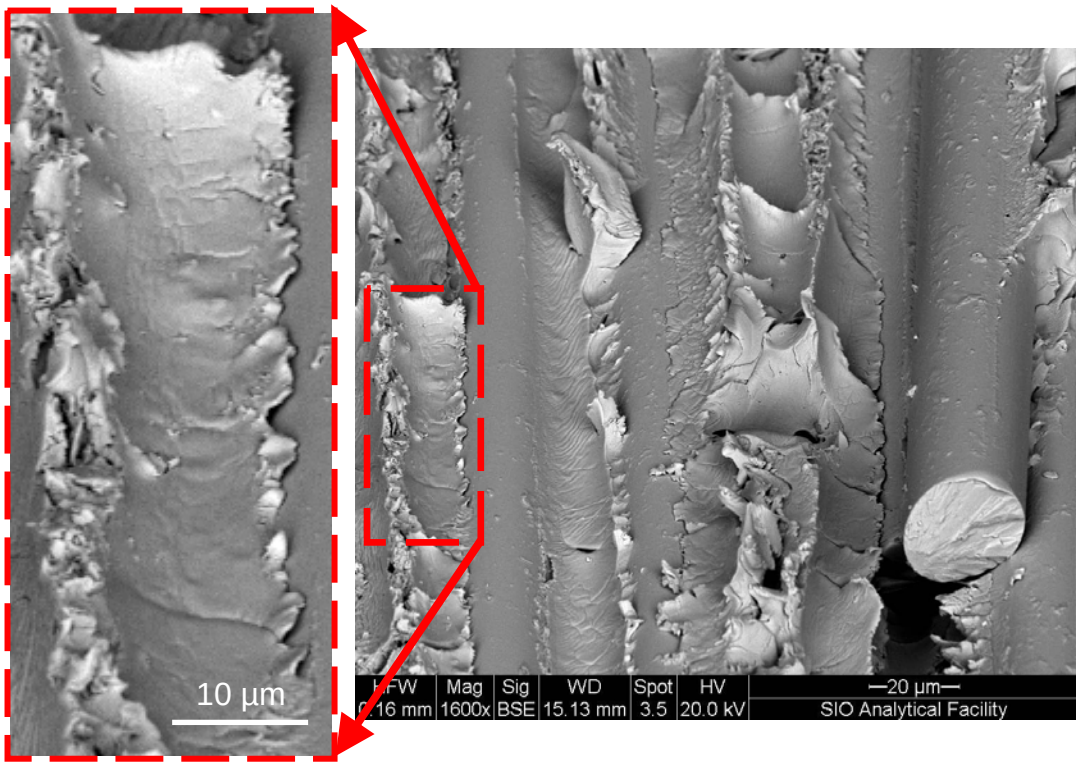

Figure 107. SEM micrograph of failed tensile specimen exposed to 40°C immersion for 12 weeks, indicating weakened polymer at fiber/matrix interface.

5.4 Relating Results of Short Beam Shear and Tension Testing

It is well known that the tensile strength is highly dependent upon interfacial adhesion. Results from short beam shear testing are primarily used to address the interlaminar shear strength (ILSS) of a composite, though it has been suggested that its use is appropriate for use as a relative measure of the fiber/matrix adhesion due to its sensitivity to through thickness longitudinal shear strength [10,11]. In the case of a pultruded composite, where the material is considered a single lamina, the shear failure should occur either in the matrix or at the interfacial level. However, because the test mode and failure modes are wholly distinct, it is difficult to quantitatively relate any short beam shear strength to tensile strength.

Exposure to low and medium humidity environments did not result in significant changes in tensile strength, though increases in SBS strength could be observed. Any increases in polymer or interphasial strength, reflected by increases in SBS strength, were not significant enough to result in increases in tensile strength.

Exposure to 75%RH at 60°C revealed a decrease in SBS strength and tensile strength and strain prior to post-conditioning. Plasticization is evidenced through the near full recovery in SBS and tensile strengths after post-conditioning and also can be detected through the decrease in tensile strain prior to post-conditioning resulting from the increased secondary modulus.

Removal of water through post-conditioning returns the tensile strength to the low end of initial scatter and the tensile strain returns to the high end of initial scatter, as shown in Figure 108 and Figure 109. Post-conditioning of this material exposed to

75%RH at 60°C, however reveals a strengthening effect as the SBS strength increases above initial values after post-conditioning, also shown in Figure 108 and Figure 109. Degradation of the interphase, also detected through increases in tanδ peak height through DMTA results discussed in Section 6.2.3.2, is likely responsible for degradation in tensile strength both before and after post-conditioning. Conversely, the increased dry tensile strain may be a consequence of the strengthening effect detected in SBS testing. A stiffer polymer network, also detected through increases in T_g, would result in a polymer which could experience greater deformation, despite a weakening of the bulk composite. Unexposed material exhibited a longitudinal splitting failure indicative of longitudinal matrix splitting. DMTA and SBS results indicate that the decreased tensile strength and increased tensile strain of the exposed material is likely a consequence of a stronger polymer network coupled with a weakened interfacial strength.

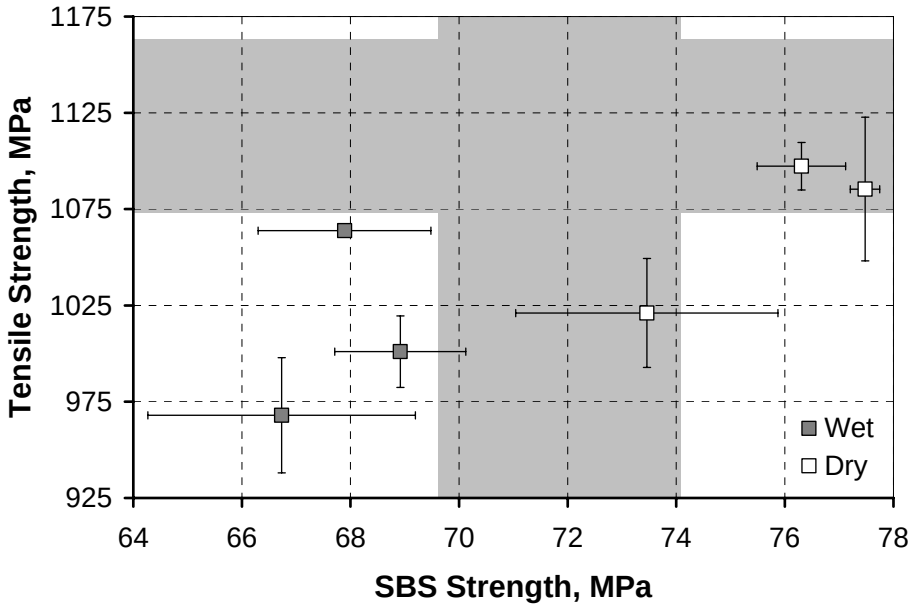

Figure 108. Tensile strength and SBS strength after exposure to 75%RH at 60°C.
Shaded region indicates baseline average and standard deviation.
Error bars indicate standard deviations.

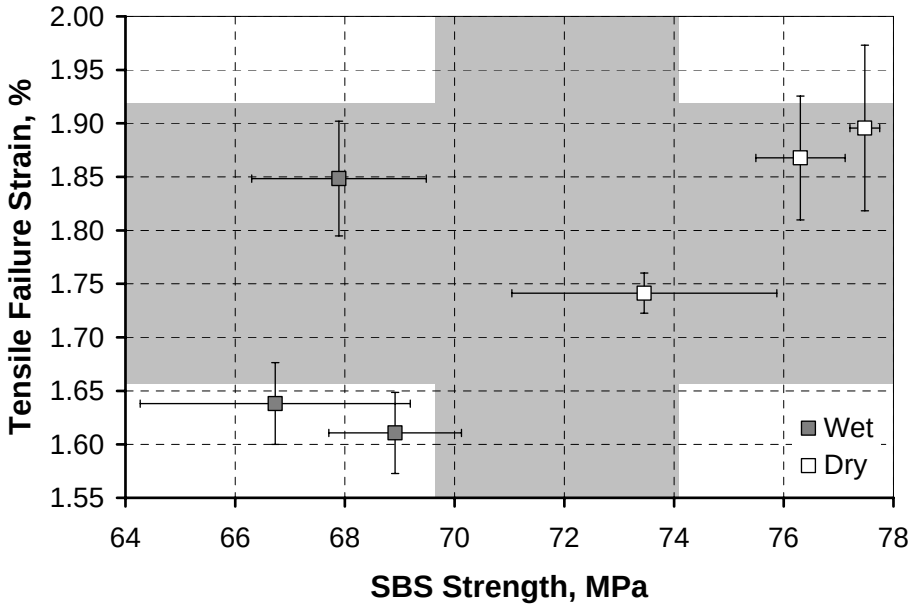

Figure 109. Tensile strain and SBS strength after exposure to 75%RH at 60°C.
Shaded region indicates baseline average and standard deviation.
Error bars indicate standard deviations.

SBS results indicate that exposure to 99%RH and immersion at 20°C results in reversible plasticization. At 40°C, exposure to 99%RH and immersion, plasticization also occurs but competes with a strengthening effect. The recovery in SBS strength and tensile failure strain after post-conditioning suggests that fibers are not damaged in these 20°C and 40°C environments over 96 weeks of exposure. Exposure to 99%RH and water immersion at 60°C permanently degrades the tensile strength at all time steps. In the first 12 weeks, the loss in SBS strength can be reversed and even increased above initial values after redrying. After 12 weeks of environmental exposure, post-conditioning results in 83% and 53% recovery in tensile strain for 99%RH and immersion, respectively. The dry SBS strength, provided in Table 29, is also greater for 99%RH after drying.

Table 29. SBS strengths and tensile strain after 12 weeks exposure to 99%RH and immersion at 60°C. Brackets indicate standard deviations.

		Wet		Dry	
	Initial	99%RH	Immersion	99%RH	Immersion
SBS (MPa)	71.9 [2.2]	65.1 [1.8]	63.4 [2.2]	75.8 [0.7]	74.4 [4.7]
Tensile Strength (MPa)	1119 [44]	760 [9]	733 [18]	850 [19]	800 [13]
Tensile Strain (%)	1.79 [0.13]	1.39 [0.06]	1.39 [0.03]	1.66 [0.08]	1.56 [0.06]
tanδ peak height	0.193 [0.011]	0.259 [0.005]	0.256 [0.009]	0.194 [0.010]	0.239 [0.010]
T_g [E''] (°C)	100.4 [2.9]	99.6 [0.7]	101.6 [0.6]	114.9 [1.3]	115.1 [0.6]

Assuming results of SBS testing reflect relative strength of the fiber/matrix interphase, it would be expected that the tensile strength would recover more after redrying. However, DMTA results presented in Table 29 indicate that there is likely

interphasial degradation occurring in the first 12 weeks of exposure as the tanδ peak height increases. Increases in T_g reveal potential further post-cure or loss of LMWS which may increase polymer strength while decreasing the failure strain. It is possible that an increase in polymer strength accounts for the increase in SBS strength while the degradation of the interface is responsible for the permanent loss in tensile strength.

After the first 12 weeks of exposure to 99%RH and immersion at 60°C, irreversible degradation of the tensile and SBS strength can be attributed to fiber pitting, revealed through SEM analysis. Fiber pitting in material exposed to 80°C saturated environments was detected in the scanning electron microscope after the first 12 weeks, leading to severe permanent degradation of material strength.

In summary, plasticization of the matrix and interphase occurs at 20°C and is reversible. Plasticization or leaching occurring in the polymer and interphase at 40°C and 60°C cannot counteract the irreversible strengthening effect due to post-cure or, more likely, leaching of LMWS and degradation occurring in these aggressive environments. After 12 weeks of exposure to 99%RH and immersion at 60°C there is a transition from reversible plasticization and strengthening, similar to that seen in material exposed to similar conditions at 40°C, to irreversible degradation of the fiber, matrix, and interphase, similar to but less severe than degradation experienced by material exposed to wet conditions at 80°C. Severe hydrolysis at 80°C leads to chemical and physical damage and permanent degradation of material strengths.

5.5 References

1. Chu, W. and V.M. Karbhari. "Effect of Water Sorption on Performance of Pultruded E-Glass/Vinylester Composites." *Journal of Materials in Civil Engineering*. Vol. 17, No. 1 (2005) 63-71.

2. Helbling, C.S. and V.M. Karbhari. "Investigation of the Sorption and Tensile Response of Pultruded E-Glass/Vinylester Composites Subjected to Hygrothermal Exposure and Sustained Strain." *Journal of Reinforced Plastics and Composites*. Vol. 27, No. 6 (2008) 613-638.

3. Kennedy, J.M., D.D. Edie, A. Banerjee, and R.J. Cano. "Characterization of Interfacial Bond Strength by Dynamic Analysis." *Journal of Composite Materials.* Vol. 26, No. 6 (1992) 869-882.

4. Rothon, R., ed. *Particulate-Filled Polymer Composites*. Longman Scientific & Technical: Essex, England, 1995.

5. Van de Velde, K. and P. Kiekens. "Effects of Chemical Environments on Pultruded E-Glass Reinforced Polyester." *Jornal of Composites Technology & Research*. Vol. 23, No. 2 (2001) 92-101.

6. Kurkjian, C.R., J.T. Krause, and U.C. Paek. "Tensile Strength Characteristics of 'Perfect' Silica Fibers." *Journal de Physique*. Vol. 43, No. 12 (1982) C9-585-586.

7. Matthewson, M.J. and C.R. Kurkjian. "Environmental Effects on the Static Fatigue of Silica Optical Fiber." *Journal of the American Society of Ceramics*. Vol. 71, No. 3 (1988) 177-183.

8. Bunker, B.C. "Moluecular mechanisms for corrosion of silica and silicate glasses." *Journal of Non-Crystalline Solids*. Vol. 179 (1994) 300-308.

9. Bascom, W.D. "Water at the Interface." *Journal of Adhesion*. Vol. 2 (1970) 161-183.

10. Drzal, L.T. and M. Madhukar. "Fibre-matrix adhesion and its relationship to composite mechanical properties." *Journal of Materials Science.* Vol. 28 (1993) 569-610.

11. Broyles, N.S., K.N.E. Verghese, R.M. Davis, J.J. Lesko, and J.S. Riffle. "Pultruded Carbon Fiber/Vinyl Ester Composites Processed with Different Fiber Sizing Agents. Part I: Processing and Static Mechanical Performance." *Journal of Materials in Civil Engineering*. Vol. 17, No. 3 (2005) 320-333.

6. Dynamic Mechanical Thermal Analysis

6.1 Background

Dynamic mechanical thermal analysis (DMTA) is a highly sensitive analytical technique for investigating characteristic transitions of polymers. Determination of the glass transition temperature, T_g, with environmental exposure can reveal plasticization through a reversible decrease in T_g or post-cure through an irreversible increase in T_g. Leaching of low molecular weight species (LMWS) may also lead to an increase in T_g as the mobility of the polymer decreases when the LMWS are removed. In addition to providing T_g for thermoset polymers, the characteristic DMTA curves introduced in the following discussion may also reveal information regarding relative crosslink density and interfacial adhesion.

The storage modulus, E', curve of a thermoset or its composite is characterized by glass transition region and the glassy and rubbery plateaus before and after T_g. T_g can be determined as the temperature at inflection point in the E' curve [1]. Strengthening of the polymer due to post-cure may also be revealed through increases in the glassy modulus. A decrease of the glassy modulus may indicate degradation of the composite material with environmental exposure. Based upon rubber elasticity theory, the rubbery plateau is assumed to correlate to changes in crosslink density of the polymer [2]. Classic rubber elasticity theory can be used to describe the average molecular weight between crosslinks, M_c, [3]

$$M_c = \frac{3RT\rho}{E'_{rp}}, \quad (1)$$

where E'_{rp} is the rubbery modulus of the unreinforced polymer, R is the gas constant, T is the temperature in Kelvin, and ρ is the density of the unreinforced polymer. This calculation of molecular weight should be taken as a qualitative representation of changes in crosslinking rather than as an absolute value, despite the acceptable order of magnitude [3]. The crosslink density, ρ_c, can be calculated as the inverse of M_c. Previous studies on the crosslinking of a vinyl-ester with styrene content indicate that increasing styrene content correlates to a decrease in crosslink density and, consequently, rubbery modulus [4-7].

DMTA testing is based upon the in phase, elastic and the out of phase plastic response of a viscoelastic material to an applied load. The storage modulus describes the elastic response while the loss modulus, E", describes the out of phase component. The breadth of the E" curve relates to the range of the glass transition region and the peak E" correlates to T_g. T_g as detected from E" should correlate to the value obtained from E', but these values will be lower than that determined from tanδ [1]. The loss modulus represents the amount of energy dissipated in the deformation process [8]. For a composite, this dissipation may originate in the viscoelastic matrix, interphase, or filler, such as glass fiber reinforcement or fillers such as kaolin clay or calcium carbonate which are commonly used in pultruded structural composites. Energy dissipation may also be related to the quality of interfacial adhesion, where lower interfacial adhesion results in greater energy loss [8]. For the material considered here, burn-off tests revealed the presence of a particulate filler confirmed to be kaolin

clay, as discussed in Section 5.3. Changes in interfacial adhesion could be attributed to changes in the adhesion of the polymer matrix to either the glass fiber reinforcement or the particulate filler. An increase in the volume fraction or size of filler will lead to an increase in *E*" [9] since the filler surface area increases with both variables.

The damping curve described by tanδ describes the ratio of the loss modulus to storage modulus. The high sensitivity of this value to changes in both *E*' and *E*" can result in curves which demonstrate unambiguous peaks, allowing for straightforward detection of T_g and other characteristic transitions. However, because of the sensitivity to changes in the storage and loss moduli, the tanδ peak value may be less consistent in the determination of T_g [1]. The height of the tanδ curve has also been related to interfacial adhesion performance [8]. An increase in damping loss, where the characteristic value is taken as the tanδ peak height, correlates to a loss in interfacial adhesion since perfect adhesion would restrict the mobility of the polymer in the immediate vicinity of the fiber reinforcement, leading to a quicker response when a load is applied. Therefore, as the fiber/matrix bond performance decreases, the tanδ peak height increases [8]. Conversely, as the degree of crosslinking increases, the system rigidity increases and can be observed in a broadened transition region and decreased tanδ values [2]. A broadening of the tanδ glass transition region has also been attributed to the presence of a stiffer interphase [1].

A drying effect is often observed in the characteristic curves of material which has been exposed to water environments [10]. The drying effect is most obvious in

the tanδ curve, where biphasic behavior may be observed through two peaks characterizing the plasticized, wet material with lower T_g and the dry material with higher T_g [11]. This drying effect may be affected by scan rate [12], as a longer time at elevated temperature will result in a drier material.

Biphasic behavior can also be observed in a two component resin [13]. In a styrene crosslinked vinyl-ester, homopolymerization of styrene may occur to form a second phase with a characteristic T_g distinct from that of the vinyl-ester. Alternatively, the components used to form vinyl-ester may react with each other during the DMTA scan, resulting in a lower T_g characteristic of the uncured polymer and a higher T_g characteristic of the polymer with higher crosslink density. Evidence of this biphasic behavior in dry vinyl ester, attributed to measurement "instability", is indicated in [14], where the biphasic behavior observed in neat vinyl ester resin is indistinguishable in the glass fiber composite. The appearance of a second peak has also been attributed to the presence of an interphase [15].

While the current study would greatly benefit from a comparison of the behaviors of neat resin and composite, it was not possible to replicate the cure schedule and formulation of the neat resin used in this pultruded material. The thermal gradients imposed upon the raw fiber and resin as they are pulled through the die are not uniform. Non-uniform resin formulation in the composite at the microscale may also result from preferential adsorption of one part of the uncured resin to the fiber surface or due to the formation of an interphase near the fiber surface [16]. The

interphase in a glass composite has been detected in DMTA tests conducted in the longitudinal direction but is indistinguishable in the transverse direction [15].

6.2 DMTA Testing Results

6.2.1 Initial Values

Values for as-received and pre-conditioned characteristic DMTA parameters are provided in Table 30. The average and standard deviation values for pre-conditioned material were obtained using DMTA results after testing of 56 specimens pre-conditioned at 40°C and 18%RH for 6 weeks. Material exposed to 40°C at 18%RH was also tested in sets of 4 after another 6, 12, 18, 24, 30, 36, 42, 48, 54, 72, 78, 96, and 102 weeks of exposure, providing an additional 52 tests. The baseline average and standard deviation were calculated using results from a total 108 tensile tests of material exposed to 40°C at 18%RH. Representative curves are presented in Figure 110 and Figure 111. DMTA results for all environmental exposures can be found in Appendix C.

Table 30. Initial DMTA values.
Brackets indicate standard deviations.

	As-Received	Pre-conditioned	Baseline
T_g (°C) (tanδ peak)	112.7 [2.6]	116.8 [4.7]	117.8 [4.2]
T_g (°C) (E" peak)	95.3 [1.7]	99.3 [2.8]	100.4 [2.8]
tanδ peak height	0.197 [0.006]	0.194 [0.010]	0.193 [0.011]
E' (GPa) (T_g - 60°C)	18.2 [0.3]	17.5 [0.7]	17.7 [0.8]
E' (GPa) (T_g + 60°C)	2.19 [0.19]	2.21 [0.14]	2.14 [0.17]

The glass transition region can be qualitatively addressed using the breadth of the tanδ curve. The glass transition region has previously be quantified as the full width at half the maximum (FWHM) of the tanδ curve [6]. For both raw and pre-

conditioned material, the FWHM is about 80°C. Consequently, the glassy and rubbery moduli are selected at T_g ± 60°C, rather than using the usual 40°C or 50°C offset, so that the *E*' value selected represents that on the glassy and rubbery plateau. Where failure occurs before T_g + 60°C, the rubbery modulus is taken as the minimum *E*' immediately before failure.

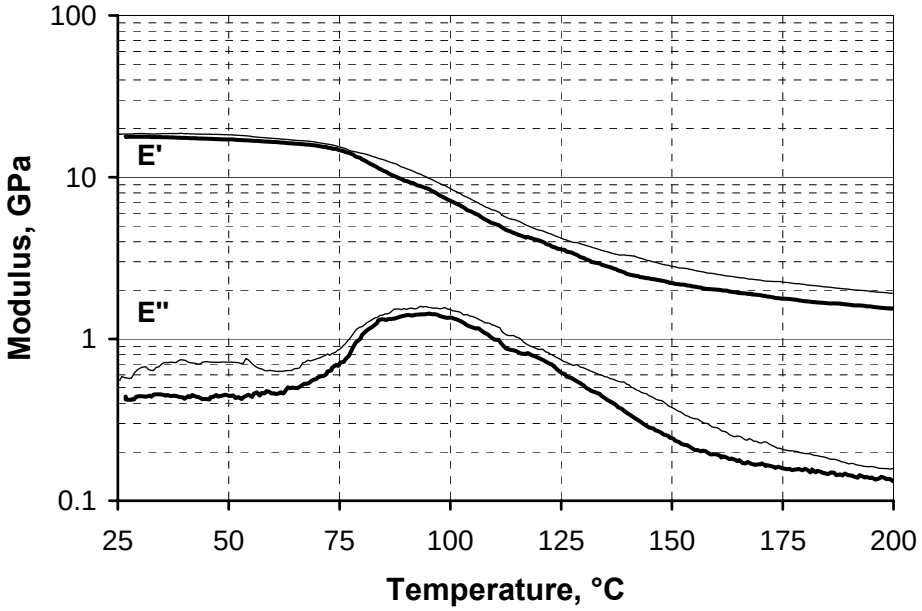

Figure 110. Representative storage and loss modulus curves of unexposed material. Thin: as-received; bold: pre-conditioned.

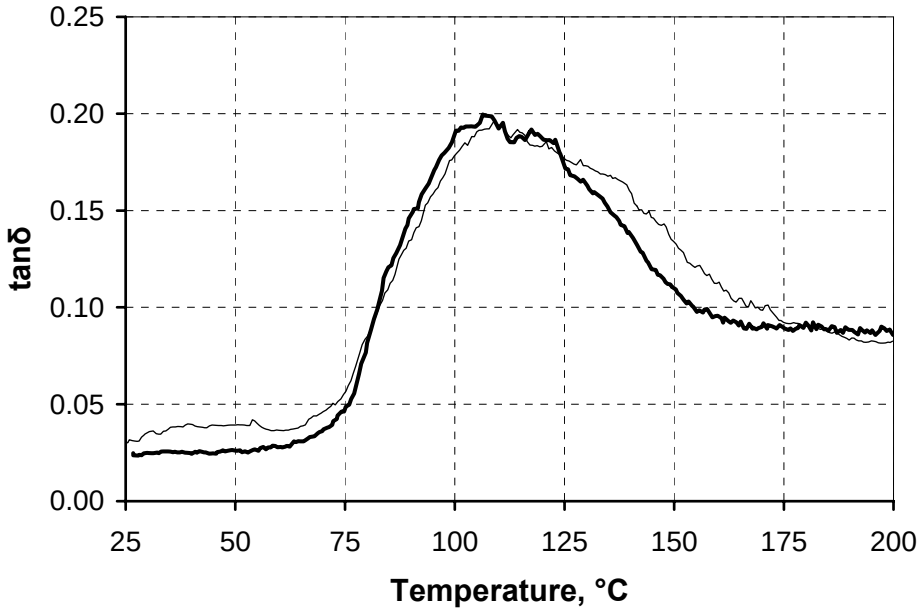

Figure 111. Representative tanδ curves of unexposed material.
Thin: as-received; bold: pre-conditioned.

6.2.2 Glass Transition Temperature

6.2.2.1 Low and Medium Humidity Results

Exposure to 18%RH and 50%RH results in subtle increases in tensile strength and strain, discussed in Section 5.1.1. The same exposures indicate clear increases in short beam shear (SBS) strength at elevated temperatures of exposure and small decreases at 20°C, as shown in Section 5.2.1. The increases in SBS strength indicate a strengthening of the polymer or interphase or a combination of both through leaching of LMWS or post-cure or a combination thereof. Redrying of the material results in observable increases of SBS strength. The small decreases in SBS strength observed at room temperature and the increases observed after redrying indicate that there is a small plasticization effect detectable through SBS testing. Comparing T_g values to

SBS strength values indicates that both plasticization and either leaching of LMWS or post-cure occurs, as seen in Figure 112 through Figure 119. These results are not surprising, as increases in T_g are often correlated with increases in polymer strengths [17], due to a tightening of the polymer network. The following discussion presents a detailed analysis of the changes in T_g, as determined using both the tanδ and E" peak, after exposure to 18%RH and 50%RH environments.

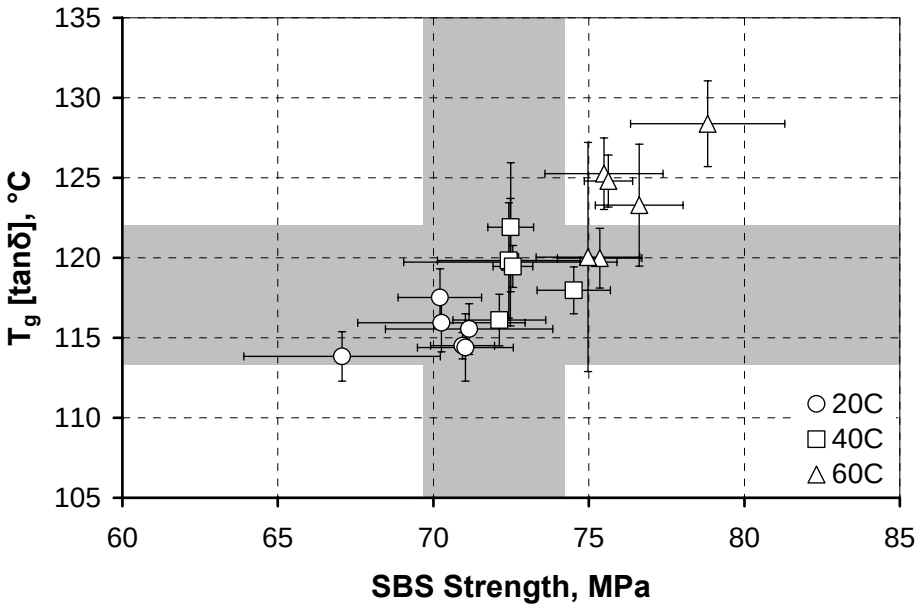

Figure 112. Wet T_g (using tanδ) and SBS strength for 18%RH exposures. Shaded region indicates baseline average and standard deviation. Error bars indicate standard deviations.

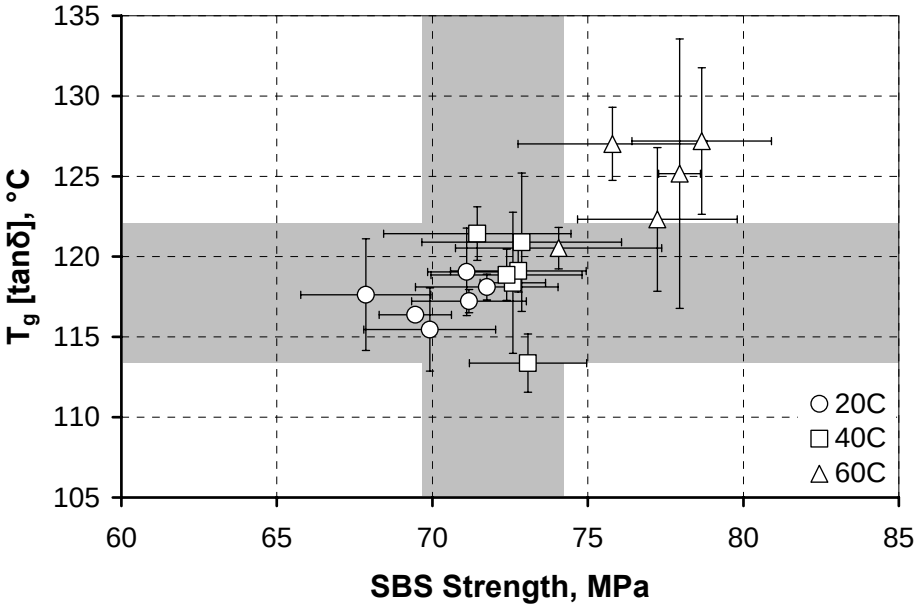

Figure 113. Dry T_g (using tanδ) and SBS strength for 18%RH exposures. Shaded region indicates baseline average and standard deviation. Error bars indicate standard deviations.

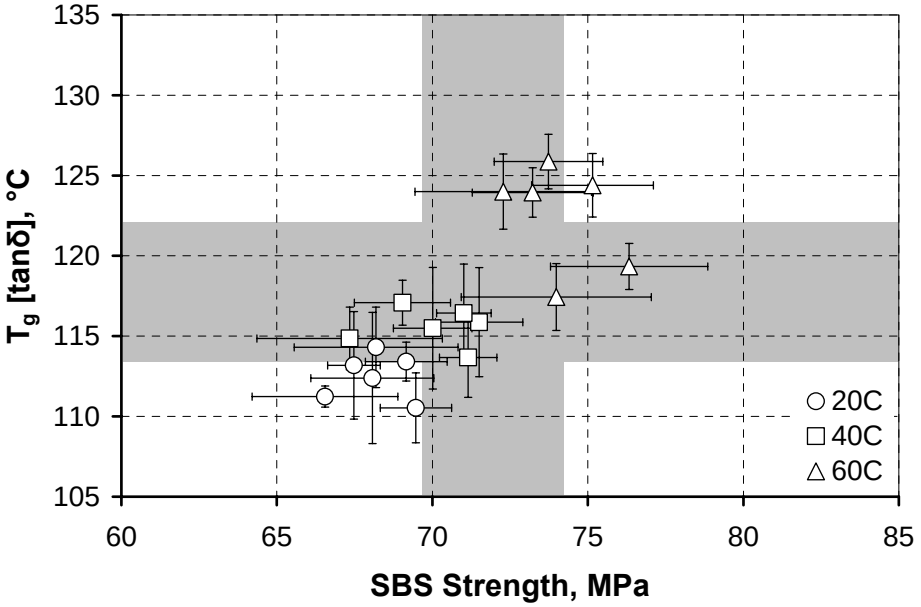

Figure 114. Wet T_g (using tanδ) and SBS strength for 50%RH exposures. Shaded region indicates baseline average and standard deviation. Error bars indicate standard deviations.

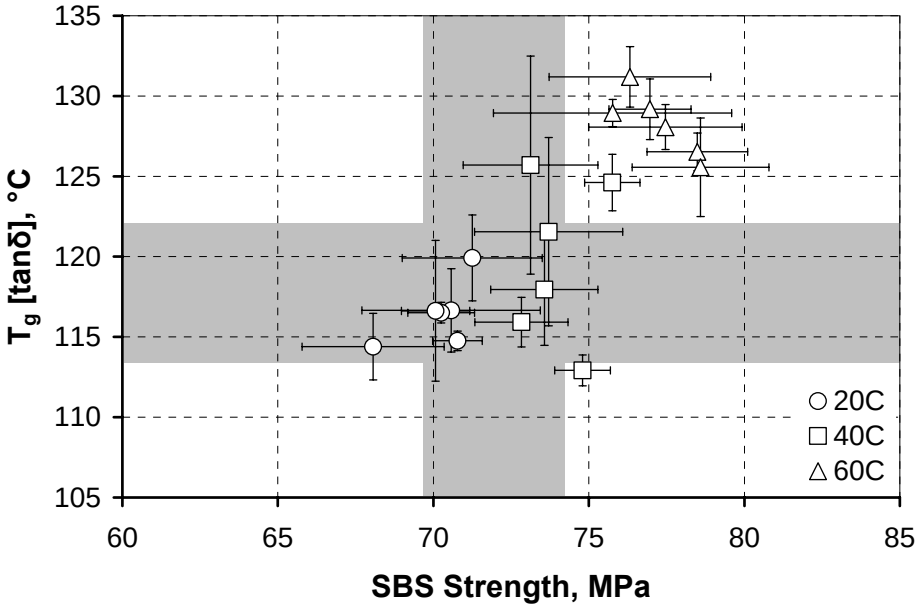

Figure 115. Dry T_g (using tanδ) and SBS strength for 50%RH exposures. Shaded region indicates baseline average and standard deviation. Error bars indicate standard deviations.

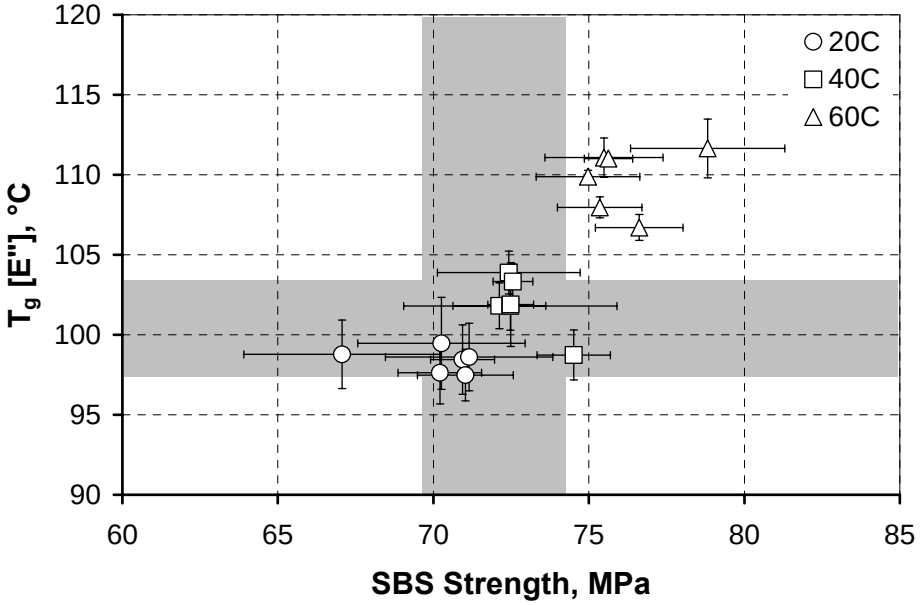

Figure 116. Wet T_g (using E") and SBS strength for 18%RH exposures. Shaded region indicates baseline average and standard deviation. Error bars indicate standard deviations.

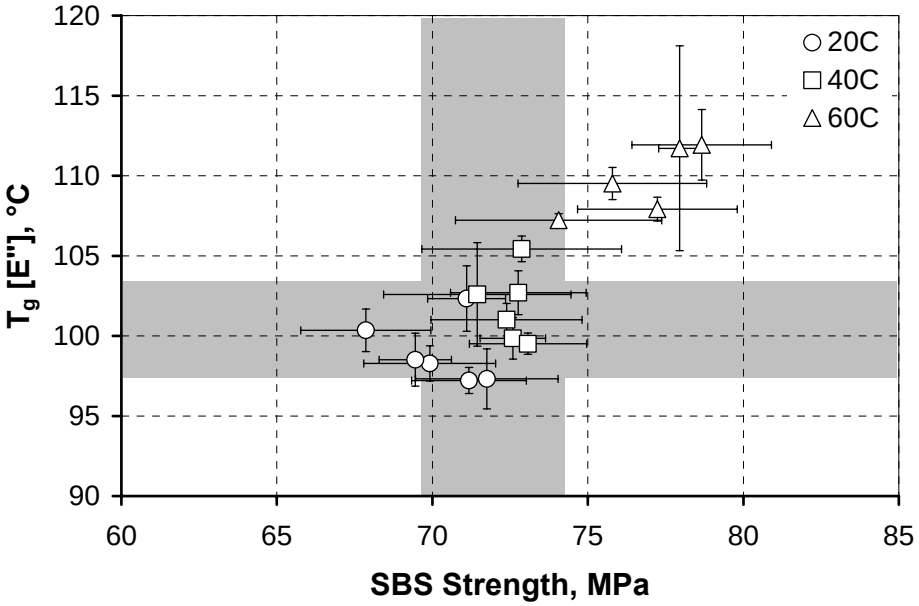

Figure 117. Dry T_g (using E") and SBS strength for 18%RH exposures. Shaded region indicates baseline average and standard deviation. Error bars indicate standard deviations.

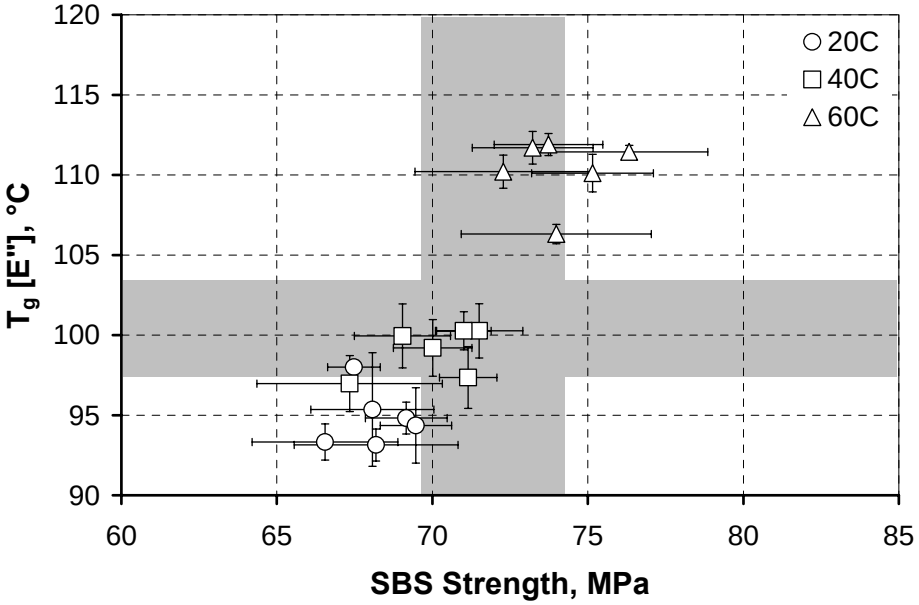

Figure 118. Wet T_g (using E") and SBS strength for 50%RH exposures. Shaded region indicates baseline average and standard deviation. Error bars indicate standard deviations.

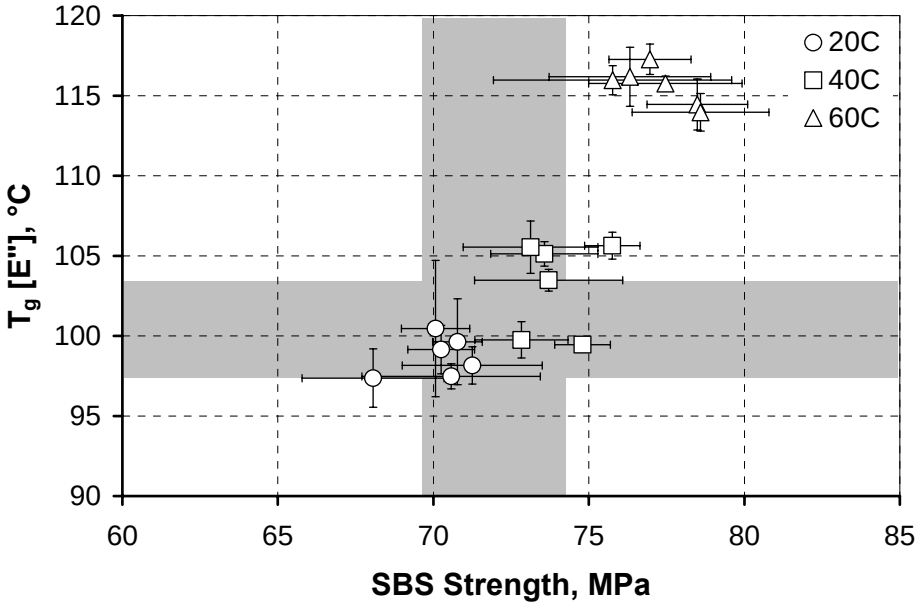

Figure 119. Dry T_g (using E") and SBS strength for 50%RH exposures. Shaded region indicates baseline average and standard deviation. Error bars indicate standard deviations.

6.2.2.1.1 T_g as Determined from tanδ Peak

Material exposed to 18%RH and 50%RH at 20°C demonstrates a small decrease in average T_g as determined using the tanδ peak. This decrease results in a T_g which is within initial scatter bounds except for two wet sets exposed to 50%RH at 20°C for 36 and 48 weeks, as shown in Figure 120 and Figure 121. Figure 122 and Figure 123 reveal a trend of increasing T_g for material exposed to low and medium relative humidity at 40°C. All T_g are within initial scatter except for that of material which was post-conditioned after exposure to 50%RH at 40°C for 96 weeks, where the T_g clearly increased. Material exposed to 18%RH and 50%RH at 60°C shows a general increase in both wet and dry T_g from the baseline value, as shown in Figure 124 and Figure 125.

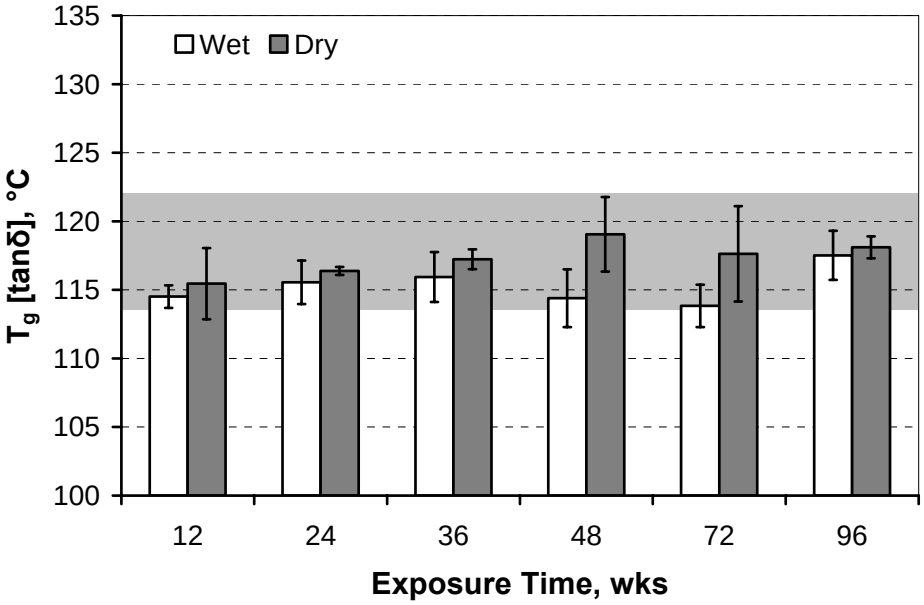

Figure 120. T_g (using tanδ) for material exposed to 20°C at 18%RH. Shaded region indicates baseline average and standard deviation. Error bars indicate standard deviations.

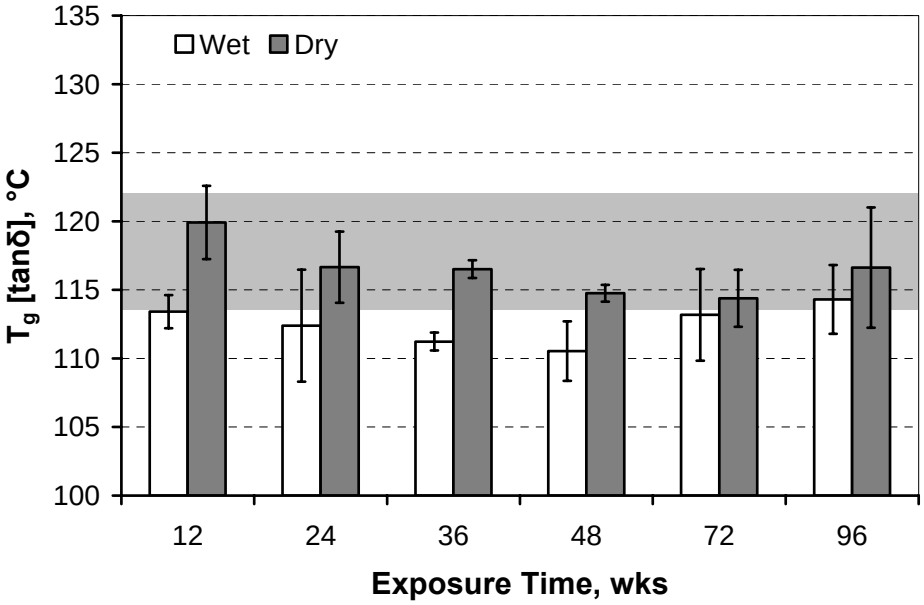

Figure 121. T_g (using tanδ) for material exposed to 20°C at 50%RH. Shaded region indicates baseline average and standard deviation. Error bars indicate standard deviations.

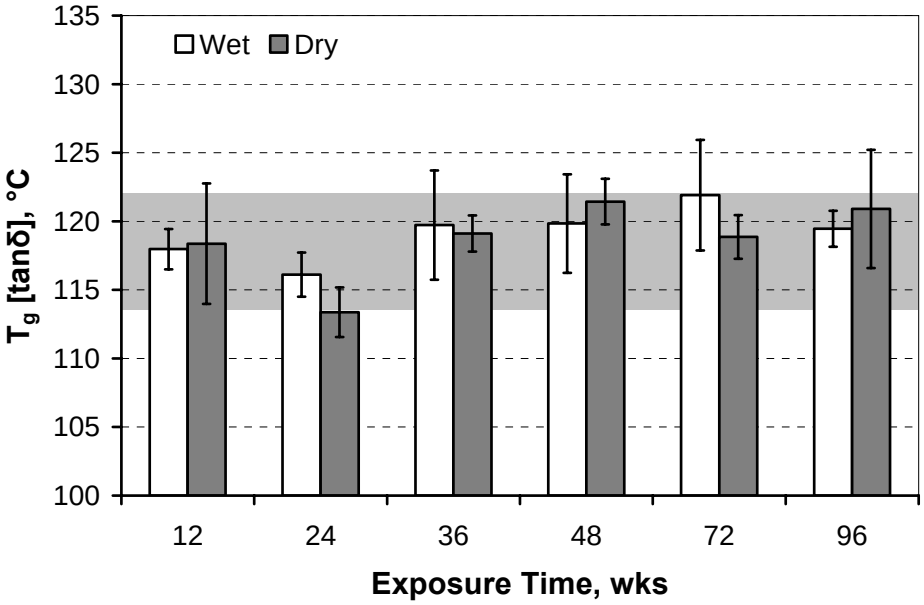

Figure 122. T_g (using tanδ) for material exposed to 40°C at 18%RH. Shaded region indicates baseline average and standard deviation. Error bars indicate standard deviations.

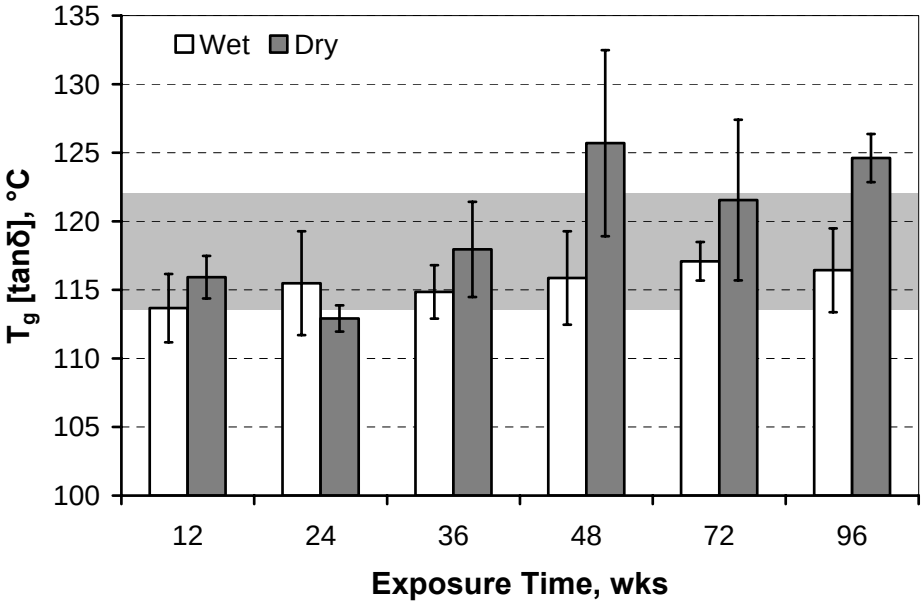

Figure 123. T_g (using tanδ) for material exposed to 40°C at 50%RH. Shaded region indicates baseline average and standard deviation. Error bars indicate standard deviations.

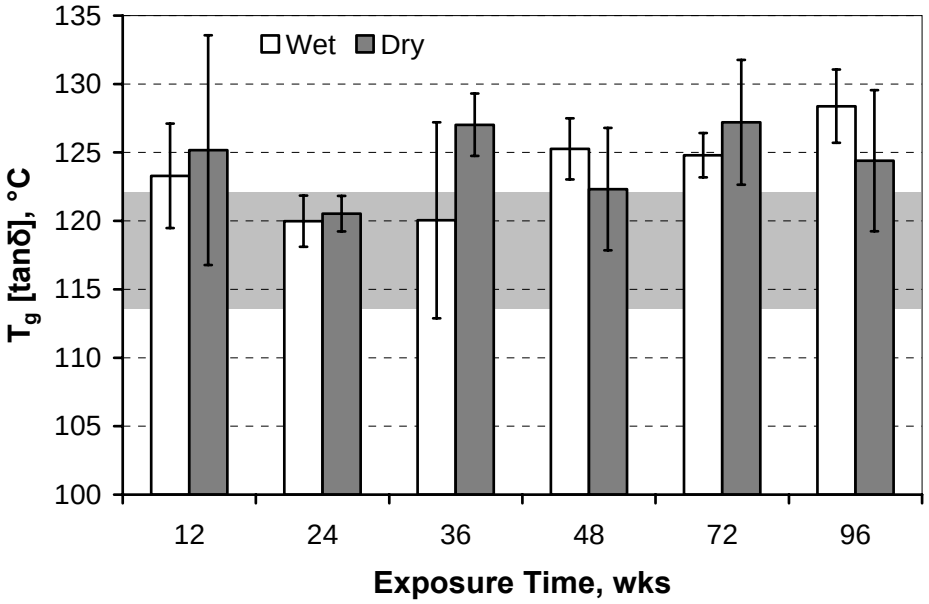

Figure 124. T_g (using tanδ) for material exposed to 60°C at 18%RH. Shaded region indicates baseline average and standard deviation. Error bars indicate standard deviations.

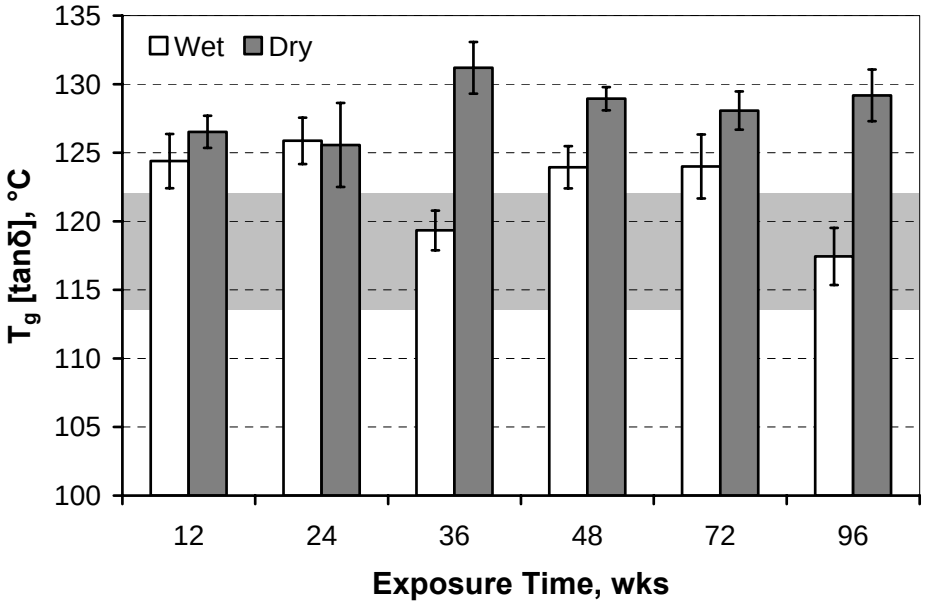

Figure 125. T_g (using tanδ) for material exposed to 60°C at 50%RH. Shaded region indicates baseline average and standard deviation. Error bars indicate standard deviations.

Exposure to room temperature leads to small moisture uptake, resulting in a depression of the average T_g. Exposure to elevated temperatures results in an increase in wet T_g for material exposed to 18%RH and an increase in dry T_g resulting from exposure to 50%RH. Increases in T_g after post-conditioning of material exposed to 50%RH indicate plasticization.

The increase in T_g seen for specimens exposed to 50%RH at 60°C tested before and after post-conditioning are likely a consequence of leaching of LMWS. Between 6 weeks and 24 weeks of exposure to 50%RH at 60°C, DMTA specimens demonstrate a steady decrease in weight, seen in Figure 126, likely a result of leaching of residual LMWS, even in the presence of water. Apparent moisture uptake in Figure 126 is calculated using the exposed, wet weight W_w and the initial, pre-conditioned weight W_0:

$$M_t = \frac{W_w - W_0}{W_0} \times 100\% \quad (2)$$

.

While SBS, moisture and tensile specimens exposed to 60°C and 50%RH do not demonstrate weight loss after post-conditioning, DMTA specimens show a slight loss in weight, seen in Figure 127, indicating loss of some material between completion of pre-conditioning and completion of post-conditioning. Weight loss is calculated using the weight after post-conditioning:

$$W_l = \frac{W_d - W_0}{W_0} \times 100\% \quad (3)$$

.

It is highly likely that this loss of material occurred during exposure to 60°C at 50%RH. While the weight loss and drops in apparent moisture uptake do not directly

correlate to changes increases in T_g, these results provide evidence for loss of LMWS during exposure to 60°C at 50%RH which may be responsible for the increase in T_g.

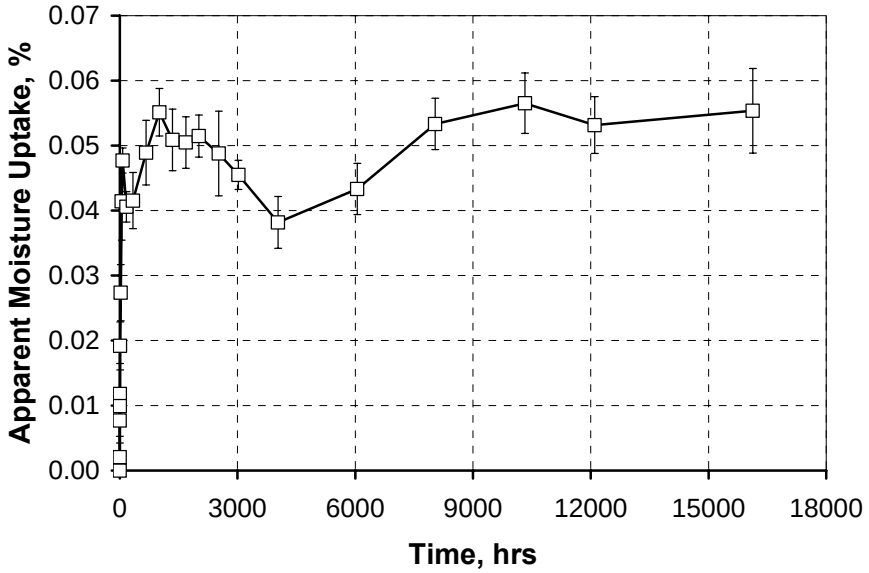

Figure 126. Moisture trend for DMTA specimens exposed to 50%RH at 60°C. Error bars indicate standard deviations.

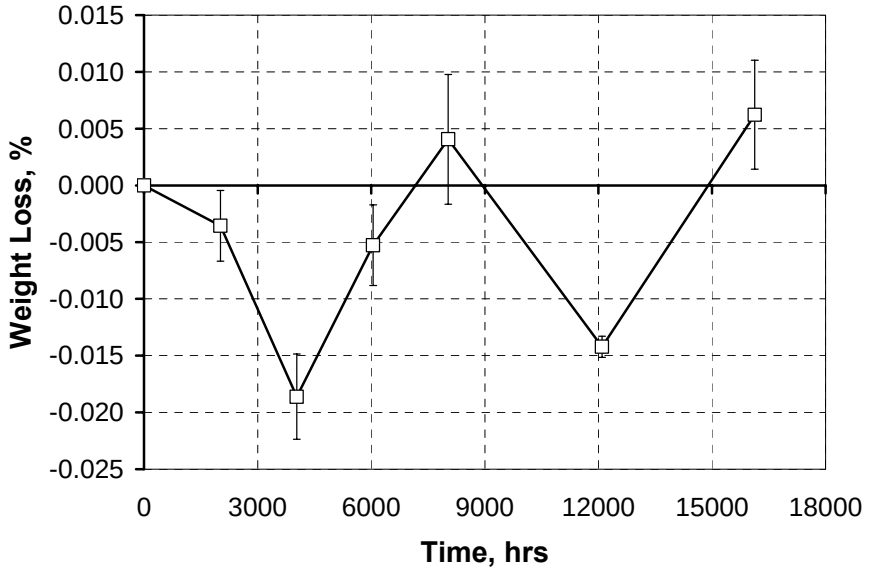

Figure 127. Weight loss of DMTA specimens post-conditioned after exposure to 50%RH at 60°C. Error bars indicate standard deviations.

6.2.2.1.2 T_g as Determined from Loss Modulus Peak

Similar trends in T_g are found when using the E" curve rather than the tanδ curve to detect T_g. Where high standard deviations indicate significant overlap of scatter for T_g values obtained using the tanδ peak, the lower scatter inherent in the T_g determined using E" peaks allows for more straightforward detection of changes in T_g. Figure 128 through Figure 133 provide T_g values, determined using E", for material exposed to 18%RH and 50%RH.

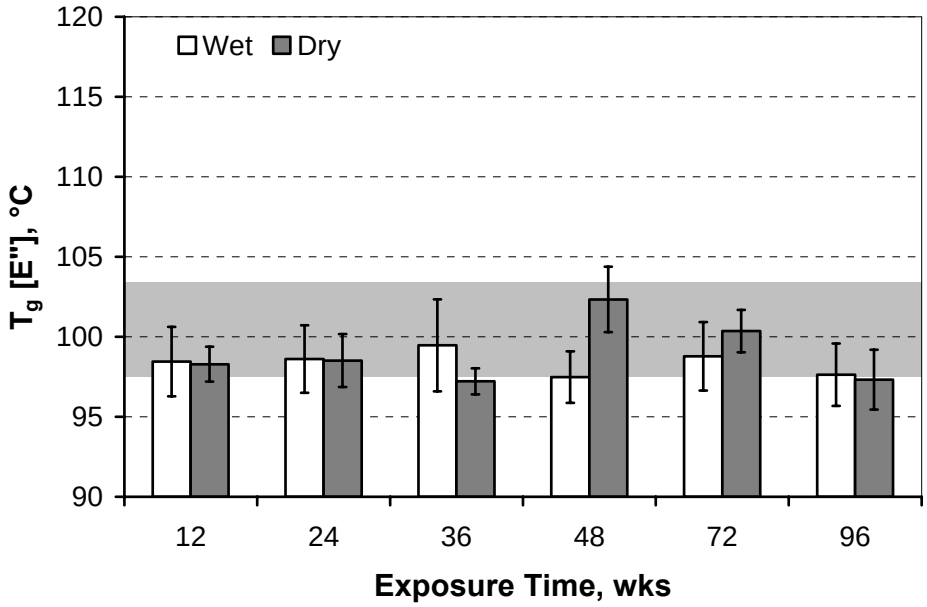

Figure 128. T_g (using E") for material exposed to 20°C at 18%RH. Shaded region indicates baseline average and standard deviation. Error bars indicate standard deviations.

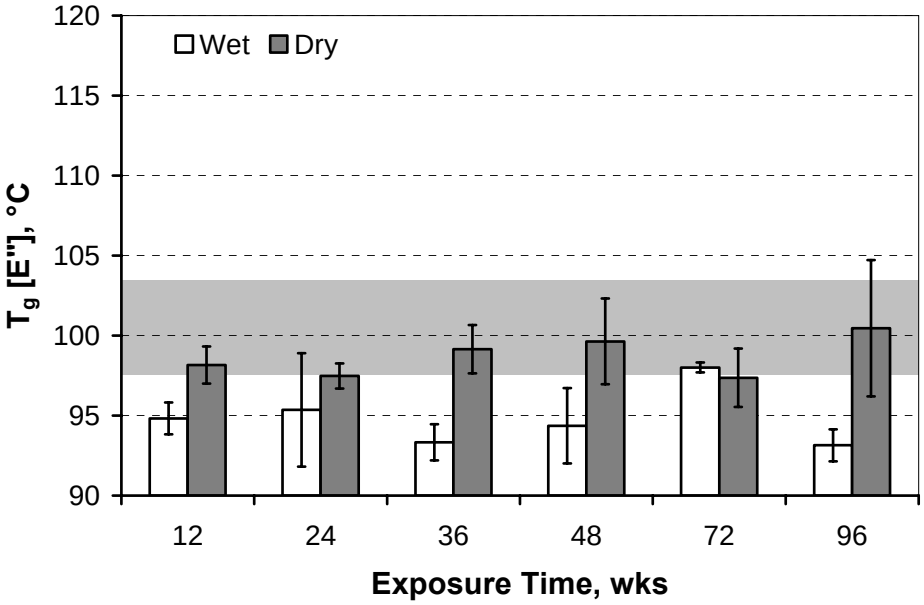

Figure 129. T_g (using E") for material exposed to 20°C at 50%RH. Shaded region indicates baseline average and standard deviation. Error bars indicate standard deviations.

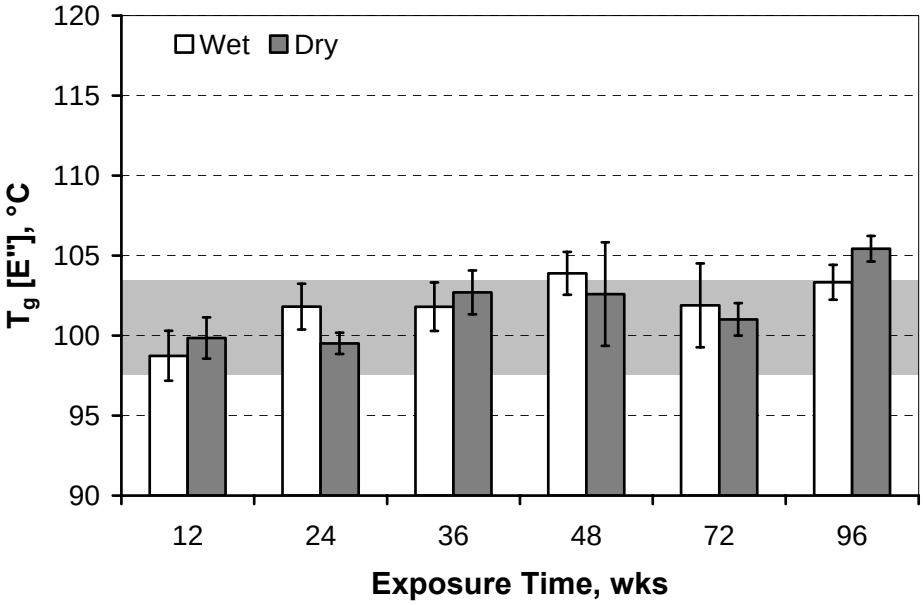

Figure 130. T_g (using E") for material exposed to 40°C at 18%RH. Shaded region indicates baseline average and standard deviation. Error bars indicate standard deviations.

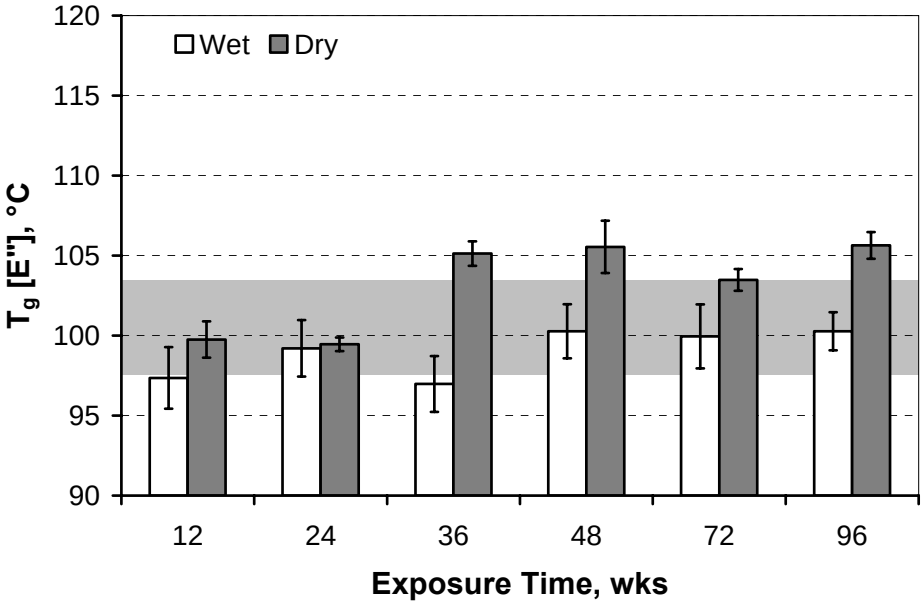

Figure 131. T_g (using E") for material exposed to 40°C at 50%RH. Shaded region indicates baseline average and standard deviation. Error bars indicate standard deviations.

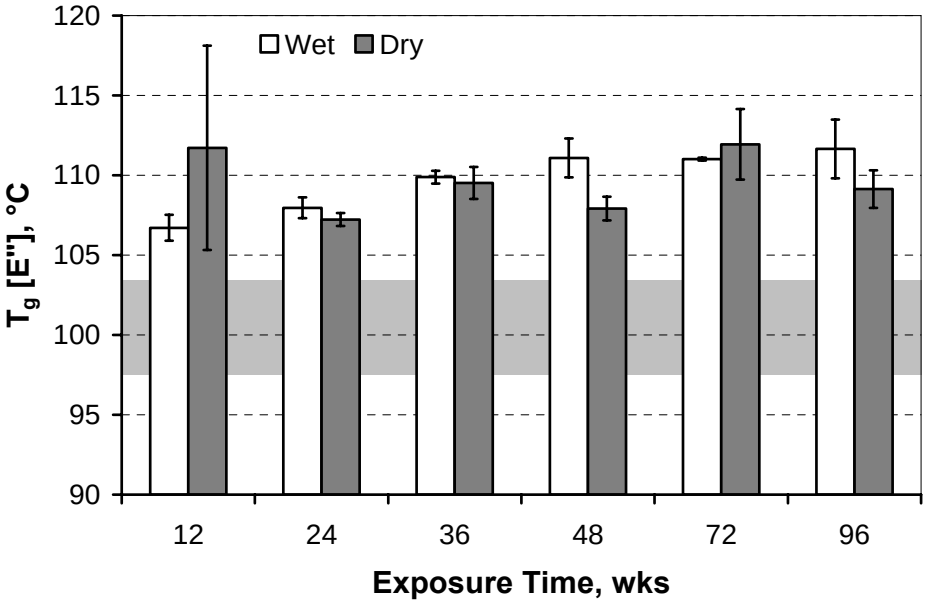

Figure 132. T_g (using E") for material exposed to 60°C at 18%RH. Shaded region indicates baseline average and standard deviation. Error bars indicate standard deviations.

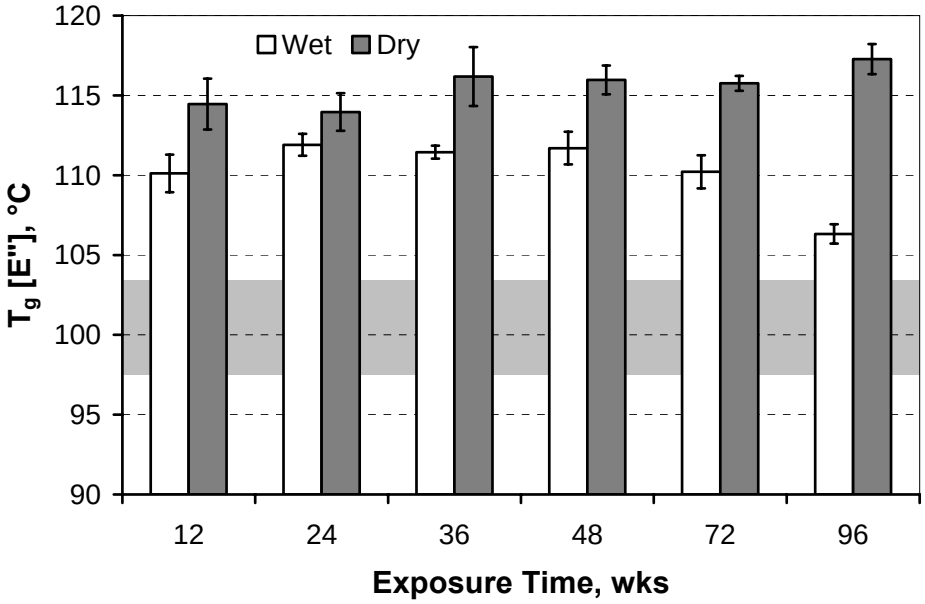

Figure 133. T_g (using E") for material exposed to 60°C at 50%RH. Shaded region indicates baseline average and standard deviation. Error bars indicate standard deviations.

Small decreases in T_g are observed in material exposed to low humidity at 20°C, as seen in Figure 128, indicating that the presence of even a small bit of moisture sorbed in a room temperature 18%RH environment results in a decrease in T_g. These water molecules may loosen the polymer network, evidenced by a lower T_g, where it requires less energy to activate segmental motion. Removal of the sorbed moisture through post-conditioning will not result in a significant shift in T_g since the apparent moisture content was so low. However, the relaxation of the polymer network may still remain, indicated by a depressed T_g which does not change between wet and dry sets. A similar phenomenon is seen in material exposed to 50%RH at 20°C, where plasticization becomes obvious and the dry T_g is about the same as that for material exposed to 18%RH at the same temperature, as shown in Figure 129.

Figure 130 illustrates a very gradual increase in T_g for material exposed to 18%RH at 40°C. While it is expected that values for the 18%RH exposure at 40°C lie within the baseline scatter since the baseline is calculated using these values, there a gradual increasing trend with time, nonetheless. A similar gradual increasing trend can be seen in Figure 131 for material which has been post-conditioned after exposure to 50%RH at 40°C where the plasticizing effect of water has been reversed. These results indicate that there is a gradual tightening of the polymer network, possibly a result of leaching of LMWS or progressive polymeric reaction at this elevated temperature.

Exposure to 60°C at 18%RH results in a T_g which gradually increases with exposure time, as shown in Figure 132. This increase in T_g is likely a consequence of leaching of LMWS in this dry environment. Figure 133 illustrates the significant increase of T_g in material exposed to 50%RH even before the removal of water through post-conditioning. The steady decrease in wet T_g from 48 weeks through 96 weeks is indicative of an increasing plasticization phenomenon, where a longer exposure to 50%RH at 60°C allows for easier activation of segmental motion in the presence of water. The discussion of the moisture sorption trend presented in Section 4.2 proposed that leaching of LMWS occurs through about 24 weeks after which the polymer network begins to relax, allowing for greater moisture sorption. The relaxation of the polymer network would allow for increased hydrogen bonding with sorbed water molecules, leading to an increased plasticization effect when water is

present. However, the leaching of LMWS would result in a tightened polymer network reflected by a progressively higher T_g after the removal of water.

6.2.2.2 75%RH Results

Material exposed to 75%RH at 60°C demonstrates an increase in T_g even before water is removed, shown in Figure 134. Because material exposed to 75%RH has a higher water content than material exposed to 50%RH at the same temperature, the it is expected that the increased plasticization effect would result in a wet T_g for material exposed to 75%RH which is lower than that for material exposed to 50%RH. The plasticization effect is reversed after redrying, whereupon the T_g of material exposed to 50%RH and 75%RH at 60°C is about the same. Again, the using the E" curve to detect T_g results in more distinct trends with lower scatter.

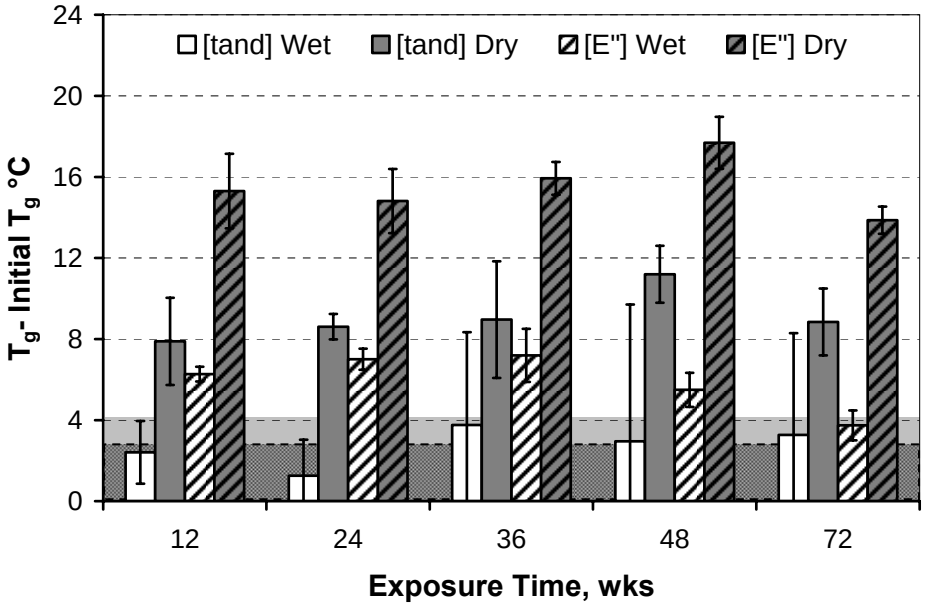

Figure 134. Change in T_g after exposure to 75%RH at 60°C. Standard deviation of baseline T_g using tanδ and E" indicated by light shaded region and dark shaded region, respectively. Error bars indicate standard deviation.

6.2.2.2.1 T_g as Determined from tanδ Peak

Investigation of the tanδ curves indicates that the T_g does not change significantly from initial values when tested immediately after exposure, as shown in Figure 134 and Figure 135. However, redrying reveals that the T_g increases from the baseline average by 7.9 [2.2] °C at just 12 weeks to 11.2 [1.4] °C at 48 weeks. The plasticization effect depressed T_g by 5.5°C [2.2] °C at 12 weeks and 8.8°C [6.8] °C at 48 weeks. Figure 135 shows that while material exposed to 50%RH at 60°C demonstrates plasticization only some of the time, the plasticization observed in material exposed to 75%RH at the same temperature is more consistent and generally more dramatic than that resulting from exposure to 50%RH. Furthermore, the dry T_g for material exposed to these two humidities are very close to each other, as seen in Figure 135, indicating that the while plasticization effects are greater with exposure to 75%RH, the increase of T_g resulting from leaching of LMWS or possible post-cure is comparable once the water is removed.

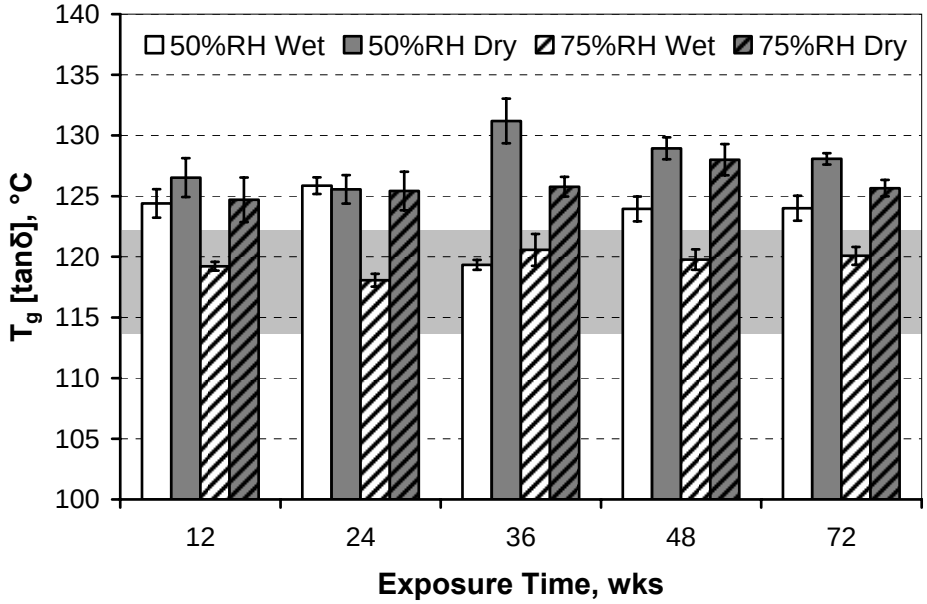

Figure 135. T_g (using tanδ) for material exposed to 50%RH and 75%RH. Shaded region indicates baseline average and standard deviation. Error bars indicate standard deviations.

6.2.2.2.2 T_g as Determined from Loss Modulus Peak

The increase in T_g resulting from post-cure or leaching of LMWS into 60°C humid environments is more pronounced when considering T_g as determined from E" rather than tanδ, even before removal of water. Figure 136 illustrates the increases in wet T_g observed for both 50%RH and 75%RH exposures at 60°C.

Testing of dry material after post-conditioning results in an increase in T_g ranging from 7.8 [1.6] °C to 12.2 [1.3] °C. The depression in this T_g resulting from plasticization has less scatter and is more dramatic than that of 5~9°C seen using the T_g determined from the tanδ peak. A more significant plasticization phenomenon is expected in higher humidity environments where the moisture uptake is greater. Again, the dry T_g for material exposed to 50%RH and 75%RH at the same temperature

are comparable, and the increase from initial values is greater for T_g determined using E" rather than tanδ.

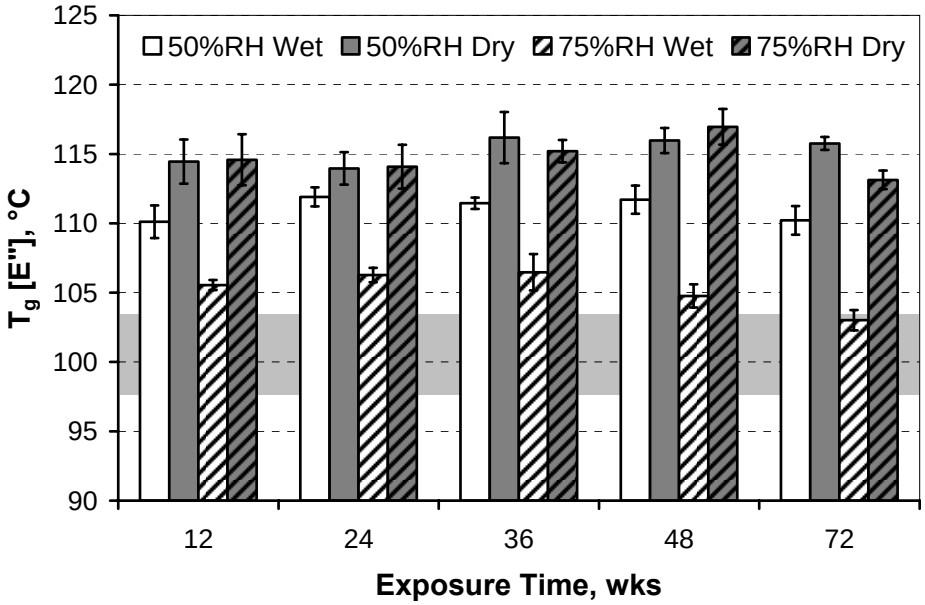

Figure 136. T_g (using E") for material exposed to 50%RH and 75%RH. Shaded region indicates baseline average and standard deviation. Error bars indicate standard deviations.

6.2.2.3 High Humidity and Immersion Results

While the effects of plasticization and leaching of LMWS are sometimes difficult to detect in material exposed to 18%RH and 50%RH, material exposed to 99%RH and immersion environments demonstrates much more plasticization. Increasing temperature of exposure results in a steady increase in T_g.

6.2.2.3.1 T_g as Determined from tanδ Peak

Using the tanδ peak, the most significant decrease in T_g from the baseline average occurs with exposure to immersion at 20°C, as seen in Figure 137 and Figure

138. In exposures at 20°C, the decrease in T_g is more dramatic after immersion in water when compared to exposure to 99%RH. The variation of T_g resulting from exposure to 40°C does not differ significantly between 99%RH and immersion. After redrying, the T_g of all material exposed to 99%RH and immersion at 20°C and 40°C are all within initial scatter. Through 36 weeks, the dry T_g of material exposed to these four environments are all within scatter range of each other. From 48 weeks on, though, material exposed to 40°C has a higher T_g than that of material exposed to 20°C, indicative of increasing rigidity in the polymer network with increasing time of exposure at 40°C.

These results provide evidence that, similar to SBS results, presented in Figure 139and Figure 140, a tightening of the polymer network does occur at 40°C, likely a result of leaching of LMWS or post-cure. Because the composite material demonstrates degradation and leaching of degraded material in 99%RH and immersion environments at elevated temperatures, it is not possible to isolate leaching of residual LMWS from leaching of degradation products.

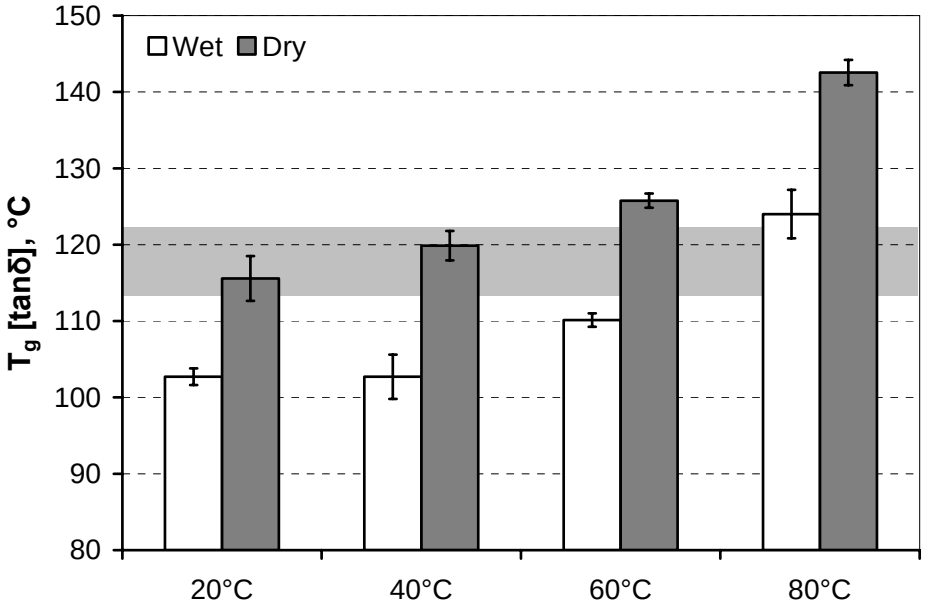

Figure 137. T_g (using tanδ) for material exposed to 99%RH for 96 weeks.
Shaded region indicates baseline average and standard deviation.
Error bars indicate standard deviations.

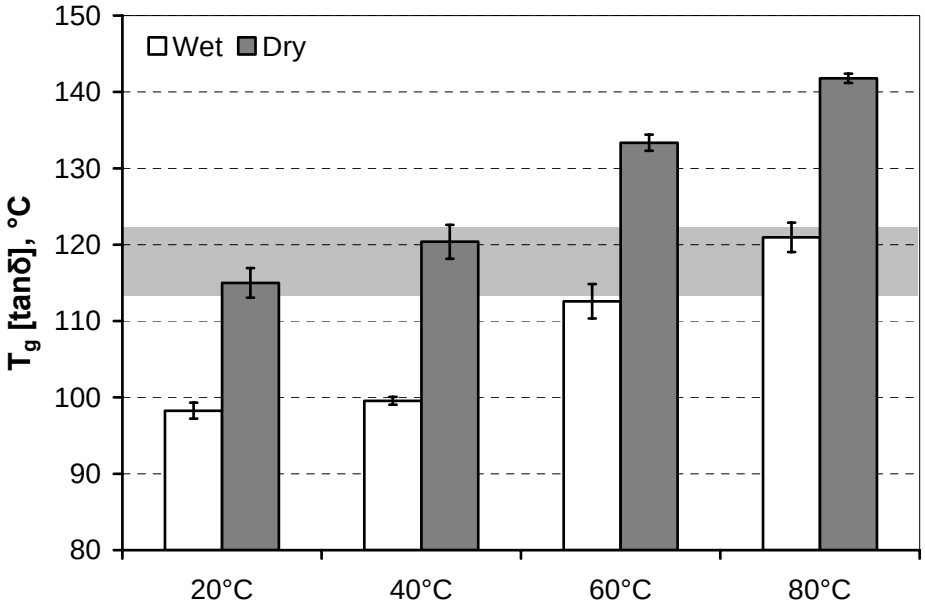

Figure 138. T_g (using tanδ) for material immersed in water for 96 weeks.
Shaded region indicates baseline average and standard deviation.
Error bars indicate standard deviations.

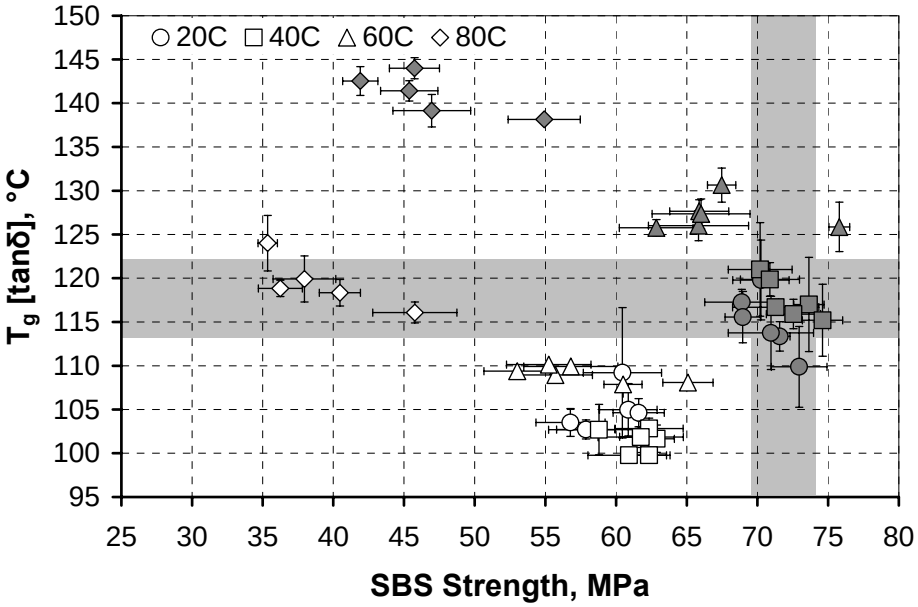

Figure 139. T_g (using tanδ) and SBS strength for 99%RH exposures. Open: wet, closed: dry. Shaded region indicates baseline average and standard deviation. Error bars indicate standard deviations.

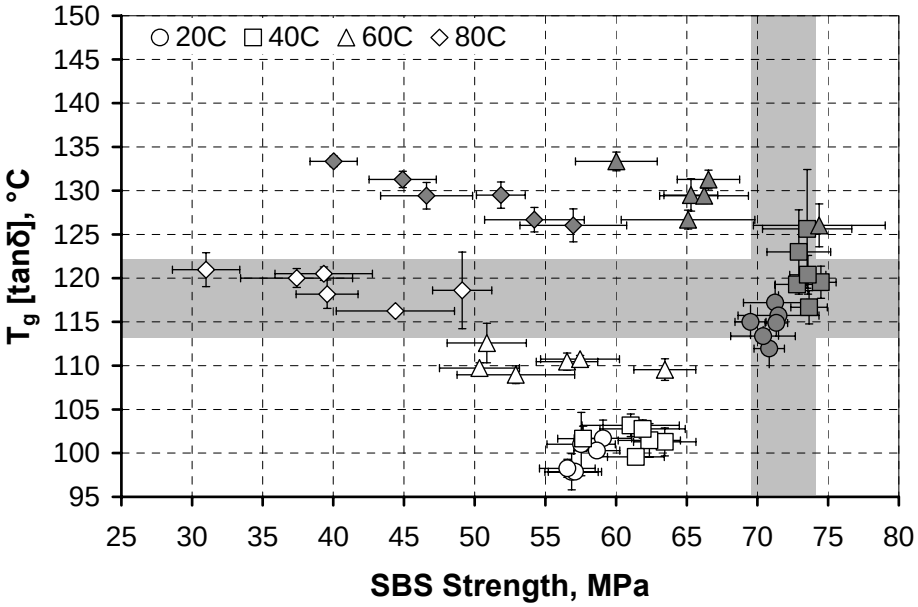

Figure 140. T_g (using tanδ) and SBS strength for immersion exposures. Open: wet, closed: dry. Shaded region indicates baseline average and standard deviation. Error bars indicate standard deviations.

For material exposed to 60°C, exposure to 99%RH consistently results in a wet T_g lower than that for material exposed to immersion. This phenomenon is demonstrated for one set tested at 96 weeks in Figure 137 and Figure 138. It is likely that the increased T_g is a consequence of leaching which occurs more readily in the liquid water exposures and leads to a strengthening effect. While greater weight loss correlates to a higher T_g, as shown in Figure 141, it also correlates to a higher temperature of exposure. The dry T_g appears to be primarily a function of temperature of exposure rather than as a function of amount of material lost to the exposure environment, although the dry T_g does appear to increase gradually over time. Figure 142 illustrates this gradual increasing T_g for material immersed in deionized water at 60°C. Similar trends are seen for 99%RH and immersion at 40°C, 60°C, and 80°C. These results indicate that while the majority of LMWS are leached into the environment in the first 12 weeks, the leaching may progress over the course of years.

With increasing temperature and moisture content, the plasticization phenomenon leads to greater changes in T_g, as Figure 143 and Figure 144 demonstrate. Figure 143 and Figure 144 plot the change in T_g from wet to dry as a function of adjusted moisture content $M_{t,a}$, where $M_{t,a}$ reflects the amount of water in degraded specimens by accounting for leaching of degraded material. $M_{t,a}$ is calculated using the wet, dry, and initial weights (W_w, W_d, and W_0):

$$M_{t,a} = \frac{W_w - W_d}{W_0} \times 100\% \quad (4)$$

The increase in T_g after post-conditioning is most significant for the material exposed to 80°C immersion where the material experiences the greatest moisture uptake and

leaches the most degraded material. It can be concluded that an increasing temperature of exposure for 99%RH and immersion exposures results in higher moisture content, plasticization, and leaching of LMWS.

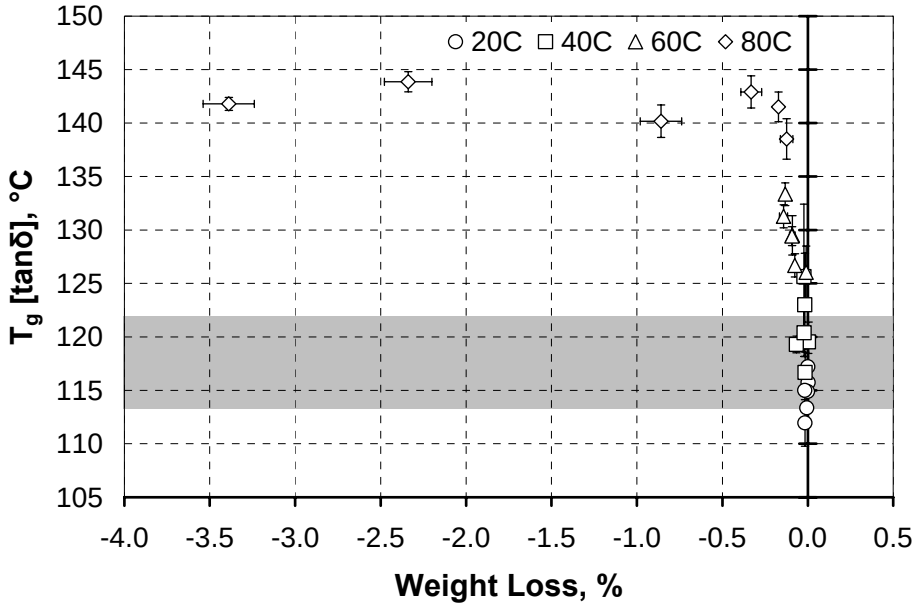

Figure 141. T_g (using tanδ) as a function of weight loss for immersion exposures.
Shaded region indicates baseline standard deviation.
Error bars indicate standard deviations.

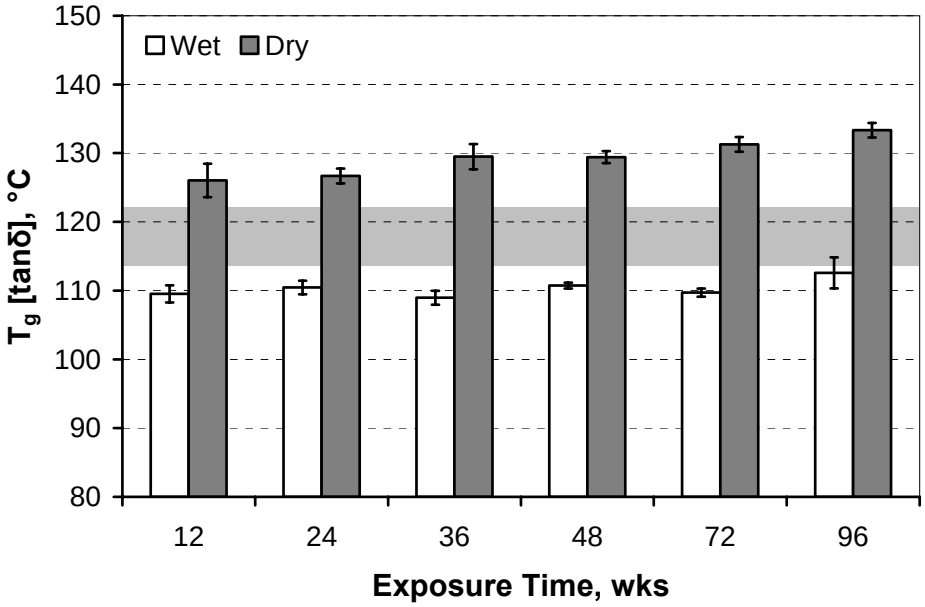

Figure 142. T_g (using tanδ) material exposed to 60°C immersion.
Shaded region indicates baseline standard deviation.
Error bars indicate standard deviations.

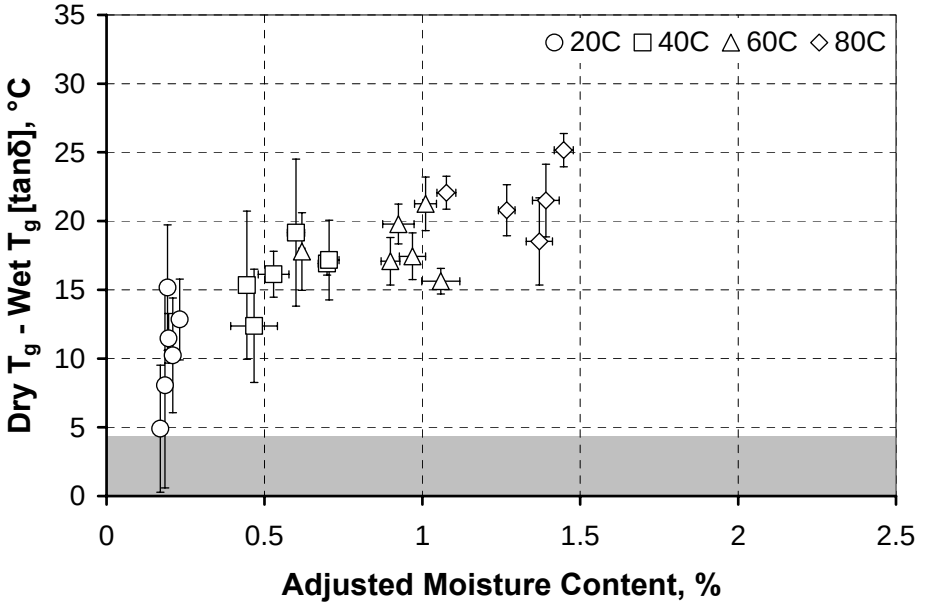

Figure 143. Regain in T_g (using tanδ) as a function of
adjusted moisture content for 99%RH exposures.
Shaded region indicates baseline standard deviation.
Error bars indicate standard deviations.

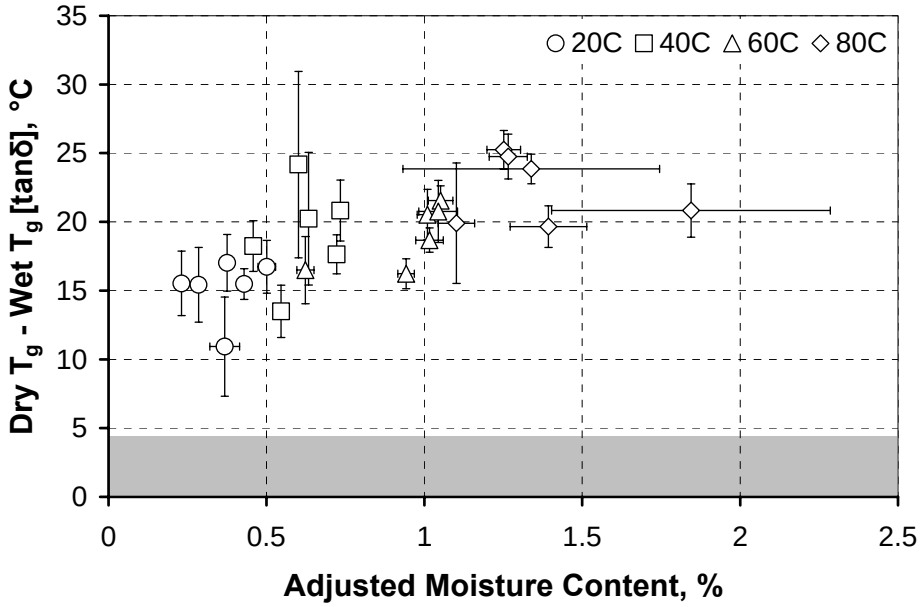

Figure 144. Regain in T_g (using tanδ) as a function of adjusted moisture content for immersion exposures. Shaded region indicates baseline standard deviation. Error bars indicate standard deviations.

6.2.2.3.2 T_g as Determined from Loss Modulus Peak

As seen in Figure 145 and Figure 146, using the E" peak to determine T_g reveals a clear plasticization effect as a function of moisture content, though the depression in T_g due to plasticization, presented in Figure 147 and Figure 148, does not demonstrate a clear trend with moisture content. The slight increase in plasticization induced by increasing moisture content is obscured by the high scatter of the calculated regain.

Figure 149 and Figure 150 provide a plot of the shift from initial to dry T_g as determined using E". The shift in T_g resulting from leaching of LMWS is lower in magnitude than that indicated by shifts in T_g using tanδ, but the scatter is also much lower. Figure 149 and Figure 150 provide a clear indication of the dependency of T_g

on moisture content, where the leaching effect is amplified for higher temperatures, as discussed in the previous section.

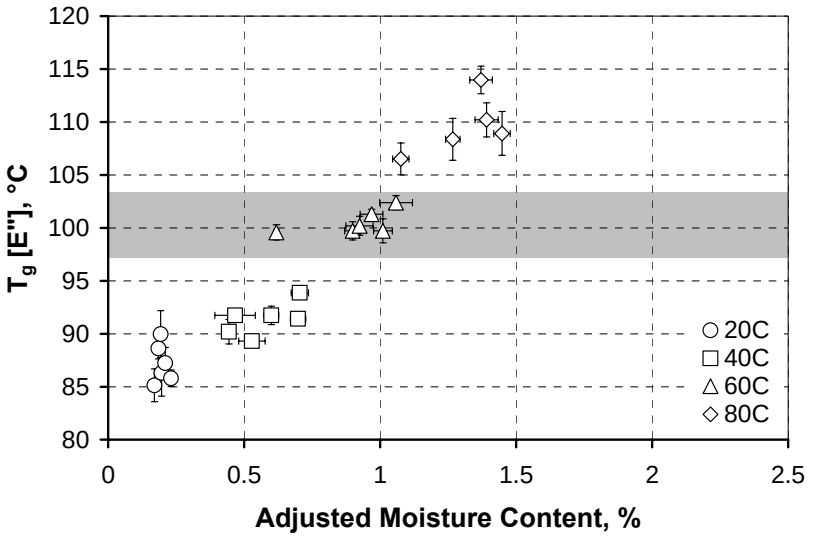

Figure 145. Wet T_g (using E") with adjusted moisture content for 99%RH exposures.
Shaded region indicates baseline average and standard deviation.
Error bars indicate standard deviations.

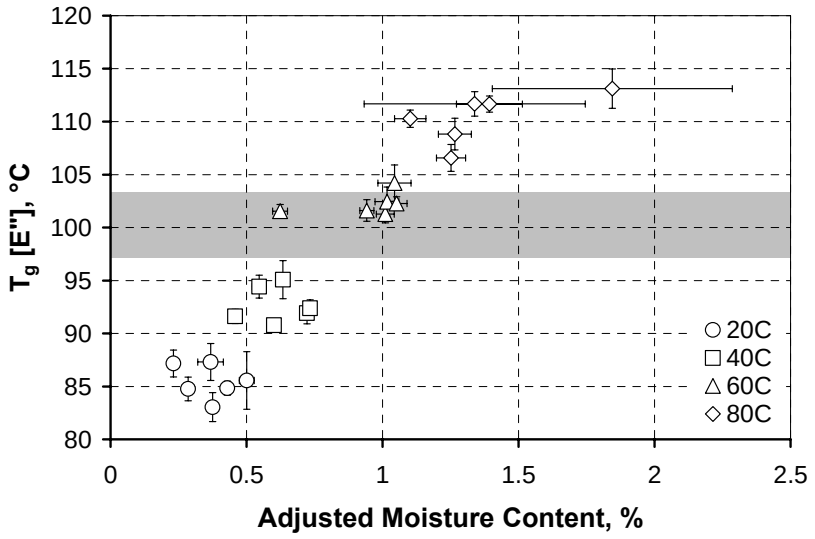

Figure 146. Wet T_g (using E") with adjusted
moisture content for immersion exposures.
Shaded region indicates baseline average and standard deviation.
Error bars indicate standard deviations.

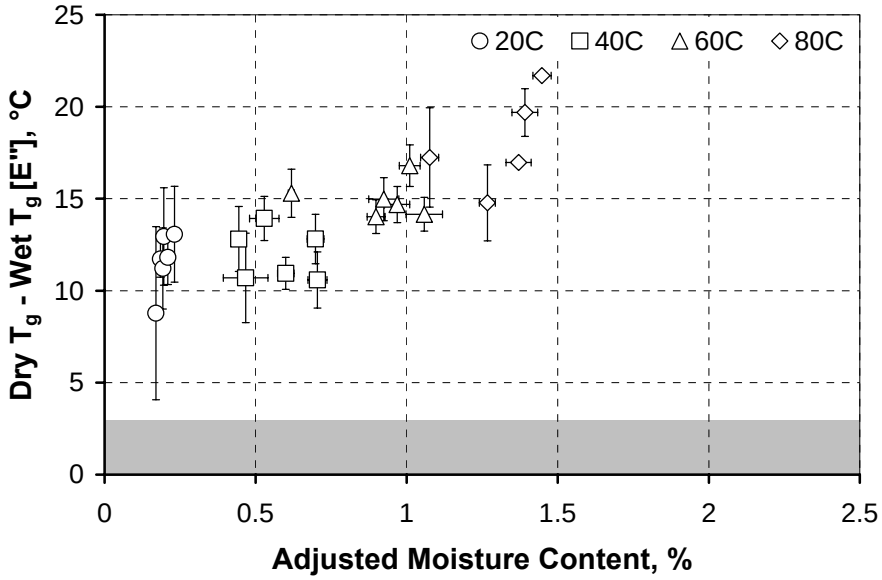

Figure 147. Regain in T_g (using E") as a function of adjusted moisture content for 99%RH exposures. Shaded region indicates baseline standard deviation. Error bars indicate standard deviations.

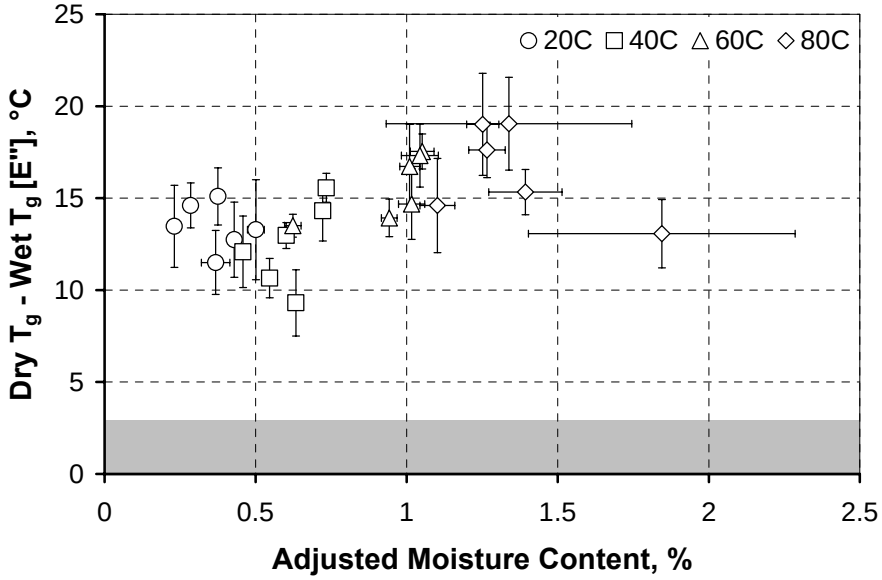

Figure 148. Regain in T_g (using E") as a function of adjusted moisture content for immersion exposures. Shaded region indicates baseline standard deviation. Error bars indicate standard deviations.

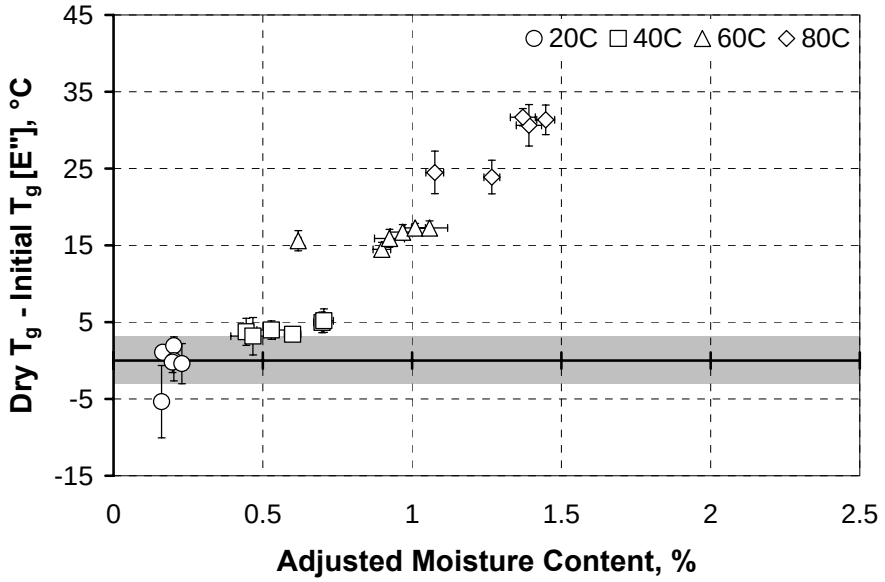

Figure 149. Change in dry T_g (using E") from initial as a function of adjusted moisture content for 99%RH exposures.
Shaded region indicates baseline standard deviation.
Error bars indicate standard deviations.

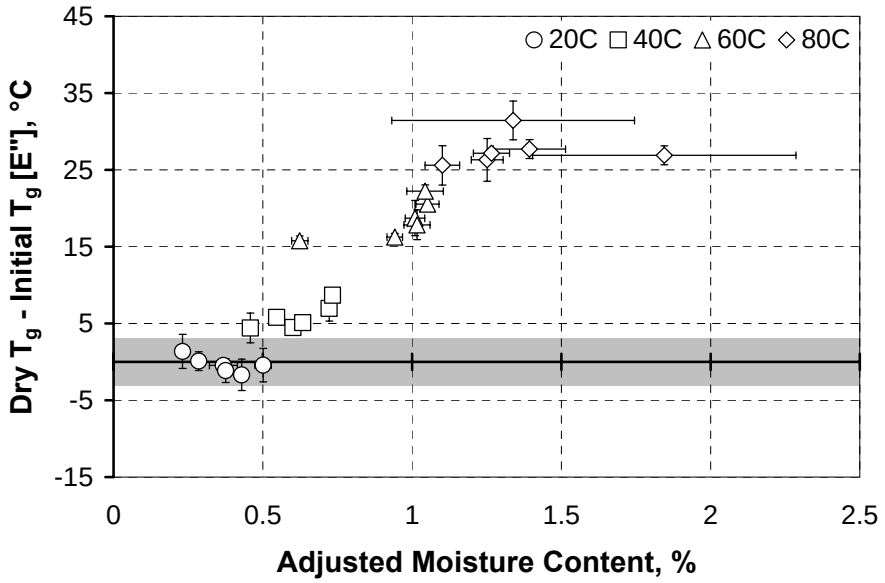

Figure 150. Change in dry T_g (using E") from initial as a function of adjusted moisture content for immersion exposures.
Shaded region indicates baseline standard deviation.
Error bars indicate standard deviations.

6.2.3 Peak Height of Damping Loss Curve

While plasticization effects are largely reversible, changes in interfacial adhesion are largely irreversible, as the SEM micrographs of failed tensile specimens, provided in Figure 151, confirm. As interfacial debonding progresses, more energy is dissipated during loading, and the tanδ peak increases [8,14,18].

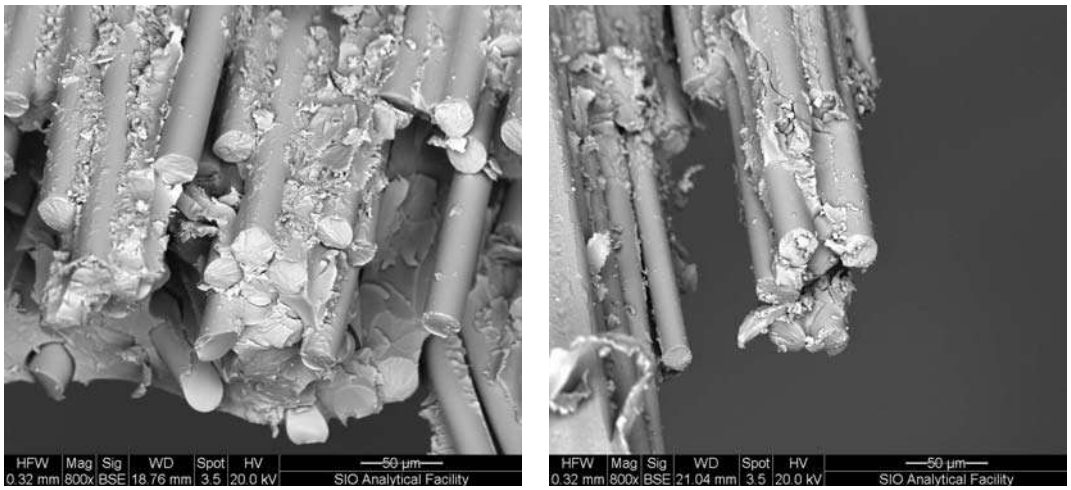

(a) (b)

Figure 151. SEM micrographs of tensile failure.
Material exposed to 60°C Immersion for 36 weeks. (a) Wet, (b) Dry.

In the case of a neat vinyl-ester resin, the tanδ peak height increases with increasing styrene content [4-7]. Because styrene acts as a chain extender [14], it is commonly observed that increasing styrene content in vinyl ester resins decreases the crosslink density, increases the mobility of the polymer chains, and consequently increases the tanδ peak height [2].

It is also well known that the presence of moisture causes a decrease in the tanδ peak height concurrent with a decrease in T_g [11,19-24]. It is possible that debonding effects in specimens tested immediately after exposure are revealed

through an increase in tanδ peak height which remains after post-conditioning [18]. A reversible or irreversible increase would indicate corresponding reversible or irreversible interfacial debonding, respectively. Similar to the moisture dependency of the plasticizing depression of T_g, the change in tanδ peak height should demonstrate a dependency on moisture content if it is related to plasticization.

6.2.3.1 Low and Medium Humidity Results

Figure 152 and Figure 153 present representative tanδ curves for material exposed to 18%RH and 50%RH. The majority of DMTA results for material exposed to 18%RH and 50%RH reveal no change in tanδ peak height except for material exposed to 50%RH at 60°C and, at two time steps, 18%RH at 60°C. One of these exceptions for 60°C exposure at 18%RH is presented in Figure 152.

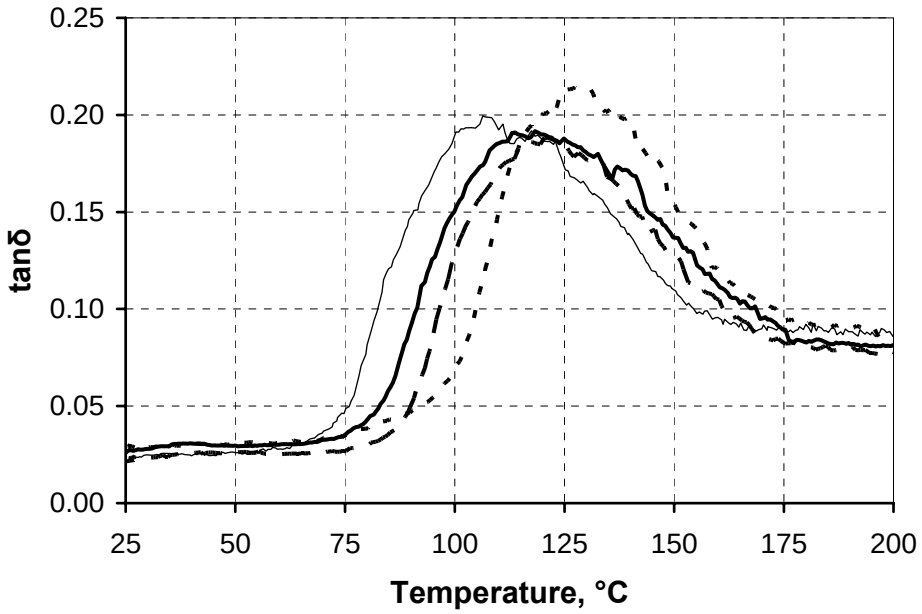

Figure 152. Damping loss curves for material exposed to 18%RH for 96 weeks. Thin——: Pre-conditioned, Bold▬▬: 20°C, — — : 40°C, - - : 60°C

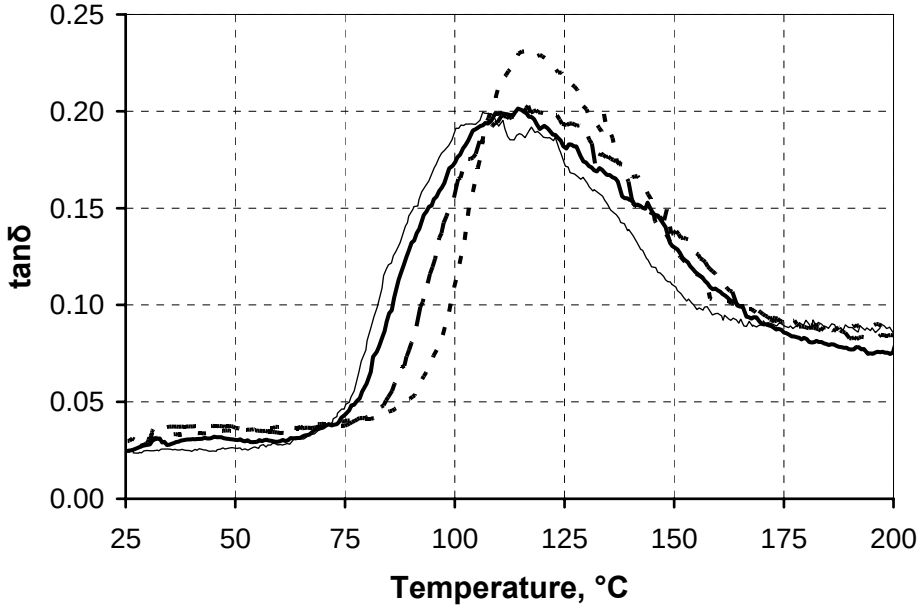

Figure 153. Damping loss curves for material exposed to 50%RH for 96 weeks. Thin Thin——: Pre-conditioned, Bold▬: 20°C, — — : 40°C, - - : 60°C

It is possible that the anomalies observed with this high temperature, low humidity exposure can be attributed to the composite's high sensitivity to moisture after long-term exposure to dry environments. It is worth noting that where the wet tanδ peak height is abnormally high, the increase in average peak height is present in only the last two of the four specimens tested. When the low humidity environment is accessed, cool air enters the environmental chamber, whereupon the relative humidity temporarily increases. After several hours of opening and closing the environmental chamber, the last few specimens have been exposed to more moisture than specimens tested earlier in the day. The isolated increase in tanδ peak height at this time can be attributed to this moisture shock inherent in testing. It is important to note here that

such environmental shock to a material conditioned in hot, dry environments such as a desert may occur in a sudden rain and will result in sudden, observable changes.

The tanδ curves for material exposed to 18%RH and 50%RH demonstrate the same general behavior, where the only major change is the onset of the glass transition region which increases with increasing temperature of exposure, narrowing the transition region. For material exposed to higher temperatures, even when the T_g value does not change, the polymer network has been tightened such that more energy is required to initiate movement of the stiffer polymer chain [25], demonstrating that, in the absence of water, thermal exposure alone results in a tightening of the molecular network. This stiffening of the polymer network is a physical mechanism likely responsible for the small increases in SBS strength observed after exposure to low humidities.

The changes for material exposed to low and medium humidity environments, 50%RH at 60°C, primarily occur in the polymer network rather than at the interphasial level. The irreversible increase in peak height observed in material exposed to 50%RH at 60°C will be discussed in Section 6.2.3.2 along with a discussion of the effects of exposure to 75%RH at the same temperature.

6.2.3.2 75%RH Results

The tanδ peak height for material exposed to 75%RH at 60°C is lower than that for material exposed to 50%RH at 60°C and, unlike the case of 50%RH exposures, the peak height increases noticeably after redrying, as indicated in Figure 154 and Figure 155. Table 31 summarizes the wet and dry average tanδ peak heights.

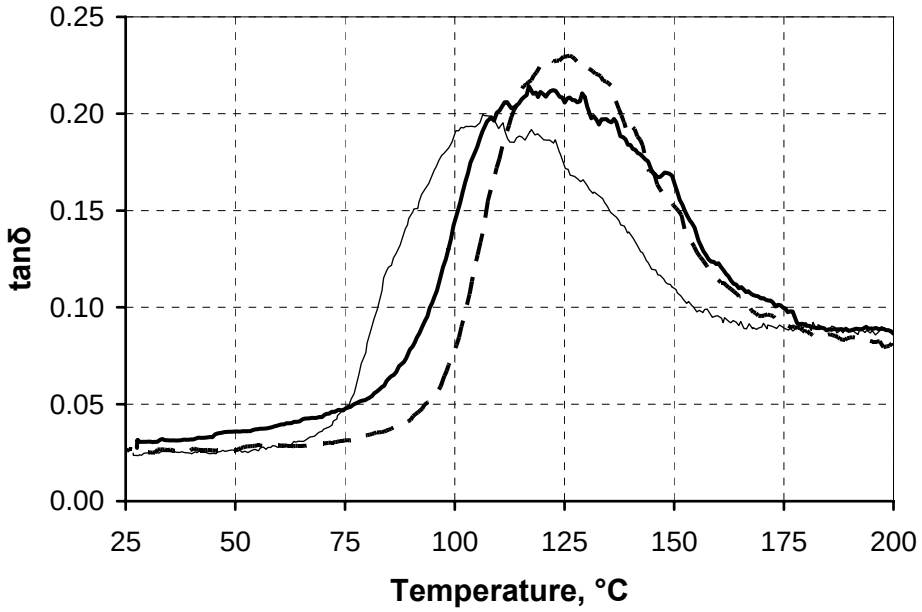

Figure 154. Damping loss curves for material exposed to 50%RH and 75%RH at 60°C for 72 weeks prior to post-conditioning. Thin: Pre-conditioned, bold: 75%RH, dashed: 50%RH.

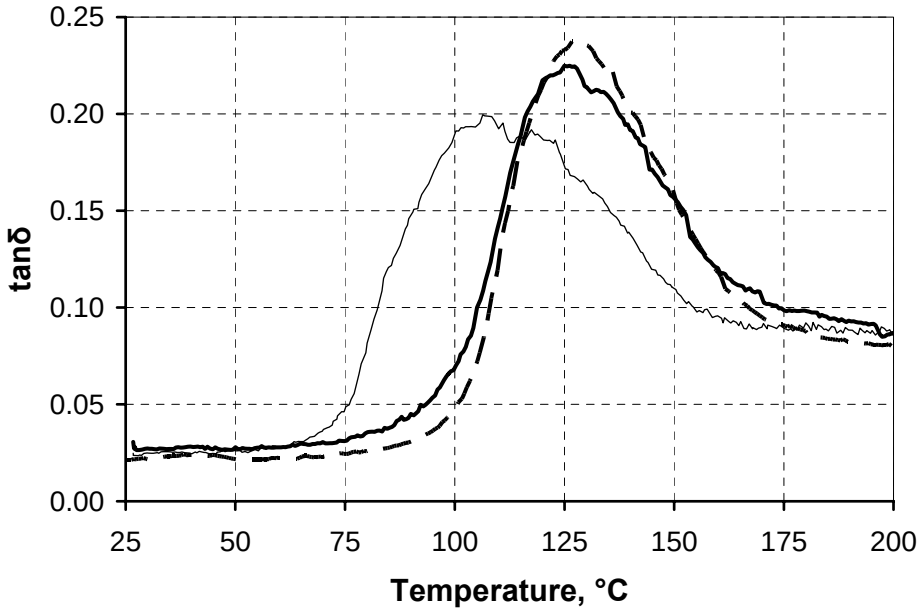

Figure 155. Damping loss curves for material exposed to 50%RH and 75%RH at 60°C for 72 weeks after post-conditioning. Thin: Pre-conditioned, bold: 75%RH, dashed: 50%RH.

Table 31. Damping loss peak heights for material exposed to 60°C at 50%RH and 75%RH
Brackets indicate standard deviations.

Time (wk)	50%RH		75%RH	
	Wet	Dry	Wet	Dry
12	0.229 [0.006]	0.222 [0.007]	0.204 [0.007]	0.221 [0.011]
24	0.227 [0.007]	0.225 [0.017]	0.214 [0.002]	0.222 [0.008]
36	0.230 [0.007]	0.236 [0.004]	0.220 [0.007]	0.229 [0.005]
48	0.235 [0.019]	0.242 [0.010]	0.212 [0.013]	0.220 [0.016]
72	0.232 [0.002]	0.233 [0.008]	0.217 [0.006]	0.221 [0.013]

This lower tanδ peak height and earlier onset of the glass transition region for wet material, shown in Figure 154 and Figure 155, indicate a plasticization effect in the presence of moisture content for both 50%RH and 75%RH exposures. The reversible broadening of the tanδ curve further indicates plasticization and drying within the polymer structure [11,23]. The plasticization phenomenon is more significant for material exposed to higher relative humidity, where the material sorbs more water. While the tanδ peak height is higher for both wet and dry material exposed to 50%RH at 60°C, the two environments considered here result in dry tanδ curves which have similar breadths and which each enter the glass transition region around the same temperature.

The lower SBS strength obtained for material exposed to 75%RH at 60°C, provided in Figure 156, further verifies the proposition that increased plasticization occurs in this environment along with leaching of LMWS. It is possible that the leaching of LMWS results in a tighter polymer network, reflected by a higher tanδ peak height and SBS strength. Figure 156 would indicate, therefore, that leaching of LMWS is less significant in a 75%RH environment, as would be expected.

Strengthening detected through SBS testing is a matrix dominated effect which results only in subtle increases in tensile properties, as discussed in Section 5.1.1. It was proposed that the degradation of tensile strength in material prior to post-conditioning was a result of both plasticization and interfacial degradation. The results presented in Figure 157 indicate that the reversible decreases in tensile strength of material exposed to 50%RH are strongly related to reversible plasticization, even as interfacial degradation is indicated through increases in tanδ.

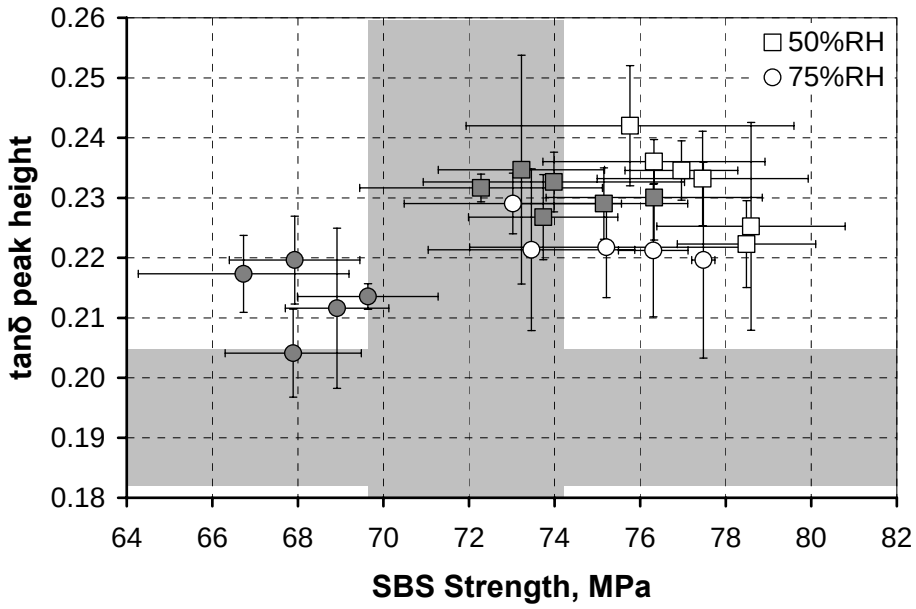

Figure 156. Short beam shear strength as related to tanδ peak height for material exposed to 50%RH and 75%RH at 60°C.
Closed: Wet; Open: Dry. Shaded region indicates baseline average and standard deviations. Error bars indicate standard deviation.

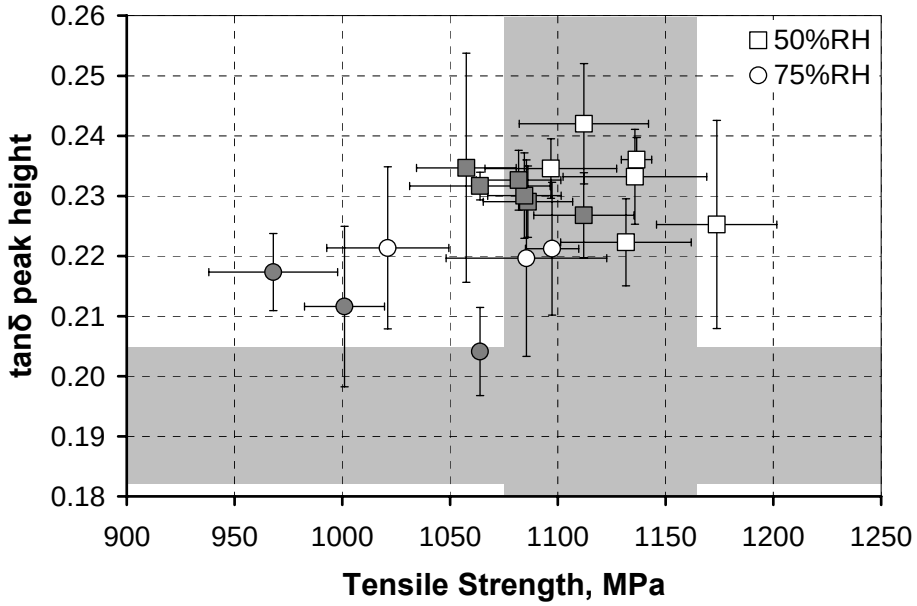

Figure 157. Tensile strength as related to tanδ peak height for material exposed to 50%RH and 75%RH at 60°C.
Closed: Wet; Open: Dry. Shaded region indicates baseline average and standard deviations. Error bars indicate standard deviation.

6.2.3.3 High Humidity and Immersion Results

Exposure to 99%RH and immersion results in an increase in tanδ peak height for both wet and dry sets. For temperatures of exposure less than 80°C, the tanδ peak height either decreases after redrying or remains within experimental scatter of the wet set. Results after 96 weeks of exposure, presented in Figure 158 and Figure 159, illustrate the general trends observed for each environment.

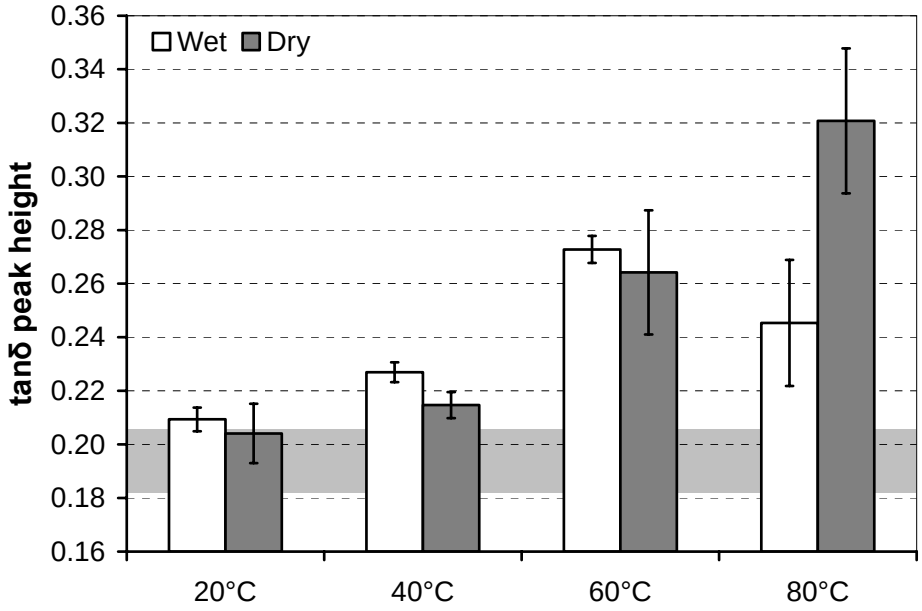

Figure 158. tanδ peak height for material exposed to 99%RH for 96 weeks.
Shaded region indicates baseline average and standard deviation.
Error bars indicate standard deviations.

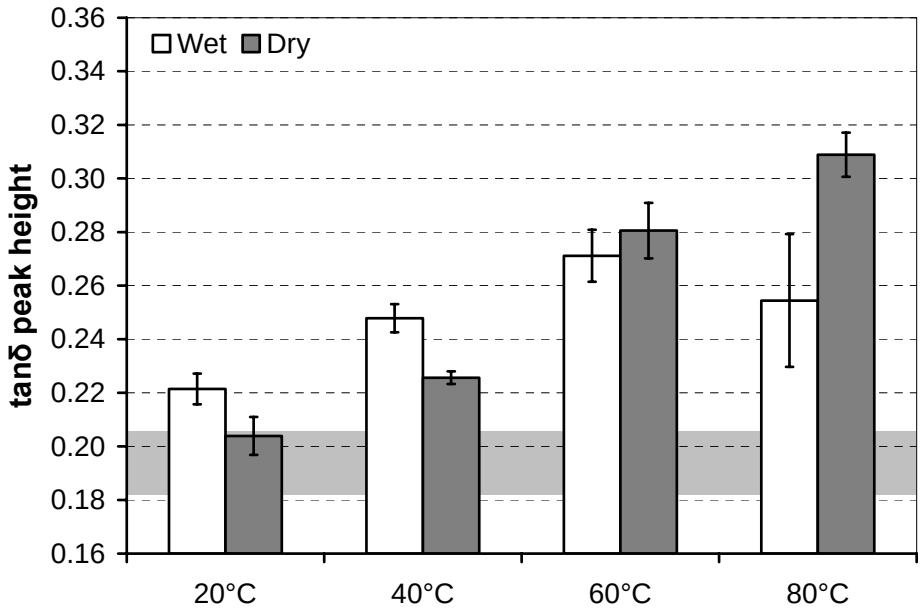

Figure 159. tanδ peak height for material immersed in water for 96 weeks.
Shaded region indicates baseline average and standard deviation.
Error bars indicate standard deviations.

The increased tanδ peak height is indicative of a both loss of interfacial adhesion as well as a possible decrease in crosslink density, where the mobility of the polymer chain increases with these modes of degradation. Where the removal of water from material exposed to 99%RH and immersion at 20°C and 40°C results in decrease in tanδ peak height, the changes are indicative of reversible reaction within the interphase and bulk matrix which would result in a partially reversible decrease in crosslink density. The irreversible nature of the increase in tanδ peak height indicates significant interfacial degradation. While chemical degradation due to hydrolysis is generally considered irreversible, a condensation or hydration reaction may occur at hydrolyzed bonds [26,27], leading to subsequent decreases in tanδ peak height.

In the first 12 weeks of exposure to 60°C in 99%RH and immersion, the tanδ peak height value decreases after post-conditioning, as shown in Figure 160, similar to the behavior seen in material exposed to high humidity and immersion at 20°C and 40°C. SBS tests reveal a transition from reversible to irreversible degradation sometime between 12 and 24 weeks, and moisture uptake trends indicate that this transition likely occurs between 18 and 24 weeks. After 12 weeks exposure to 99%RH at 60°C, the tanδ peak height decreases after post-conditioning similar to behavior exhibited in material exposed to lower temperatures of immersion and 99%RH through 96 weeks. From 24 weeks on, material exposed to 99%RH at 60°C indicates irreversible increases in tanδ peak height, in following with the transitions seen in SBS and gravimetric data.

For 60°C immersion, however, a significant decrease in tanδ peak height occurs beyond this expected transition period at 24 weeks. It is unclear why the change in tanδ peak height demonstrates such high reversibility beyond this time period since irreversible degradation is indicated in the tanδ peak height from 36 weeks on. Nonetheless, the changes in tanδ peak height correlate with reversible changes in SBS strength, seen in Figure 161. In the transition from reversible to irreversible degradation, it is highly likely that severe interfacial debonding has occurred, reflected by the clear increase in the tanδ peak height from the baseline.

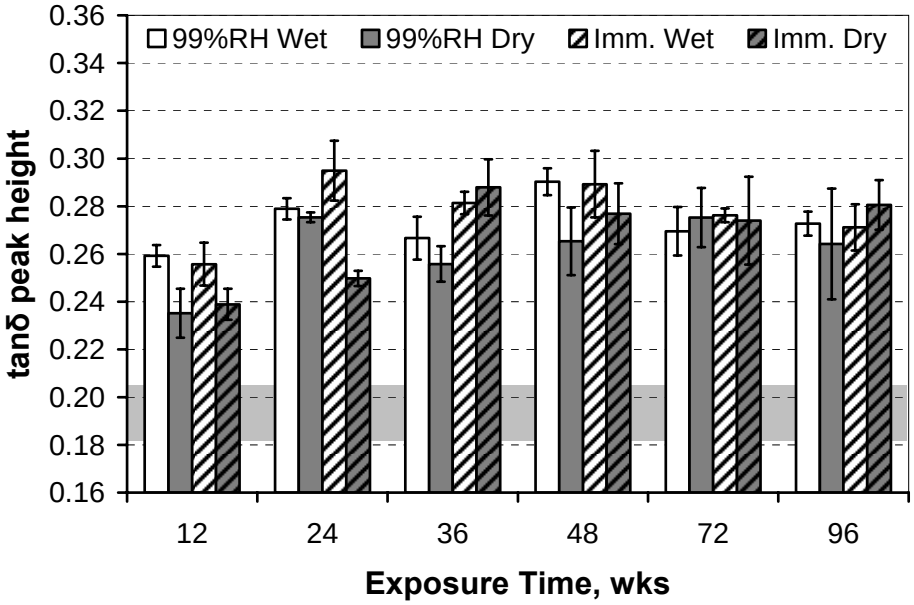

Figure 160. tanδ peak height for material exposed to 99%RH and immersion (Imm.) at 60°C. Shaded region indicates baseline average and standard deviation. Error bars indicate standard deviations.

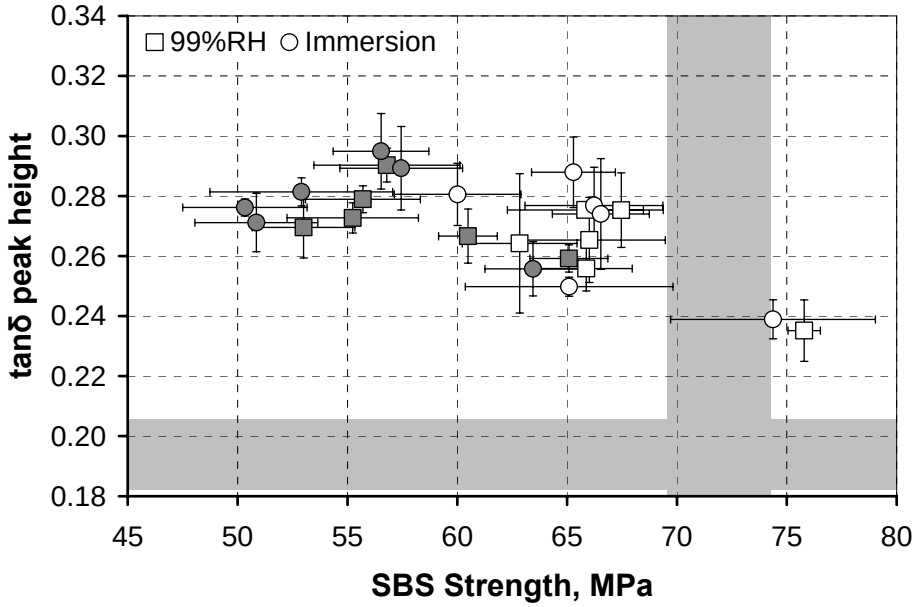

Figure 161. Short beam shear strength as related to tanδ peak height for material exposed to 99%RH and immersion at 60°C. Closed: Wet; Open: Dry. Shaded region indicates baseline average and standard deviations. Error bars indicate standard deviations.

In the case of immersion at 60°C, the tanδ peak height is larger for wet sets than for dry sets at 12 weeks, indicating a reversible decrease in crosslink density. By 96 weeks exposure, the wet tanδ peak height is less than but within experimental scatter of the dry, similar to changes seen at 80°C. In these aggressive environments, because of the irreversible nature of the severe interfacial degradation, the increases in tanδ peak height after redrying indicate significant plasticization.

For material exposed to 99%RH and immersion at 80°C, there is a marked increase in tanδ peak height after redrying, indicating significant plasticization of the polymer matrix and possibly the interphase. It is also possible that a loss of degraded material in the form of LMWS in the post-conditioning environment results in this increase in tanδ peak height. Scanning electron microscopy, such as Figure 162,

indicates that the severe interfacial degradation is not reversible. Because of the severity of the interfacial degradation experienced in 80°C saturated environments, it can be concluded that the change between wet and dry sets is directly related to plasticization of the polymer since the interfacial degradation is demonstrably irreversible.

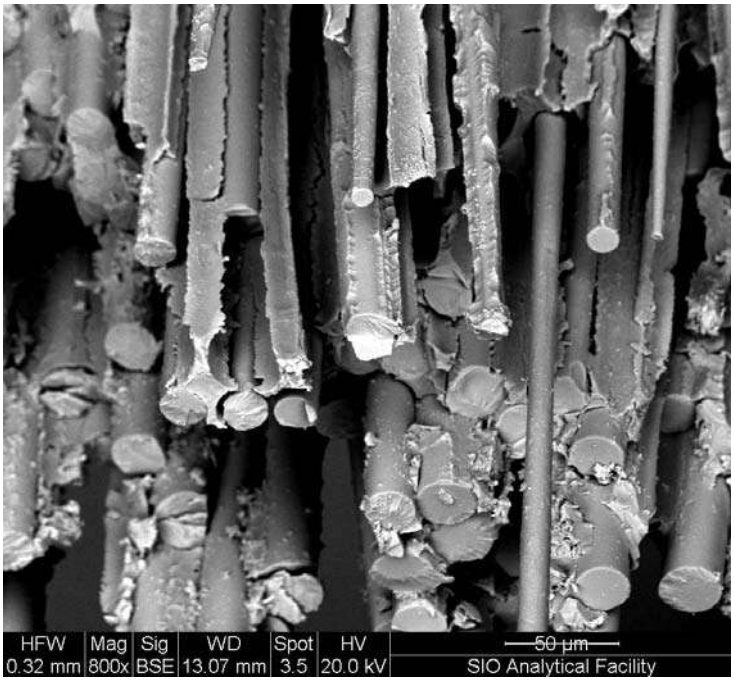

Figure 162. SEM of failed dry tensile specimen exposed to 80°C immersion. Tested after post-conditioning.

6.2.4 Storage Modulus Results

While changes are seen in the rubbery modulus, as expected, the glassy modulus does not change prior to irreversible degradation of the constituent elements, where severe permanent degradation of the tensile strength is also observed, as seen in Figure 163. Changes observed in the glassy modulus can be correlated to physical degradation of the polymer matrix and fiber reinforcement in this system, as is detected by weight loss of the composite after redrying, Figure 164, indicating leaching of degraded material. This trend is fundamentally qualitative. Validation on other composite systems must be performed before general conclusions can be made.

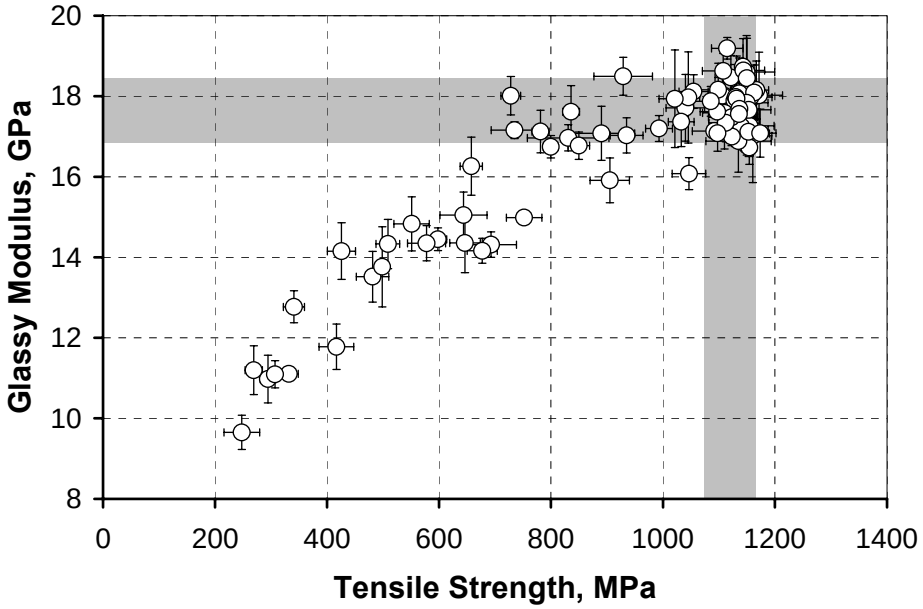

Figure 163. Glassy modulus [$E'(T_g\text{-}60°C)$] and tensile strength for all dry sets. Shaded region indicates baseline averages and standard deviations. Error bars indicate standard deviations.

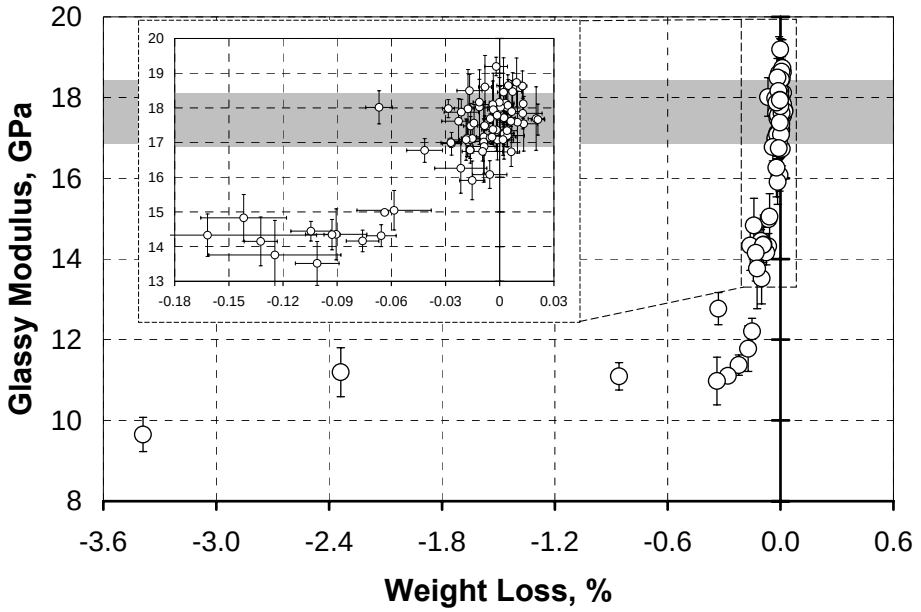

Figure 164. Glassy modulus [$E'(T_g$-60°C)] versus weight loss after redrying. Shaded region indicates baseline average and standard deviation. Error bars indicate standard deviations.

The rubbery modulus can reveal changes in average crosslink density of the polymer matrix. An increase in M_c, as calculated according to Equation 1 in Section 6.1, correlates to a decrease in rubbery modulus and crosslink density ρ_c. An observed change in M_c with exposure could be a consequence of hydrolysis where scission of crosslinks leads to increasing M_c or it could indicate post-cure where additional crosslinks are formed, decreasing the value of M_c. Leaching of styrene or other LMWS would result in an increase in an increased M_c as the LMWS are lost and the average molecular weight between crosslinks increases.

This interpretation is in apparent contrast to studies concerning the effect of styrene content on neat vinyl-ester resins where it has been shown that decreasing styrene content leads to lower M_c and increased tanδ peak height due to increased

linear polymerization [4-7]. A loss of LMWS after curing would result in a more open polymer network, leading to higher M_c and tanδ peak height.

Since these changes due to leaching of LMWS are reversible, post-conditioning should result in a subsequent increase in tanδ peak height as plasticization is reversed. If any change in average molecular weight between crosslinks is observed with post-conditioning after leaching, it might be reflected through increased M_c since water may effectively act to crosslink the polymer even as it plasticizes the resin.

In the case of hydrolysis, the hydrolytic attack of the crosslink creates longer polymer chains with fewer crosslinks and, therefore, higher mobility, as indicated by increases in tanδ peak height with M_c. Where hydration or condensation reactions occur to reverse the chain scission, decreases in both tanδ and M_c should be seen after redrying. Figure 165 and Figure 166 demonstrate that where tanδ decreases after redrying, so does M_c, indicating a reversible reaction responsible for a decrease in crosslink density. The condensation reaction on hydrolyzed species appears to occur only in material which has been exposed to 99%RH and immersion at 40°C and 60°C. Material exposed to high humidity and immersion at 20°C does not demonstrate any change in M_c outside initial scatter. Therefore, it can be concluded that hydrolysis occurs at elevated temperatures only.

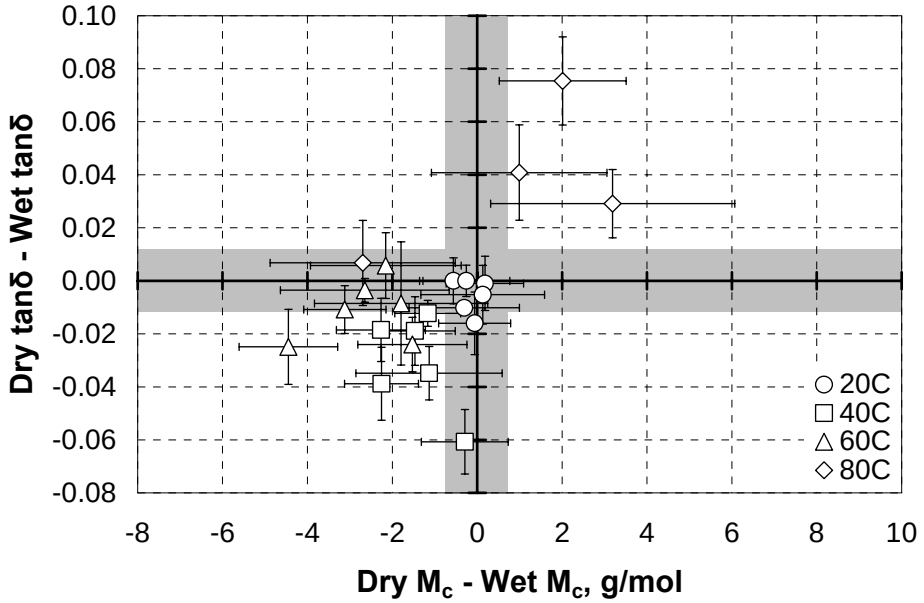

Figure 165. Changes in tanδ and M_c after redrying for 99%RH exposures.
Shaded regions indicate baseline standard deviations.
Error bars indicate standard deviations.

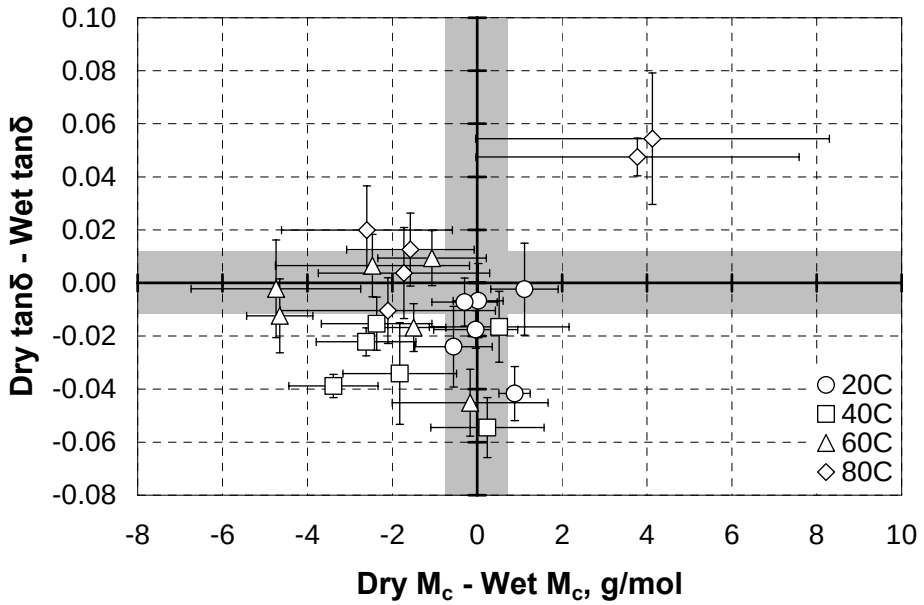

Figure 166. Changes in tanδ and M_c after redrying for immersion exposures.
Shaded regions indicate baseline standard deviations.
Error bars indicate standard deviations.

Material exposed to 80°C demonstrates a decrease in rubbery modulus after post-conditioning reflecting an increase in M_c. Because most interfacial and fiber chemical degradation is shown to be irreversible after exposure to 80°C immersion and 99%RH, it is possible that the decrease in crosslink density indicates a decrease in hydrogen bonding as water is removed.

For 18%RH and 50%RH exposures at 20°C and 40°C, the tanδ and M_c values stay within initial scatter bounds, as shown in Figure 167 and Figure 168. For 60° exposures at 18%RH, 50%RH, and 75%RH, there is a clear increase in both tanδ peak height and M_c, where it is likely that there is leaching of residual volatiles. The molecular weight between crosslinks increases with increasing relative humidity only at 60°C. At 75%RH, the changes in tanδ peak height and M_c after redrying, shown in Figure 169, indicate that the presence of water not only plasticizes the resin but is also responsible for a decrease in crosslink density which can be partially reversed upon post-conditioning. In contrast, Figure 169 reveals that post-conditioning does not results in changes in tanδ peak height and M_c beyond initial scatter range. Furthermore, the increase in tanδ peak height from baseline values indicates that there is some interphasial degradation, possibly a consequence of hydrolytic degradation.

Post-conditioning of material exposed to 75%RH lowers M_c such that the dry M_c is in the vicinity of that for material exposed to 50%RH, as seen in Figure 169. The higher moisture content resulting from exposure to 75%RH at 60°C is not only responsible for plasticization but also for a reversible decrease in crosslink density not seen after exposure to lower humidities.

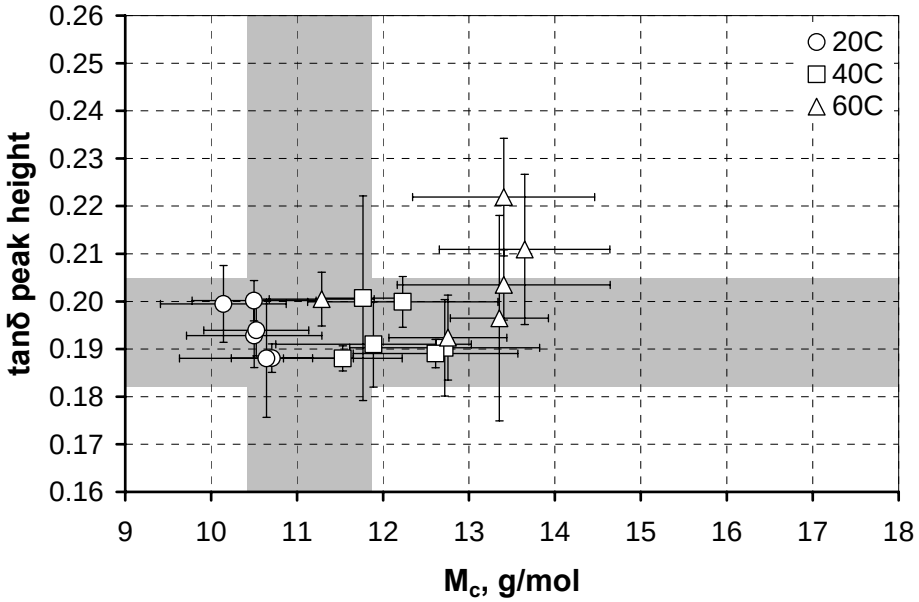

Figure 167. Wet tanδ peak height and M_c for 18%RH exposures. Shaded regions indicate baseline averages and standard deviations. Error bars indicate standard deviations.

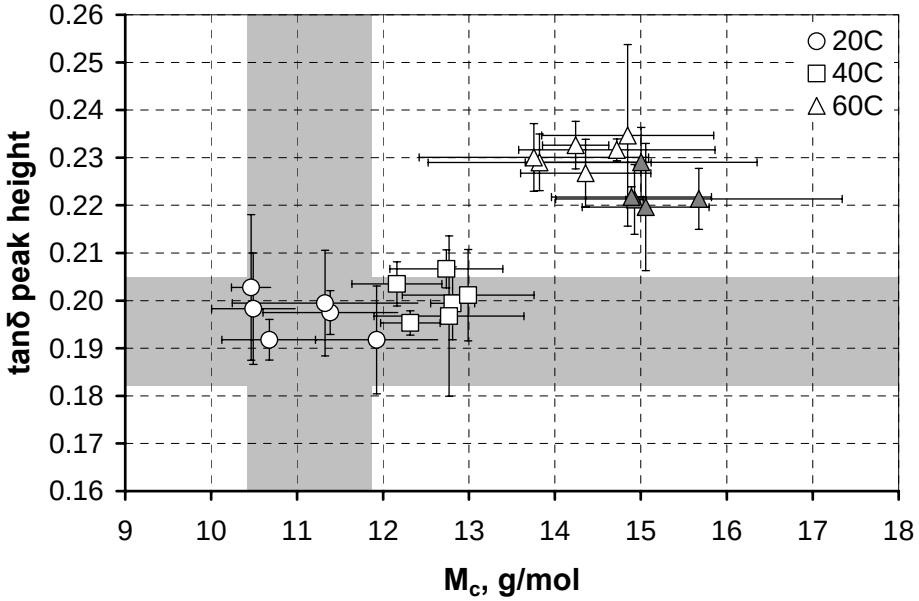

Figure 168. Wet tanδ peak height and M_c for 50%RH and 75%RH exposures. Open: 50%RH, closed: 75%RH. Shaded regions indicate baseline averages and standard deviations. Error bars indicate standard deviations.

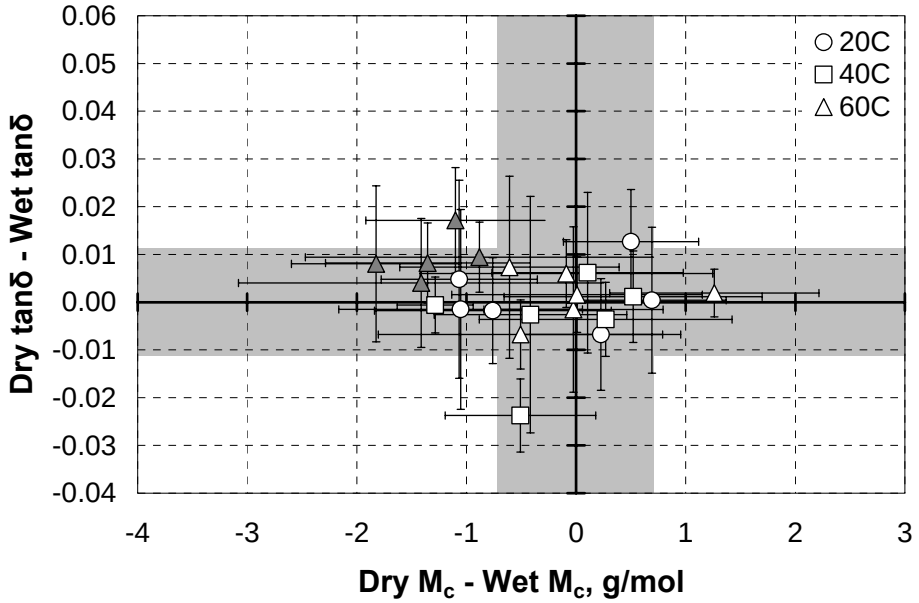

Figure 169. Changes in tanδ and M_c after redrying for 50%RH and 75%RH exposures. Open: 50%RH, closed: 75%RH. Shaded regions indicate baseline standard deviations. Error bars indicate standard deviations.

6.3 Summary

DMTA results for 75%RH exposure support evidence of plasticization seen through increases in tensile failure strain and interphasial degradation seen in decreases in tensile strength, discussed in Section 5.1.2.

DMTA testing confirmed plasticization as a reversible mechanism of physical degradation responsible for decreases in tensile strength and SBS strength. Plasticization was also confirmed where increases in the secondary modulus were observed, theorized to be a consequence of fiber alignment as the plasticized resin deformed at high strains. The change in T_g resulting from the removal of water was shown to be highly dependent on the temperature of exposure in Section 6.2.2.3.1, indicating increased plasticization and/or leaching of LMWS with increasing

temperature. Recovery of SBS strength was shown to be predominantly independent of temperature in Section 5.2.3 for exposures up to 60°C. At 80°C, the severe material degradation experienced in 99%RH and immersion conditions was demonstrated by clear decreases in glass modulus and a decreased capacity for recovery in SBS strength.

Increases in T_g with increasing temperature of exposure corroborate the strengthening effect detected in SBS testing for all environmental conditions. In the first 12 weeks of exposure, material exposed to 99%RH and immersion at 60°C demonstrated reversible degradation concurrent with a strengthening effect, also seen in similar 40°C wet environments. The reversible degradation was attributed primarily to plasticization which weakened the polymer matrix and interphase while Strengthening of the polymer was attributed primarily to leaching of LMWS. At 40°C and 60°C decreases in M_c after post-conditioning of material exposed to 99%RH and water immersion indicate that a dehydration reaction may have led to recovery in polymer strength as the effects of hydrolysis were partly reversed.

While the changes in the chemical makeup of the polymer structure, reflected through changes in rubbery modulus, did not change through 96 weeks, somewhere between 18 and 24 weeks, the degradation resulting from exposure to 99%RH and immersion at 60°C transitioned from reversible to irreversible. From 24 weeks on, even as the tensile strength did not demonstrate a change in degradation mode, SBS, DMTA, and gravimetric results indicated irreversible degradation of the interface along with fiber pitting, confirmed through SEM investigations.

6.4 References

1. Akay, M. "Aspects of Dynamic Mechanical Analysis in Polymeric Composites." *Composites Science and Technology*. Vol. 47 (1993) 419-423.

2. Nielsen, L.E. "Cross-Linking—Effect on Physical Properties of Polymers." *Journal of Macromolecular Science – Reviews in Macromolecular Chemistry*. Vol. C3, No. 1 (1969) 69-103.

3. DeNeve, B. and M.E.R. Shanahan. "Water Absorption by an epoxy resin and its effect on the mechanical properties and infra-red spectra." *Polymer*. Vol. 34, No. 24 (1993) 5099-5105.

4. Auad, M.L., M. Aranguren, and J. Borrajo. "Epoxy-Based Divinyl Ester Resin/Styrene Copolymers: Composition Dependence of the Mechanical and Thermal Properties." *Journal of Applied Polymer Science*. Vol. 66 (1997) 1059-1066.

5. Shan, L., C.G. Robertson, K.N.E. Verghese, E. Burts, J.S. Riffle, T.C. Ward, and K.L. Reifsnider. "Influence of Vinyl Ester/Styrene Network Structure on Thermal and Mechanical Behavior." *Journal of Applied Polymer Science*. Vol. 80 (2001) 917-927.

6. Scott, T.F., W.D. Cook, and J.S. Forsythe. "Kinetics and network structure of thermally cured vinyl ester resins." *European Polymer Journal*. Vol. 38, No. 4 (2002) 705-716.

7. Rodriguez, E., M. Larranaga, I. Mondragon, and A. Vazquez. "Relationship Between the Network Morphology and Properties of Commercial Vinyl Ester Resins." *Journal of Applied Polymer Science*. Vol. 100 (2006) 3895-3903.

8. Kennedy, J.M., D.D. Edie, A. Banerjee, and R.J. Cano. "Characterization of Interfacial Bond Strength by Dynamic Analysis." *Journal of Composite Materials*. Vol. 26, No. 6 (1992) 869-882.

9. Iisaka, K. and K. Shibayama. "Effect of Filler Particle Size on Dynamic Mechanical Properties of Poly(methyl Methacrylate)." *Journal of Applied Polymer Science*. Vol. 22 (1978) 1321-1330.

10. Xian, G. and V.M. Karbhari. "Segmental relaxation of water-aged ambient cured epoxy." *Polymer Degradation and Stability*. Vol. 92, No. 9 (2007) 1650-1659.

11. Gupta, V.B., L.T. Drzal, and M.J. Rich. "The Physical Basis of Moisture Transport in a Cured Epoxy Resin System." *Journal of Applied Polymer Science*. Vol. 30 (1985) 4467-4493.

12. Soulier, J.P., R. Berreut, A. Chateauminois, B. Chabert, and R. Gauthier. "Interactions of fibre-reinforced epoxy composites with different salt water solutions including isotonic liquid." *Polymer Communications*. Vol. 29 (1988) 243-246.

13. Mijovic, J. and K.-F. Lin. "Time-Dependent Changes in Morphology of Neat and Reinforced Epoxy Resins Part I:. Neat Epoxies." *Journal of Applied Polymer Science*. Vol. 32 (1986) 3211-3227.

14. Fraga, A.N., V.A. Alvarez, A. Vazquez, and O. De La Osa. "Relationship Between Dynamic Mechanical Properties and Water Absorption of Unsaturated Polyester and Vinyl Ester Glass Fiber Composites." *Journal of Composite Materials*. Vol. 37, No. 17 (2003) 1553-1574.

15. Reed, K.E. "Dynamic Mechanical Analysis of Fiber Reinforced Composites." *Polymer Composites*. Vol. 1, No. 1 (1980) 44-49.

16. Verghese, K.N.E., R.E. Jensen, J.J. Lesko, and T.C. Ward. "Effects of molecular relaxation behavior on sized carbon fiber-vinyl ester matrix composite properties." *Polymer*. Vol. 42 (2001) 1633-1645.

17. Morgan, R.J., F-M. Kong, and C.M. Walkup. "Structure-property relations of polyethertriamine-cured bisphenol-A-diglycidyl ether epoxies." *Polymer*. Vol. 25 (1984) 275-386

18. Lee, M.C. and N.A. Peppas. "Water Transport in Graphite/Epoxy Composites." *Journal of Applied Polymer Science*. Vol. 47 (1993) 1349-1359.

19. Mijovic, J. and K.-F. Lin. "The Effect of Hygrothermal Fatigue on Physical/Mechanical Properties and Morphology on Neat Epoxy Resin and Graphite/Epoxy Composite." *Journal of Applied Polymer Science*. Vol. 30 (1985) 2527-2549.

20. Mijovic, J. and S.A. Weinstein. "Moisture Diffusion into a graphite-epoxy composite." *Polymer Communications*. Vol. 26 (1985) 237-239.

21. Barton, J.M. and D.C.L. Greenfield. "The Use of Dynamic Mechanical Methods to Study the Effect of Absorbed Water on Temperature-dependent Properties of an Epoxy Resin-Carbon Fibre Composite." *British Polymer Journal*. Vol. 18, No. 1 (1986) 51-56.

22. Nogueira, P., C. Ramirez, A. Torres, M.J. Abad, J. Cano, J. Lopez, I. Lopez-Bueno, and L. Barral. "Effect of Water Sorption on the Structure and Mechanical Properties of an Epoxy Resin System." *Journal of Applied Polymer Science*. Vol. 80 (2001) 71-80.

23. Xian, G. and V. Karbhari. "DMTA Based Investigation of Hygrothermal Ageing of an Epoxy System Used in Rehabilitation." *Journal of Applied Polymer Science*. Vol. 104 (2007) 1084-1094.

24. Perrux, D. and C. Suri. "A study of the coupling between the phenomena of water absorption and damage in glass/epoxy composite pipes." *Composites Science and Technology*. Vol. 57 (1997) 1403-1413.

25. Kaplan, D.S. "Structure-Property Relationships in Copolymers to Composite: Molecular Interpretation of the Glass Transition Phenomenon." *Journal of Applied Polymer Science*. Vol. 20 (1976) 2615-2629.

26. Bunker, B.C. "Molecular mechanisms for corrosion of silica and silicate glasses." *Journal of Non-Crystalline Solids*. Vol. 179 (1994) 300-308.

27. Ishida, H. and J.L. Koenig. "The Reinforcement Mechanism of Fiber-Glass Reinforced Plastics under Wet Conditions: A Review." *Polymer Engineering and Science*. Vol. 18, No. 2 (1978) 128-145.

7. Predictive Degradation Models

7.1 Overview

Accelerated testing should be implemented with predictive degradation models to estimate a material property for the duration of a structure's service life. These degradation models should also allow for the most accurate prediction possible so that the amount of material required to maintain a critical design level for the duration of the service life can be minimized in order to reduce weight, labor, and cost.

The difficulty in predictive modeling lies with the application of a simplistic empirical model which generally cannot take into account the various chemical, physical, and physio-mechanical mechanisms of degradation. Furthermore, employing a single model for all environmental exposures assumed that the modes of degradation do not change over time or between environments. The most rigorous predictive model would require the isolation of mechanisms of degradation and would allow for transitions between these mechanisms.

In the following analysis, the Arrhenius rate, crack propagation, time-temperature-superposition (TTS), and a moisture dependent degradation model, all introduced in Section 2.5.1, are employed to predict short beam shear (SBS) strength, tensile strength, and tensile strain with environmental exposure. An empirically based predictive degradation model is developed here for application to SBS results. Predictions are made for both wet and dry material properties. The multicomponent

degradation model is also employed using experimental DMTA results to predict the wet tensile strength resulting from immersion in deionized water.

A fundamental limiting assumption of these models is that the mechanisms of degradation are uniform for all moist environments. A transition in mechanisms may be identified through a non-linear Arrhenius plot, where the mechanisms governing degradation may vary between temperatures and humidity and so may be described by two characteristic activation energies. In order to account for transitions in degradation mode between environments, the empirically based degradation model developed in this chapter accounts for plasticization in environments with relative humidities 75%RH and above but not in lower humidity environments. The theoretically based moisture dependent degradation model does assume a transition in degradation mode due to water clustering; however, its application to the degradation of tensile modulus is only moderately successful since the degradation of the tensile modulus is minimal and high in scatter.

Because no significant changes in tensile modulus occurred over two years of exposure, it is not considered in time based predictive models. The tensile modulus did demonstrate a subtle decreasing trend with increasing moisture content, as discussed in Section 5.1, but the scatter for the modulus of exposed material remained within initial scatter. Because the moisture dependent degradation model was developed specifically using the Young's modulus, the moisture dependent degradation model is the only model to consider the longitudinal tensile modulus.

Because no significant changes in material properties were observed in 18%RH and 50%RH exposures, time based predictive models are not applied to results from these environments. In the case of 40°C high humidity and immersion environments, the strengthening effect introduced in Section 5.2.3 led to SBS strengths which were above the baseline average after post-conditioning. Consequently, these dry SBS results are not considered in the application of time based prediction models.

Similarly, an increase in tensile strain was observed after post-conditioning of specimens exposed to 99%RH and immersion at 20°C. This increase in tensile strain after post-conditioning is partly a consequence of the reversal of plasticization in the matrix. The increase above initial scatter range may be related to predominantly irreversible interfacial debonding which occurs in the wet environments. While exposed material demonstrates ductile matrix failure concurrent with debonding prior to post-conditioning, as seen in Figure 170, post-conditioning leads to more brittle matrix failure along with interfacial failure, as seen in Figure 171. After post-conditioning the loss of adhesion between the fiber and matrix may allow for the fibers to be loaded to a higher strain and may also allow for a larger strain from the initial onset of failure at the maximum load to complete failure at zero load. Consequently, the increased strain of the post-conditioned material exposed to 99%RH and immersion at 20°C are not considered in the analysis of dry tensile strains.

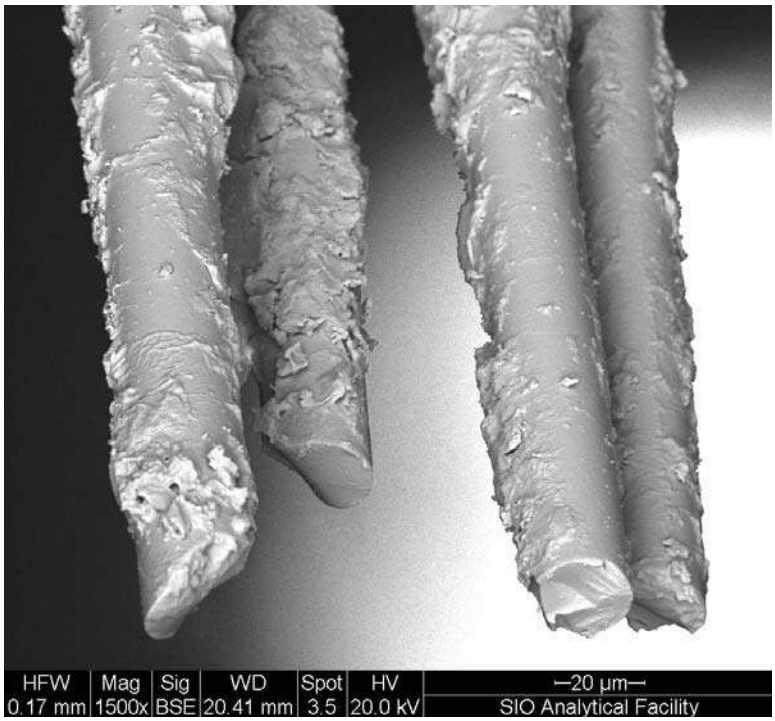

Figure 170. SEM of failed wet tensile specimen exposed to 20°C immersion for 12 weeks.

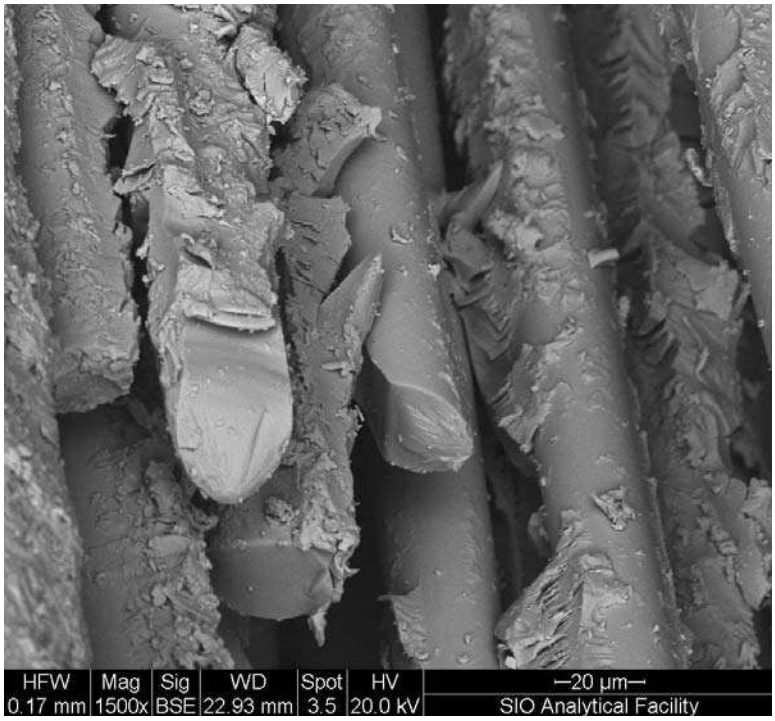

Figure 171. SEM of failed dry tensile specimen exposed to 20°C immersion for 24 weeks.

7.2 Arrhenius Rate Degradation Model

The Arrhenius rate degradation model [1], introduced in Section 2.5.1.1, was employed by fitting data to

$$\frac{P_0 - P(t)}{P_0} = B \ln t \tag{1}$$

where P is the material property at time t, P_0 is the baseline initial property value, and B is the unitless Arrhenius rate degradation model parameter. Here, B has been calculated using time in weeks. Calculated values of B are summarized in Table 32.

Table 32. Arrhenius rate degradation model parameters.

	SBS Strength		Tens. Strength		Tens. Strain	
Env.	Wet B	Dry B	Wet B	Dry B	Wet B	Dry B
6X	0.015	-0.012	0.028	0.014	0.016	-0.006
2H	0.045	0.005	0.038	0.006	0.019	—
4H	0.039	—	0.078	0.058	0.039	0.018
6H	0.054	0.019	0.127	0.110	0.085	0.062
8H	0.130	0.100	0.193	0.185	0.166	0.157
2I	0.053	0.004	0.038	0.005	0.013	—
4I	0.040	—	0.090	0.076	0.050	0.035
6I	0.064	0.023	0.140	0.124	0.098	0.082
8I	0.120	0.088	0.193	0.186	0.163	0.153

The thermal dependence of the degradation parameter B should be described by the Arrhenius relation

$$B = B_o \exp\left[\frac{-E_B}{RT}\right], \tag{2}$$

where B_o is a pre-exponential factor and E_B is the activation rate for the degradation process. Activation energies for the Arrhenius rate degradation model parameters are provided in Table 33, with Arrhenius plots in Figure 172 through Figure 174.

In the case of 75%RH exposures, dry material properties result in a negative value of B, indicating increases in material properties. For environments where redrying resulted in returns to initial baseline values, the dry sets were removed for the purpose of analysis of thermal trends since both negative and positive values of B cannot be accounted for in the Arrhenius relation. At 75%RH, it is expected that exposure to temperatures other than 60°C would result in $B < 0$ for dry properties, so dry B values for 75%RH have been included in Table 32 for guidance.

Table 33. Activation energies E_B (kJ/mol)
for Arrhenius rate degradation model parameters.

	SBS Strength		Tens. Strength		Tens. Strain	
Env.	Wet	Dry	Wet	Dry	Wet	Dry
99%RH	14	39	23	48	31	50
Immersion	12	41	23	49	36	34

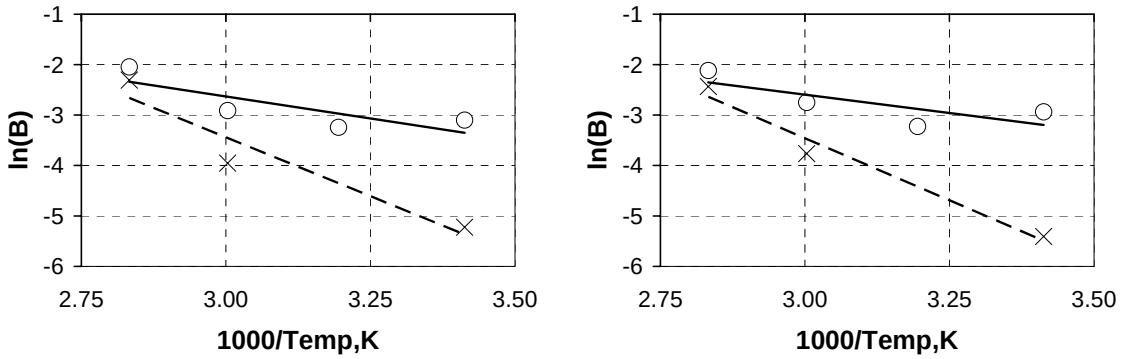

(a) (b)

Figure 172. Arrhenius plots of Arrhenius rate degradation parameters for SBS strength. (a) 99%RH, (b) immersion; ○ wet; × dry.

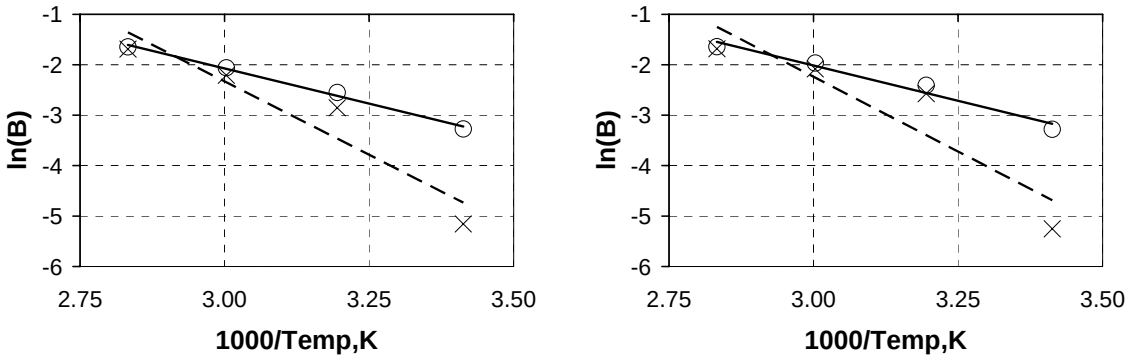

Figure 173. Arrhenius plots of Arrhenius rate degradation parameters for tensile strength. (a) 99%RH, (b) immersion; ○ wet; × dry.

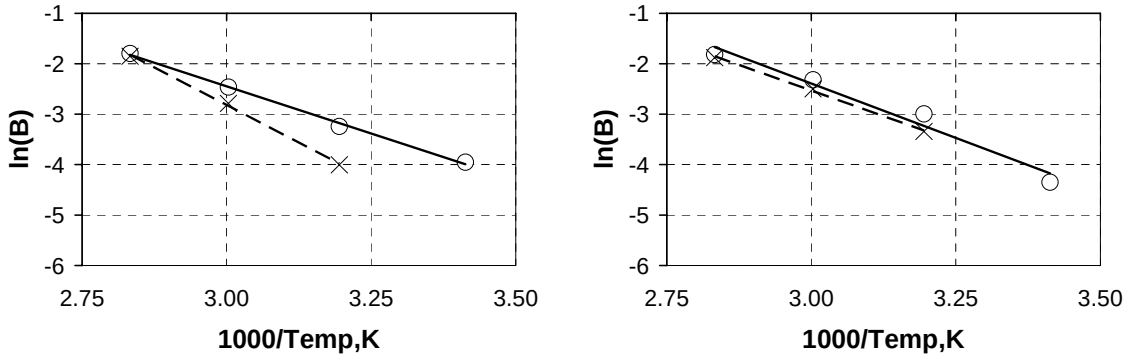

Figure 174. Arrhenius plots of Arrhenius rate degradation parameters for tensile strain. (a) 99%RH, (b) immersion; ○ wet; × dry.

Degradation parameters are higher for "wet" material than for "dry" material, as shown in Table 32. Post-conditioning of material leads to partial recovery of material properties by reversing plasticization and possible interfacial degradation, as discussed in Section 6.2.2 and Section 6.2.3. The analysis in Section 6.2.4 also indicates that the removal of water leads to an increase in crosslink density. Degradation of dry material should be more difficult to activate since the aggravating

effects of water have been reversed. This analysis is supported by the higher values of E_B determined for the degradation trends of "dry" material, provided in Table 33.

SBS strength demonstrates the least severe degradation, indicated by lower values of B in Table 32, when compared to tensile strength and strain for all exposures except for those at 20°C. The activation energies for SBS strength degradation indicate that while the rates of degradation may be less for SBS strength degradation than for degradation of tensile properties, the degradation process is most easily activated for SBS. If it is assumed that a combination of interphasial and matrix shear failure are responsible for SBS failure, the degradation of these constituent strengths is less aggressive but more easily activated than for longitudinal tensile parameters.

When comparing results for degradation rates and activation energies of tensile strength and strain in Table 32 and Table 33, the lower values of E_B in and higher values of B for tensile strength further support evidence that degradation of tensile strength is more aggressive than that of tensile failure strain. Because tensile strain is largely dominated by fiber failure strain, the degradation of failure strain should be controlled primarily by the degradation of the fiber whereas degradation of the tensile strength is dependent upon the degradation of fiber, matrix, and interphasial strengths. Thus, it is expected that the activation energy for degradation of tensile strength is lower than for tensile strain since its degradation is more easily activated.

The aggravating effect of water on the degradation of tensile strength can be seen through greater values in B in Table 32 for immersion exposures where moisture sorption is slightly greater than for 99%RH at similar time periods. Degradation of

tensile strain appears to be more easily activated with exposure to immersion, possibly due to the leaching of degraded products where hydrolytic degradation of the fibers occurs. Removal of the water would also make the matrix more brittle, reducing the failure strain of the dry matrix and, consequently, the dry composite. Figure 175 and Figure 176 indicate that the presence of water in "wet" material leads to more ductile matrix failure. Exposure to immersion environments should therefore result in activation energies which are lower for "dry" material than for "wet" material, as indicated in Table 33.

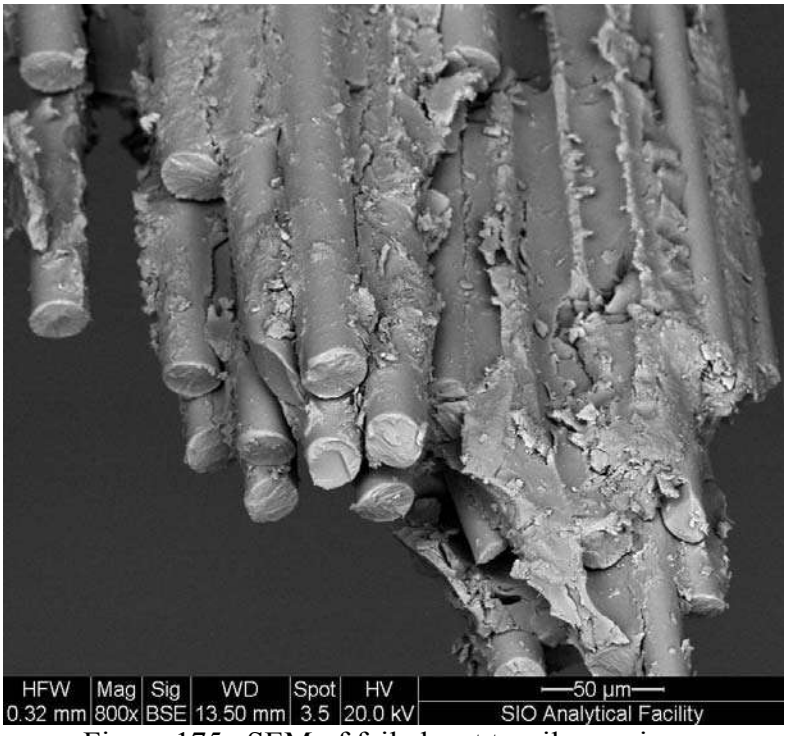

Figure 175. SEM of failed wet tensile specimen exposed to 60°C immersion for 24 weeks.

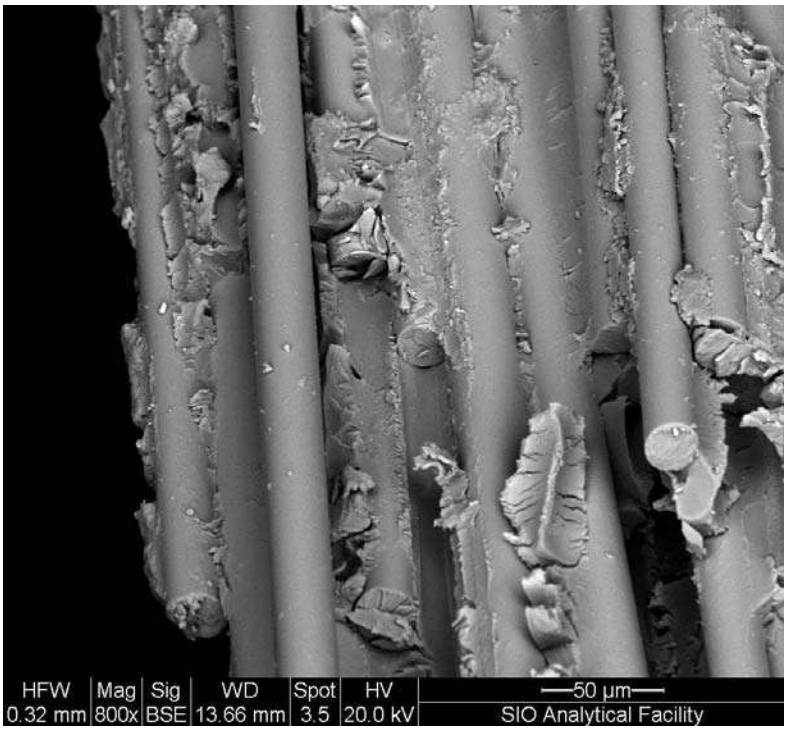

Figure 176. SEM of failed dry tensile specimen exposed to 60°C immersion for 24 weeks.

The dry E_B for strength degradation is anywhere from 24 to 29 kJ/mol greater than the wet E_B. While E_B for the degradation of tensile failure strain after exposure to 99%RH is 18 kJ/mol greater for wet than for dry, the dry E_B is actually 2 kJ/mol less for immersion environments, indicating the detrimental effect of removing water on the degradation rate of the failure strain. When considering wet/dry cyclic environments, significant attention should be paid to the changes in failure strain.

For hot water bath accelerated testing, it may not always be realistic to conduct tests on both wet and dry specimens. In order to gain an understanding of the rate of irreversible degradation using the Arrhenius rate degradation model, the addition of at least 25 kJ/mol to the wet activation energy may be appropriate.

7.3 Time Temperature Superposition

Phani and Bose [2] proposed a simplified version of the time-temperature superposition (TTS) degradation model where the property P at some time t can be described, using the initial property value P_0 and the property P_∞ as $t \rightarrow \infty$, via

$$\frac{P(t) - P_\infty}{P_0 - P_\infty} = \exp\left[\frac{-t}{\tau}\right], \tag{3}$$

where τ is the characteristic relaxation time. Mathematically, this model restricts $P_0 \geq P(t) > P_\infty$. It may be possible to account for increases in P by selecting some $P_0 < P(t) < P_\infty$, where degradation does not occur after the initial increase in $P(t)$. Relaxation times τ were calculated using P_∞ values presented in Table 34. Calculated values of τ are summarized in Table 35.

Table 34. P_∞ values used for calculation of TTS relaxation times.

Property	Wet	Dry
SBS Strength (MPa)	31.0	40.0
Tensile Strength (MPa)	234	248
Tensile Strain (%)	0.548	0.572

Table 35. Relaxation times (yr) for TTS degradation model.

	SBS Strength		Tens. Strength		Tens. Strain	
Env.	Wet τ	Dry τ	Wet τ	Dry τ	Wet τ	Dry τ
6 X	9.2	—	6.9	13.5	9.3	—
2 H	3.3	22.3	5.8	25.2	12.4	—
4 H	3.9	—	2.4	3.1	4.4	9.3
6 H	2.5	5.6	1.1	1.4	1.6	2.2
8 H	0.5	0.5	0.4	0.4	0.3	0.4
2 I	2.8	26.0	5.7	27.3	16.9	—
4 I	3.9	—	1.9	2.2	3.3	4.2
6 I	2.0	4.4	0.9	1.1	1.3	1.5
8 I	0.6	0.7	0.3	0.3	0.3	0.4

τ can be described by the Arrhenius relation for thermal dependency using a pre-exponential factor τ_o and activation energy E_τ.

$$\tau = \tau_o \exp\left[\frac{-E_\tau}{RT}\right], \tag{4}$$

It should be noted that τ is implemented as a relaxation time rather than a rate parameter, so its thermal dependency will be reflected through a negative activation energy such that τ decreases with temperature. Activation energies for the crack propagation characteristic degradation rates are provided in Table 36, with Arrhenius plots in Figure 177 through Figure 179.

The results presented in Table 35 and Table 36 demonstrate similar trends as those observed for the Arrhenius rate degradation model, discussed in the previous section. The TTS model has major advantages in that it allows for $P_\infty > 0$ and allows for increases from P_0.

Table 36. Activation energies E_τ (kJ/mol) for crack propagation degradation model.

	SBS Strength		Tens. Strength		Tens. Strain	
Env.	Wet	Dry	Wet	Dry	Wet	Dry
99%RH	-25	-51	-38	-59	-52	-66
Immersion	-22	-49	-41	-60	-55	-52

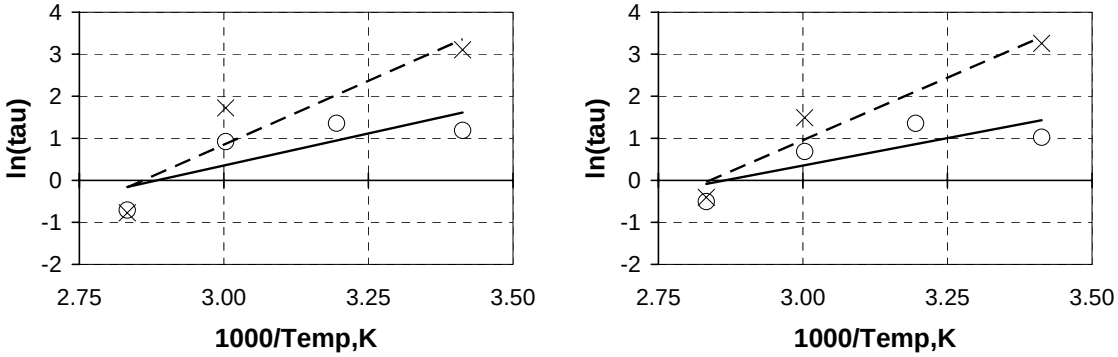

(a) (b)

Figure 177. Arrhenius plots of relaxation times for SBS strength.
(a) 99%RH, (b) immersion; ○ Wet; × Dry.

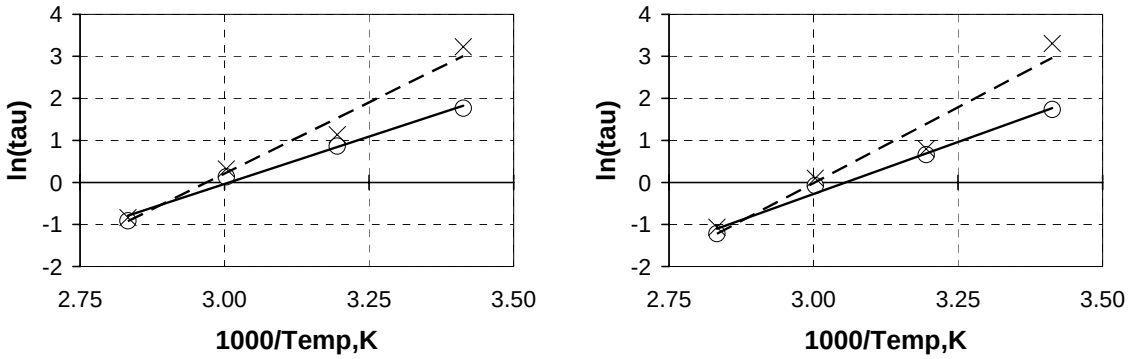

(a) (b)

Figure 178. Arrhenius plots of relaxation times for tensile strength.
(a) 99%RH, (b) immersion; ○ Wet; × Dry.

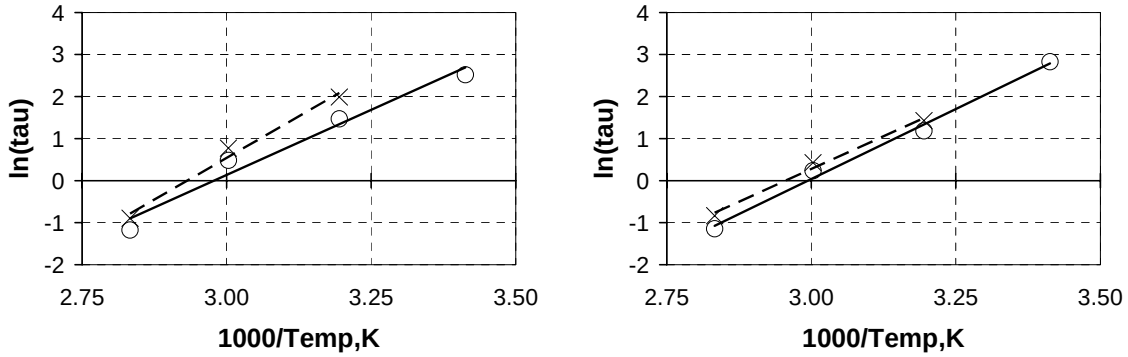

(a) (b)

Figure 179. Arrhenius plots of relaxation times for tensile strain.
(a) 99%RH, (b) immersion; ○ Wet; × Dry.

7.4 Crack Propagation Degradation Model

The crack propagation degradation model [3], introduced in Section 2.5.1.3, was employed by fitting data to

$$\frac{P(t)}{P_0} = \frac{1}{\sqrt{1+kt}} \tag{5}$$

where P is the material property at time t, P_0 is the baseline initial property value, and k is the characteristic degradation rate which incorporates environmental effects such

as temperature. While the model was developed for tensile strength, it shall be extended to tensile strain and SBS strength here.

When $P(t) > P_0$, Equation 5 requires that $k < 0$, resulting in values of P/P_0 which grow by several orders of magnitudes over short periods of time. Consequently, this model is not applicable to changes in material properties where $P > P_0$. Calculated values of k are summarized in Table 37.

Table 37. Characteristic degradation rates (yr^{-1}) for crack propagation model.

	SBS Strength		Tens. Strength		Tens. Strain	
Env.	Wet k	Dry k	Wet k	Dry k	Wet k	Dry k
6X	0.14	—	0.26	0.12	0.16	—
2H	0.39	0.04	0.32	0.07	0.12	—
4H	0.32	—	0.97	0.67	0.38	0.21
6H	0.53	0.16	2.84	2.06	1.27	0.87
8H	2.93	1.69	12.45	10.35	6.84	5.64
2I	0.47	0.03	0.33	0.06	0.09	—
4I	0.33	—	1.29	1.04	0.53	0.39
6I	0.69	0.21	4.02	2.92	1.76	1.33
8I	2.40	1.26	13.79	11.60	6.12	5.10

The thermal dependence of the degradation parameter k should be described by the Arrhenius relation

$$k = k_o \exp\left[\frac{-E_k}{RT}\right], \tag{6}$$

where k_o is a pre-exponential factor and E_k is the activation rate for the degradation process. Activation energies for the crack propagation characteristic degradation rates are provided in Table 38, with Arrhenius plots in Figure 180 through Figure 182.

The results presented in Table 37 and Table 38 demonstrate similar trends as those observed for the Arrhenius rate and TTS degradation model. While the crack

propagation degradation model does not allow for increases from initial material properties, it does restrict the change in properties to a positive value as *t* increases.

Table 38. Activation energies E_k (kJ/mol) for crack propagation degradation model.

	SBS Strength		Tens. Strength		Tens. Strain	
Env.	Wet	Dry	Wet	Dry	Wet	Dry
99%RH	27	49	52	70	57	75
Immersion	37	49	53	73	60	59

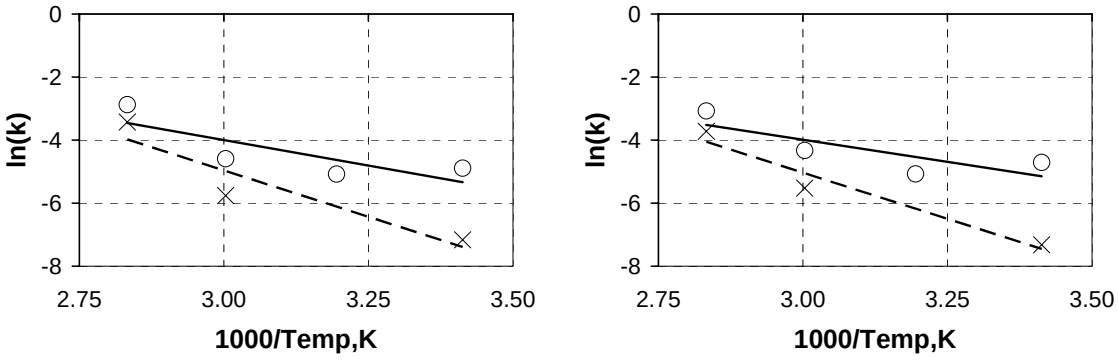

(a) (b)

Figure 180. Arrhenius plots of crack propagation degradation rates for SBS strength. (a) 99%RH, (b) immersion; ○ wet; × dry.

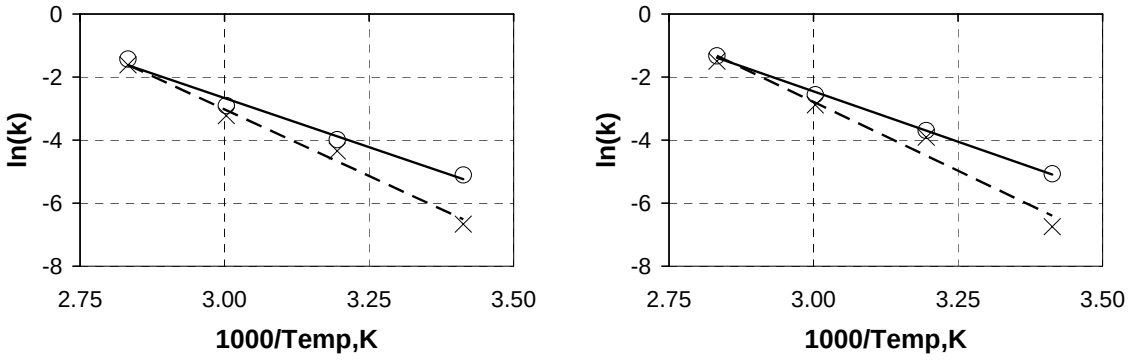

(a) (b)

Figure 181. Arrhenius plots of crack propagation degradation rates for tensile strength. (a) 99%RH, (b) immersion; ○ wet; × dry.

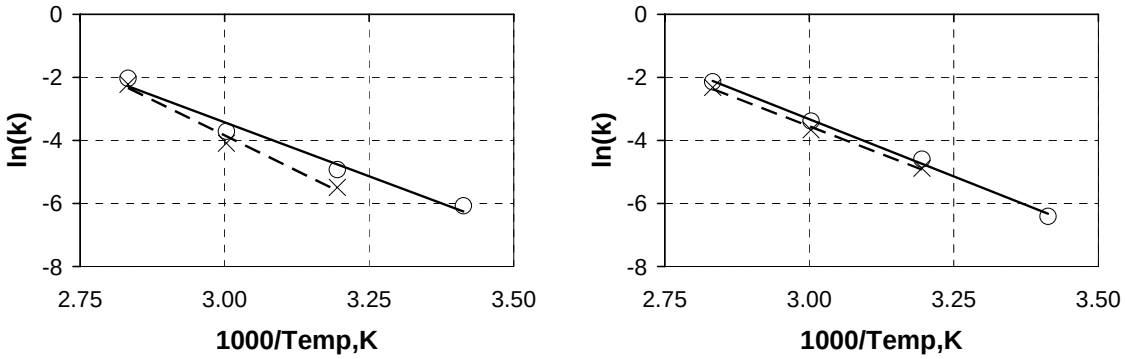

Figure 182. Arrhenius plots of crack propagation degradation rates for tensile strain. (a) 99%RH, (b) immersion; ○ wet; × dry.

7.5 Equivalent Temperature

While equivalent temperatures have previously been proposed [4] to represent time variant environments, as discussed in Section 2.5.1.7, an alternative definition of equivalent temperature is defined here which can be applied to any model employing the Arrhenius relation for developing thermal trends.

It is first assumed that a change in property after exposure to some static temperature T_1 and relative humidity RH_1 can be described by the same relationship at having been exposed to immersion at some other temperature T_e:

$$P(T_1, RH_1, t) = P(T_e, t). \tag{7}$$

Most degradation models integrate the Arrhenius relation into the specified degradation rate parameter, such as B for the Arrhenius rate degradation model and k for the crack propagation degradation model. Consequently, the characteristic degradation rate parameter for any environment can be described at an equivalent

temperature of immersion using the activation energy and pre-exponential coefficient established for immersion exposures.

$$A(T_1, RH_1) = A_{0,i} \exp\left[\frac{-E_{A,i}}{RT_e}\right], \tag{8}$$

where A is a degradation rate parameter, such as B or k, determined for some exposure to T_1 and RH_1 and $A_{0,i}$ and $E_{A,i}$ are the corresponding pre-exponential factor and activation energy for immersion exposures. Therefore, the equivalent temperature for immersion, T_e, is then

$$T_e = \frac{E_{A,i}}{R(\ln A_{0,i} - \ln A)}. \tag{9}$$

Applying this methodology to 75%RH and 99%RH wet results and 99%RH dry results, equivalent temperatures of immersion were determined for humid environments where degradation was observed. Results are summarized for the Arrhenius rate degradation model in Table 39. Equivalent temperatures determined for the TTS and crack propagation degradation model are comparable, as would be expected since B, τ, and k demonstrate similar thermal dependency.

Table 39. Equivalent temperatures (°C) for Arrhenius rate degradation model.

	SBS Strength		Tens. Strength		Tens. Strain	
Env.	Wet	Dry	Wet	Dry	Wet	Dry
6 X	-30	—	8	—	**21**	—
2 H	26	25	17	13	24	—
4 H	**17**	—	40	49	40	**24**
6 H	**38**	50	59	61	58	53
8 H	109	89	76	71	76	80

It is not surprising that equivalent temperatures of immersion for 99%RH environments are very close to the temperatures of exposure at 99%RH. Furthermore,

the slight decrease observed in wet SBS strength after exposure to 75%RH resulted in an unrealistic sub-zero temperature of immersion.

In general, equivalent temperatures of immersion were calculated except for SBS strengths resulting from exposure to 80°C at 99%RH, where the SBS strengths at each time step were observed to be lower than for immersion exposures. The higher equivalent temperatures of immersion provided in Table 39 for 20°C results at 99%RH and for dry tensile strain at 40°C and 99%RH are considered a consequence of error which is inherent in the line fitting process.

Experimental results can only be compared for calculated T_e of 20°C, 40°C, 60°C, or 80°C. Those calculated T_e which are differentiated from the actual temperature of exposure by more than 5°C and which are within 5°C of one of the four experimental T_e are indicated in bold in Table 39. Most experimental trends for humid environments with these distinct equivalent temperatures closely resemble the experimental trend for immersion in the specified equivalent temperature. A comparison is provided in Figure 183 through Figure 186. Unfortunately, 99%RH exposure at 60°C cannot be compared to 50°C immersion since that temperature of immersion was not considered in this study.

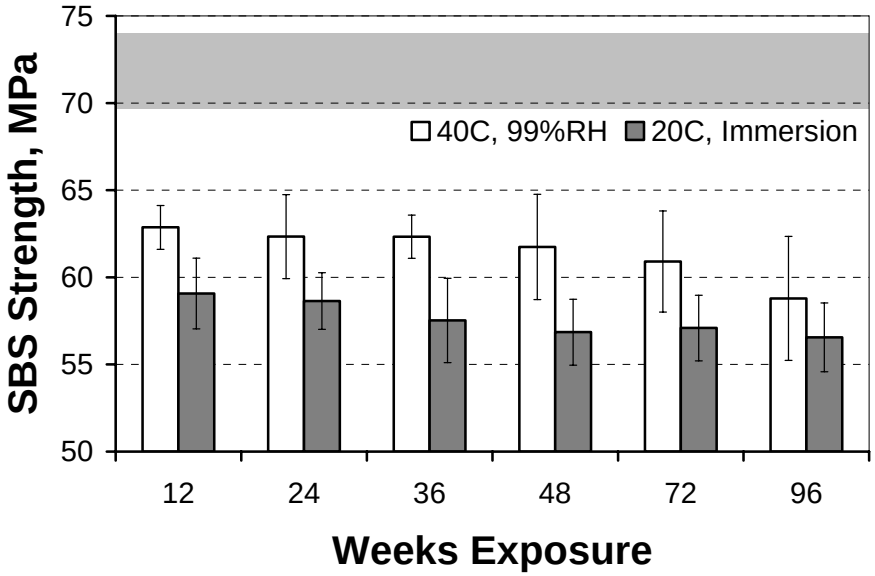

Figure 183. Comparison of wet SBS strength
after exposure to 40°C at 99%RH and 20°C immersion.
Shaded region indicates baseline average and standard deviation.
Error bars indicate standard deviations.

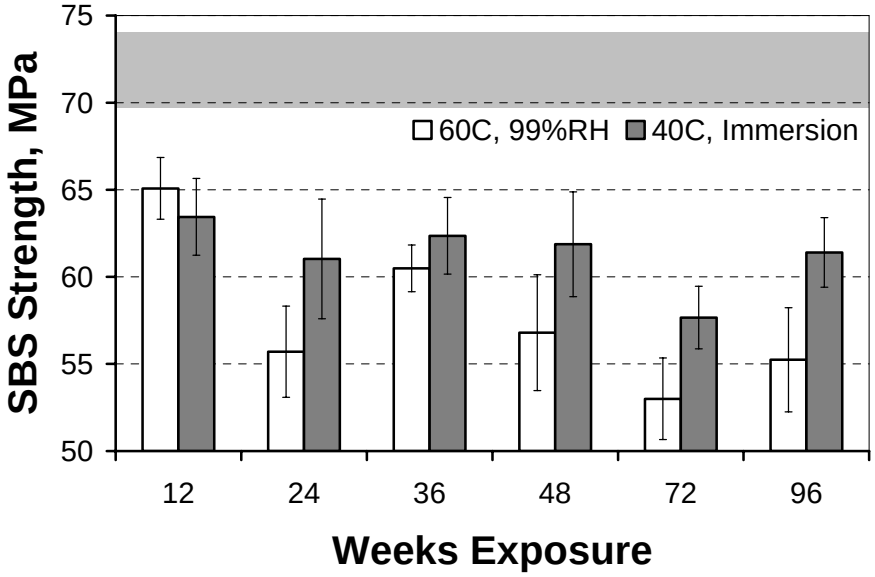

Figure 184. Comparison of wet SBS strength
after exposure to 60°C at 99%RH and 40°C immersion.
Shaded region indicates baseline average and standard deviation.
Error bars indicate standard deviations.

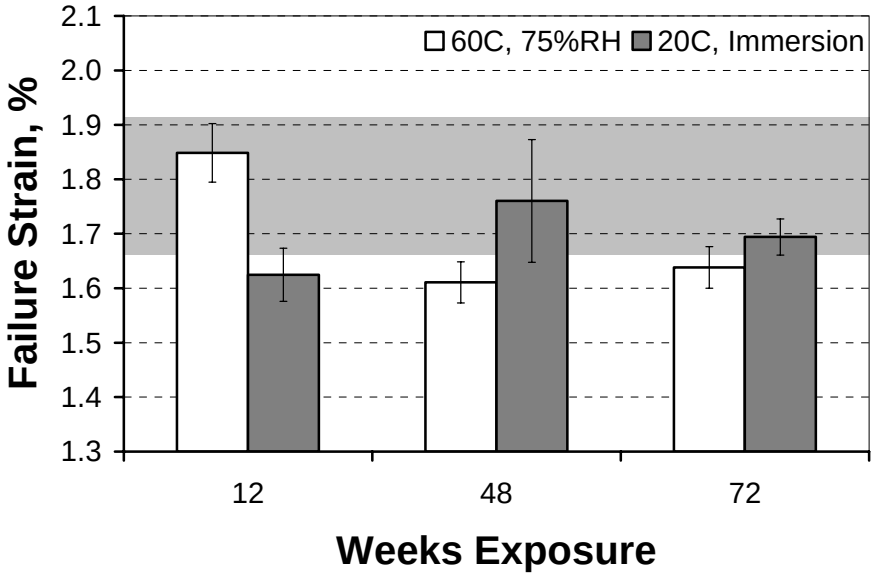

Figure 185. Comparison of wet tensile failure strain
after exposure to 60°C at 75%RH and 20°C immersion.
Shaded region indicates baseline average and standard deviation.
Error bars indicate standard deviations.

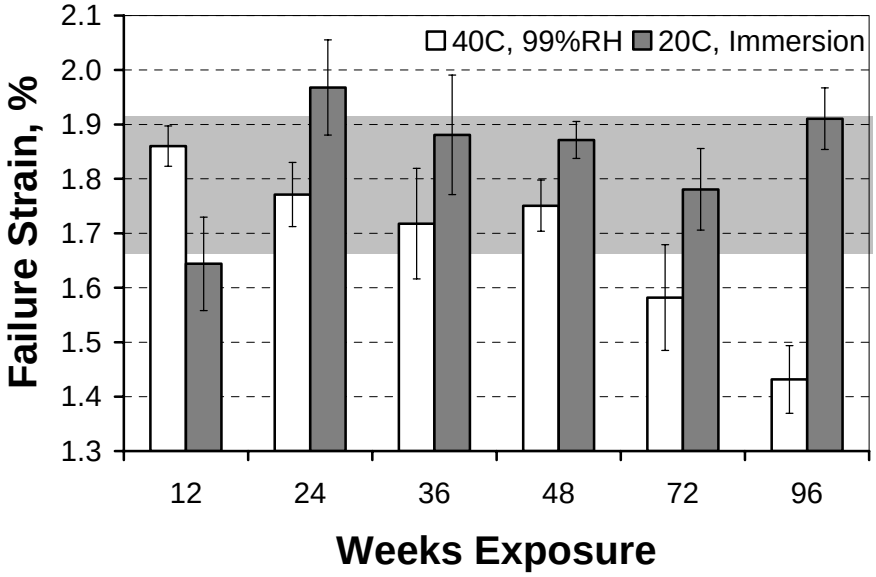

Figure 186. Comparison of dry tensile failure strain
after exposure to 40°C at 99%RH and 20°C immersion.
Shaded region indicates baseline average and standard deviation.
Error bars indicate standard deviations.

Most comparable trends appear to be within scatter range of each other, though degradation may be consistently underestimated, as in Figure 183, or overestimate, as in Figure 184, the material property.

For wet tensile strains, exposure to water immersion at 20°C results in significant decreases after just 12 weeks which are not seen after 12 weeks exposure to 75%RH at 60°C, as seen in Figure 185. After 12 weeks, however, the wet tensile strains for the two exposure conditions appear to be within scatter range of each other. Because a shortage of material prevented tensile testing for the 75%RH exposure between 12 and 48 weeks, it is unclear how the trends replicate each other for intermediate times.

The degradation of the dry tensile strain for material exposed to 99%RH at 40°C remains within baseline scatter for the first 48 weeks, seen in Figure 186, similar to results for 20°C immersion. From 72 weeks on, the dry failure strain demonstrates irreversible degradation not seen in material immersed in 20°C deionized water, where fiber pitting is likely less severe.

7.6 Moisture Dependent Degradation

In this section, three moisture dependent degradation models will be employed. The first considers the tensile modulus as a function of moisture content based on a derivation relating the modulus to the hydrogen bonding within a polymeric material [5] and will be discussed in Section 7.6.1. The second model, addressed in Section 7.6.2, adopts an empirically based exponential degradation model which allows for a non-zero strength as moisture content becomes very large. In Section 7.6.3, a third

model is developed to predict the SBS strength as a function of moisture content. It shall consider the observable increases in SBS strength resulting form exposure at elevated temperatures as well as plasticization and degradation resulting from prolonged exposure to water.

7.6.1 Theoretically Based Moisture Dependent Degradation Model

The moisture dependent degradation models presented in Section 2.5.1.4 are independent of time save for predictions in moisture content which could be made using diffusion models. The analysis here employs a theoretical model relating the disruption of inter-chain hydrogen bonds by water to the change in moduli based upon analysis of materials such as cellulose, nylon, and wool [5]. Because the tensile modulus does not demonstrate significant changes with time here, it was not employed in temporally based degradation models earlier. However, the wet tensile modulus does demonstrate a subtle decreasing trend with increasing moisture content, as discussed in Section 5.1.

The model [5] states that in Region I under a critical moisture content, w_c, the modulus E changes from an initial value of E_0 with increasing moisture content M_t, given in grams of water per grams of sorbent here

$$E = E_0 \exp\left[-\frac{1}{3}\cdot\frac{M_t}{W}\right], \qquad M_t < w_c \qquad (10)$$

where W is the "hypothetical quantity of water required to provide one molecule for each OH" or any other group on the sorbing polymer molecule which may establish a

hydrogen bond with water [5]. Above the critical moisture content, which is theorized to be on the order of the BET adsorbed monolayer [5], in Region II,

$$E = E_0 \exp\left[\frac{1}{3}\cdot\frac{w_c}{W}(CI-1)\right]\exp\left[-\frac{CI}{3}\cdot\frac{M_t}{W}\right], \qquad M_t > w_c \qquad (11)$$

where *CI* is the average cooperative index referring to the total number of inter-chain bonds broken by a single water molecule.

It shall first be assumed that w_c is greater than the observed M_{max} resulting from exposure to 75%RH, which was 0.15 [0.02] % for tensile specimens exposed to 75%RH at 60°C. For $M_t < w_c$, tensile moduli from 50%RH and 75%RH exposures were used to calculate *W* using Equation 10. Since the modulus for 18%RH exposures were about the initial value with high scatter in moisture contents and no clear trend, as discussed in Section 5.1, these results were not used. For $M_t > w_c$, results for 99%RH and immersion exposure were used at all temperatures to calculate w_c and *CI*. Using the wet tensile modulus, resulting values of *W*, w_c, and *CI* are presented in Table 40.

Table 40. Parameters for theoretically based moisture dependent degradation model.

W (g H_2O / g sorbent)	0.073
w_c (g H_2O / g sorbent)	0.140
CI	0.943

First and foremost, the critical moisture content w_c is determined as 14 %, while it was assumed to be 0.15 %. While this result is not reasonable and implies invalidity of the model, the values determined for *W* and *CI* are reasonable, and their theoretical implications are discussed below.

W can be theoretically calculated with knowledge of then number of sites available for hydrogen bonding and the molecular weight of the sorbent repeating unit. The proposed structure of a model vinyl-ester [6,7] indicates that there are three types of sites available for hydrogen bonding, identified as ester, ether, and hydroxyl groups, all of which could possibly establish hydrogen bonds [8,9]. Using the structure proposed in Section 2.1.1.1 [7], there are two ether groups and one hydroxyl group in the repeating unit with a molecular weight of 152 g/mol. External of the repeating unit, there are two esters, including four oxygen molecules, and a hydroxyl in the chemical structure with a molecular weight of 122 g/mol. The number average molecular weight of one commercial vinyl-ester is given as 2.0 kg/mol [6], implying that there are about 12 repeating units in one commercial vinyl-ester. Assuming this structure is correct, *W* can be calculated as

$$W = \frac{3 \times 12 \times 18\ \text{g/mol} + 5 \times 18\ \text{g/mol}}{12 \times 152\ \text{g/mol} + 122\ \text{g/mol}} = 0.379\ \text{g}\ H_2O\ /\ \text{g sorbent}\,.$$

The calculated *W* is about five times greater than the experimentally determined value of 0.073. The calculation provided above assumes that water will establish a hydrogen bond at every available site, when it is known that hydrogen bonding is much more likely with hydroxyl groups [8].

The average cooperative index *CI* of 0.943 indicates that a single water molecule breaks just one hydrogen bond as it interacts strongly with the bulk polymer. While this result is reasonable, it indicates that water clustering is unlikely since $CI \leq 1$. It should be reiterated that *CI* is the average value and accounts for the presence of

clustering which is likely at hydroxyl groups ($CI_{OH} > 1$) and less likely at ester and ether groups ($CI_{CO} \approx 0$) [8].

The critical moisture content w_c was determined to be much greater than the maximum observed moisture content in this composite system. A moisture content of 14 % for this material system would be indicative of severe degradation. Because w_c was determined to be much greater than the assumed 0.15 %, it should be restated that the model will not be continuous as it transitions for Region I to Region II. Figure 187 provides a comparison of experimental and theoretical results. Figure 188 provides the same results on a smaller scale, where the high scatter in experimental results can be identified, along with discontinuity between Region I and Region II.

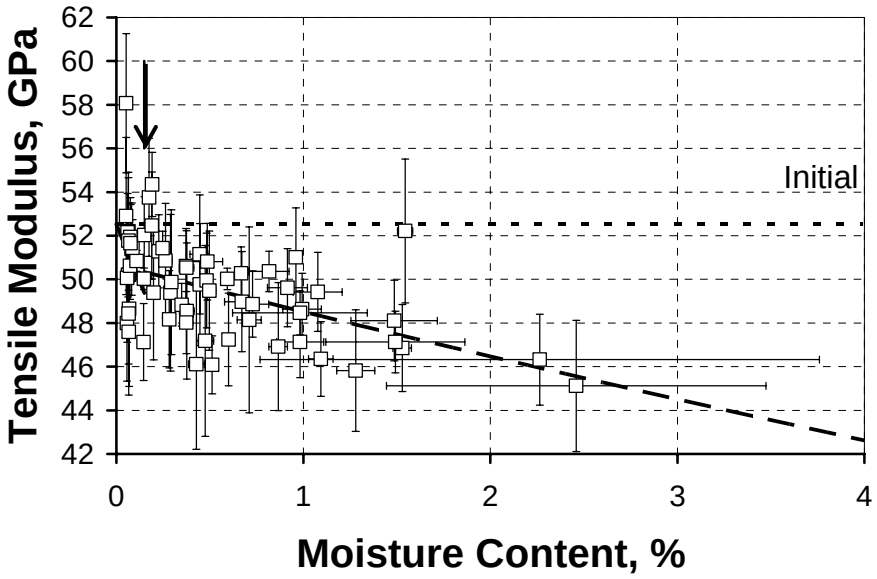

Figure 187. Moisture degradation predictive model and wet tensile modulus. □: Experimental, - - : average initial modulus, ——: Region I for $M_t < w_c$ (not visible below markers), — — : Region II for $M_t > w_c$. ↓ indicates w_c used in calculations. Error bars indicate standard deviation.

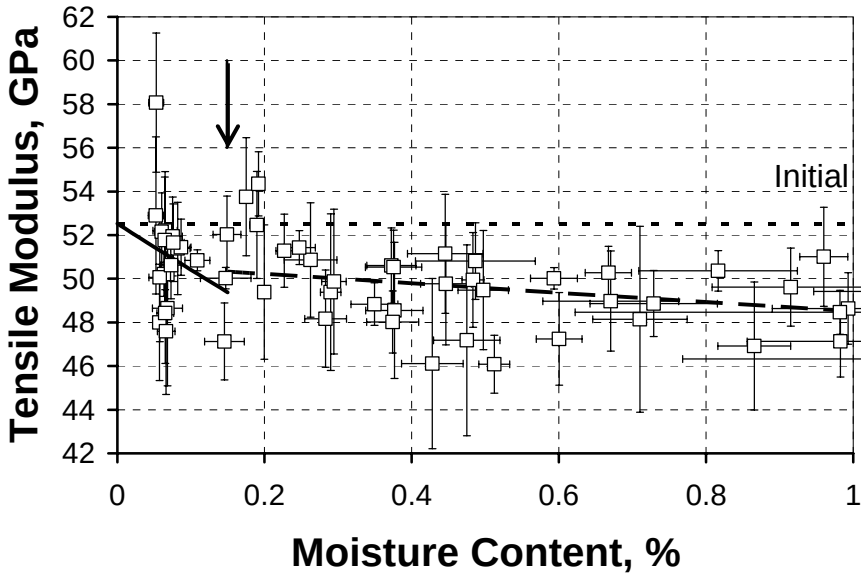

Figure 188. Moisture degradation predictive model and wet tensile modulus. Plotted through M_t = 1 %. □: Experimental, - - : average initial modulus, ——: Region I for $M_t < w_c$, — — : Region II for $M_t > w_c$. ↓ indicates w_c used in calculations. Error bars indicate standard deviation.

7.6.2 Empirically Based Moisture Dependent Degradation Model

An alternative moisture degradation model was introduced in Section 2.5.1.4, and has been generalized here for a property P, which reaches P_∞ as the moisture content $M_t \rightarrow \infty$ from P_0 at $t = 0$:

$$\frac{P_0 - P(t)}{P_0 - P_\infty} = \exp(-CM_t), \tag{12}$$

where C is the empirically determined moisture dependent degradation parameter. While M_t should theoretically reach a finite M_∞ as $t \rightarrow \infty$, it may be possible for severe degradation to result in sudden, dramatic moisture uptake where $M_\infty \rightarrow \infty$ for $t \rightarrow \infty$.

To obtain C values, Equation 12 was fitted using strength and strain results for material exposed to 50%RH, 75%RH, 99%RH and immersion for all temperatures.

Property values for material exposed to 18%RH were not considered since these low humidity exposures tended to result in slight increases in property values with high scatter. Because the small moisture content in material exposed to 50%RH did appear to result in slight plasticization, as elucidated in Section 5.1.1 and Section 5.2.1, these results were included in the following analysis.

For each temperature of exposure, P and M_t results for material exposed to all humidities and immersion at that temperature were used to determine C from Equation 12. It was assumed that the changes in material properties resulted from interaction with a specific moisture content at a particular temperature, characterized by C, and so the degradation observed in dry results resulted from the same moisture content used to determine the degradation in material tested in the wet state. Where leaching of degraded species from SBS specimens was observed, in high humidity environments at 40°C, 60°C and 80°C and in immersion environments at 20°C, 40°C, 60°C, and 80°C as indicated in Section 4.3, adjusted moisture contents were used in place of apparent moisture contents so that the effect of moisture sorption alone could be considered. Leaching of degraded material from tensile specimens was noted in 99%RH at 60°C and 80°C and in immersion environments at 40°C, 60°C, and 80°C.

The P_∞ values used in Equation 12 were distinct for wet and dry sets and are summarized in Table 34 in Section 7.3. Calculated values of C are summarized in Table 41.

Table 41. Degradation parameter ($\%^{-1}$) for empirically based moisture dependent degradation model.

Temperature (°C)	SBS Strength		Tens. Strength		Tens. Strain	
	Wet *C*	Dry *C*	Wet *C*	Dry *C*	Wet *C*	Dry *C*
20	1.23	0.15	0.74	0.10	0.34	—
40	0.48	—	1.06	0.83	0.58	0.34
60	0.52	0.20	1.28	1.05	0.88	0.66
80	1.25	1.18	1.79	1.57	1.79	1.36

The thermal dependence of the degradation parameter *C* should be described by the Arrhenius relation

$$C = C_o \exp\left[\frac{-E_C}{RT}\right], \tag{13}$$

where C_o is a pre-exponential factor and E_C is the activation rate for the degradation process. Activation energies for the moisture dependent degradation model are provided in Table 42, with Arrhenius plots in Figure 189 through Figure 191. Figure 192 and Figure 193 demonstrate typical degradation trends for this moisture dependent model. Adjusted moisture contents are provided in Figure 192 and Figure 193, where leaching of degraded material occurred.

Table 42. Activation Energies E_C (kJ/mol) for moisture dependent degradation.
* If 20°C exposure is omitted from Arrhenius plot, E_C = 15 kJ/mol for dry tensile strength.

SBS Strength		Tens. Strength		Tens. Strain	
Wet	Dry	Wet	Dry	Wet	Dry
- 0.49	25	12	38 *	23	31

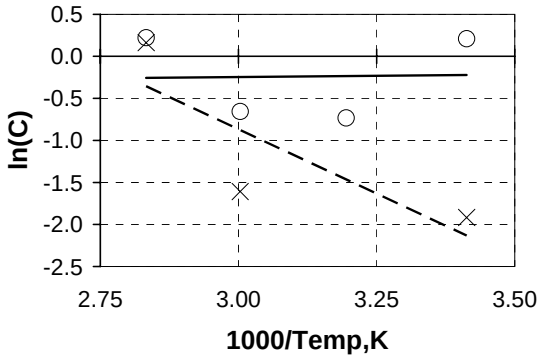

Figure 189. Arrhenius plots of moisture dependent degradation parameter for SBS strength.
○ Wet; × Dry.

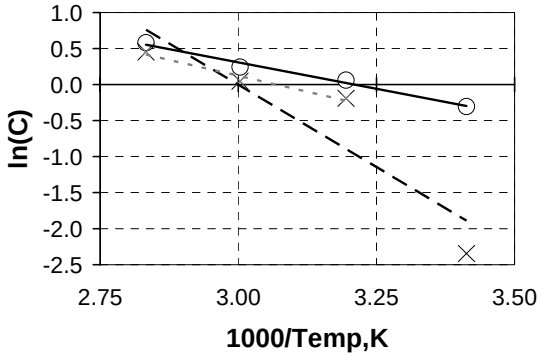

Figure 190. Arrhenius plots of moisture dependent degradation parameter for tensile strength.
○ Wet; × Dry. Dashed lines indicate line fit for dry *C* values. — —: 20°C, 40°C, 60°C, 80°C environments. - - -: 40°C, 60°C, 80°C exposures.

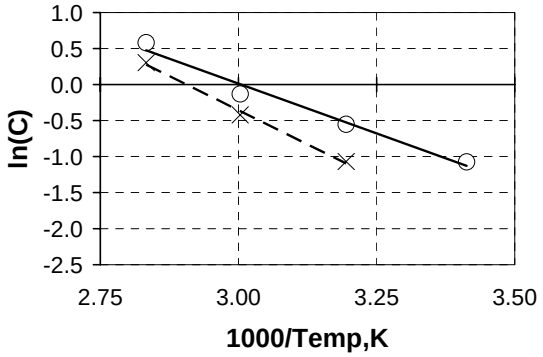

Figure 191. Arrhenius plots of moisture dependent degradation parameter for tensile strain.
○ Wet; × Dry.

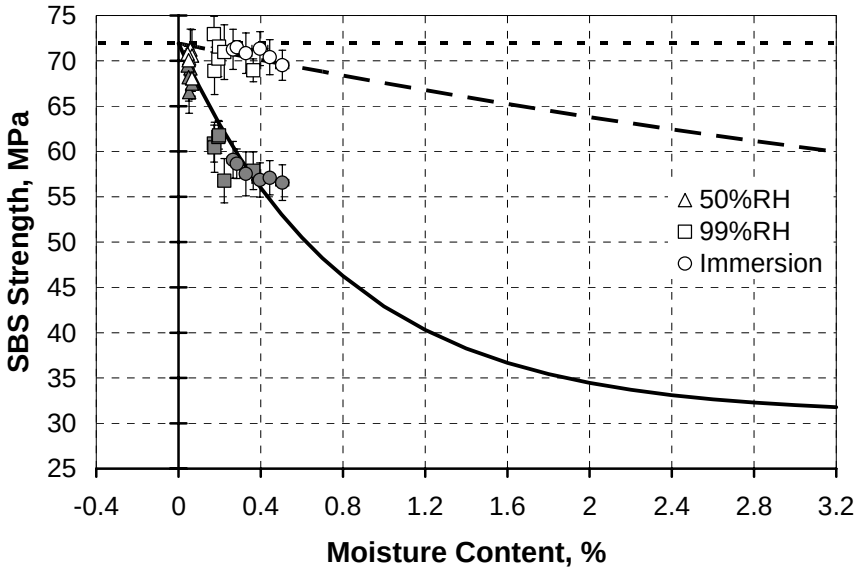

Figure 192. Predictions of SBS strength for material exposed to 20°C. Closed: wet, open: dry. ——: wet predictions, — — : dry predictions, - - - : baseline average. Error bars indicate standard deviations. Apparent moisture content is provided for 50%RH and 99%RH results; adjusted moisture content is provided for immersion results, where leaching of degraded species occurred.

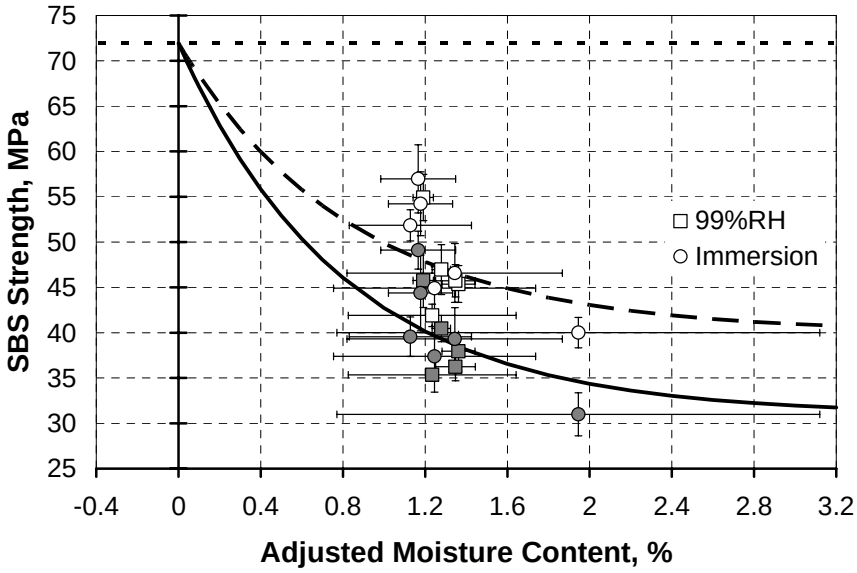

Figure 193. Predictions of SBS strength for material exposed to 80°C. Closed: wet, open: dry. ——: wet predictions, — — : dry predictions, - - - : baseline average. Error bars indicate standard deviations. Adjusted moisture content is provided for immersion results, where leaching of degraded species occurred.

The values of *C* for wet SBS strength degradation indicate that the degradation experienced in 20°C exposures closely resembles that resulting from 80°C exposures, though Figure 192 and Figure 193 indicate that the experimental results are not as similar as the values of *C* suggest. In the case of SBS specimens exposed to 20°C, reversible plasticization was responsible for the decrease in wet SBS strength, while degradation of the fiber and matrix are attributed for the severe degradation of SBS strength in material exposed to 80°C. At 40°C and 60°C, the primary mechanisms responsible for degradation of the wet SBS strength are plasticization and strengthening due to leaching of LMWS or post-cure, as discussed in Section 5.2. In 99%RH and immersion environments at 60°C, fiber degradation is also observed. Consequently, the competing mechanisms of degradation and strengthening result in moisture dependent degradation parameters which are not adequately described by a single activation energy, as seen in Figure 189.

While post-conditioning results in near full recovery of the SBS strength in material exposed to 20°C environments due to reversible plasticization, the degradation of the fiber and polymer in material exposed to 80°C does not allow for much recovery in SBS strength. Consequently, the *C* value is very similar for 80°C exposures both before and after post-conditioning, though the dry *C* value is less, as expected.

Degradation of the SBS strength of post-conditioned material results in a *C* with an activation energy which is 26 kJ/mol greater than that of material tested prior to post-conditioning. This positive activation energy for the moisture dependent

degradation parameter characteristic of the SBS strength for dry material reveals the irreversible nature of the degradation of material tested before post-conditioning.

The moisture dependent degradation parameters for tensile strength and strain are several times larger than that for the degradation of SBS strength for all temperatures of exposure except 20°C. Plasticization has already been introduced as a significant mechanism for degradation of the wet SBS strength. In the case of tensile properties, Section 5.1.3 addresses the near complete recovery of tensile strength and the increases in tensile strain observed after post-conditioning in material exposed to 20°C. Section 7.1 reviews this increase as a reason for the omission of dry tensile strain for the calculation of C at 20°C. The significant recovery in tensile strength results in a value of C which is much lower for material exposed to 20°C than for material exposed to wet environments at higher temperatures. Figure 190 demonstrates the effect that the lower magnitude of C calculated for the degradation of dry tensile strengths has on the Arrhenius plot. Removing C determined for 20°C dry results from the Arrhenius plot results in a 61% decrease in activation energy from 38 kJ/mol to 15 kJ/mol.

Consequently, the difference between the reversible and irreversible degradation of tensile strength may be summarized through the 3 kJ/mol difference between wet and dry activation energies of 12 kJ/mol and 15 kJ/mol, respectively. It is not surprising that activation energies for degradation of wet and dry tensile strain are larger than for tensile strength and that the difference between E_C for tensile strain is larger at 8 kJ/mol. The presence of water results in some plasticization of the

polymer matrix which results in lower tensile strains at low temperatures of exposure, as elucidated in the discussion on tensile strain throughout Section 5.1. These degradation trends also account for the degradation of E-glass fiber reinforcement at high temperatures and moisture content which result significant irreversible degradation of the failure strain. Because the interfacial degradation is primarily irreversible, the difference between the activation energies for tensile strengths before and after post-conditioning should be the lowest, while plasticization observed through SBS testing is most significant, as revealed through the larger difference in E_C.

The activations energies for this empirically based moisture dependent degradation model allow for determination of material properties independent of environmental moisture content, e.g. relative humidity, provided that the moisture has an observable effect on material properties.

7.6.3 Predictive Modeling of Short Beam Shear Strength with Exposure

An empirical model may be developed for the prediction of short beam shear strength as a function of moisture content. The physical mechanisms of degradation of plasticization and strengthening due to leaching of LMWS were integrated into this model through additive degradation terms. Chemical and physio-mechanical degradation due to hydrolysis and interfacial debonding were incorporated using an exponentially based moisture dependent degradation parameter.

Results presented in Section 5.2 indicated that there was a consistent difference between wet and dry SBS strengths for material exposed to 99%RH and water immersion resulting from the reversible effects of plasticization. The average

difference between the wet and SBS strengths for material exposed to 99%RH and immersion was 10.52 MPa. Exposure to 50%RH resulted in a difference on average of 3.0 MPa, which was on the order of a standard deviation for a single set of SBS strength measurements. There was no consistent difference between wet and dry strengths for material exposed to 18%RH. Material exposed to 75%RH recovered 6.9 MPa after the removal of water. Because the difference between wet and dry SBS strengths of material exposed to 50%RH was on the order of a standard deviation of a set of 5 SBS strengths, it was assumed in the application of this model that plasticization did not occur in 18%RH or 50%RH environments. Despite a lower average difference between wet and dry SBS strengths resulting from exposure to 75%RH, it was assumed for the purposes of this model that plasticization resulting from this 75%RH exposure could be represented by the average plasticization adjustment of 10.52 MPa determined fro 99%RH and immersion exposures. Defining R as the recovery in SBS strength after post-conditioning, the wet SBS strength $S_w$can be determined using the dry SBS strength S_d via

$$S_w = S_d - R. \tag{14}$$

For 18%RH and 50%RH exposures, $R = 0$. For environmental exposures of 75%RH and above, $R = 10.52$ MPa.

The strengthening effect was determined using results from 18%RH and 50%RH exposures at the elevated temperatures of 40°C and 60°C and was assumed to hold for 99%RH and immersion at higher temperatures. Because there were no humid environments considered below 99%RH at 80°C, it was assumed that the

strengthening effect could be linearly extrapolated from lower temperatures of exposure to predict strengthening at 80°C. While strengthening did not occur in 20°C exposures, there was a slight decrease SBS strength. While it is likely that the restructuring of the polymer network was a consequence of small water uptake, the weakening effect may incorporated in the strengthening term to account for subtle plasticization effects. To determine the strengthening effect, the average difference between the dry SBS strength S_d and baseline SBS strength S_0 for material exposed to low and medium humidities at 20°C, 40°C, and 60°C was calculated and was found to be -1.74 MPa, 1.32 MPa, and 4.94 MPa, respectively. An empirical constant A can be introduced to describe the strengthening effect at a temperature of exposure T using a reference temperature T_0 via

$$S_d = S_0 + (T - T_0)A. \tag{15}$$

Using average values of $S_d - S_0$ for each environmental exposure independent of time, T_0 and A were determined to be 31°C and 0.1669 MPa/°C, respectively.

To determine the effects of degradation, it was assumed that irreversible degradation of SBS strength was dependent upon the amount of moisture sorbed. Where irreversible degradation was observed in 60°C and 80°C exposures, an exponential empirical relationship was employed after

$$S_d = S_0 \exp(-D \cdot M_t). \tag{16}$$

where D is an empirical parameter describing the degradation of S_d. and M_t is the moisture content. In these highly degraded specimens, leaching of degraded material occurred, requiring the use of adjusted moisture content in order to consider the effect

of the amount of water present in the material. D was calculated using average values of $S_d - S_0$ for each hot, moist environmental exposure independent of time. Material exposed to 99%RH and immersion at 60°C demonstrated a transition from reversible to irreversible degradation somewhere between 12 and 24 weeks, as indicated through SBS and DMTA results which were discussed in Sections 5.2.3 and 6.2.3.3. Consequently, dry SBS strengths obtained after just 12 weeks exposure to 99%RH and immersion at 60°C were not included in the calculation of D. D was found to be 0.2385 $\%^{-1}$.

Subsequently, the wet SBS strength can be predicted as a function of moisture content and temperature of exposure

$$S_w = \left[S_0 + A\left(T - T_0\right)\right]\exp\left(-D \cdot M_t\right) - R\,. \tag{17}$$

Table 43 provides empirically derived constants for the composite under consideration.

Table 43. Constants for empirical SBS degradation model.
Note that for 18%RH or 50%RH exposures, $R = 0$.
For calculation of dry SBS strength, it should be assumed $R = 0$.

A	0.1669 MPa/°C
T_0	31°C
D	0.2385 $\%^{-1}$
R	10.52 MPa

The reversible plasticization term R should only be used when deriving wet short beam shear strengths in wet environments with a relative humidity of at least 75%RH and should be set to zero for lower humidity environments. When calculating dry short beam shear strengths Equation 17 should still be used with the same moisture content used for wet predictions, but R should be set equal to zero since the

dry environment describes irreversible changes in SBS strength due to post-cure and the ingress of moisture.

Figure 194 and Figure 195 provide a comparison of experimental and predicted results for wet and dry sets. Correlation coefficients for wet and dry predictions were 0.874 and 0.733, respectively. Correlation coefficients for predictions corresponding to each environmental exposure were calculated using both wet and dry results and are provided in Table 44.

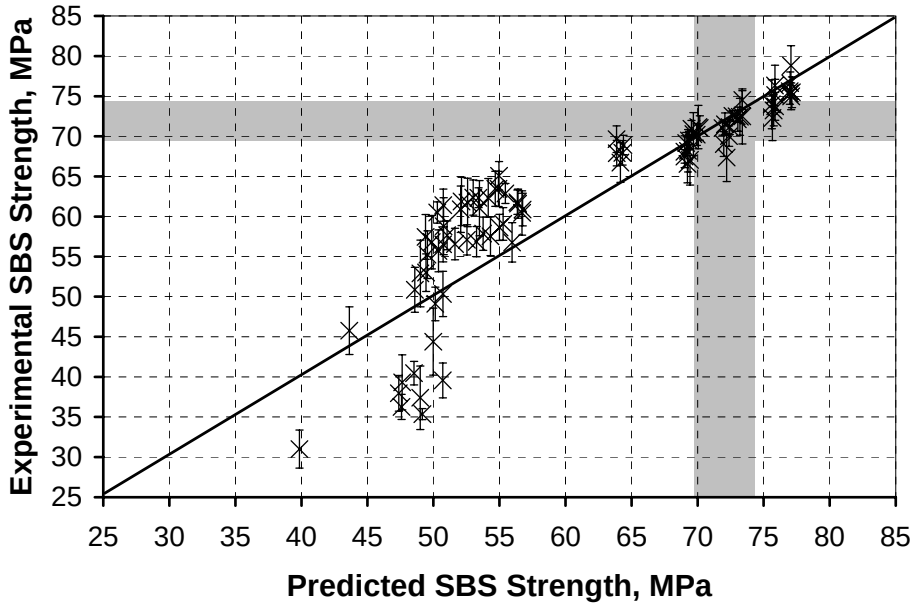

Figure 194. Comparison of experimental and predicted wet SBS strengths.
Error bars indicate standard deviations.
Shaded region indicates baseline average and standard deviation.

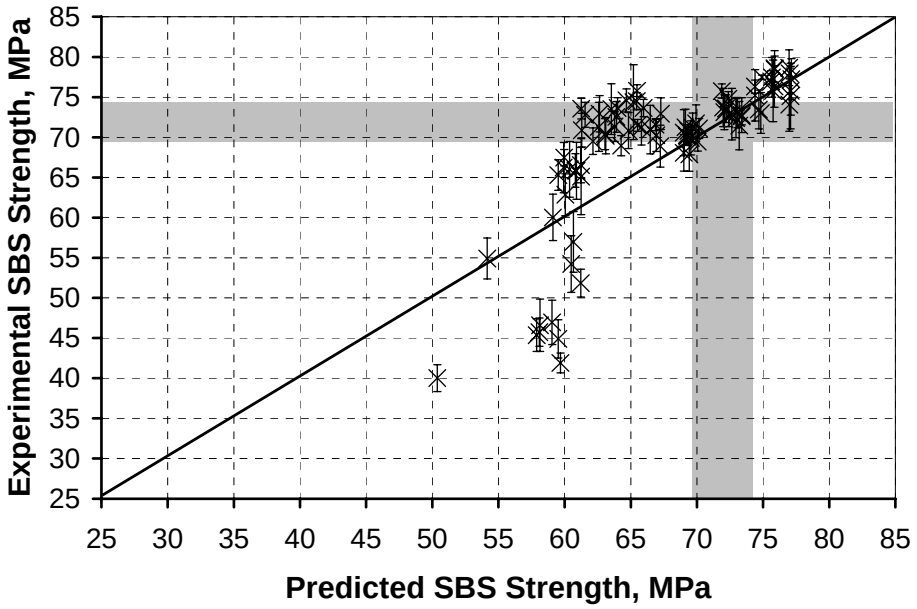

Figure 195. Comparison of experimental and predicted dry SBS strengths.
Error bars indicate standard deviations.
Shaded region indicates baseline average and standard deviation.

Table 44. Correlation coefficients for SBS strength predictions.
Each correlation coefficient accounts for both wet and dry predictions.

Env.	Correlation Coefficient
2L	0.616
4L	0.175
6L	-0.039
2M	0.258
4M	-0.101
6M	0.288
6X	0.925
2H	0.968
4H	0.989
6H	0.920
8H	0.752
2I	0.989
4I	0.977
6I	0.920
8I	0.865

The correlation coefficients calculated for 18%RH and 50%RH exposures indicate that predictions are quite poor. However, it is worth noting that of the 72 predictions made for the wet and dry SBS strength in 6 environments at 6 time steps, 72% of the calculated strengths are within a standard deviation of the experimental results. It may be desirable to investigate further the distribution of the predicted and experimental SBS strengths which are within one standard deviation but which result in low correlation coefficients.

Table 44 further indicates that predictions for the SBS strength of material exposed to 99%RH and immersion at 80°C are less accurate than for lower temperature high humidity and immersion environments. Equation 17 consistently overestimated the SBS strength by 9.51 [3.99] MPa. This overestimation is a result of the assumed strengthening effect. If the strengthening effect is assumed to be zero, predictions are closer to but still greater than experimental measurements. In this hot wet environment, pitting of the fiber and hydrolysis of the polymer resin and interphase leads to severe weakening of the composite along with significant leaching of degraded species. The transition and degree of degradation modes is not accounted for in this simplistic empirical model.

7.7 Multicomponent Degradation

The multicomponent degradation model takes into account degradation of the glass fiber and plasticization of the resin matrix [10]. Based on the weakest link model assuming a Weibull distribution for fiber strength, the strength P at some time t can be determined with the characteristic value of the Weibull distribution μ, an

ineffective length δ, and the debond length L_d, and the parameter describing the dispersion of the Weibull distribution m [10]:

$$\frac{P(t)}{P_0} = \frac{\{\mu(t)[\delta(t) + L_d(t)]me\}^{-\frac{1}{m}}}{\{\mu(0)[\delta(0) + L_d(0)]me\}^{-\frac{1}{m}}} \tag{18}$$

where P_0 is the strength at $t = 0$ and e is the base of natural logarithms. The characteristic value of the Weibull distribution is defined as [10]

$$\mu(t) = \frac{1}{L}\left\{\frac{\Gamma\left(1 + m^{-1}\right)}{\sigma(t)}\right\}^{-\frac{1}{m}} \tag{19}$$

where σ is the average fiber strength obtained using a gage length of L.

Consequently, Equation 18 reduces to

$$\frac{P(t)}{P_0} = \frac{\sigma(t)}{\sigma(0)}\left[\frac{\delta(t) + L_d(t)}{\delta(0) + L_d(0)}\right]^{-\frac{1}{m}} \tag{20}$$

where the debond length is described by empirical parameters κ and λ defined in [10]

$$L_d(t) = \kappa + \lambda \ln t\,, \tag{21}$$

and the ineffective or stress transfer length is provided as [10,11]

$$\delta = \frac{d_f}{2}\left[\left(\frac{1 - \sqrt{V_f}}{\sqrt{V_f}}\right)\left(\frac{E_f}{G_m(t)}\right)\right]^{-1/2} \cosh^{-1}\left[\frac{1 + (1 - \varphi)^2}{2(1 - \varphi)}\right] \tag{22}$$

where d_f is the fiber diameters, V_f is the fiber volume fraction, E_f is the fiber modulus, and φ is the stress intensity factor defined as the ratio of the stress from the end of the ineffective length δ away from the broken end of the fiber to a point far away from the

break. For an arbitrary stress development of φ=0.9, the $\cosh^{-1}$ term simplifies to 2.302.

G_m is the matrix shear modulus which will change with hygrothermal exposure and can be described using $G_{m\infty}$ to describe the longterm modulus with the wet and dry glass transition temperatures T_{gw} and T_{gd}, the temperature of exposure T, and a reference temperature T_0:

$$G_m = G_{m\infty}\sqrt{\frac{T_{gw}-T}{T_{gd}-T_0}}\,. \tag{23}$$

The fiber strength is provided in [10], using the modified stress corrosion model:

$$\sigma\left(t_f, t_a\right) = \left[\frac{t_f}{BS_0^{N-2}\left(1+\alpha t_a\right)^{-\beta(N-2)}}\right]^{-1/N}. \tag{24}$$

where t_f is the time to failure, t_a is the aging time, N is the susceptibility, B is an empirical parameter relating to stress corrosion, and α and β are empirical constants describing zero-stress aging of the fiber. The fiber strength used in the Weibull distribution can be described assuming that the aging time t_a and the time to failure of the fiber are equivalent.

However, research has shown that the characteristic value of the Weibull distribution μ does not change significantly with environmental exposure [12,13]. Therefore, rather than calculating $\sigma(t)$, it may be assumed that $\mu(t) = \mu(0)$, simplifying Equation 18 to

$$\frac{P(t)}{P_0} = \left[\frac{\delta(t) + L_d(t)}{\delta(0) + L_d(0)}\right]^{-\frac{1}{m}} \tag{25}$$

Predictions were made using experimentally determined $V_f = 0.68$, $d_f = 18$ μm, and $T_0 = 10$°C. It was assumed that $E_f = 73$ GPa for glass fiber and $G_{m\infty} = 1.1$ GPa for vinyl-ester [14]. Predictions are presented in Table 45, comparing the predictions made using Equation 25 to tensile strengths of material exposed to immersion environments prior to post-conditioning.

Table 45. Tensile strength predictions for immersion exposures made using multicomponent degradation model. Brackets indicate standard deviations.

Exposure		**Lengths**		**Tensile Strength (MPa)**	
Temp.	**Time (wk)**	**δ (m)**	**L_d (m)**	**Predicted**	**Experimental**
20°C	12	5.15×10^{-6}	2.62×10^{-3}	1075	1021 [11]
	24	5.15×10^{-6}	2.74×10^{-3}	1070	988 [12]
	36	5.21×10^{-6}	2.81×10^{-3}	1066	976 [19]
	48	5.12×10^{-6}	2.86×10^{-3}	1064	981 [21]
	72	5.14×10^{-6}	2.94×10^{-3}	1061	923 [14]
	96	5.12×10^{-6}	2.99×10^{-3}	1059	912 [20]
40°C	12	4.77×10^{-6}	2.62×10^{-3}	1075	873 [15]
	24	4.84×10^{-6}	2.74×10^{-3}	1070	818 [21]
	36	4.71×10^{-6}	2.81×10^{-3}	1066	777 [22]
	48	4.76×10^{-6}	2.86×10^{-3}	1064	750 [10]
	72	4.78×10^{-6}	2.94×10^{-3}	1061	681 [20]
	96	4.73×10^{-6}	2.99×10^{-3}	1059	621 [15]
60°C	12	4.46×10^{-6}	2.62×10^{-3}	1075	733 [18]
	24	4.47×10^{-6}	2.74×10^{-3}	1070	608 [42]
	36	4.41×10^{-6}	2.81×10^{-3}	1066	571 [33]
	48	4.45×10^{-6}	2.86×10^{-3}	1064	530 [42]
	72	4.41×10^{-6}	2.94×10^{-3}	1061	461 [23]
	96	4.46×10^{-6}	2.99×10^{-3}	1059	377 [28]
80°C	12	4.08×10^{-6}	2.62×10^{-3}	1075	438 [32]
	24	4.00×10^{-6}	2.74×10^{-3}	1070	359 [21]
	36	4.04×10^{-6}	2.81×10^{-3}	1066	331 [22]
	48	4.12×10^{-6}	2.86×10^{-3}	1064	273 [6]
	72	4.08×10^{-6}	2.94×10^{-3}	1061	244 [13]
	96	4.12×10^{-6}	2.99×10^{-3}	1059	234 [15]

A major obstacle in implementing this degradation model lies in the relative magnitudes of δ and L_d, as seen in Table 45. The debond length provided in [10] indicates that $L_d \sim 10^{-3}$ m while $\delta \sim 10^{-6}$ m. Therefore, the changes in G_m calculated using Equation 23 will result in changes in δ which have little effect on the value of $\delta + L_d$. In other words, Equation 21 describing $L_d(t)$ governs the outcome of Equation 25. Table 45 reveals that because the subtle changes in δ do not affect $\delta + L_d$, the predicted strengths are the same for all environments and vary only with time. This uniformity is also a consequence of the fact that κ and λ values are provided for 95°C water immersion only and are assumed to hold for all immersion temperatures.

While implementation of this model would allow for accelerated testing to be performed through DMTA tests, the multicomponent degradation model does not successfully model the degradation of the glass fiber composite in a series of environments.

7.8 Predictions

Because it is highly desirable to use predictive modeling in civil structure design, the results of most importance for degradation models are those for in-service environments. While in-service conditions will naturally be time variant, a worst case scenario of constant exposure to liquid water at 20°C could be assumed. It is further possible that conditions close to 99%RH at 40°C may temporarily occur in hot, humid environments. It is encouraging that exposure at 50%RH or less does not result in significant degradation of the E-glass/vinyl-ester composite under consideration here.

Previous analysis [15] has indicated that exposure conditions of 45°C and 85%RH should provide adequate representation of the most aggressive worldwide environmental conditions. Because there is no 85%RH environment considered in this study, exposure to 75%RH at 60°C shall be taken as an adequate representation of a humid environment near 85%RH.

Predictive degradation curves through 75 years are presented in Figure 196 through Figure 204, illustrating the predictions for wet material properties after exposure to 20°C immersion, 40°C at 99%RH, and 60°C at 75%RH. Figure 205 through Figure 213 present the same plots through 3 years. Standard deviations in Figure 196 through Figure 204 are smaller than the markers used to plot results.

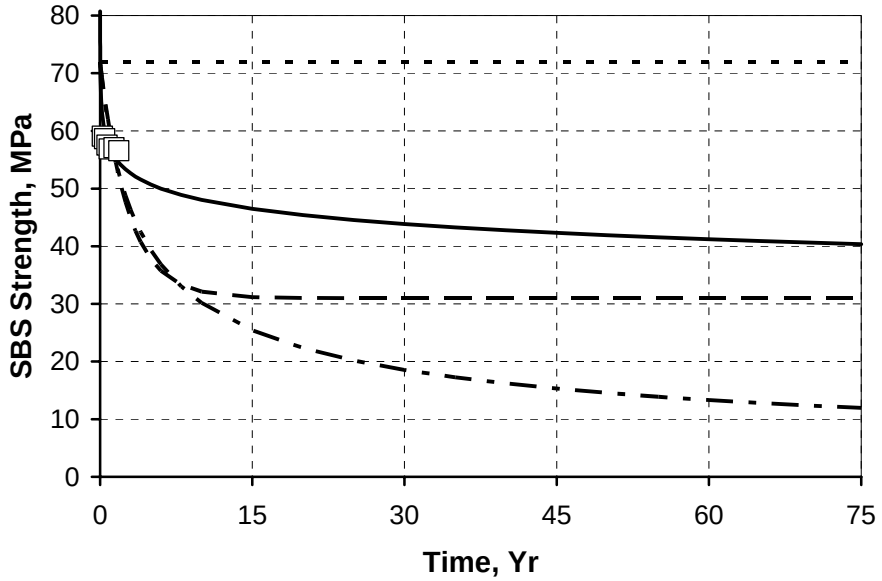

Figure 196. Predictions of SBS strength for immersion at 20°C through 75 yrs.
□: Experimental, - - : initial, ——: Arrhenius rate degradation model,
— — : TTS, — - : crack propagation degradation model.
Error bars indicate standard deviations.

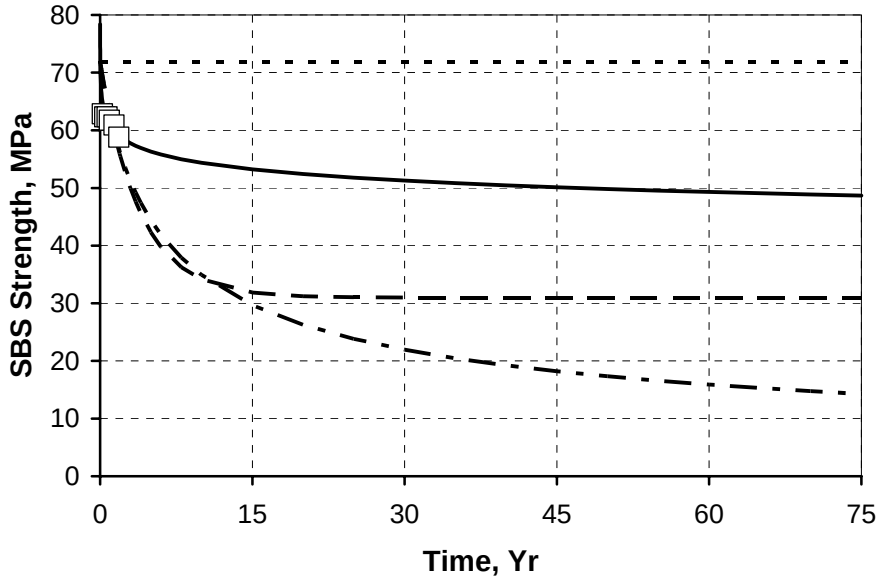

Figure 197. Predictions of SBS strength for 99%RH at 40°C through 75 yrs.
□: Experimental, - - : initial, ——: Arrhenius rate degradation model,
— — : TTS, — - : crack propagation degradation model.
Error bars indicate standard deviations.

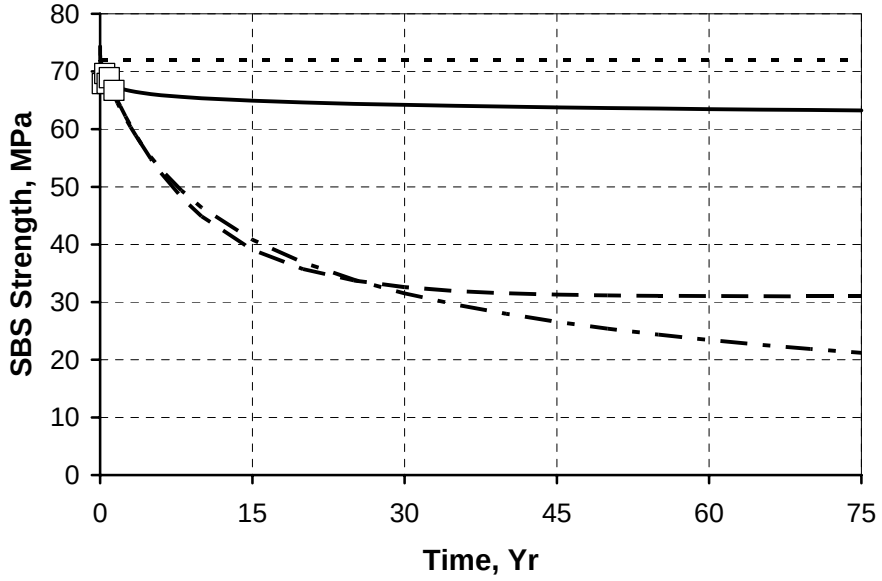

Figure 198. Predictions of SBS strength for 75%RH at 60°C through 75 yrs.
□: Experimental, - - : initial, ——: Arrhenius rate degradation model,
— — : TTS, — - : crack propagation degradation model.
Error bars indicate standard deviations.

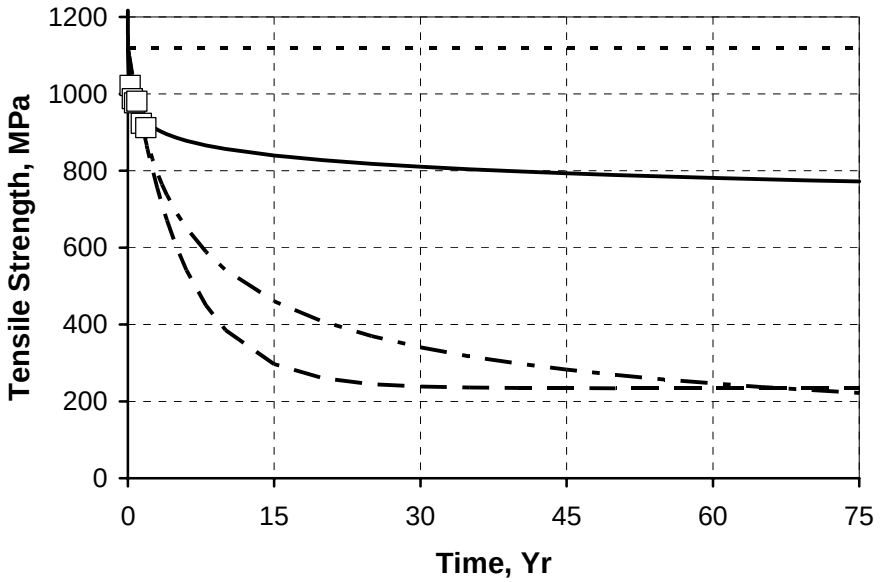

Figure 199. Predictions of tensile strength for immersion at 20°C through 75 yrs.
□: Experimental, - - : initial, ——: Arrhenius rate degradation model,
— — : TTS, — - : crack propagation degradation model.
Error bars indicate standard deviations.

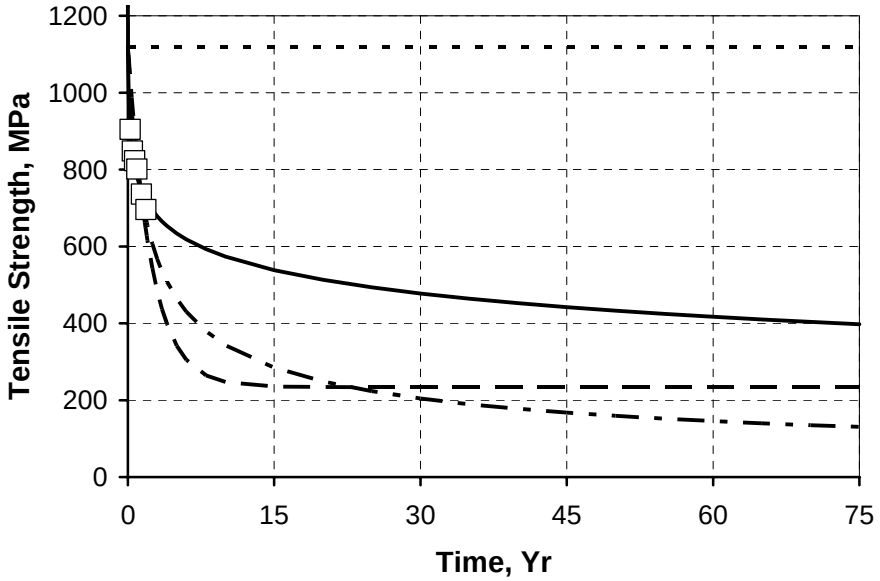

Figure 200. Predictions of tensile strength for 99%RH at 40°C through 75 yrs.
□: Experimental, - - : initial, ——: Arrhenius rate degradation model,
— — : TTS, — - : crack propagation degradation model.
Error bars indicate standard deviations.

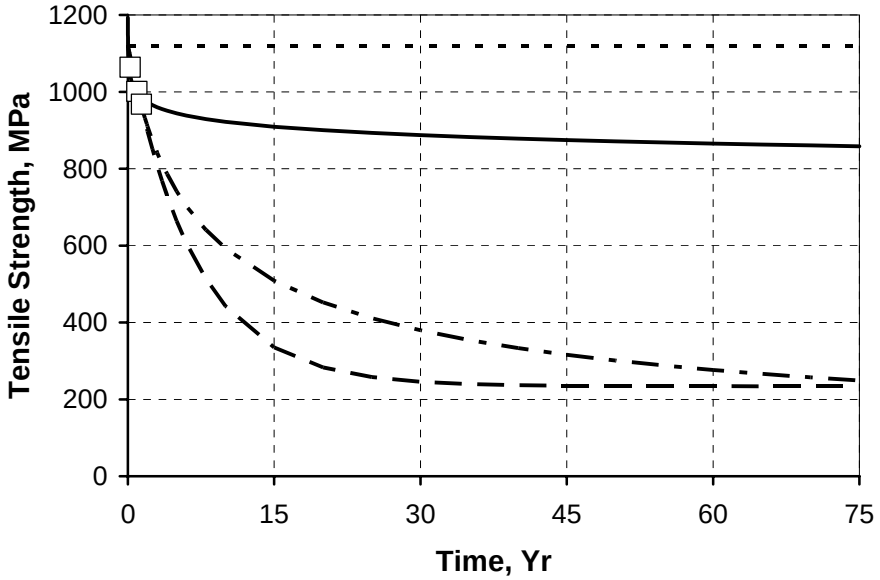

Figure 201. Predictions of tensile strength for 75%RH at 60°C through 75 yrs.
□: Experimental, - - : initial, ——: Arrhenius rate degradation model,
— — : TTS, — - : crack propagation degradation model.
Error bars indicate standard deviations.

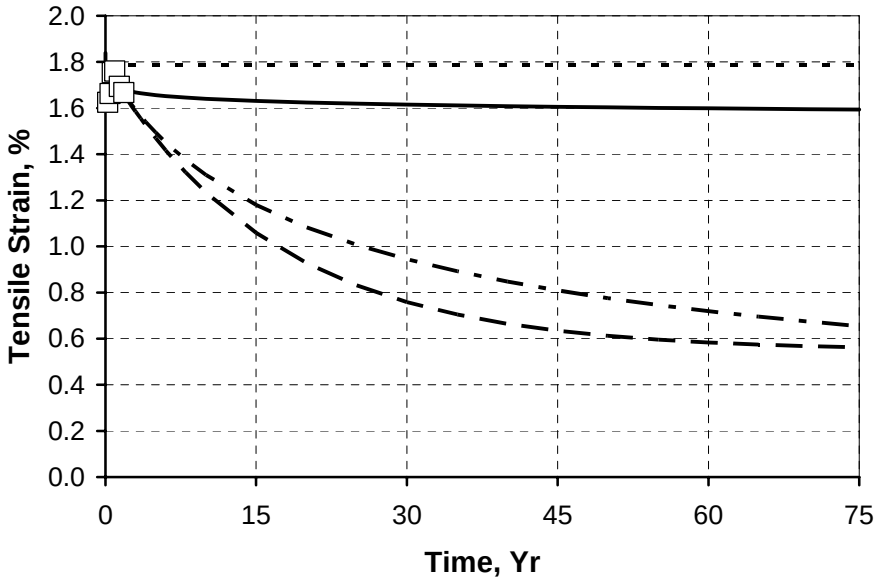

Figure 202. Predictions of tensile strain for immersion at 20°C through 75 yrs.
□: Experimental, - - : initial, ——: Arrhenius rate degradation model,
— — : TTS, — - : crack propagation degradation model.
Error bars indicate standard deviations.

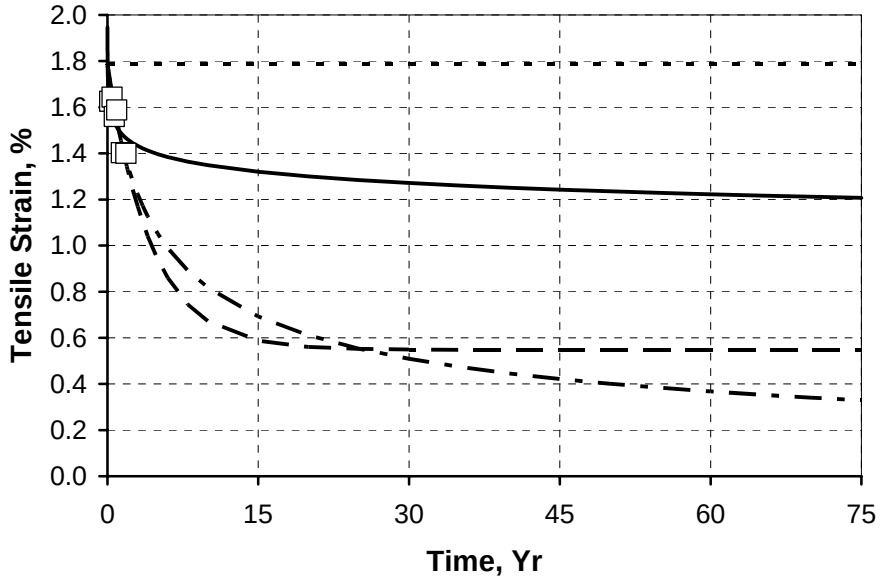

Figure 203. Predictions of tensile strain for 99%RH at 40°C through 75 yrs.
□: Experimental, - - : initial, ——: Arrhenius rate degradation model,
— — : TTS, — - : crack propagation degradation model.
Error bars indicate standard deviations.

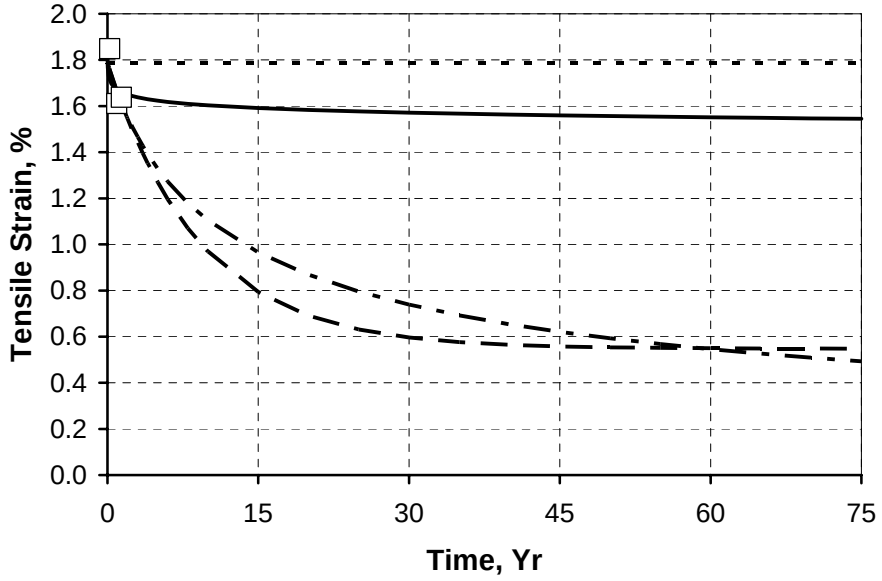

Figure 204. Predictions of tensile strain for 75%RH at 60°C through 75 yrs.
□: Experimental, - - : initial, ——: Arrhenius rate degradation model,
— — : TTS, — - : crack propagation degradation model.
Error bars indicate standard deviations.

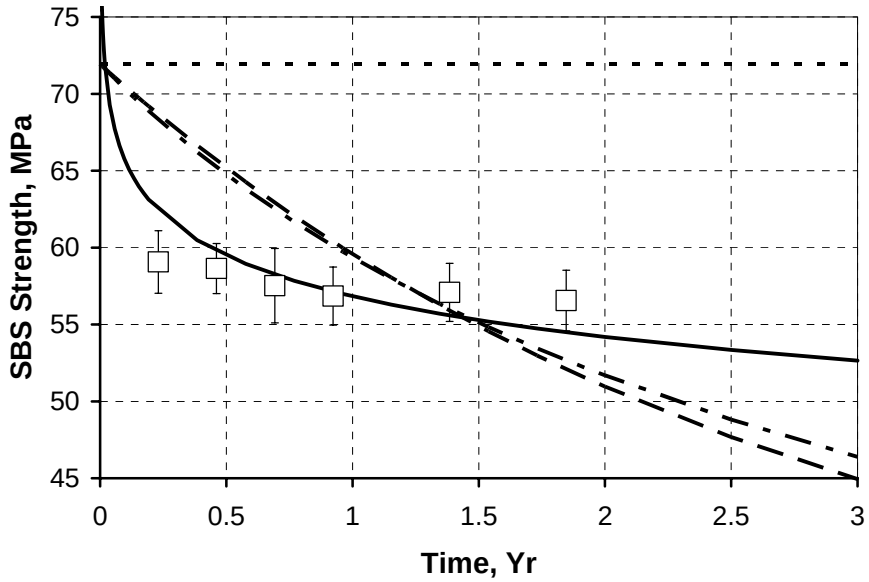

Figure 205. Predictions of SBS strength for immersion at 20°C through 3 yrs.
□: Experimental, - - : initial, ——: Arrhenius rate degradation model,
— — : TTS, — - : crack propagation degradation model.
Error bars indicate standard deviations.

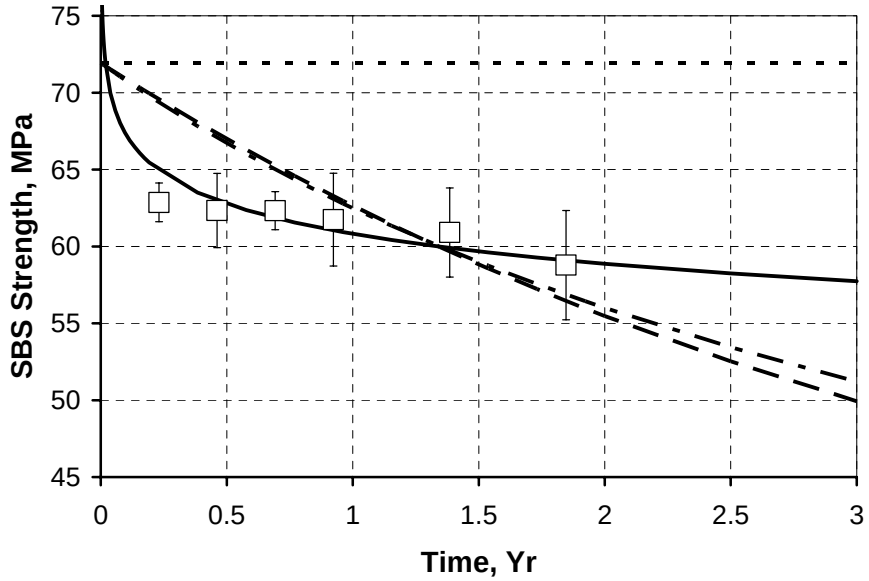

Figure 206. Predictions of SBS strength for 99%RH at 40°C through 3 yrs.
□: Experimental, - - : initial, ——: Arrhenius rate degradation model,
— — : TTS, — - : crack propagation degradation model.
Error bars indicate standard deviations.

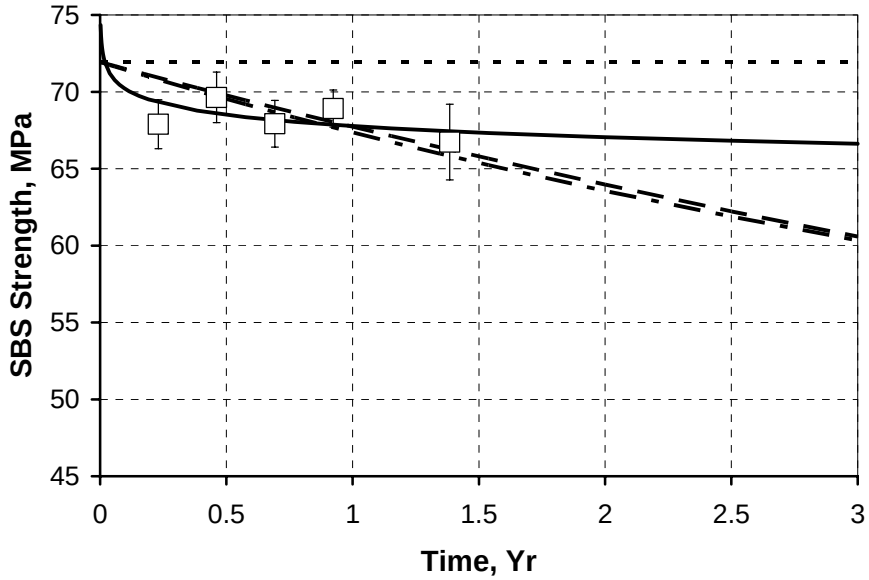

Figure 207. Predictions of SBS strength for 75%RH at 60°C through 3 yrs.
□: Experimental, - - : initial, ——: Arrhenius rate degradation model,
— — : TTS, — - : crack propagation degradation model.
Error bars indicate standard deviations.

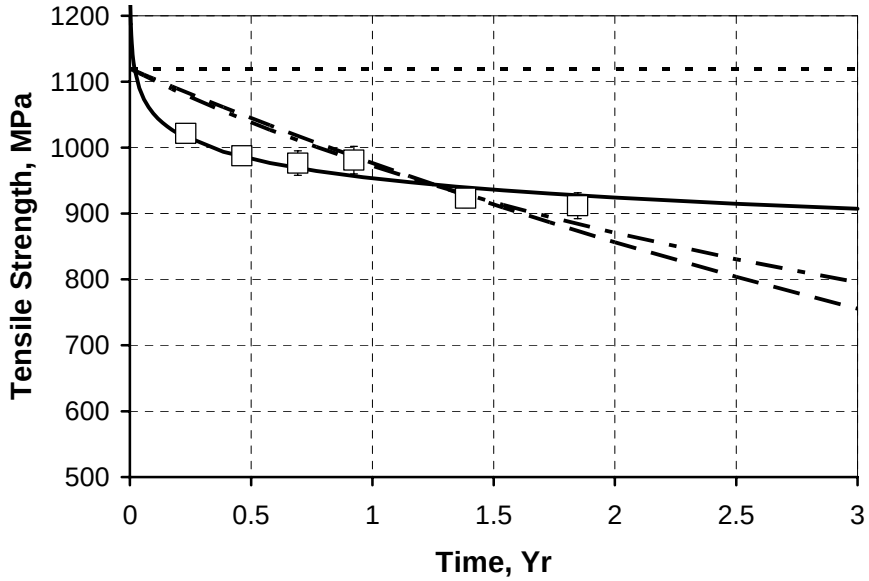

Figure 208. Predictions of tensile strength for immersion at 20°C through 3 yrs.
□: Experimental, - - : initial——: Arrhenius rate degradation model,
— — : TTS, — - : crack propagation degradation model.
Error bars indicate standard deviations.

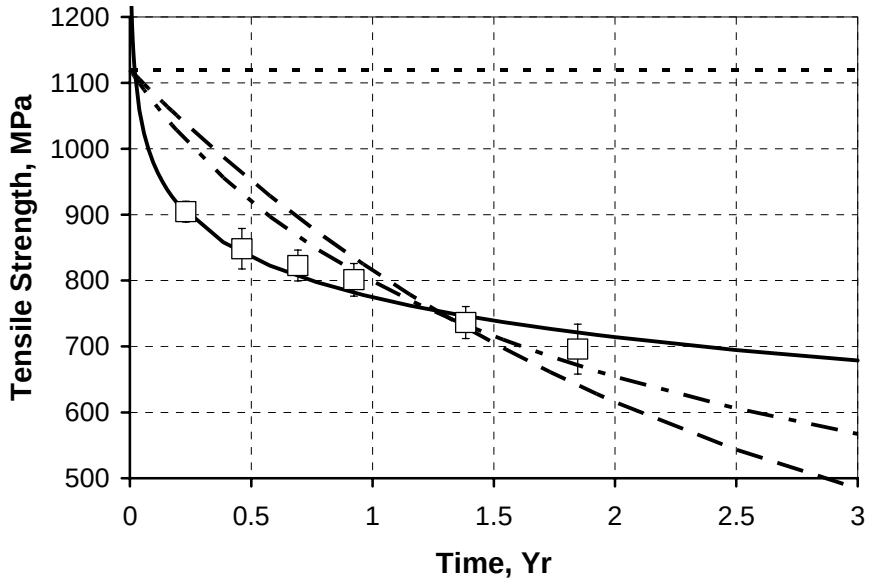

Figure 209. Predictions of tensile strength for 99%RH at 40°C through 3 yrs.
□: Experimental, - - : initial, ——: Arrhenius rate degradation model,
— — : TTS, — - : crack propagation degradation model.
Error bars indicate standard deviations.

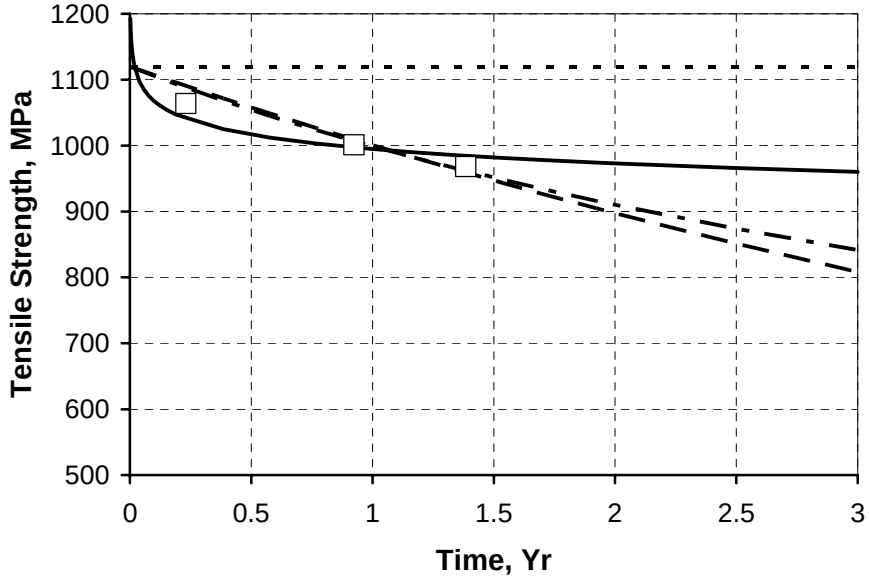

Figure 210. Predictions of tensile strength for 75%RH at 60°C through 3 yrs.
□: Experimental, - - : initial, ——: Arrhenius rate degradation model,
— — : TTS, — - : crack propagation degradation model.
Error bars indicate standard deviations.

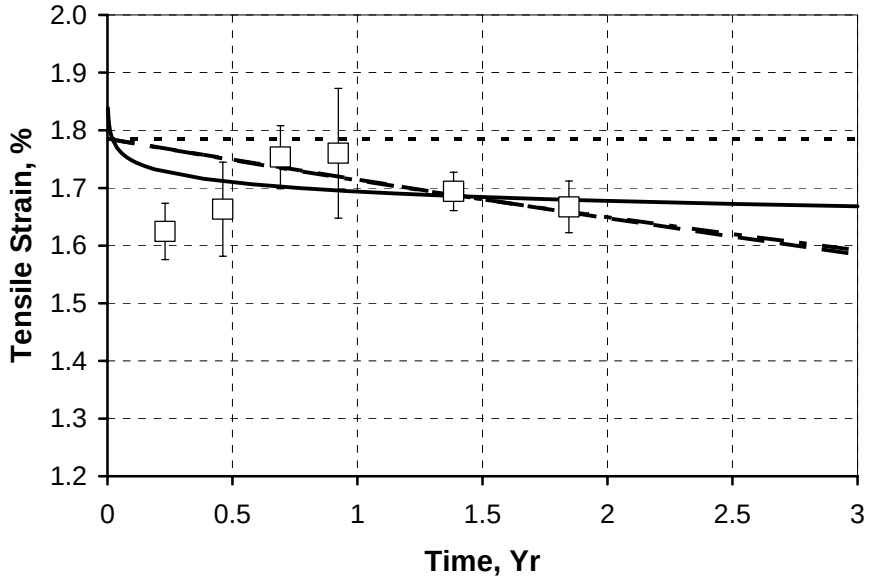

Figure 211. Predictions of tensile strain for immersion at 20°C through 3 yrs.
□: Experimental, - - : initial, ——: Arrhenius rate degradation model,
— — : TTS, — - : crack propagation degradation model.
Error bars indicate standard deviations.

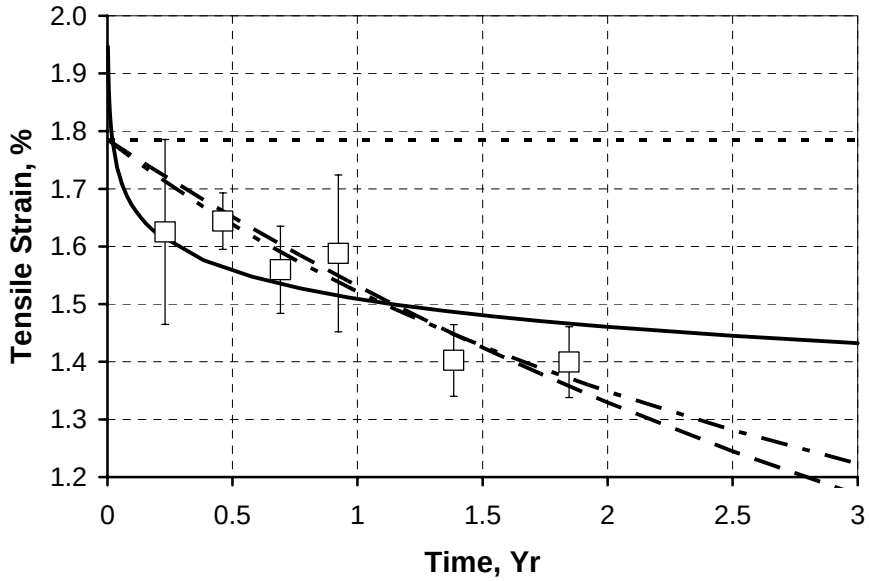

Figure 212. Predictions of tensile strain for 99%RH at 40°C through 3 yrs.
□: Experimental, - - : initial, ——: Arrhenius rate degradation model,
— — : TTS, — - : crack propagation degradation model.
Error bars indicate standard deviations.

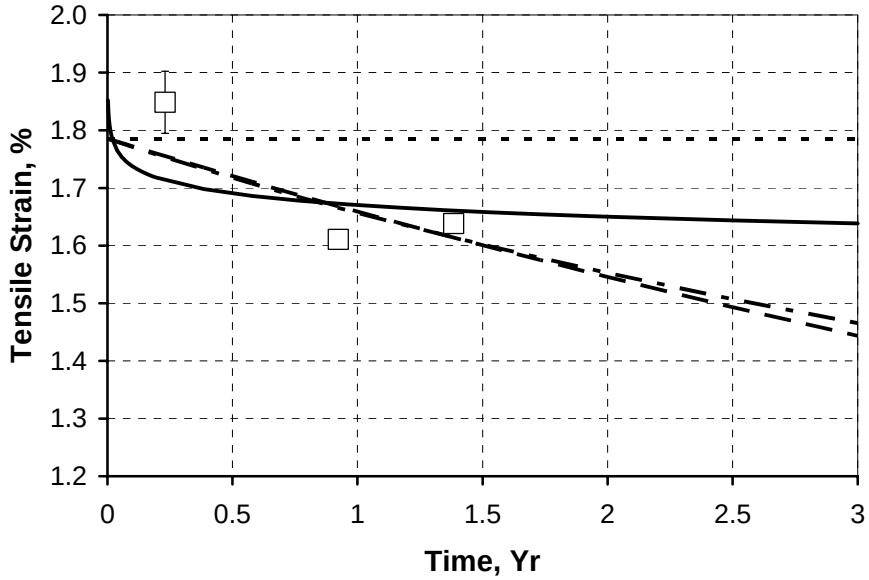

Figure 213. Predictions of tensile strain for 75%RH at 60°C through 3 yrs.
□: Experimental, - - : initial, ——: Arrhenius rate degradation model,
— — : TTS, — - : crack propagation degradation model.
Error bars indicate standard deviations.

Figure 205 through Figure 213 indicate that at early times up through about 1 to 1.5 years, the TTS and crack propagation degradation model tends to be an overestimate of experimental results while the Arrhenius rate degradation model appears to match degradation through these times well. At later times, the TTS and crack propagation model tends to model results more accurately, while the Arrhenius rate degradation model predicts larger values than are observed. It is interesting to note in Figure 196 through Figure 204 that TTS and crack propagation degradation model predict similar tensile strength and failure strain after 75 years, while SBS predictions are much higher using TTS since TTS assumes a non-zero P_{∞}.

In order to compare predictive results, the design code used in ACI-440 will be introduced here [16]. Provided a mean tensile strength $f_{u,ave}$ with standard deviation σ, ACI-440 provides the guaranteed tensile strength f_{fu}* as [16]

$$f_{fu}^{*} = f_{u,ave} - 3\sigma \tag{26}$$

and the design tensile strength f_{fu} as

$$f_{fu} = C_E f_{fu}^{*}, \tag{27}$$

where C_E is an environmental reduction factor dependent on fiber type and in-service environmental conditions. A table of C_E values is provided in Table 46.

Table 46. Environmental reduction factors per ACI-440 [16].

Exposure Condition	Fiber Type	C_E
Not exposed to earth and weather	Carbon	1.0
	Glass	0.8
	Aramid	0.9
Exposed to earth and weather	Carbon	0.9
	Glass	0.7
	Aramid	0.8

For the E-glass/vinyl-ester under consideration here, using baseline values, the guaranteed tensile strength is 988 MPa. For service conditions where contact with earth and water is unlikely, the design tensile strength is 790 MPa while exposure to earth and water requires a design value of 692 MPa. Because most civil applications will require an externally bonded E-glass/vinyl-ester material to be exposed to the elements, the latter design value will be used.

Using the latter design value, which is 62% of the baseline average tensile strength, Table 47 summarizes the time required for a material to reach this design parameter from initial values.

Table 47. Time (yr) to reach ACI-440 design tensile strength for harsh environmental conditions using degradation models.

Exposure condition	Arrhenius rate degradation	TTS	Crack Propagation
20°C Immersion	802	4.0	5.4
40°C 99%RH	3	1.7	1.8
60°C 75%RH	27,000	4.9	6.9

According to Table 47, the most conservative calculation indicates that it would take 1.7 years for the longitudinal tensile strength of the concerned glass composite to reach the specified design value of 692 MPa. That prediction is made for environmental conditions of 40°C and 99%RH, where 1.8 years (96 weeks) of exposure results in a wet tensile strength of 696 [38] MPa. The composite does not reach the specified design strength through 96 weeks exposure to 75%RH at 60°C or 20°C immersion. The Arrhenius rate degradation model clearly underestimates the tensile strength after just two years exposure to this harsh environment.

It can be concluded that implementing the Arrhenius rate degradation model could lead to a significant reduction in the safety factor for a structure in service. It should further be noted that predictions for the time to reach the ACI-440 design value using the Arrhenius rate degradation model are anywhere from 1.7 to 5,500 times larger than the predicted times using the TTS or crack propagation degradation model. It should raise significant concern, however, that the more conservative predictive models implemented here indicate that the E-glass/vinyl-ester composite will take less than 10 years to degrade below its design tensile strength for environments considered in Table 47. These results cannot be corroborated without continued long term testing.

Results presented in Figure 200 and Figure 203 and Table 47 indicate that predictions are more conservative using the TTS degradation model, as opposed to the crack propagation degradation model, for the 99%RH condition at 40°C through the first 25 years of exposure. Using results from 20°C immersion and 60°C and 75%RH exposures, the TTS model remains more conservative through at least 60 years. The TTS model will not, however, predict a material property below the minimum observed in the most harsh environment if that minimum value is used in the derivation of relaxation times. While the TTS based degradation model is generally more conservative through the first couple of decades, it will not allow for a material property to go below that observed in accelerated testing. Therefore, if the TTS is to be implemented, environmental exposures should be selected judiciously for accelerated testing.

A main goal of accelerated testing is to predict the strength of a material through the entirety of a material's service life so that the structure will maintain the design strength for the duration of a structure's service life. To do this, the strength of the material at the end of a specified service life shall be used to establish a reduction factor. Currently, ACI-440 assumes that a glass fiber composite exposed to earth and water will retain 70% of its initial guaranteed strength through its service life, as noted in Table 46.

The service life for a structure may vary, however. Composites used in retrofitting of civil infrastructure are designed for a service life of 35 years. While civil structures are generally designed for a total service life of 50 years, civil

structures are currently seeing service lives of 75 years and should be expected to stay in service through 100 years. Therefore, composites used in civil infrastructure could be designed for a service life of 35 years but may remain in service upwards of 100 years.

The Arrhenius rate, TTS, and crack propagation degradation models are employed here to predict the percent retention of the initial guaranteed strength for this glass fiber composite after 35, 50, 75, and 100 years. Calculations are made using predictive degradation trends obtained for the three environments considered to be representative of worst case in-service conditions. Results are presented in Table 48 through Table 51.

Table 48. Percent retention of guaranteed tensile strength after 35 year service life. Guaranteed tensile strength is 988 MPa.

Exposure condition	Arrhenius rate degradation	TTS	Crack Propagation
20°C Immersion	81.3 %	23.9 %	32.1 %
40°C 99%RH	47.0 %	23.7 %	19.2 %
60°C 75%RH	89.3 %	24.2 %	35.9 %

Table 49. Percent retention of guaranteed tensile strength after 50 year service life. Guaranteed tensile strength is 988 MPa.

Exposure condition	Arrhenius rate degradation	TTS	Crack Propagation
20°C Immersion	79.8 %	23.7 %	27.2 %
40°C 99%RH	43.8 %	23.7 %	16.1 %
60°C 75%RH	88.2 %	23.7 %	30.5 %

Table 50. Percent retention of guaranteed tensile strength after 75 year service life. Guaranteed tensile strength is 988 MPa.

Exposure condition	Arrhenius rate degradation	TTS	Crack Propagation
20°C Immersion	78.1 %	23.7 %	22.4 %
40°C 99%RH	40.2 %	23.7 %	13.2 %
60°C 75%RH	86.9 %	23.7 %	25.2 %

Table 51. Percent retention of guaranteed tensile strength after 100 year service life. Guaranteed tensile strength is 988 MPa.

Exposure condition	Arrhenius rate degradation	TTS	Crack Propagation
20°C Immersion	76.9 %	23.7 %	19.5 %
40°C 99%RH	37.7 %	23.7 %	11.5 %
60°C 75%RH	86.0 %	23.7 %	21.9 %

The TTS degradation model indicates that after just 35 years, the tensile strength will reach 24% of the guaranteed strength for all environmental exposures. The predicted tensile strength is nearly constant after 35 years using this model due to the allowance for a non-zero P_∞ of 24% which is determined from tensile tests of material exposed to the most aggressive environment. Consequently, the TTS model suggests $C_E = 0.24$ should be used rather than 0.7.

Based upon immersion at 20°C and exposure to 75%RH at 60°C, the more conservative crack propagation degradation model indicates that a $C_E = 0.2$ would be appropriate, while the Arrhenius rate degradation model suggests $C_E = 0.8$. It is worth noting that the Arrhenius rate degradation model results in a C_E which is actually higher than that that recommended by ACI-440. However, results also indicate that the Arrhenius rate degradation model is non-conservative.

40°C exposure at 99%RH indicate that the design strength should be 12% or 38% the guaranteed strength using the crack propagation and Arrhenius rate degradation models, respectively. This accelerated test environment will be more aggressive than field conditions since constant exposure to 99%RH at 40°C is not expected.

While use of the Arrhenius rate degradation model would demand a lower design strength, it may result in non-conservative design values. The time temperature superposition model results in a more conservative C_E based upon the lowest tensile strength observed in accelerated testing and could require as much as three times as much material. The more conservative $C_E = 0.24$ determined using the TTS degradation model is recommended for use in composite design. However, it is important to note that the calculation of the recommended lower design factor is fundamentally dependent upon the lowest tensile strength observed in environmental testing, P_∞, and the guaranteed tensile strength. Therefore, the C_E may vary between material systems or accelerated test programs, where more or less aggressive environments may be used. If the standard 60°C immersion environment used for accelerated testing is employed to determine the reduction factor, then $C_E = 0.38$ instead of 0.24.

Because the use of the TTS degradation model results in a much lower C_E than is specified by ACI-440 and because the Arrhenius rate degradation model results in a $C_E > 0.7$ using non-conservative predictions, it is clear that further standardization and execution of accelerated testing is needed to verify C_E for a range of material systems.

This analysis indicates that a value of C_E significantly lower than that recommended by ACI-440 should be used.

7.9 References

1. Litherland, K.L., D.R. Oakley, and B.A. Proctor. "The use of accelerated ageing procedures to predict the long term strength of GRC composites." *Cement and Concrete Research*. Vol. 11 (1981) 455-466.

2. Phani, K.K. and N.R. Bose. "Hydrothermal ageing of CSM-laminate during water immersion – an acousto-ultrasonic study." *Journal of Materials Science*. Vol. 21 (1986) 3633-3637.

3. Purnell, P., N.R. Short, and C.L. Page. "A static fatigue model for the durability of glass fibre reinforced cement." *Journal of Materials Science*. Vol. 26 (2001) 5385-5390.

4. Purnell, P. "Interpretation of climatic temperature variations for accelerated ageing models." *Journal of Materials Science*. Vol. 39 (2004) 113-118.

5. Nissan, A.H. "H-Bond Dissociation in Hydrogen Bond Dominated Solids." *Macromolecules*. Vol. 9, No. 5 (1976) 840-850.

6. Rodriguez, E., M. Larranaga, I. Mondragon, and A. Vazquez. "Relationship between the Network Morphology and Properties of Commercial Vinyl Ester Resins." *J. of Applied Polymer Science*. Vol. 100 (2006) 3895-3903.

7. Apicella, A., C. Migliaresi, L. Nicolais, L. Iaccarino, and S. Roccotelli. "The water aging of unsaturated polyester-based composites: influence of resin chemical structure." *Composites*. Vol. 14, No. 4 (1983) 387-392.

8. Mijovic, J. and H. Zhang. "Molecular Dynamics Simulation Study of Motions and Interactions of Water in a Polymer Network." *J. Phys Chem. B.* Vol. 108 (2004) 2557-2563.

9. Antoon, M.K., J.L. Koenig, and T. Serafini. "Fourtier-Transform Infrared Strudy of the Reversible Interaction of Water and a Crosslinked Epoxy Matrix." *Journal of Polymer Science*. Vol. 19 (1981) 1567-1575.

10. Barbero, E.J. and T.M. Damiani. "Phenomenological Prediction of tensile Strength of E-glass Composites." *Journal of Reinforced Plastics and Composites*. Vol. 22, No. 4 (2003) 373-394.

11. Beltzer, A.I., M. Piau, and Y. Weitsman. "Note on the ineffective length of a fiber." *Mechanics of Materials*. Vol. 13, No. 4 (1992) 285-294.

12. Gao, S.L., E. Maeder, A. Abdkader, and P. Offermann. "Environmental resistance and mechanical performance of alkali-resistant glass fibers with surface sizings." *Jounral of Non-Crystalline Solids*. Vol. 325 (2003) 230-241.

13. Brown, E.N., A.K. Davis, K.D. Jonnalagadda, and N.R. Sottos. "Effect of surface treatment on the hydrolytic stability of E-glass fiber bundle tensile strength." *Composites Science and Technology*. Vol. 65 (2005) 129-136.

14. Daniel, I.M. and O. Ishai. "Engineering Mechanics of Composite Materials." Oxford University Press: New York, 2006.

15. Collings, T.A. "The effect of observed climatic conditions on the moisture equilibrium level of fibre-reinforced plastics." *Composites*. Vol. 17, No. 1 (1986) 33-41.

16. ACI-440.2R-02. *Guide to the Design and Construction of Externally Bonded FRP Systems for Strengthening Concrete Structures*. American Concrete Institute: Farmington Hills, MI, 2002.

8. Conclusions

Hot water immersion accelerated testing of a model E-glass/vinyl-ester composite has been performed and complemented with environmental testing in static, humid environments at the same temperatures. Short beam shear (SBS) testing and dynamic mechanical thermal analysis (DMTA) were conducted concurrent with tensile testing in order to gain an understanding of the modes of moisture degradation which are responsible for decreases in tensile strength. Predictive degradation models were applied to tensile strengths obtained through 96 weeks where degradation led to tensile strengths beyond baseline scatter. The Arrhenius rate degradation model resulted in non-conservative strength predictions for lower temperatures of exposure at late times while the time temperature superposition (TTS) model predicted non-conservative values at early times.

It was found that plasticization was most significant in immersion environments but could be detected in humid environments as low as 50%RH. Plasticization led to reversible decreases in tensile strength. Interfacial debonding was detected through increases in the DMTA tanδ peak heights and was found to lead to irreversible decreases in tensile strength.

Irreversible degradation or pitting of the glass fiber reinforcement was observed in 99%RH and immersion conditions at 60°C and 80°C. In material exposed to 80°C immersion, fiber pitting was localized adjacent to kaolin particulate filler in the vinyl-ester matrix. Kaolin, a hydrous alumina silicate, may slow down initial

degradation but shows clear indications of aggravating the fiber pitting process. The filler's hydrophilic nature provides high energy sites where pitting initiation is more favorable and leads to degradation of the matrix as the bond between the polymer matrix and kaolin filler itself deteriorates. While kaolin clay may be an effective processing aid, these results suggest that further study is required to address whether kaolin filler content accelerates the degradation process of a glass fiber composite in moist environments.

Hydrolysis could also be detected in material exposed to 40°C and 60°C in 99%RH and water immersion. Post-conditioning of material exposed to 40°C and 60°C environments resulted in partial recovery of changes in the rubbery modulus indicating that the hydrolyzed species may have experienced a condensation reaction.

A matrix dominated strengthening effect was detected through increases in SBS strengths observed at 40°C and 60°C, where increases in the glass transition temperature, T_g. These results indicated a increase in matrix and interfacial bond strength which occurs at elevated temperatures at all humidity levels and in immersion environments. The strengthening effect could not be detected in fiber dominated longitudinal tensile testing.

Tightening of the polymer network was evident in gravimetric observations, as well. At 60°C in 18%RH, weight loss was observed, possibly due to leaching of LMWS or residual moisture content not removed in pre-conditioning, leading to a stiffening of the polymer network. In 50%RH at 60°C, moisture uptake demonstrated a Fickian trend at early times, followed indications of weight loss, attributed to

leaching of LMWS, and then a slight weight gain, possibly due to further moisture uptake in the polymer network where relaxation of the polymer structure occurs at elevated temperature. Similar behavior was observed in 75%RH at the same temperature, though only weight loss was observed after apparent equilibrium. Relaxation of the polymer network in 75%RH at 60°C could not be detected through gravimetric observations.

At 40°C in 18%RH, a gradual weight gain was observed over 96 weeks, indicating slight polymer relaxation. At 50%RH and 40°C, a linearly asymptotic trend after pseudo-equilibrium was reached indicated relaxation which was more significant in the 40°C environment where there was less leaching of LMWS. Relaxation was not observed in 20°C exposures at low and medium humidities.

Exposure to 99%RH and immersion environments at 20°C, 40°C, 60°C, and 80°C resulted in apparent equilibrium moisture uptake at 60°C and 80°C only. Two stage moisture sorption was observed in 60°C immersion and 99%RH environments only, beginning around 18 weeks. These environments also demonstrated a transition in degradation mode from strengthening and reversible plasticization at 12 weeks to irreversible degradation of the matrix and fiber reinforcement from 24 weeks on. Results for material exposed to 60°C indicate that there is also a transition in diffusion mechanisms between 75%RH and 99%RH, but this threshold for this transition could not be identified since no humidities were considered within that range.

The moisture uptake trends in these room temperature environments could be approximated as Fickian in 50%RH and 75%RH environments only. Anomalous

behavior was observed in 99%RH and immersion exposures, where 60°C high humidity and immersion demonstrated two stage anomalous sorption. At 60°C and 80°C in 99%RH and immersion, degradation and leaching of degraded species could be detected through apparent moisture uptake trends where a maximum moisture uptake was reached followed by a decrease in weight, indicating the loss of degraded material to these environments was greater than the uptake of water. Leaching of degraded material was much more severe in immersion environments than in 99%RH exposures.

Structural modification diffusion theory was used to model non-Fickian behavior for all environmental conditions. The structural modification factor successfully accounted for relaxation phenomena as wells as leaching of LMWS such as unpolymerized styrene and degraded material after Fickian dominated diffusion no longer dominated.

Freundlich's relation was determined to be the most adequate isotherm available, despite its theoretical constraints. While Freundlich's relation is derived for an adsorbed monolayer, it is one of the few isotherms which allows for an isotherm which describes an increasing M_{max} with increasing vapor pressure where the slope of the isotherm also increases with partial pressure. The isotherm could not, however, address the discrepancy between equilibrium moisture contents in 99%RH and immersion environments, also known as Schroeder's paradox.

Differences between 99%RH and immersion exposures could be detected beyond equilibrium contents through mechanical testing and DMTA. While

experimental results were similar for these high humidity and immersion exposures, subtle differences could be identified and are summarized in Table 52.

Table 52. Summary of phenomena observed in 99%RH and immersion environments.

Environment	99%RH	Immersion
Larger diffusion coefficients		×
Greater M_{max}		×
Greater leaching of degraded material		×
Greater interfacial debonding (using SBS strengths and tanδ peak height)		×
Greater strengthening effect		×
Greater loss in tensile strength with time		×
Greater loss in tensile strain with time		×
Greater loss in SBS strength with time		×
Higher degradation rate parameters		×
Greater activation energies (diffusion and degradation rates)	×	

Degradation models were used to predict the tensile strength of the mode E-glass/vinyl-ester composite through a series of possible service lives. Composites in civil infrastructure are primarily used as retrofits which are designed for 35 year service lives. Bridges are designed for a 50 year service life, even as they are seeing actual service lives in the range of 75 to 100 years. Predictive degradation models were only applied to the degradation of tensile strengths for material exposed to 75%RH and above. Exposure to 18%RH and 50%RH resulted in tensile properties which remained within initial scatter for 96 weeks.

The Arrhenius rate degradation model was found to be non-conservative through the conclusion of 96 weeks of testing while the crack propagation and time temperature superposition degradation models were non-conservative through the first year of testing. Predictions made by the crack propagation and TTS degradation models were more accurate at later times than predictions made using the Arrhenius

rate degradation model. However, the crack propagation and TTS models were more conservative than the Arrhenius rate model, leading to lower environmental degradation reduction factors C_E than are recommended by ACI-440. ACI-440 recommends $C_E = 0.7$ for outdoor exposure of glass fiber composites. Using the recommended TTS model, it was determined that $C_E = 0.24$ is more appropriate than $C_E = 0.7$. It is important to note that the C_E calculated using TTS is determined by the lowest tensile strength observed in environmental testing. Additional environmental tests may lead to a higher C_E if less aggressive environments are used. Ultimately, the predictions of degradation models can only be verified through further environmental testing.

In general, exposure to field conditions of 50%RH and lower should allow for a long service life. Interfacial degradation and hydrolysis seen in the single 75%RH environment considered shows cause for concern and requires further attention in future studies. High humidity service conditions near 99%RH may result in a service life as low as 4 or 5 years at 20°C, as determined through predictive degradation models fit to available data. Exposure to liquid water leads to leaching of degraded material, resulting in lower material strengths. Prolonged contact with water should be avoided in order to reduce this leaching.

Future work should concentrate on degradation mechanisms resulting from exposure to relative humidities above 50%RH in the range of 75%RH. There appears to be a transition in degradation modes between 75%RH and 99%RH, and identification of this threshold would contribute to a greater understanding of

degradation mechanisms of glass composites in humid and liquid water environments. Monitoring the degradation of tensile strengths observed in higher humidity environments would allow for the implementation of available degradation models which account for the effects of relative humidity.

Appendix A. Summary of Diffusion Results

A.1 Fickian Diffusion Parameters

Table A.1. Fickian diffusion parameters for moisture specimens using apparent moisture trends.

Env.	M_∞ (%)	D (10^{-8} mm^2/s)
2L	0.033	0.46
4L	0.032	0.28
6L	- 0.014	8.64
2M	0.057	5.89
4M	0.060	26.8
6M	0.074	48.7
6X	0.148	78.7
2H	0.269	2.19
4H	0.666	2.28
6H	0.894	2.50
8H	1.229	6.07
2I	0.393	1.35
4I	0.586	3.40
6I	0.846	3.97
8I	0.998	12.8

Table A.2. Fickian diffusion parameters for moisture specimens using adjusted moisture trends.

Env.	M_∞ (%)	D (10^{-8} mm^2/s)
2H	1.468	0.032
4H	1.468	0.170
6H	1.468	0.846
8H	1.468	3.74
2I	2.068	0.031
4I	2.068	0.102
6I	2.068	0.259
8I	2.068	0.990

Table A.3. Fickian diffusion parameters for SBS specimens using apparent moisture trends.

Env.	M_∞ (%)	D (10^{-8} mm^2/s)
2L	0.040	0.64
4L	0.046	0.60
6L	- 0.025	66.3
2M	0.066	3.08
4M	0.090	14.0
6M	0.066	110
6X	0.132	142
2H	0.223	5.48
4H	0.732	2.44
6H	0.631	10.7
8H	1.038	13.6
2I	0.443	1.46
4I	0.682	3.61
6I	0.647	11.8
8I	0.843	30.4

Table A.4. Fickian diffusion parameters for SBS specimens using adjusted moisture trends.

Env.	M_∞ (%)	D (10^{-8} mm^2/s)
2H	1.362	0.04
4H	1.362	0.28
6H	1.362	1.26
8H	1.362	7.09
2I	1.945	0.05
4I	1.945	0.15
6I	1.945	0.68
8I	1.945	4.74

Table A.5. Fickian diffusion parameters for DMTA specimens using apparent moisture trends.

Env.	M_∞ (%)	D (10^{-8} mm^2/s)
2L	0.031	0.14
4L	0.015	0.96
6L	- 0.025	19.9
2M	0.061	3.84
4M	0.080	11.5
6M	0.057	95.9
6X	0.131	108
2H	0.231	2.75
4H	0.700	2.95
6H	0.614	10.7
8H	1.169	8.29
2I	0.483	1.12
4I	0.712	2.54
6I	0.684	9.16
8I	1.080	17.9

Table A.6. Fickian diffusion parameters for DMTA specimens using adjusted moisture trends.

Env.	M_∞ (%)	D (10^{-8} mm^2/s)
2H	1.448	0.03
4H	1.448	0.22
6H	1.448	1.04
8H	1.448	5.17
2I	1.845	0.06
4I	1.845	0.16
6I	1.845	0.70
8I	1.845	3.81

Table A.7. Fickian diffusion parameters for tension specimens using apparent moisture trends.

Env.	M_∞ (%)	D (10^{-8} mm^2/s)
2L	0.049	7.88
4L	0.021	2.52
6L	- 0.097	55.6
2M	0.069	6.16
4M	0.109	8.60
6M	0.087	18.0
6X	0.152	56.4
2H	0.290	2.21
4H	0.520	2.82
6H	0.545	9.41
8H	1.362	4.58
2I	0.372	1.61
4I	0.604	2.58
6I	0.645	7.69
8I	0.990	17.5

Table A.8. Fickian diffusion parameters for tension specimens using adjusted moisture trends.

Env.	M_∞ (%)	D (10^{-8} mm^2/s)
2H	1.529	0.03
4H	1.529	0.12
6H	1.529	0.32
8H	1.529	3.41
2I	2.459	0.02
4I	2.459	0.06
6I	2.459	0.18
8I	2.459	0.97

A.2 Structural Modification Diffusion Parameters

Table A.9. Structural modification diffusion parameters for moisture specimens using apparent moisture trends.

Env.	$M_{o\infty}$ (%)	D (10^{-7} mm^2/s)	k (10^{-4} s$^{-0.5}$)
2L	0.017	0.22	-0.18
4L	0.001	1.48	34.7
6L	- 0.005	2.19	1.36
2M	0.054	0.78	0.01
4M	0.042	5.02	1.30
6M	0.053	8.43	0.49
6X	0.145	8.13	-0.03
2H	0.097	2.06	2.29
4H	0.250	1.62	1.99
6H	0.754	0.52	0.33
8H	1.342	0.49	-0.21
2I	0.187	0.82	1.45
4I	0.413	0.68	0.56
6I	2.374	0.040	-1.17
8I	5.869	0.037	-2.13

Table A.10. Structural modification diffusion parameters for moisture specimens using adjusted moisture trends.

Env.	$M_{o\infty}$ (%)	D (10^{-7} mm^2/s)	k (10^{-4} s$^{-0.5}$)
6H	0.685	0.71	0.67
8H	1.212	0.62	0.35
4I	0.281	1.68	1.93
6I	0.359	2.20	2.85
8I	0.494	4.75	3.98

Table A.11. Structural modification diffusion parameters for SBS specimens using apparent moisture trends.

Env.	$M_{o\infty}$ (%)	D (10^{-7} mm^2/s)	k (10^{-4} s$^{-0.5}$)
2L	0.012	0.002	0.63
4L	0.025	1.38	-0.26
6L	- 0.020	0.54	-0.22
2M	0.053	1.13	0.08
4M	0.039	6.85	1.60
6M	0.050	2.88	0.31
6X	0.112	19.7	0.02
2H	0.096	3.63	2.55
4H	0.357	1.34	1.31
6H	0.879	0.55	0.004
8H	2.180	0.28	-1.13
2I	0.147	1.46	2.72
4I	0.399	1.06	0.96
6I	2.220	0.11	-1.26
8I	2.413	0.31	-1.80

Table A.12. Structural modification diffusion parameters for SBS specimens using adjusted moisture trends.

Env.	$M_{o\infty}$ (%)	D (10^{-7} mm^2/s)	k (10^{-4} s$^{-0.5}$)
4H	0.341	1.02	1.55
6H	0.637	1.32	0.95
8H	0.811	2.33	1.12
2I	0.136	1.97	3.50
4I	0.328	2.05	1.82
6I	0.411	2.34	2.43
8I	0.673	4.58	1.91

Table A.13. Structural modification diffusion parameters for DMTA specimens using apparent moisture trends.

Env.	$M_{o\infty}$ (%)	D (10^{-7} mm^2/s)	k (10^{-4} s$^{-0.5}$)
2L	0.013	0.11	-0.03
4L	0.006	0.09	0.10
6L	- 0.013	6.87	1.48
2M	0.057	1.14	-0.19
4M	0.038	4.62	1.18
6M	0.047	14.0	0.18
6X	0.131	9.67	-0.25
2H	0.138	1.37	0.83
4H	0.280	1.88	2.00
6H	0.786	0.77	0.22
8H	1.528	0.60	-4.76
2I	0.141	2.22	3.12
4I	0.381	1.01	1.12
6I	0.864	0.62	0.89
8I	5.192	0.08	-1.68

Table A.14. Structural modification diffusion parameters for DMTA specimens using adjusted moisture trends.

Env.	$M_{o\infty}$ (%)	D (10^{-7} mm^2/s)	k (10^{-4} s$^{-0.5}$)
4H	0.265	2.11	2.27
6H	0.735	0.83	0.57
8H	1.190	0.88	0.29
2I	0.143	1.54	3.16
4I	0.362	1.12	1.40
6I	0.976	0.63	0.28
8I	0.974	2.19	0.65

Table A.15. Structural modification diffusion parameters for tension specimens using apparent moisture trends.

Env.	$M_{o\infty}$ (%)	D (10^{-7} mm^2/s)	k (10^{-4} s$^{-0.5}$)
2L	0.027	2.58	0.07
4L	- 0.005	3.61	-5.12
6L	- 0.046	58.4	-1.13
2M	0.065	0.56	-0.03
4M	0.040	6.33	1.82
6M	0.048	44.8	0.40
6X	0.139	6.73	0.09
2H	0.102	1.93	2.37
4H	0.285	1.33	1.01
6H	0.416	1.23	1.50
8H	0.982	1.06	0.61
2I	0.123	2.48	2.72
4I	0.345	0.96	0.93
6I	1.851	0.10	-1.03
8I	4.980	0.06	-2.11

Table A.16. Structural modification diffusion parameters for tension specimens using adjusted moisture trends.

Env.	$M_{o\infty}$ (%)	D (10^{-7} mm^2/s)	k (10^{-4} s$^{-0.5}$)
6H	0.433	1.54	1.38
8H	0.680	2.21	2.08
4I	0.251	1.81	2.09
6I	0.551	1.13	1.21
8I	0.581	5.08	3.09

A.3 Two Phase Fickian Diffusion Parameters

Two phase Fickian diffusion was employed for moisture specimens only.

Table A.17. Two Phase Fickian diffusion parameters for moisture specimens using apparent moisture trends.

Env.	M_1 (%)	M_2 (%)	D_1 (10^{-7} mm^2/s)	D_2 (10^{-7} mm^2/s)
2L	0.017	0.016	2.54	0.014
4L	0.009	0.031	59.7	0.366
6L	- 0.005	- 0.016	14.8	0.076
2M	0.054	0.011	7.79	0.0004
4M	0.040	0.049	44.2	0.533
6M	0.053	0.021	79.0	0.536
6X	0.145	0.003	81.6	0.973
2H	0.123	0.145	7.39	0.577
4H	0.257	0.409	8.41	0.511
6H	0.754	0.194	4.92	0.601
8H	1.449	- 0.220	5.75	1.58
2I	0.187	0.206	3.93	0.625
4I	0.413	0.173	5.20	0.649
6I	2.374	- 3.019	1.79	0.307
8I	5.868	-10.645	3.59	0.502

Table A.18. Two Phase Fickian diffusion parameters for moisture specimens using adjusted moisture trends.

Env.	M_1 (%)	M_2 (%)	D_1 (10^{-7} mm^2/s)	D_2 (10^{-7} mm^2/s)
6H	0.685	0.331	5.09	0.709
8H	1.212	0.256	5.24	0.979
4I	0.281	0.428	6.59	0.585
6I	0.359	0.685	8.84	0.809
8I	0.494	1.574	20.2	0.568

A.4 Langmuir Diffusion Parameters

Table A.19. Langmuir diffusion parameters for moisture specimens using apparent moisture trends.

Env.	M_∞ (%)	D (10^{-6} mm^2/s)	α (10^{-8} s^{-1})	β (10^{-8} s^{-1})
2L	0.033	2.73	2.60	12.8
4L	0.032	0.03	2.50	19.7
6L	- 0.021	0.54	1.42	3.58
2M	0.065	0.22	0.71	0.16
4M	0.089	0.98	2.92	2.37
6M	0.074	1.58	4.72	1.62
6X	0.148	1.99	- 0.75	- 0.02
2H	0.269	0.23	3.40	2.92
4H	0.666	0.22	2.51	2.37
6H	0.948	2.04	10.3	42.0
8H	1.229	2.50	23.3	59.5
2I	0.393	1.76	5.21	15.6
4I	0.586	0.37	6.60	6.88
6I	0.845	0.13	- 0.78	- 0.15
8I	0.998	0.53	- 6.42	- 1.31

Table A.20. Langmuir diffusion parameters for moisture specimens using adjusted moisture trends.

Env.	M_∞ (%)	D (10^{-6} mm^2/s)	α (10^{-8} s^{-1})	β (10^{-8} s^{-1})
4H	1.468	0.20	0.49	1.53
6H	1.468	0.29	1.38	2.01
8H	1.468	2.62	15.9	53.1
2I	2.068	0.30	0.21	2.17
4I	2.068	0.22	0.36	1.53
6I	2.068	0.31	0.78	1.96
8I	2.068	0.82	3.76	8.04

Table A.21. Langmuir diffusion parameters for SBS specimens using apparent moisture trends.

Env.	M_∞ (%)	D (10^{-6} mm^2/s)	α (10^{-8} s^{-1})	β (10^{-8} s^{-1})
2L	0.040	5.30	0.09	0.16
4L	0.045	10.7	1.29	3.73
6L	- 0.025	7.30	4.60	14.0
2M	0.066	0.38	3.08	0.58
4M	0.090	15.0	3.46	3.14
6M	0.066	9.05	0.36	0.07
6X	0.132	9.92	2.36	1.30
2H	0.364	0.73	1.00	1.46
4H	0.732	0.25	3.25	2.59
6H	0.908	60.2	16.7	3.34
8H	1.038	0.46	- 11.4	- 0.04
2I	0.443	12.3	5.18	13.0
4I	0.682	0.50	7.46	11.1
6I	0.839	0.31	9.90	12.2
8I	0.843	0.88	- 7.25	- 0.47

Table A.22. Langmuir diffusion parameters for SBS specimens using adjusted moisture trends.

Env.	M_∞ (%)	D (10^{-6} mm^2/s)	α (10^{-8} s^{-1})	β (10^{-8} s^{-1})
4H	1.362	0.20	0.67	1.33
6H	1.362	0.19	0.43	0.19
8H	1.362	1.66	16.3	23.7
2I	1.945	0.56	0.34	2.84
4I	1.945	0.45	0.40	1.20
6I	1.945	0.26	0.48	0.66
8I	1.945	0.43	0.46	0.33

Table A.23. Langmuir diffusion parameters for DMTA specimens using apparent moisture trends.

Env.	M_∞ (%)	D (10^{-6} mm^2/s)	α (10^{-8} s^{-1})	β (10^{-8} s^{-1})
2L	0.031	0.65	2.34	11.7
4L	0.015	31.4	- 0.28	- 0.32
6L	- 0.036	11.2	1.11	1.43
2M	0.061	0.34	- 0.70	- 0.10
4M	0.080	0.51	2.42	1.99
6M	0.057	3.76	- 0.38	- 0.05
6X	0.131	3.00	- 4.35	- 0.09
2H	0.231	0.35	2.90	1.44
4H	0.700	0.55	5.60	10.1
6H	0.910	2.89	12.2	48.7
8H	1.169	1.05	15.8	12.0
2I	0.483	1.51	4.12	10.2
4I	0.712	0.36	4.24	3.98
6I	0.924	0.671	9.60	18.5
8I	1.080	0.674	- 7.41	- 0.33

Table A.24. Langmuir diffusion parameters for DMTA specimens using adjusted moisture trends.

Env.	M_∞ (%)	D (10^{-6} mm^2/s)	α (10^{-8} s^{-1})	β (10^{-8} s^{-1})
6H	1.448	0.44	1.60	2.36
8H	1.448	1.42	12.1	18.6
4I	1.845	0.23	0.42	1.27
6I	1.845	0.16	0.24	0.22
8I	1.845	0.67	1.84	1.88

Table A.25. Langmuir diffusion parameters for tension specimens using apparent moisture trends.

Env.	M_∞ (%)	D (10^{-6} mm^2/s)	α (10^{-8} s^{-1})	β (10^{-8} s^{-1})
2L	0.049	1.39	1.74	205
4L	0.021	0.16	- 0.56	- 0.38
6L	-0.097	82.2	- 2.70	- 1.07
2M	0.069	0.36	- 1.46	0.05
4M	0.109	1.73	1.60	1.70
6M	0.087	0.95	2.00	0.98
6X	0.152	5.48	1.89	0.14
2H	0.290	9.04	7.01	- 44.2
4H	0.520	0.21	4.02	3.58
6H	0.901	0.46	3.65	4.64
8H	1.362	0.27	6.55	2.64
2I	0.372	4.60	5.17	11.2
4I	0.604	0.19	3.28	1.88
6I	0.867	0.83	8.32	14.2
8I	0.990	0.52	- 7.02	- 0.96

Table A.26. Langmuir diffusion parameters for tension specimens using adjusted moisture trends.

Env.	M_∞ (%)	D (10^{-6} mm^2/s)	α (10^{-8} s^{-1})	β (10^{-8} s^{-1})
6H	1.545	0.42	0.96	2.24
8H	1.545	2.30	15.1	66.6
4I	2.459	0.19	0.24	1.30
6I	2.459	0.12	0.12	0.22
8I	2.459	2.97	4.44	25.4

Appendix B. Summary of Mechanical Testing

B.1 Tensile Results

Table B.1. Wet tensile results for 18%RH environments.
Brackets indicate standard deviations.

Exposure Condition	Time (wk)	Strength (MPa)	Modulus (GPa)	Failure Strain (%)
20°C 18%RH	12	1070 [19]	55.0 [2.3]	1.78 [0.04]
	24	1161 [27]	52.4 [3.6]	1.80 [0.07]
	36	1120 [29]	49.8 [3.5]	1.90 [0.12]
	48	1195 [19]	51.7 [1.2]	1.91 [0.04]
	72	1113 [9]	59.6 [1.2]	1.88 [0.03]
	96	1186 [31]	51.1 [2.0]	1.97 [0.08]
40°C 18%RH	12	1067 [13]	51.6 [2.2]	1.76 [0.001]
	24	1152 [21]	49.7 [2.3]	1.93 [0.08]
	36	1137 [44]	51.1 [2.8]	1.91 [0.08]
	48	1130 [40]	50.2 [3.2]	1.84 [0.10]
	72	1099 [31]	52.2 [1.2]	1.79 [0.02]
	96	1136 [47]	52.0 [1.9]	1.89 [0.07]
60°C 18%RH	12	1099 [89]	50.4 [2.4]	1.89 [0.10]
	24	1126 [49]	48.8 [2.1]	1.94 [0.08]
	36	1137 [28]	50.6 [1.1]	1.92 [0.05]
	48	1131 [24]	50.2 [2.7]	1.93 [0.09]
	72	1155 [22]	49.5 [3.5]	1.84 [0.13]
	96	1107 [32]	51.0 [2.0]	1.85 [0.06]

Table B.2. Wet tensile results for 50%RH and 75%RH environments. Brackets indicate standard deviations.

Exposure Condition	Time (wk)	Strength (MPa)	Modulus (GPa)	Failure Strain (%)
20°C 50%RH	12	1040 [30]	58.1 [3.2]	1.61 [0.07]
	24	1054 [33]	52.2 [2.7]	1.53 [0.08]
	36	1093 [22]	50.2 [2.1]	1.84 [0.07]
	48	1153 [17]	52.2 [1.8]	1.86 [0.05]
	72	1084 [27]	50.2 [1.0]	1.83 [0.02]
	96	1123 [11]	50.1 [2.9]	1.91 [0.09]
40°C 50%RH	12	1075 [10]	52.9 [3.6]	1.76 [0.05]
	24	1107 [13]	48.7 [3.6]	1.89 [0.12]
	36	1121 [47]	51.9 [1.8]	1.85 [0.04]
	48	1133 [19]	50.6 [1.5]	1.83 [0.04]
	72	1107 [23]	51.4 [2.1]	1.77 [0.07]
	96	1096 [16]	50.8 [0.5]	1.84 [0.01]
60°C 50%RH	12	1086 [21]	48.0 [2.7]	1.94 [0.09]
	24	1112 [23]	48.4 [2.3]	1.88 [0.08]
	36	1084 [17]	51.8 [2.9]	1.84 [0.08]
	48	1058 [23]	47.6 [2.9]	1.91 [0.07]
	72	1064 [33]	51.4 [1.3]	1.70 [0.05]
	96	1082 [20]	51.7 [1.8]	1.81 [0.05]
60°C 75%RH	12	1064 [1]	47.1 [1.8]	1.85 [0.05]
	48	1001 [19]	50.0 [0.5]	1.61 [0.04]
	72	968 [30]	52.0 [1.8]	1.64 [0.04]

Table B.3. Wet tensile results for 99%RH environments.
Brackets indicate standard deviations.

Exposure Condition	Time (wk)	Strength (MPa)	Modulus (GPa)	Failure Strain (%)
20°C 99%RH	12	974 [32]	53.8 [2.7]	1.62 [0.08]
	24	992 [23]	54.3 [1.5]	1.48 [0.08]
	36	969 [51]	49.4 [3.1]	1.74 [0.09]
	48	985 [35]	51.3 [1.7]	1.69 [0.04]
	72	918 [17]	49.4 [3.6]	1.67 [0.10]
	96	934 [15]	50.9 [2.6]	1.68 [0.07]
40°C 99%RH	12	905 [16]	48.5 [3.1]	1.63 [0.16]
	24	848 [31]	48.0 [1.4]	1.64 [0.05]
	36	823 [23]	49.8 [2.8]	1.56 [0.08]
	48	801 [25]	46.1 [3.9]	1.59 [0.14]
	72	736 [24]	51.1 [2.7]	1.40 [0.06]
	96	696 [38]	50.8 [1.8]	1.40 [0.06]
60°C 99%RH	12	760 [9]	49.5 [2.7]	1.39 [0.06]
	24	655 [44]	48.1 [4.3]	1.39 [0.08]
	36	622 [12]	49.0 [2.3]	1.32 [0.06]
	48	577 [37]	48.9 [1.5]	1.25 [0.05]
	72	515 [36]	50.4 [0.9]	1.09 [0.05]
	96	456 [28]	49.6 [1.8]	0.96 [0.06]
80°C 99%RH	12	427 [10]	46.4 [1.7]	0.94 [0.01]
	48	294 [15]	46.9 [2.0]	0.66 [0.04]
	72	277 [8]	52.5 [3.3]	0.56 [0.02]

Table B.4. Wet tensile results for immersion environments.
Brackets indicate standard deviations.

Exposure Condition	Time (wk)	Strength (MPa)	Modulus (GPa)	Failure Strain (%)
20°C Immersion	12	1021 [11]	52.5 [2.5]	1.62 [0.05]
	24	988 [12]	5.14 [0.8]	1.66 [0.08]
	36	976 [19]	48.2 [2.2]	1.75 [0.05]
	48	981 [21]	49.9 [3.3]	1.76 [0.11]
	72	923 [14]	48.8 [1.0]	1.69 [0.03]
	96	912 [20]	50.6 [1.7]	1.67 [0.04]
40°C Immersion	12	873 [15]	50.5 [1.7]	1.54 [0.03]
	24	818 [21]	47.2 [4.4]	1.64 [0.11]
	36	777 [22]	49.9 [2.2]	1.50 [0.04]
	48	750 [10]	46.1 [1.3]	1.45 [0.15]
	72	681 [20]	47.2 [2.1]	1.38 [0.02]
	96	621 [15]	50.3 [1.2]	1.27 [0.02]
60°C Immersion	12	733 [18]	50.0 [0.5]	1.39 [0.03]
	24	608 [42]	46.9 [2.9]	1.33 [0.12]
	36	571 [33]	51.0 [2.3]	1.16 [0.04]
	48	530 [42]	48.6 [1.6]	1.17 [0.09]
	72	461 [23]	47.1 [1.6]	1.04 [0.04]
	96	377 [28]	48.5 [1.0]	0.83 [0.05]
80°C Immersion	12	438 [32]	49.4 [1.8]	0.92 [0.06]
	24	359 [21]	45.8 [2.8]	0.85 [0.08]
	36	331 [22]	48.1 [1.8]	0.73 [0.05]
	48	273 [6]	47.1 [1.4]	0.64 [0.01]
	72	244 [13]	46.3 [2.1]	0.56 [0.03]
	96	234 [15]	45.1 [3.0]	0.55 [0.02]

Table B.5. Dry tensile results for 18%RH environments.
Brackets indicate standard deviations.

Exposure Condition	Time (wk)	Strength (MPa)	Modulus (GPa)	Failure Strain (%)
20°C 18%RH	12	1121 [28]	55.0 [1.4]	1.61 [0.05]
	24	1151 [30]	50.8 [0.8]	1.91 [0.02]
	36	1136 [32]	47.0 [2.3]	2.01 [0.07]
	48	1172 [42]	49.1 [3.0]	1.96 [0.08]
	72	1108 [37]	49.9 [1.7]	1.85 [0.07]
	96	1157 [38]	49.7 [3.4]	1.99 [0.09]
40°C 18%RH	12	1128 [40]	50.2 [2.3]	1.94 [0.06]
	24	1154 [10]	49.7 [1.6]	1.94 [0.03]
	36	1144 [38]	52.2 [1.6]	1.86 [0.05]
	48	1167 [22]	50.3 [1.3]	1.95 [0.07]
	72	1140 [17]	50.7 [0.6]	1.79 [0.02]
	96	1129 [25]	53.2 [0.5]	1.81 [0.01]
60°C 18%RH	12	1153 [32]	50.5 [3.0]	1.91 [0.12]
	24	1130 [11]	52.2 [4.1]	1.89 [0.11]
	36	1123 [42]	48.6 [1.3]	2.00 [0.03]
	48	1099 [50]	49.2 [2.9]	1.90 [0.10]
	72	1123 [28]	50.1 [1.6]	2.00 [0.05]
	96	1123 [20]	51.6 [1.3]	1.81 [0.05]

Table B.6. Dry tensile results for 50%RH and 75%RH environments. Brackets indicate standard deviations.

Exposure Condition	Time (wk)	Strength (MPa)	Modulus (GPa)	Failure Strain (%)
20°C 50%RH	12	1117 [10]	55.5 [0.6]	1.68 [0.03]
	24	1109 [26]	49.0 [3.0]	1.93 [0.06]
	36	1153 [37]	48.6 [2.4]	1.94 [0.09]
	48	1161 [26]	54.1 [1.9]	1.85 [0.05]
	72	1136 [25]	49.6 [1.6]	1.89 [0.05]
	96	1149 [50]	50.4 [1.2]	1.98 [0.04]
40°C 50%RH	12	1150 [15]	50.1 [1.2]	1.94 [0.05]
	24	1135 [58]	50.7 [2.5]	1.92 [0.12]
	36	1163 [14]	49.5 [1.7]	1.95 [0.08]
	48	1149 [38]	49.8 [2.1]	1.93 [0.07]
	72	1110 [39]	51.4 [4.1]	1.75 [0.10]
	96	1153 [39]	52.1 [2.1]	1.84 [0.06]
60°C 50%RH	12	1132 [30]	52.0 [2.9]	1.87 [0.10]
	24	1174 [28]	48.7 [1.5]	2.01 [0.04]
	36	1137 [7]	48.8 [2.9]	1.90 [0.10]
	48	1112 [30]	48.2 [1.9]	1.93 [0.06]
	72	1136 [33]	51.0 [2.3]	1.90 [0.05]
	96	1097 [31]	52.3 [1.8]	1.80 [0.06]
60°C 75%RH	12	1097 [12]	51.0 [2.0]	1.87 [0.06]
	48	1085 [37]	51.1 [2.4]	1.90 [0.08]
	72	1021 [28]	52.0 [0.8]	1.74 [0.02]

Table B.7. Dry tensile results for 99%RH environments.
Brackets indicate standard deviations.

Exposure Condition	Time (wk)	Strength (MPa)	Modulus (GPa)	Failure Strain (%)
20°C 99%RH	12	1143 [8]	55.3 [1.4]	1.66 [0.05]
	24	1122 [37]	50.0 [2.2]	1.91 [0.09]
	36	1160 [34]	47.6 [1.6]	2.00 [0.05]
	48	1092 [39]	52.0 [2.8]	1.87 [0.08]
	72	1055 [26]	49.7 [1.9]	1.84 [0.05]
	96	1040 [24]	50.7 [1.3]	1.90 [0.03]
40°C 99%RH	12	1032 [23]	49.4 [1.3]	1.86 [0.04]
	24	935 [29]	49.5 [2.1]	1.77 [0.06]
	36	929 [52]	50.0 [3.2]	1.72 [0.10]
	48	890 [59]	49.0 [0.8]	1.75 [0.05]
	72	831 [73]	49.5 [2.8]	1.58 [0.10]
	96	735 [42]	52.9 [1.5]	1.43 [0.06]
60°C 99%RH	12	850 [19]	49.5 [2.6]	1.66 [0.08]
	24	752 [32]	48.9 [2.6]	1.54 [0.09]
	36	693 [46]	48.3 [2.2]	1.48 [0.04]
	48	644 [42]	46.3 [3.3]	1.44 [0.12]
	72	598 [16]	46.8 [1.8]	1.27 [0.04]
	96	509 [21]	52.2 [3.6]	1.03 [0.05]
80°C 99%RH	12	481 [29]	47.9 [2.3]	1.03 [0.02]
	48	332 [17]	50.9 [0.1]	0.69 [0.04]
	72	295 [14]	49.8 [1.5]	0.62 [0.01]

Table B.8. Dry tensile results for immersion environments.
Brackets indicate standard deviations.

Exposure Condition	Time (wk)	Strength (MPa)	Modulus (GPa)	Failure Strain (%)
20°C Immersion	12	1106 [22]	53.9 [2.0]	1.64 [0.09]
	24	1155 [44]	49.1 [3.1]	1.97 [0.09]
	36	1149 [16]	51.4 [4.0]	1.88 [0.11]
	48	1115 [28]	51.3 [1.8]	1.87 [0.03]
	72	1046 [30]	51.7 [2.4]	1.78 [0.07]
	96	1045 [20]	50.4 [2.0]	1.91 [0.06]
40°C Immersion	12	993 [24]	50.2 [1.2]	1.80 [0.04]
	24	905 [35]	52.5 [2.7]	1.64 [0.08]
	36	836 [15]	51.0 [2.4]	1.62 [0.09]
	48	781 [15]	48.4 [1.7]	1.64 [0.03]
	72	728 [18]	50.6 [1.6]	1.41 [0.06]
	96	658 [20]	50.0 [3.8]	1.33 [0.07]
60°C Immersion	12	799 [13]	49.7 [1.1]	1.56 [0.06]
	24	677 [27]	50.0 [1.8]	1.38 [0.02]
	36	646 [27]	48.4 [3.7]	1.36 [0.06]
	48	578 [34]	49.3 [1.8]	1.25 [0.05]
	72	551 [32]	48.6 [1.9]	1.14 [0.06]
	96	426 [25]	51.0 [2.2]	0.91 [0.06]
80°C Immersion	12	498 [11]	47.5 [3.2]	1.09 [0.05]
	24	417 [31]	49.7 [0.8]	0.89 [0.04]
	36	341 [19]	46.2 [1.5]	0.78 [0.05]
	48	307 [15]	45.7 [3.2]	0.70 [0.05]
	72	269 [15]	43.6 [1.1]	0.64 [0.04]
	96	248 [32]	45.9 [2.0]	0.57 [0.04]

B.2 Short Beam Shear Results

Table B.9. Wet SBS strengths for 18%RH environments.
Brackets indicate standard deviations.

Exposure Condition	Time (wk)	SBS Strength (MPa)
20°C 18%RH	12	70.9 [1.0]
	24	71.2 [2.7]
	36	70.3 [2.7]
	48	71.0 [1.5]
	72	67.1 [3.2]
	96	70.2 [1.3]
40°C 18%RH	12	74.5 [1.2]
	24	72.1 [1.5]
	36	72.5 [3.4]
	48	72.4 [2.3]
	72	72.5 [0.7]
	96	72.6 [0.6]
60°C 18%RH	12	76.6 [1.4]
	24	75.3 [1.4]
	36	75.0 [1.7]
	48	75.5 [1.9]
	72	75.6 [0.8]
	96	78.8 [2.5]

Table B.10. Wet SBS strengths for 50%RH and 75%RH environments. Brackets indicate standard deviations.

Exposure Condition	Time (wk)	SBS Strength (MPa)
20°C 50%RH	12	69.2 [1.3]
	24	68.1 [2.0]
	36	66.5 [2.3]
	48	69.5 [1.1]
	72	67.5 [0.8]
	96	68.2 [2.6]
40°C 50%RH	12	71.2 [0.9]
	24	70.0 [1.3]
	36	67.3 [3.0]
	48	71.5 [1.4]
	72	69.0 [1.5]
	96	71.0 [0.9]
60°C 50%RH	12	75.2 [2.0]
	24	73.7 [1.7]
	36	76.3 [2.5]
	48	73.2 [1.9]
	72	72.3 [2.8]
	96	74.0 [3.1]
60°C 75%RH	12	67.9 [1.6]
	24	69.6 [1.6]
	36	67.9 [1.5]
	48	68.9 [1.2]
	72	66.7 [2.5]

Table B.11. Wet SBS strengths for 99%RH environments.
Brackets indicate standard deviations.

Exposure Condition	Time (wk)	SBS Strength (MPa)
20°C 99%RH	12	60.9 [2.0]
	24	60.4 [2.8]
	36	61.6 [1.8]
	48	61.8 [1.5]
	72	56.8 [2.4]
	96	57.9 [2.1]
40°C 99%RH	12	62.9 [1.3]
	24	62.3 [2.4]
	36	62.3 [1.2]
	48	61.7 [3.0]
	72	60.9 [2.9]
	96	58.8 [3.6]
60°C 99%RH	12	65.1 [1.8]
	24	55.7 [2.6]
	36	60.5 [1.3]
	48	56.8 [3.3]
	72	53.0 [2.3]
	96	55.2 [3.0]
80°C 99%RH	12	45.8 [3.0]
	24	40.5 [1.5]
	36	38.0 [2.2]
	48	36.2 [1.6]
	72	35.4 [0.7]

Table B.12. Wet SBS strengths for immersion environments. Brackets indicate standard deviations.

Exposure Condition	Time (wk)	SBS Strength (MPa)
20°C Immersion	12	59.1 [2.0]
	24	58.6 [1.6]
	36	57.5 [2.4]
	48	56.9 [1.9]
	72	57.1 [1.9]
	96	56.6 [2.0]
40°C Immersion	12	63.4 [2.2]
	24	61.0 [3.4]
	36	62.4 [2.2]
	48	61.9 [3.0]
	72	57.7 [1.8]
	96	61.4 [2.0]
60°C Immersion	12	63.4 [2.2]
	24	56.5 [2.2]
	36	52.9 [4.2]
	48	57.4 [2.8]
	72	50.3 [2.8]
	96	50.9 [2.8]
80°C Immersion	12	49.1 [2.1]
	24	44.4 [4.2]
	36	39.6 [2.2]
	48	39.3 [3.4]
	72	37.4 [4.0]
	96	31.0 [2.4]

Table B.13. Dry SBS strengths for 18%RH environments.
Brackets indicate standard deviations.

Exposure Condition	Time (wk)	SBS Strength (MPa)
20°C 18%RH	12	69.9 [2.1]
	24	69.5 [1.2]
	36	71.2 [1.8]
	48	71.1 [1.3]
	72	67.9 [2.1]
	96	71.8 [2.3]
40°C 18%RH	12	72.6 [1.1]
	24	73.1 [1.9]
	36	72.8 [2.2]
	48	71.4 [3.0]
	72	72.4 [2.4]
	96	72.9 [3.2]
60°C 18%RH	12	77.9 [0.7]
	24	74.1 [3.3]
	36	75.8 [3.0]
	48	77.2 [2.6]
	72	78.7 [2.2]
	96	75.1 [4.1]

Table B.14. Dry SBS strengths for 50%RH and 75%RH environments. Brackets indicate standard deviations.

Exposure Condition	Time (wk)	SBS Strength (MPa)
20°C 50%RH	12	71.3 [2.2]
	24	70.6 [2.9]
	36	70.3 [1.1]
	48	70.8 [0.8]
	72	68.1 [2.3]
	96	70.1 [1.1]
40°C 50%RH	12	72.8 [1.5]
	24	74.8 [0.9]
	36	73.6 [1.7]
	48	73.1 [2.2]
	72	73.7 [2.4]
	96	75.8 [0.9]
60°C 50%RH	12	78.5 [1.6]
	24	78.6 [2.2]
	36	76.3 [2.6]
	48	75.8 [3.8]
	72	77.5 [2.5]
	96	77.0 [1.3]
60°C 75%RH	12	76.3 [0.8]
	24	75.2 [3.2]
	36	73.0 [2.5]
	48	77.5 [0.3]
	72	73.5 [2.4]

Table B.15. Dry SBS strengths for 99%RH environments. Brackets indicate standard deviations.

Exposure Condition	Time (wk)	Strength (MPa)
20°C 99%RH	12	72.9 [2.0]
	24	68.9 [2.6]
	36	70.2 [2.0]
	48	71.6 [0.7]
	72	71.0 [3.0]
	96	69.0 [1.3]
40°C 99%RH	12	73.6 [1.1]
	24	74.6 [1.4]
	36	72.5 [1.9]
	48	70.2 [2.3]
	72	71.3 [3.1]
	96	70.9 [2.1]
60°C 99%RH	12	75.8 [0.7]
	24	65.8 [3.5]
	36	65.9 [2.1]
	48	66.0 [3.5]
	72	67.5 [1.0]
	96	62.8 [2.6]
80°C 99%RH	12	54.9 [2.5]
	24	47.0 [2.8]
	36	45.4 [2.0]
	48	45.7 [1.8]
	72	41.9 [1.2]

Table B.16. Dry SBS strengths for immersion environments. Brackets indicate standard deviations.

Exposure Condition	Time (wk)	SBS Strength (MPa)
20°C Immersion	12	71.3 [2.2]
	24	71.5 [0.7]
	36	70.8 [2.2]
	48	71.3 [1.9]
	72	70.4 [1.9]
	96	69.5 [1.7]
40°C Immersion	12	74.5 [1.1]
	24	73.6 [1.3]
	36	73.5 [3.2]
	48	72.9 [2.3]
	72	72.8 [1.6]
	96	73.6 [1.3]
60°C Immersion	12	74.4 [4.7]
	24	65.1 [4.7]
	36	65.3 [1.9]
	48	66.2 [3.1]
	72	66.5 [2.2]
	96	60.0 [2.9]
80°C Immersion	12	57.0 [3.8]
	24	54.2 [3.5]
	36	51.8 [1.7]
	48	46.6 [3.2]
	72	44.9 [2.4]
	96	40.0 [1.7]

Appendix C. Summary of DMTA Results

C.1 Glass Transitions Temperatures and tanδ Peak Heights

Table C.1. Wet T_g and tanδ for 18%RH environments.
Brackets indicate standard deviations.

Exposure Condition	Time (wk)	T_g [tanδ] (°C)	T_g [E''] (°C)	tanδ pk height
20°C 18%RH	12	114.5 [0.8]	98.4 [2.2]	0.193 [0.007]
	24	115.6 [1.6]	98.6 [2.1]	0.199 [0.008]
	36	115.9 [1.8]	99.5 [2.9]	0.200 [0.004]
	48	114.4 [2.1]	97.5 [1.6]	0.188 [0.003]
	72	113.8 [1.5]	98.8 [2.1]	0.188 [0.012]
	96	117.5 [1.8]	97.6 [2.0]	0.194 [0.005]
40°C 18%RH	12	118.0 [1.5]	98.7 [1.6]	0.188 [0.003]
	24	116.1 [1.6]	101.8 [1.4]	0.191 [0.009]
	36	119.7 [4.0]	101.8 [1.5]	0.200 [0.005]
	48	119.8 [3.6]	103.9 [1.3]	0.201 [0.021]
	72	121.9 [4.0]	101.9 [2.6]	0.190 [0.010]
	96	119.5 [1.3]	103.3 [1.1]	0.189 [0.003]
60°C 18%RH	12	123.3 [3.8]	106.7 [0.8]	0.200 [0.006]
	24	120.0 [1.9]	108.0 [0.7]	0.192 [0.009]
	36	120.0 [7.2]	109.9 [0.4]	0.196 [0.022]
	48	125.3 [2.2]	111.1 [1.2]	0.222 [0.012]
	72	124.8 [1.6]	111.0 [0.1]	0.203 [0.007]
	96	128.4 [2.7]	111.7 [1.8]	0.211 [0.016]

Table C.2. Wet T_g and tanδ for 50%RH and 75%RH environments. Brackets indicate standard deviations.

Exposure Condition	Time (wk)	T_g [tanδ] (°C)	T_g [E''] (°C)	tanδ pk height
20°C 50%RH	12	113.4 [1.2]	94.8 [1.0]	0.192 [0.004]
	24	112.4 [4.1]	95.4 [3.5]	0.198 [0.005]
	36	111.2 [0.7]	93.3 [1.1]	0.198 [0.012]
	48	110.5 [2.2]	94.4 [2.4]	0.192 [0.011]
	72	113.2 [3.3]	98.0 [0.3]	0.203 [0.015]
	96	114.3 [2.5]	93.1 [1.0]	0.199 [0.011]
40°C 50%RH	12	113.7 [2.5]	97.4 [1.9]	0.195 [0.003]
	24	115.5 [3.8]	99.2 [1.8]	0.199 [0.008]
	36	114.9 [2.0]	97.0 [1.8]	0.204 [0.005]
	48	115.9 [3.4]	100.3 [1.7]	0.197 [0.017]
	72	117.1 [1.4]	100.0 [2.0]	0.201 [0.010]
	96	116.4 [3.1]	100.3 [1.2]	0.207 [0.004]
60°C 50%RH	12	124.4 [2.0]	110.1 [1.2]	0.229 [0.006]
	24	125.9 [1.7]	111.9 [0.7]	0.227 [0.007]
	36	119.3 [1.4]	111.4 [0.4]	0.230 [0.007]
	48	123.9 [1.5]	111.7 [1.0]	0.235 [0.019]
	72	124.0 [2.3]	110.2 [1.0]	0.232 [0.002]
	96	117.4 [2.1]	106.3 [0.6]	0.233 [0.005]
60°C 75%RH	12	119.2 [1.5]	105.5 [0.4]	0.204 [0.007]
	24	118.1 [1.8]	106.3 [0.5]	0.214 [0.002]
	36	120.6 [4.6]	106.5 [1.3]	0.220 [0.007]
	48	119.8 [6.8]	104.8 [0.8]	0.212 [0.013]
	72	12.01 [5.0]	103.0 [0.7]	0.217 [0.006]

Table C.3. Wet T_g and tanδ for 99%RH environments.
Brackets indicate standard deviations.

Exposure Condition	Time (wk)	T_g [tanδ] (°C)	T_g [E''] (°C)	tanδ pk height
20°C 99%RH	12	105.0 [3.0]	85.1 [1.5]	0.199 [0.009]
	24	109.2 [7.5]	88.6 [1.0]	0.207 [0.006]
	36	104.6 [1.6]	90.0 [2.2]	0.205 [0.002]
	48	101.9 [1.8]	86.3 [2.2]	0.203 [0.006]
	72	103.5 [1.6]	87.2 [1.5]	0.207 [0.007]
	96	102.7 [1.1]	85.8 [0.8]	0.209 [0.004]
40°C 99%RH	12	101.7 [1.6]	90.2 [1.2]	0.230 [0.004]
	24	102.8 [1.2]	91.7 [0.5]	0.244 [0.009]
	36	99.8 [0.7]	89.3 [0.1]	0.248 [0.010]
	48	101.8 [1.2]	91.7 [0.9]	0.231 [0.005]
	72	99.8 [0.8]	91.4 [0.5]	0.235 [0.009]
	96	102.7 [2.9]	93.9 [0.6]	0.227 [0.004]
60°C 99%RH	12	108.1 [0.7]	99.6 [0.7]	0.259 [0.005]
	24	108.9 [0.9]	99.7 [0.9]	0.279 [0.004]
	36	107.9 [1.4]	100.2 [0.9]	0.267 [0.009]
	48	109.9 [0.4]	101.3 [0.5]	0.290 [0.006]
	72	109.4 [0.8]	99.7 [1.1]	0.270 [0.010]
	96	110.1 [0.9]	102.4 [0.7]	0.273 [0.005]
80°C 99%RH	12	116.1 [1.2]	106.5 [1.5]	0.296 [0.004]
	24	118.3 [1.5]	108.4 [2.0]	0.299 [0.010]
	36	119.9 [2.6]	110.2 [1.6]	0.279 [0.011]
	48	118.8 [0.9]	108.9 [2.1]	0.278 [0.002]
	72	124.0 [3.2]	11.40 [1.3]	0.245 [0.024]

Table C.4. Wet T_g and tanδ for immersion environments.
Brackets indicate standard deviations.

Exposure Condition	Time (wk)	T_g [tanδ] (°C)	T_g [E''] (°C)	tanδ pk height
20°C Immersion	12	101.7 [2.1]	87.2 [1.3]	0.202 [0.017]
	24	100.3 [0.8]	84.8 [1.1]	0.208 [0.017]
	36	101.0 [3.6]	87.3 [1.7]	0.220 [0.007]
	48	97.9 [2.1]	83.0 [1.4]	0.217 [0.009]
	72	97.9 [0.7]	84.8 [0.7]	0.213 [0.015]
	96	98.3 [1.0]	85.6 [2.7]	0.221 [0.006]
40°C Immersion	12	101.3 [1.6]	91.6 [0.7]	0.233 [0.013]
	24	10.32 [1.3]	94.4 [1.1]	0.248 [0.011]
	36	101.5 [1.9]	90.8 [0.5]	0.242 [0.003]
	48	102.8 [1.1]	95.1 [1.8]	0.256 [0.019]
	72	101.6 [1.4]	91.9 [1.0]	0.245 [0.004]
	96	99.6 [0.5]	92.4 [0.8]	0.248 [0.005]
60°C Immersion	12	109.5 [1.2]	101.6 [0.6]	0.256 [0.009]
	24	110.5 [1.0]	101.6 [1.0]	0.295 [0.013]
	36	109.0 [1.0]	101.3 [0.8]	0.281 [0.005]
	48	110.7 [0.4]	102.4 [1.4]	0.289 [0.014]
	72	109.7 [0.6]	102.3 [0.6]	0.276 [0.003]
	96	112.6 [2.3]	104.2 [1.7]	0.271 [0.010]
80°C Immersion	12	118.6 [4.4]	110.3 [0.8]	0.302 [0.004]
	24	116.3 [0.3]	106.6 [1.3]	0.288 [0.014]
	36	118.2 [1.6]	108.8 [1.5]	0.284 [0.017]
	48	120.5 [0.8]	111.7 [0.8]	0.297 [0.014]
	72	120.0 [1.1]	111.7 [1.1]	0.258 [0.007]
	96	121.0 [1.9]	113.1 [1.9]	0.254 [0.025]

Table C.5. Dry T_g and tanδ for 18%RH environments.
Brackets indicate standard deviations.

Exposure Condition	Time (wk)	T_g [tanδ] (°C)	T_g [E''] (°C)	tanδ pk height
20°C 18%RH	12	115.5 [2.6]	98.3 [1.1]	0.179 [0.014]
	24	116.4 [0.3]	98.5 [1.7]	0.191 [0.004]
	36	117.2 [0.7]	97.2 [0.8]	0.195 [0.008]
	48	119.1 [2.7]	102.3 [2.0]	0.204 [0.009]
	72	117.6 [3.5]	100.4 [1.3]	0.204 [0.008]
	96	118.1 [0.8]	97.3 [1.9]	0.189 [0.013]
40°C 18%RH	12	118.4 [1.3]	99.9 [1.3]	0.202 [0.005]
	24	113.4 [0.7]	99.5 [0.7]	0.177 [0.011]
	36	119.1 [1.4]	102.7 [1.4]	0.195 [0.009]
	48	121.4 [3.2]	102.6 [3.2]	0.204 [0.013]
	72	118.9 [1.0]	101.0 [1.0]	0.191 [0.007]
	96	120.9 [0.8]	105.4 [0.8]	0.185 [0.014]
60°C 18%RH	12	125.2 [8.4]	111.7 [6.4]	0.198 [0.012]
	24	120.5 [1.3]	107.2 [0.4]	0.184 [0.009]
	36	127.0 [2.3]	10.95 [1.0]	0.225 [0.006]
	48	122.3 [4.5]	107.9 [0.7]	0.206 [0.011]
	72	127.2 [4.6]	111.9 [2.2]	0.195 [0.009]
	96	124.4 [5.1]	109.1 [1.2]	0.196 [0.003]

Table C.6. Dry T_g and tanδ for 50%RH and 75%RH environments. Brackets indicate standard deviations.

Exposure Condition	Time (wk)	T_g [tanδ] (°C)	T_g [E''] (°C)	tanδ pk height
20°C 50%RH	12	119.9 [2.7]	98.2 [1.2]	0.204 [0.011]
	24	116.7 [2.6]	97.5 [0.8]	0.196 [0.021]
	36	116.5 [0.6]	99.2 [1.5]	0.192 [0.010]
	48	114.8 [0.6]	99.6 [2.7]	0.197 [0.021]
	72	114.4 [2.1]	97.4 [1.8]	0.203 [0.009]
	96	116.6 [4.4]	100.5 [4.3]	0.198 [0.006]
40°C 50%RH	12	115.9 [1.5]	99.8 [1.1]	0.195 [0.006]
	24	112.9 [1.0]	99.5 [0.4]	0.176 [0.004]
	36	117.9 [3.5]	105.1 [0.8]	0.201 [0.025]
	48	125.7 [6.8]	105.5 [1.6]	0.203 [0.002]
	72	121.6 [5.9]	103.5 [0.7]	0.202 [0.006]
	96	124.6 [1.8]	105.6 [0.8]	0.203 [0.008]
60°C 50%RH	12	126.5 [1.2]	114.5 [1.6]	0.222 [0.007]
	24	125.6 [3.1]	114.0 [1.2]	0.225 [0.017]
	36	131.2 [1.9]	116.2 [1.8]	0.236 [0.004]
	48	128.9 [0.8]	116.0 [0.9]	0.242 [0.010]
	72	128.1 [1.4]	115.8 [0.5]	0.233 [0.008]
	96	129.2 [1.9]	117.3 [0.9]	0.235 [0.005]
60°C 75%RH	12	124.7 [2.2]	114.6 [1.8]	0.221 [0.011]
	24	125.4 [0.6]	114.1 [1.6]	0.222 [0.008]
	36	125.8 [2.9]	115.2 [0.8]	0.229 [0.005]
	48	128.0 [1.4]	117.0 [1.3]	0.220 [0.016]
	72	125.7 [1.7]	113.1 [0.7]	0.221 [0.13]

Table C.7. Dry T_g and tanδ for 99%RH environments.
Brackets indicate standard deviations.

Exposure Condition	Time (wk)	T_g [tanδ] (°C)	T_g [E''] (°C)	tanδ pk height
20°C 99%RH	12	109.9 [4.6]	93.9 [4.7]	0.199 [0.009]
	24	117.3 [1.5]	100.3 [0.5]	0.207 [0.006]
	36	119.8 [4.6]	101.2 [1.2]	0.195 [0.002]
	48	113.4 [1.7]	99.3 [2.7]	0.187 [0.012]
	72	113.8 [4.2]	99.1 [1.4]	0.206 [0.010]
	96	115.6 [2.9]	98.9 [2.6]	0.204 [0.011]
40°C 99%RH	12	117.0 [5.4]	103.0 [1.8]	0.211 [0.013]
	24	115.2 [4.1]	102.4 [2.4]	0.184 [0.012]
	36	115.9 [1.7]	103.2 [1.2]	0.213 [0.008]
	48	121.0 [5.3]	102.7 [0.7]	0.212 [0.012]
	72	116.7 [0.6]	104.2 [1.3]	0.196 [0.014]
	96	119.9 [1.9]	104.5 [1.5]	0.215 [0.005]
60°C 99%RH	12	125.9 [2.8]	114.9 [1.3]	0.235 [0.010]
	24	126.0 [1.7]	113.7 [0.9]	0.275 [0.002]
	36	127.7 [1.3]	115.2 [1.2]	0.256 [0.008]
	48	127.4 [1.7]	116.0 [1.0]	0.265 [0.014]
	72	130.6 [1.9]	116.5 [0.6]	0.275 [0.012]
	96	125.8 [0.9]	116.5 [0.9]	0.264 [0.023]
80°C 99%RH	12	138.2 [0.3]	123.8 [2.8]	0.308 [0.016]
	24	139.1 [1.9]	123.1 [2.2]	0.305 [0.018]
	36	141.1 [1.2]	129.9 [2.7]	0.320 [0.013]
	48	144.0 [1.2]	130.6 [1.9]	0.307 [0.017]
	72	142.5 [1.7]	130.9 [1.1]	0.321 [0.027]

Table C.8. Dry T_g and tanδ for immersion environments.
Brackets indicate standard deviations.

Exposure Condition	Time (wk)	T_g [tanδ] (°C)	T_g [E''] (°C)	tanδ pk height
20°C Immersion	12	117.2 [2.3]	100.6 [2.2]	0.200 [0.005]
	24	115.7 [2.7]	99.4 [1.2]	0.201 [0.011]
	36	112.0 [2.2]	98.8 [0.9]	0.178 [0.010]
	48	114.9 [1.5]	98.1 [1.6]	0.210 [0.004]
	72	113.4 [1.1]	97.6 [2.0]	0.189 [0.006]
	96	115.0 [1.9]	98.9 [2.2]	0.204 [0.007]
40°C Immersion	12	119.5 [1.8]	103.7 [1.9]	0.217 [0.008]
	24	116.7 [1.9]	105.1 [0.7]	0.193 [0.005]
	36	125.6 [6.8]	103.8 [0.7]	0.226 [0.010]
	48	123.0 [4.8]	104.4 [0.7]	0.222 [0.005]
	72	119.3 [0.8]	106.2 [1.7]	0.207 [0.002]
	96	120.4 [2.2]	108.0 [0.3]	0.226 [0.002]
60°C Immersion	12	126.0 [2.4]	115.1 [0.6]	0.239 [0.007]
	24	126.7 [1.1]	115.5 [0.5]	0.250 [0.003]
	36	129.5 [1.8]	118.0 [2.3]	0.288 [0.012]
	48	129.4 [0.9]	117.1 [1.9]	0.277 [0.013]
	72	131.3 [1.1]	119.8 [0.9]	0.274 [0.018]
	96	133.3 [1.1]	121.5 [0.8]	0.281 [0.010]
80°C Immersion	12	138.5 [1.9]	124.9 [2.6]	0.292 [0.012]
	24	141.5 [1.4]	125.6 [2.8]	0.301 [0.005]
	36	142.9 [1.5]	126.4 [0.6]	0.304 [0.005]
	48	140.2 [1.5]	127.0 [1.2]	0.304 [0.017]
	72	143.9 [0.9]	130.7 [2.5]	0.305 [0.001]
	96	141.8 [0.6]	126.2 [1.2]	0.309 [0.008]

C.2 Storage Moduli

Table C.9. Wet storage moduli for 18%RH environments. Brackets indicate standard deviations.

Exposure Condition	Time (wk)	$E'[T_g$-60°C] (GPa)	$E'[T_g$+60°C] (GPa)
20°C 18%RH	12	17.28 [0.87]	2.26 [0.19]
	24	18.31 [0.95]	2.36 [0.16]
	36	17.52 [0.20]	2.25 [0.17]
	48	18.78 [0.53]	2.21 [0.10]
	72	18.60 [1.22]	2.24 [0.21]
	96	18.51 [0.63]	2.26 [0.15]
40°C 18%RH	12	18.20 [0.33]	2.16 [0.12]
	24	18.21 [0.58]	2.11 [0.22]
	36	17.89 [0.85]	2.05 [0.17]
	48	18.68 [0.54]	2.13 [0.10]
	72	16.68 [0.63]	1.98 [0.18]
	96	17.42 [0.30]	1.99 [0.17]
60°C 18%RH	12	17.84 [0.81]	2.25 [0.13]
	24	17.68 [0.46]	1.98 [0.10]
	36	17.53 [0.37]	1.89 [0.11]
	48	16.91 [0.49]	1.91 [0.16]
	72	17.50 [0.82]	1.91 [0.19]
	96	18.48 [0.71]	1.89 [0.14]

Table C.10. Wet storage moduli for 50%RH and 75%RH environments. Brackets indicate standard deviations.

Exposure Condition	Time (wk)	$E'[T_g$-60°C] (GPa)	$E'[T_g$+60°C] (GPa)
20°C 50%RH	12	16.96 [1.14]	2.21 [0.12]
	24	17.87 [0.55]	2.07 [0.14]
	36	17.58 [0.89]	2.24 [0.10]
	48	16.95 [0.40]	1.97 [0.14]
	72	17.94 [1.07]	2.26 [0.05]
	96	17.53 [0.59]	2.11 [0.21]
40°C 50%RH	12	17.69 [0.41]	1.97 [0.05]
	24	17.26 [0.53]	1.91 [0.06]
	36	17.75 [1.05]	2.01 [0.10]
	48	18.10 [0.32]	1.94 [0.14]
	72	17.01 [0.76]	1.90 [0.12]
	96	17.20 [0.23]	1.94 [0.12]
60°C 50%RH	12	18.04 [0.53]	1.83 [0.18]
	24	16.80 [0.32]	1.77 [0.10]
	36	16.55 [0.41]	1.84 [0.18]
	48	16.71 [0.56]	1.71 [0.12]
	72	17.27 [1.06]	1.73 [0.14]
	96	18.15 [0.42]	1.76 [0.06]
60°C 75%RH	12	16.07 [0.49]	1.66 [0.02]
	24	17.40 [0.47]	1.67 [0.12]
	36	16.72 [0.78]	1.68 [0.13]
	48	16.94 [0.53]	1.66 [0.07]
	72	17.75 [0.88]	1.60 [0.19]

Table C.11. Wet storage moduli for 99%RH environments. Brackets indicate standard deviations.

Exposure Condition	Time (wk)	$E'[T_g$-60°C] (GPa)	$E'[T_g$+60°C] (GPa)
20°C 99%RH	12	17.07 [1.04]	1.93 [0.13]
	24	17.48 [0.87]	2.15 [0.14]
	36	17.15 [0.31]	2.05 [0.07]
	48	17.66 [0.68]	2.06 [0.16]
	72	18.10 [1.44]	2.09 [0.15]
	96	17.22 [0.45]	1.99 [0.14]
40°C 99%RH	12	18.32 [0.74]	1.73 [0.09]
	24	18.05 [0.73]	1.67 [0.12]
	36	18.83 [0.09]	1.66 [0.20]
	48	16.28 [0.85]	1.51 [0.10]
	72	17.65 [0.15]	1.53 [0.06]
	96	17.68 [0.58]	1.56 [0.02]
60°C 99%RH	12	17.33 [0.81]	1.51 [0.14]
	24	15.45 [0.52]	1.05 [0.08]
	36	15.44 [0.51]	1.01 [0.04]
	48	14.61 [0.35]	0.97 [0.04]
	72	14.99 [0.63]	1.04 [0.06]
	96	15.60 [0.37]	1.04 [0.07]
80°C 99%RH	12	1.320 [0.38]	0.90 [0.05]
	24	13.19 [0.42]	0.88 [0.03]
	36	11.77 [0.13]	0.88 [0.03]
	48	11.54 [0.40]	0.81 [0.03]
	72	11.43 [0.67]	0.75 [0.01]

Table C.12. Wet storage moduli for immersion environments. Brackets indicate standard deviations.

Exposure Condition	Time (wk)	$E'[T_g$-60°C] (GPa)	$E'[T_g$+60°C] (GPa)
20°C Immersion	12	17.42 [0.71]	2.20 [0.15]
	24	17.55 [0.65]	2.22 [0.04]
	36	17.82 [1.21]	2.02 [0.07]
	48	16.77 [0.72]	197 [0.08]
	72	17.35 [0.68]	1.94 [0.10]
	96	19.03 [0.66]	2.01 [0.16]
40°C Immersion	12	18.02 [0.44]	1.87 [0.08]
	24	17.53 [0.61]	1.66 [0.15]
	36	17.45 [1.25]	1.53 [0.06]
	48	17.27 [0.91]	1.44 [0.12]
	72	17.68 [0.37]	1.48 [0.10]
	96	17.90 [0.61]	1.44 [0.09]
60°C Immersion	12	17.66 [0.59]	1.52 [0.04]
	24	14.79 [0.46]	1.10 [0.05]
	36	15.16 [0.70]	1.05 [0.11]
	48	14.45 [0.85]	0.94 [0.03]
	72	14.51 [0.51]	0.97 [0.08]
	96	14.82 [0.33]	1.00 [0.06]
80°C Immersion	12	13.51 [0.76]	0.96 [0.04]
	24	12.68 [0.46]	0.85 [0.05]
	36	11.90 [0.48]	0.82 [0.06]
	48	11.91 [0.12]	0.80 [0.01]
	72	10.02 [0.54]	0.84 [0.02]
	96	9.92 [0.39]	0.78 [0.03]

Table C.13. Dry storage moduli for 18%RH environments. Brackets indicate standard deviations.

Exposure Condition	Time (wk)	$E'[T_g$-60°C] (GPa)	$E'[T_g$+60°C] (GPa)
20°C 18%RH	12	18.47 [0.54]	2.21 [0.24]
	24	18.13 [0.55]	2.31 [0.26]
	36	17.49 [0.28]	2.09 [0.14]
	48	18.02 [1.07]	2.26 [0.20]
	72	18.63 [0.44]	2.12 [0.22]
	96	17.98 [0.64]	2.11 [0.15]
40°C 18%RH	12	17.89 [0.90]	2.13 [0.06]
	24	16.73 [0.42]	1.89 [0.20]
	36	18.64 [0.18]	2.22 [0.13]
	48	18.16 [0.72]	2.03 [0.14]
	72	17.25 [0.31]	1.86 [0.09]
	96	17.54 [0.79]	1.92 [0.18]
60°C 18%RH	12	17.12 [0.42]	1.92 [0.07]
	24	17.98 [0.26]	1.92 [0.16]
	36	17.48 [0.65]	1.94 [0.12]
	48	18.16 [0.66]	1.90 [0.11]
	72	17.00 [0.13]	1.91 [0.11]
	96	16.90 [0.43]	1.74 [0.16]

Table C.14. Dry storage moduli for 50%RH and 75%RH environments. Brackets indicate standard deviations.

Exposure Condition	Time (wk)	$E'[T_g$-60°C] (GPa)	$E'[T_g$+60°C] (GPa)
20°C 50%RH	12	17.32 [0.43]	2.15 [0.11]
	24	18.02 [0.51]	2.32 [0.25]
	36	17.08 [0.57]	2.21 [0.16]
	48	17.16 [0.52]	2.19 [0.08]
	72	18.07 [0.88]	2.11 [0.15]
	96	18.60 [0.91]	2.26 [0.06]
40°C 50%RH	12	18.45 [0.99]	2.24 [0.04]
	24	16.89 [0.77]	1.99 [0.12]
	36	18.09 [0.68]	2.11 [0.15]
	48	17.84 [0.44]	1.95 [0.09]
	72	17.59 [0.89]	1.85 [0.15]
	96	17.66 [0.45]	1.94 [0.19]
60°C 50%RH	12	17.94 [1.06]	1.92 [0.12]
	24	17.08 [0.06]	1.77 [0.11]
	36	17.69 [0.14]	1.89 [0.12]
	48	17.34 [0.47]	1.79 [0.09]
	72	17.56 [0.54]	1.73 [0.07]
	96	17.62 [0.16]	1.66 [0.11]
60°C 75%RH	12	17.08 [0.45]	1.81 [0.11]
	24	17.38 [0.39]	1.87 [0.09]
	36	17.78 [0.38]	1.80 [0.19]
	48	17.88 [0.37]	1.92 [0.13]
	72	17.94 [1.21]	1.78 [0.9]

Table C.15. Dry storage moduli for 99%RH environments. Brackets indicate standard deviations.

Exposure Condition	Time (wk)	$E'[T_g$-60°C] (GPa)	$E'[T_g$+60°C] (GPa)
20°C 99%RH	12	18.73 [0.70]	2.04 [0.12]
	24	17.69 [0.92]	2.25 [0.22]
	36	17.02 [1.16]	2.19 [0.25]
	48	17.14 [0.18]	2.12 [0.12]
	72	18.12 [0.42]	2.09 [0.17]
	96	17.71 [0.83]	2.04 [0.26]
40°C 99%RH	12	17.37 [0.61]	2.03 [0.20]
	24	17.03 [0.44]	1.75 [0.14]
	36	18.50 [0.47]	1.86 [0.13]
	48	17.08 [0.67]	1.83 [0.09]
	72	16.97 [0.33]	1.86 [0.13]
	96	17.16 [0.21]	1.76 [0.10]
60°C 99%RH	12	16.77 [0.34]	1.73 [0.16]
	24	14.99 [0.03]	1.24 [0.12]
	36	14.32 [0.32]	1.22 [0.06]
	48	15.05 [0.57]	1.23 [0.08]
	72	14.45 [0.28]	1.20 [0.10]
	96	14.33 [0.61]	1.18 [0.11]
80°C 99%RH	12	16.52 [0.63]	1.08 [0.09]
	24	12.21 [0.33]	0.89 [0.06]
	36	11.37 [0.25]	0.83 [0.07]
	48	11.11 [0.13]	0.80 [0.04]
	72	10.98 [0.59]	0.82 [0.09]

Table C.16. Dry storage moduli for immersion environments. Brackets indicate standard deviations.

Exposure Condition	Time (wk)	$E'[T_g$-60°C] (GPa)	$E'[T_g$+60°C] (GPa)
20°C Immersion	12	18.02 [0.44]	2.06 [0.09]
	24	17.27 [0.74]	2.31 [0.13]
	36	16.78 [0.24]	1.92 [0.04]
	48	19.19 [0.27]	2.09 [0.13]
	72	16.08 [0.40]	2.12 [0.16]
	96	17.97 [1.13]	2.11 [0.20]
40°C Immersion	12	17.20 [0.32]	1.89 [0.24]
	24	15.91 [0.56]	1.68 [0.10]
	36	17.62 [0.65]	1.91 [0.16]
	48	17.13 [0.53]	1.69 [0.12]
	72	18.01 [0.48]	1.96 [0.06]
	96	16.26 [0.72]	1.78 [0.10]
60°C Immersion	12	16.75 [0.28]	1.74 [0.16]
	24	14.16 [0.31]	1.15 [0.12]
	36	14.36 [0.74]	1.23 [0.06]
	48	14.35 [0.44]	1.19 [0.08]
	72	14.83 [0.67]	1.26 [0.10]
	96	14.15 [0.70]	1.11 [0.11]
80°C Immersion	12	13.76 [0.99]	1.10 [0.11]
	24	11.78 [0.56]	0.95 [0.02]
	36	12.77 [0.40]	0.95 [0.06]
	48	11.09 [0.34]	0.89 [0.06]
	72	11.20 [0.60]	0.79 [0.10]
	96	9.65 [0.43]	0.73 [0.09]